Synthesis of Water Stable Organometallic $^{99(m)}$Tc- and Re Complexes Containing Arene- or N-Heterocyclic Carbene Ligands

---

Dissertation

zur

Erlangung der naturwissenschaftlichen Doktorwürde
(Dr. sc. nat.)

vorgelegt der

Mathematisch-naturwissenschaftlichen Fakultät

der

Universität Zürich

von

Michael Benz

von

Marbach SG

Promotionskomitee

Prof. Dr. Roger Alberto (Vorsitz)

Prof. Dr. Cristina Nevado

Dr. Henrik Braband (Betreuung der Dissertation)

Zürich, 2016

Table of Contents

1 Glossary and Summary

1.1 Compounds in this Thesis

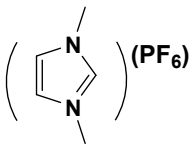

(L1-H)(PF6)

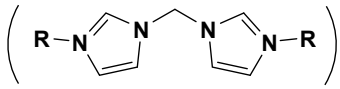

R = Me (L2-H2)(PF6)2
R = Et (L3-H2)(PF6)2

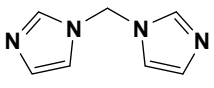

L4

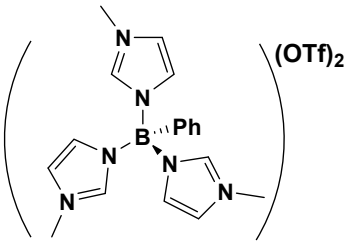

(L5-H3)(OTf)2

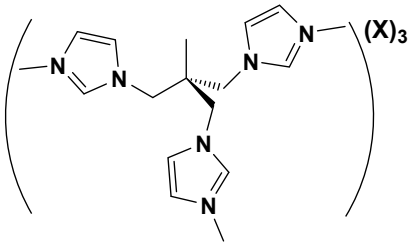

(L6-H3)(X)3 (X = Br, PF6)

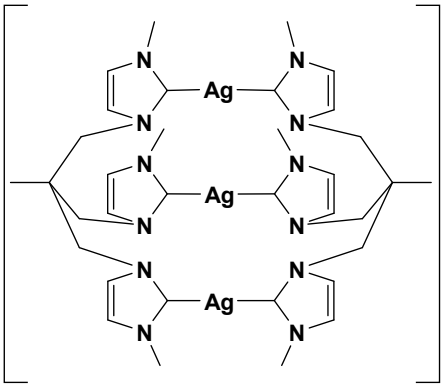

[7]3+

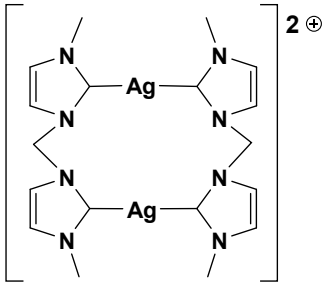

[6]2+

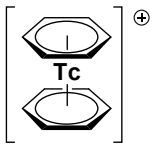

[1]+

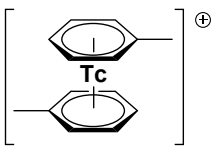

[2]+

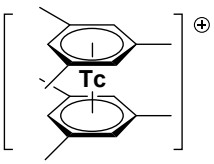

[3]+

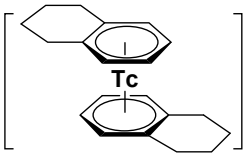

[4]+

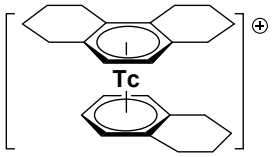

[5]+

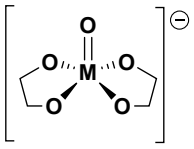

M = 99Tc ([8]-)
M = Re ([15]-)

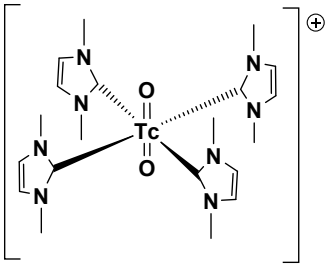

[9]+

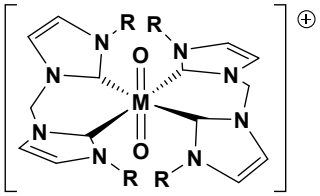

M = 99Tc, R = Me ([10]+)
M = 99Tc, R = Et ([11]+)
M = Re, R = Me ([16]+)

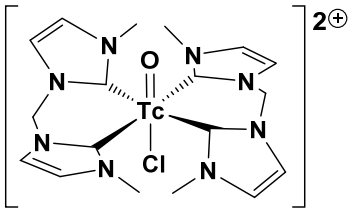

M = ^{99}Tc ([12]$^{2+}$)
M = Re ([17]$^{2+}$)

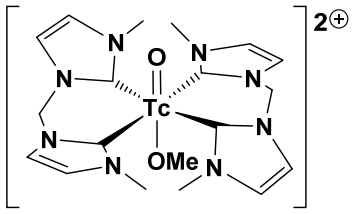

[13]$^{2+}$

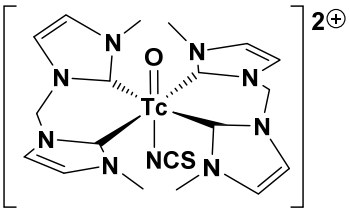

[14]$^{2+}$

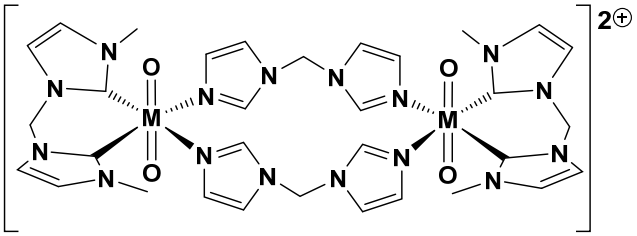

M = ^{99}Tc ([18]$^{2+}$)
M = Re ([19]$^{2+}$)

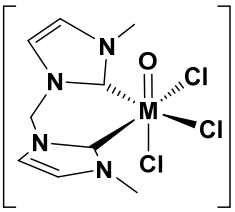

M = ^{99}Tc ([20])
M = Re ([21])

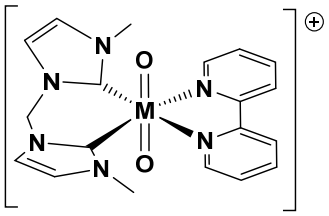

M = ^{99}Tc ([22]$^{+}$)
M = Re ([23]$^{+}$)

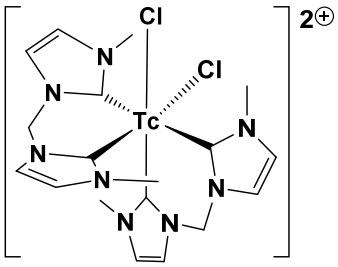

[24]$^{2+}$

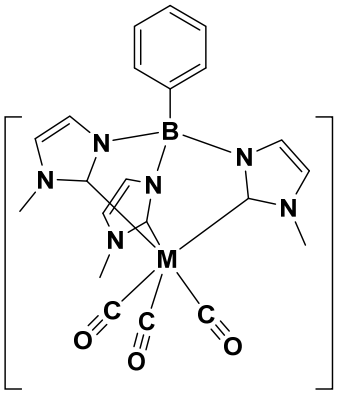

M = ^{99}Tc ([28])
M = Re ([25])

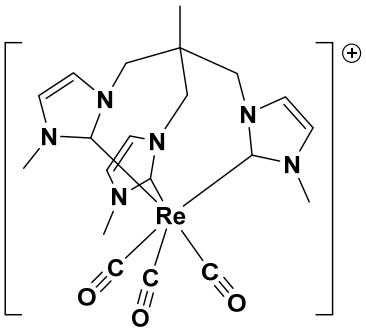

[26]$^{+}$

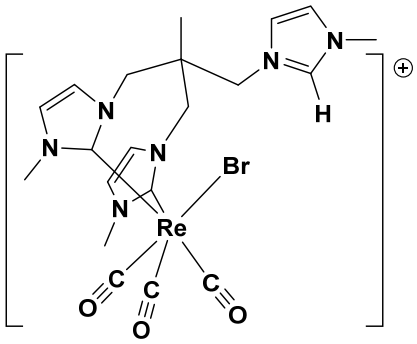

[27]$^{+}$

1.2 List of Abbreviations

bipy	2,2'-bipyridine
boc	COO^tBu
boc-ser-OBz-H	boc-*L*-serine benzyl ester
cat-H_2	catechol
Cp	cyclopentadienyl
Cp*	pentamethylcyclopentadienyl
CV	cyclic voltammetry
dab-H_2	1,2-diaminobenzene
DHA	donor-H-acceptor
DMF	dimethylformamide
DMSO	dimethyl sulfoxide
DPMA-H_2	2-(diphenylphosphinomethyl)aniline
dppd-H_2	N,N'-bis[2-(diphenylphosphino)-phenyl]propane-1,3-diamine
DPV	differential pulse voltammetry
EI	electron ionization
ESI	electrospray ionization
glyc-H_2	ethylene glycol
HPLC	high-performance liquid chromatography
HR	high-resolution
IL	ionic liquid
Im	imidazole
IR	infrared
L^R_B	1,1′-methylene-3,3′-dialkyl-4,4′-diimidazoline-2,2′-diylidene (R = Me, ^{i}Pr. Bz)
LDA	lithium diisopropylamide
L^{Et}	1,3-diethyl-4,5-dimethylimidazoline-2-ylidene
L^{iPr}	1,3-diisopropyl-4,5-dimethylimidazoline-2-ylidene
LMCT	ligand-to-metal charge-transfer
L^{Me}	1,3,4,5-tetramethylimidazoline-2-ylidene
L^{Ph}	1,3,4-triphenyl-1,2,4-triazoline-5-ylidene
L^{Py}	1-(2-pyridyl)-3-methylimidazoline-2-ylidene

LSC	liquid scintillation counting
Me_3tacn	1,4,7-trimethyl-1,4,7-triazacyclononane
MOF	metal organic framework
MS	mass spectrometry
MTBE	methyl *tert*-butyl ether
NHC	N-heterocyclic carbene
NMR	nuclear magnetic resonance
NOE	nuclear Overhauser effect
o-apdpp-H	(*o*-aminophenyl)diphenylphosphine
OHPhen	1,2,3,4,5,6,7,8-octahydrophenanthrene
ORTEP	Oak Ridge thermal ellipsoid plot
$OSiMe_2OSiMe_2O$	1,1,3,3-tetramethyldisiloxane-1,3-diolato
OTf	trifluoromethanesulfonate
$PhNPPh_3$	tetraphenylphosphine imide
PUREX	plutonium uranium redox extraction
py	pyridine
SHE	standard hydrogen electrode
SNHC	saturated imidazoline-2-ylidene
SPECT	single-photon emission computed tomography
tacn-R	1,4,7-triazacyclononane and derivatives
TEAP	triethylammonium phosphate
TFA	trifluoroacetic acid
THF	tetrahydrofuran
TLC	thin-layer chromatography
TMSOTf	trimethylsilyl trifluoromethanesulfonate
Tp	trispyrazolylborate
Tp^{Me}	tris(3-methylpyrazolyl)borate
TSB	tetradentate N_2O_2 Schiff base
UV-Vis	ultraviolet–visible

1.3 Published Parts of this Thesis

From Tc^{VII} to Tc^{I}; Facile Syntheses of bis-Arene Complexes $[^{99(m)}Tc(arene)_2]^+$ from Pertechnetate, Benz, M.; Braband, H.; Schmutz, P.; Halter, J.; Alberto, R. *Chem. Sci.* **2015**, *6*, 165-169.

Toward Organometallic ^{99m}Tc Imaging Agents: Synthesis of Water-Stable ^{99}Tc-NHC Complexes, Benz, M.; Spingler, B.; Alberto, R.; Braband, H. *J. Am. Chem. Soc.* **2013**, *135*, 17566-17572.

1.4 Summary

Water stable organometallic $^{99(m)}$Tc complexes containing arene and N-heterocyclic carbene (NHC) ligands were successfully synthesized. Three different methods for the preparation of $[^{99}Tc(arene)_2]^+$ complexes were developed, starting from $(NH_4)[^{99}TcO_4]$, $(K)[^{99}TcO_4]$ or $(K)_2[^{99}TcCl_6]$ using either $AlCl_3$ and Zn, or exclusively $AlCl_3$, as reagents besides the corresponding arene. While reactions using benzene require the presence of Zn for the reduction, reactions using toluene, mesitylene and tetralin proceed to $[^{99}Tc(arene)_2]^+$ using only $AlCl_3$ as a reagent. Formation of a significant amount of side products by transalkylation reactions was only observed in the synthesis of $[^{99}Tc(tetralin)_2]^+$. The side product $[^{99}Tc(tetralin)(OHPhen)]^+$ (OHPhen = 1,2,3,4,5,6,7,8-octahydrophenanthrene) was unambiguously identified. $[Al(DMF)_6][^{99}TcCl_6](Cl)\cdot DMF$ (DMF = dimethylformamide) and $[^{99}Tc(benzene)_2][^{99}TcCl_5(OH_2)]$ were identified as intermediates of the formation of $[^{99}Tc(arene)_2]^+$, which indicates that the reaction starting from $[^{99(m)}TcO_4]^-$ proceeds via the formation of $[^{99(m)}TcCl_6]^{2-}$. The water stable $[^{99}Tc(arene)_2]^+$ complexes have been fully characterized, including the determination of their electrochemical potentials and structural characterization using X-ray diffraction experiments. The synthetic knowledge gained with ^{99}Tc was successfully translated to ^{99m}Tc chemistry, where a novel ionic liquid-based extraction of $[^{99m}TcO_4]^-$ from the saline to the organic solvent was employed. The synthesis of $[^{99(m)}Tc(arene)_2]^+$ complexes starting from $[^{99(m)}TcO_4]^-$ represents a significant improvement of previously reported synthetic procedures and makes this very important class of organometallic ^{99m}Tc complexes accessible for further radiopharmaceutical investigations.

The preparation of $\{^{99}TcO_2\}$-NHC complexes was significantly improved by starting from $[^{99}TcO(glyc)_2]^-$ (glyc = ethylene glycolato) instead of the base sensitive $[^{99}TcOCl_4]^-$. Reaction with the monodentate NHC 1,3-dimethylimidazoline-2-ylidene (**L1**) gave $[^{99}TcO_2(\mathbf{L1})_4]^+$, which was fully characterized despite its tendency to hydrolyze in the presence of H_2O. Reaction of $[^{99}TcO(glyc)_2]^-$ with the bidentate NHCs 1,1′-methylene-3,3′-dimethyl-4,4′-diimidazoline-2,2′-diylidene (**L2**) and 1,1′-methylene-3,3′-diethyl-4,4′-diimidazoline-2,2′-diylidene (**L3**) gave $[^{99}TcO_2(\mathbf{L})_2]^+$ (**L** = **L2**, **L3**) which are the first water stable ^{99}Tc-NHC complexes. An alternative method was developed, in which $[^{99}TcO(glyc)_2]^-$ was reacted with $(\mathbf{L}\text{-}H_2)^{2+}$ in the presence of NEt_3 to give $[^{99}TcO_2(\mathbf{L})_2]^+$ (**L** = **L2**, **L3**). The high stability of these complexes allows the conversion of the $\{^{99}TcO_2\}^+$ core to the $\{^{99}TcO\}^{3+}$ core using HCl by protonation of one O^{2-} ligand, which is subsequently exchanged for a Cl^- ligand. The reaction is fully reversible, since the resulting $[^{99}TcOCl(\mathbf{L2})_2]^{2+}$ forms again $[^{99}TcO_2(\mathbf{L2})_2]^+$ in the presence of OH^- or large quantities of H_2O. $[^{99}TcOCl(\mathbf{L2})_2]^{2+}$ was derivatized with X^-, which led to the corresponding complexes $[^{99}TcOX(\mathbf{L2})_2]^{2+}$ (X = OMe, NCS). Due to the tendency of $[^{99}TcOX(\mathbf{L2})_2]^{2+}$ (X = Cl, OMe, NCS) to form $[^{99}TcO_2(\mathbf{L2})_2]^+$ in aqueous media, these complexes are not suitable for an application with ^{99m}Tc. However, the presented chemistry of $[^{99}TcOX(\mathbf{L2})_2]^{2+}$ has important implications for the *in vivo* chemistry of $[^{99m}TcO_2(\mathbf{L2})_2]^+$, since the $\{^{99(m)}TcO_2\}^+$ core in this complex has to be considered labile at low pH. The preparation of $[ReO_2(\mathbf{L2})_2]^+$ was also achieved following the same procedure as for ^{99}Tc. In contrast to the results with ^{99}Tc, formation of *cis*- and

trans-$[ReO_2(\mathbf{L2})_2]^+$ was observed. Exclusive formation of the thermodynamic product *trans*-$[ReO_2(\mathbf{L2})_2]^+$ was observed when $[ReO(glyc)_2]^-$ was reacted with $(\mathbf{L2}\text{-}H_2)^{2+}$ and NEt_3 in refluxing CH_2Cl_2. While the preparation of $[ReOCl(\mathbf{L2})_2]^{2+}$ and its derivatives was not as thoroughly investigated as with ^{99}Tc, the feasibility of this reaction was proven by the structural characterization of *trans*-$[ReOCl(\mathbf{L2})_2]^{2+}$ by X-ray diffraction experiments. A synthetic procedure to novel dimeric M-NHC complexes (M = Re, ^{99}Tc) was developed. $[MO_2(\mathbf{L2})(\mathbf{L4})]_2^{2+}$ (**L4** = bisimidazol-1-ylmethane) was prepared by reaction of $[MO(glyc)_2]^-$ with 1 eq. of $(\mathbf{L2}\text{-}H_2)^{2+}$ and **L4** in the presence of NEt_3. Two conformers of $[MO_2(\mathbf{L2})(\mathbf{L4})]_2^{2+}$ were identified with X-ray diffraction experiments. When $[MO_2(\mathbf{L2})(\mathbf{L4})]_2^{2+}$ was treated with HCl, the formation of $[MOCl_3(\mathbf{L2})]$ was observed. $[MOCl_3(\mathbf{L2})]$ is a promising starting material for the preparation of M-NHC complexes containing only two NHCs. This was tested with 2,2'-bipyridine (bipy) as a model ligand. Reaction of $[MOCl_3(\mathbf{L2})]$ with bipy in aqueous solution gave $[MO_2(\mathbf{L2})(bipy)]^+$. The synthesis of $[^{99m}TcO_2(\mathbf{L2})_2]^+$ was tested starting from $[^{99m}TcO_4]^-$ via the intermediate $[^{99m}TcO(glyc)_2]^-$. However, the presence of excess $SnCl_2$ in the reaction led to a reduction of the formed $[^{99m}TcO_2(\mathbf{L2})_2]^+$ to $[^{99m}TcCl_2(\mathbf{L2})_2]^{2+}$, which was proven by the synthesis of *cis*-$[^{99}TcCl_2(\mathbf{L2})_2]^{2+}$ from $[^{99}TcO_2(\mathbf{L2})_2]^+$ by reaction with excess $SnCl_2$. The elucidation of this side reaction is presumably the key for the development of a high-yield synthesis of $^{99m}Tc^V$-NHC complexes, in the future. The synthesis of low-valent *fac*-$\{M(CO)_3\}^+$-NHC complexes was tested with the tridentate NHCs $(PhB(^{Me}Im)_3)^-$ ($\mathbf{L5}^-$) and 1,1,1-tris[(3-methylimidazoline-2-ylidene)-methyl]ethane (**L6**). $[Re(\mathbf{L5})(CO)_3]$ and $[Re(\mathbf{L6})(CO)_3]^+$ were prepared by reaction of $[ReBr_3(CO)_3]^{2-}$ with $\mathbf{L5}^-$ or **L6**. The side product $[ReBr(\mathbf{L6}\text{-}H)(CO)_3]^+$ was structurally characterized by X-ray diffraction experiments. Formation of $[ReBr(\mathbf{L6}\text{-}H)(CO)_3]^+$ was prevented when the Br^- ligands of $[ReBr_3(CO)_3]^{2-}$ were precipitated prior to reaction using AgOTf (OTf = trifluoromethanesulfonate). Following the synthetic procedure for the preparation of $[Re(\mathbf{L5})(CO)_3]$, $[^{99}Tc(\mathbf{L5})(CO)_3]$ was prepared. The decomposition of $[^{99}Tc(\mathbf{L5})(CO)_3]$ was observed during purification and only trace amounts of $[^{99}Tc(\mathbf{L5})(CO)_3]$ were obtained. Similar decomposition reactions were observed for $[Re(\mathbf{L5})(CO)_3]$. Although the exact mechanism of decomposition is unclear, spectroscopic evidence showed that the decomposition reaction was presumably initiated by protonation of one NHC to give $[Re(\mathbf{L5}\text{-}H)(CO)_3]^+$.

The described results are an important contribution to the organometallic chemistry of Re- and ^{99m}Tc complexes with arene- and NHC ligands and pave the way for the further development of applications in this field.

1.5 Zusammenfassung

Wasserstabile organometallische $^{99(m)}$Tc Komplexe mit Aren- und N-heterocyclischen Carben (NHC)-Liganden wurden erfolgreich synthetisiert. Drei verschiedene Methoden für die Herstellung von $[^{99}Tc(Aren)_2]^+$ Komplexen wurden entwickelt, ausgehend von $(NH_4)[^{99}TcO_4]$, $(K)[^{99}TcO_4]$ oder $(K)_2[^{99}TcCl_6]$ mittels Umsetzung mit $AlCl_3$ und Zn, oder nur $AlCl_3$, als Reagenzien im entsprechenden Aren. Während Reaktionen mit Benzol nur mit Zn als Reduktionsmittel ablaufen, führen Reaktionen mit Toluol, Mesitylen oder Tetralin unter ausschliesslicher Verwendung von $AlCl_3$ als Reagenz zu den entsprechenden $[^{99}Tc(Aren)_2]^+$ Komplexen. Die Bildung einer signifikanten Menge Nebenproduktes wurde nur bei der Synthese von $[^{99}Tc(Tetralin)_2]^+$ beobachtet. Das Nebenprodukt konnte eindeutig als $[^{99}Tc(Tetralin)(OHPhen)]^+$ (OHPhen = OHPhen = 1,2,3,4,5,6,7,8-Octahydrophenanthren) identifiziert werden. $[Al(DMF)_6][^{99}TcCl_6](Cl)\cdot DMF$ (DMF = Dimethylformamid) und $[^{99}Tc(Benzol)_2]$-$[^{99}TcCl_5(OH_2)]$ wurden mittels Röntgenstrukturanalyse als Intermediate bei der Bildung von $[^{99}Tc(Aren)_2]^+$ identifiziert, was darauf hinweist, dass die Reaktion ausgehend von $[^{99(m)}TcO_4]^-$ über die Bildung von $[^{99(m)}TcCl_6]^{2-}$ verläuft. Die wasserstabilen $[^{99}Tc(Aren)_2]^+$ Komplexe wurden vollständig charakterisiert, einschliesslich der Bestimmung ihrer elektrochemischen Potentiale und ihrer Röntgenstruktur. Die synthetischen Erkenntnisse aus der ^{99}Tc-Chemie wurden für die Synthese der entsprechenden ^{99m}Tc-Komplexe verwendet. Dabei wurde eine neuartige Extraktionsmethode für den Phasentransfer von der wässrigen in die organische Phase verwendet, in welcher $[^{99m}TcO_4]^-$ mittels einer ionischen Flüssigkeit in die organische Phase extrahiert wird. Die entwickelte Synthese von $[^{99(m)}Tc(Aren)_2]^+$ Komplexen ausgehend von $[^{99(m)}TcO_4]^-$ repräsentiert eine signifikante Verbesserung gegenüber bisher veröffentlichten synthetischen Prozeduren und macht diese sehr interessante Klasse von metallorganischen ^{99m}Tc Komplexen für weitere radiopharmazeutische Untersuchungen zugänglich

Die Herstellung von $\{^{99}TcO_2\}^+$-NHC Komplexen wurde signifikant verbessert, indem $[^{99}TcO(Glyc)_2]^-$ (Glyc = Ethylenglycolat) anstelle des basensensitiven $[^{99}TcOCl_4]^-$ als Startverbindung verwendet wurde. Die Reaktion mit dem monodentaten NHC 1,3-Dimethylimidazolin-2-yliden (**L1**) führte zur Isolierung von $[^{99}TcO_2(\mathbf{L1})_4]^+$, welches trotz seiner Tendenz zur Hydrolyse in Gegenwart von H_2O vollständig charakterisiert werden konnte. Reaktion mit den bidentaten NHCs 1,1′-Methylen-3,3′-dimethyl-4,4′-diimidazolin-2,2′-diyliden (**L2**) und 1,1′-Methylen-3,3′-diethyl-4,4′-diimidazolin-2,2′-diyliden (**L3**) ergab $[^{99}TcO_2(\mathbf{L})_2]^+$ (**L** = **L2**, **L3**), welche die ersten wasserstabilen ^{99}Tc-NHC Komplexe sind. Eine alternative Synthesemethode wurde entwickelt, in welcher $[^{99}TcO(glyc)_2]^-$ direkt mit $(\mathbf{L}\text{-}H_2)^{2+}$ und NEt_3 zu $[^{99}TcO_2(\mathbf{L})_2]^+$ umgesetzt wurde. The hohe Stabilität dieser Komplexe erlaubt die Umwandlung des $\{^{99}TcO_2\}^+$ Zentrums zum $\{^{99}TcO\}^{3+}$ Zentrum mittels Protonierung eines O^{2-} Liganden und anschliessendem Austausch durch Cl^-. Diese Reaktion ist vollständig reversibel und das resultierende $[^{99}TcOCl(\mathbf{L2})_2]^{2+}$ reagiert in der Anwesenheit von OH^- oder einem grossem Überschuss H_2O wieder zu $[^{99}TcO_2(\mathbf{L2})_2]^+$. $[^{99}TcOCl(\mathbf{L2})_2]^{2+}$ wurde mit X^- derivatisiert, was zu den entsprechenden $[^{99}TcOX(\mathbf{L2})_2]^{2+}$ Komplexen führt (X = OMe, NCS). Wegen der Tendenz von

$[^{99}TcOX(\mathbf{L2})_2]^{2+}$ (X = Cl, OMe, NCS) in wässriger Lösung $[^{99}TcO_2(\mathbf{L2})_2]^{+}$ zu bilden, ist diese Derivatisierung nicht für die Anwendung mit ^{99m}Tc geeignet. Allerdings hat die untersuchte Chemie von $[^{99}TcOX(\mathbf{L2})_2]^{2+}$ Komplexen wichtige Implikationen für die *in vivo* Chemie von $[^{99m}TcO_2(\mathbf{L2})_2]^{+}$, da das $\{^{99m}TcO_2\}^{+}$ Zentrum in diesem Komplex bei niedrigem pH als nicht inert angesehen werden muss. Die Synthese von $[ReO_2(\mathbf{L2})_2]^{+}$ wurde analog zu ^{99}Tc durchgeführt. Im Gegensatz zu den Resultaten mit ^{99}Tc wurde bei der Synthese von $[ReO_2(\mathbf{L2})_2]^{+}$ auch die Bildung des *cis*- und *trans*-Produktes beobachtet. Bei der Reaktion von $[ReO(glyc)_2]^{-}$ mit $(\mathbf{L2}\text{-}H_2)^{2+}$ und NEt_3 in refluxierendem CH_2Cl_2 wurde die ausschliessliche Bildung des thermodynamischen Produktes *trans*-$[ReO_2(\mathbf{L2})_2]^{+}$ beobachtet. Die Synthese von $[ReOCl(\mathbf{L2})_2]^{2+}$ und seinen Derivatkomplexen wurde nicht so eingehend studiert wie mit ^{99}Tc, aber die Machbarkeit dieser Reaktion wurde durch die Röntgenstrukturanalyse von *trans*-$[ReOCl(\mathbf{L2})_2]^{2+}$ bewiesen. Eine Synthese von neuartigen Dimerkomplexen des Typs $[MO_2(\mathbf{L2})(\mathbf{L4})]_2^{2+}$ wurde entwickelt (M = Re, ^{99}Tc, **L4** = Bisimidazol-1-ylmethan). $[MO_2(\mathbf{L2})(\mathbf{L4})]_2^{2+}$ wird durch Reaktion von $[ReO(glyc)_2]^{-}$ mit $(\mathbf{L2}\text{-}H_2)^{2+}$ und **L4** in der Gegenwart von NEt_3 hergestellt. Zwei Konformere von $[MO_2(\mathbf{L2})(\mathbf{L4})]_2^{2+}$ wurden mittels Röntgenstrukturanalyse identifiziert. Wenn $[MO_2(\mathbf{L2})(\mathbf{L4})]_2^{2+}$ mit HCl umgesetzt wird, wird die Bildung von $[MOCl_3(\mathbf{L2})]$ beobachtet. $[MOCl_3(\mathbf{L2})]$ ist ein vielversprechendes Startmaterial für die Synthese von Komplexen mit nur zwei NHC Liganden. Dies wurde mit dem Modelliganden 2,2'-Bipyridin (Bipy) getestet. Die Reaktion von $[MOCl_3(\mathbf{L2})]$ mit Bipy in wässriger Lösung führt zur Bildung von $[MO_2(\mathbf{L2})(Bipy)]^{+}$. Die Synthese von $[^{99m}TcO_2(\mathbf{L2})_2]^{+}$ ausgehend von $[^{99m}TcO_4]^{-}$ über die Bildung des Intermediates $[^{99m}TcO(glyc)_2]^{-}$ wurde getestet. Allerdings führte die Anwesenheit eines Überschusses an $SnCl_2$ in der Reaktionslösung zur Reduktion des gebildeten $[^{99m}TcO_2(\mathbf{L2})_2]^{+}$ zu $[^{99m}TcCl_2(\mathbf{L2})_2]^{2+}$, was durch die Synthese von *cis*-$[^{99}TcCl_2(\mathbf{L2})_2]^{2+}$ mittels Reaktion von $[^{99}TcO_2(\mathbf{L2})_2]^{+}$ mit einem Überschuss $SnCl_2$ bewiesen wurde. Die Aufklärung dieser Nebenreaktion ist vermutlich der Schlüssel zu einer zukünftigen Synthese von $^{99m}Tc^{V}$-NHC Komplexen in hoher Ausbeute. Die Synthese von niedervalenten *fac*-$\{M(CO)_3\}^{+}$-NHC Komplexen wurde mit den tridentaten NHC Liganden $(PhB(^{Me}Im)_3)^{-}$ ($\mathbf{L5}^{-}$) und 1,1,1-Tris[(3-methylimidazolin-2-yliden)-methyl]ethan (**L6**) getestet. Die Komplexe $[Re(\mathbf{L5})(CO)_3]$ und $[Re(\mathbf{L6})(CO)_3]^{+}$ wurden durch die Reaktion von $[ReBr_3(CO)_3]^{2-}$ mit $\mathbf{L5}^{-}$ respektive **L6** erhalten. $[ReBr(\mathbf{L6}\text{-}H)(CO)_3]^{+}$ wurde durch Röntgenstrukturanalyse als Nebenprodukt identifiziert. Die Bildung von $[ReBr(\mathbf{L6}\text{-}H)(CO)_3]^{+}$ wird durch die Fällung der Br^{-} Liganden in $[ReBr_3(CO)_3]^{2-}$ mittels AgOTf (OTf = Trifluormethansulfonat) vor der Reaktion verhindert. $[^{99}Tc(\mathbf{L5})(CO)_3]$ wurde analog zu $[Re(\mathbf{L5})(CO)_3]$ synthetisiert. Während der Aufreinigung wurde jedoch die Zersetzung von $[^{99}Tc(\mathbf{L5})(CO)_3]$ beobachtet. Ähnliche Zersetzungsreaktionen wurden für $[Re(\mathbf{L5})(CO)_3]$ beobachtet. Obwohl der exakte Mechanismus der Zersetzungsreaktion nicht bekannt ist, zeigen spektroskopische Untersuchungen, dass eine Protonierung eines NHC Liganden unter Bildung von $[Re(\mathbf{L5}\text{-}H)(CO)_3]^{+}$ vermutlich die Zersetzung einleitet.

Die beschriebenen Resultate sind ein wichtiger Beitrag zur metallorganischen Chemie von Re- und $^{99(m)}$Tc mit Aren- und NHC Liganden und sind wegweisend für die weitere Entwicklung von Anwendungen in diesem Bereich.

2 Introduction

In the last decades, organometallic chemistry gained more and more importance for the development of novel biologically active compounds. Selected examples are $\{M(Cp)\}^{+}$- (M = Fe, Ru, Os; Cp = cyclopentadienyl), $\{M(arene)\}^{2+}$- (M = Ru, Os) and $\{M(NHC)\}^{+}$ complexes (M = Ag, Au; NHC = N-heterocyclic carbene), that have been studied for their antimicrobial properties or antiproliferative activity against cancer cells.[1-4] Surprisingly, the coordination chemistry of technetium is significantly lagging behind this trend in bioinorganic chemistry. To push the organometallic $^{99(m)}$Tc chemistry forward and to close gaps in the fundamental knowledge of organometallic $^{99(m)}$Tc chemistry, arenes and NHCs have been studied as ligand systems in this thesis. Besides the impact of this work on fundamental $^{99(m)}$Tc chemistry, the resulting new class of compounds has a high potential for nuclear medicinal applications.

2.1 A Brief Introduction to Technetium

Technetium (Tc) is the lightest element without any stable isotopes. The low natural abundance of Tc is the reason for its relatively late discovery in 1937 by Perrier and Segrè.[5,6] Since then, $^{99(m)}$Tc chemistry has continuously become more and more important. The significance of fundamental $^{99(m)}$Tc chemistry is mainly explained by the importance of ^{99m}Tc in nuclear medicine, where it is used as a nuclide in single-photon emission computed tomography (SPECT). ^{99m}Tc is a γ-emitter with a half life time ($t_{1/2}$) of approximately 6 h and a decay energy of 140 keV (Figure 1, a)), which make ^{99m}Tc an ideal nuclide for the application with SPECT.[7] The development of the ^{99}Mo/^{99m}Tc generator, from which ^{99m}Tc is readily available as a saline solution of $[^{99m}TcO_4]^-$ for the application in nuclear medicine (Figure 1, b)), has led to a great interest in $^{99(m)}$Tc chemistry that is still vivid until today.[8,9] While the main interest in the fundamental chemistry of ^{99}Tc stems from the application of ^{99m}Tc in nuclear medicine, the impact of fundamental ^{99}Tc chemistry on environmental chemistry should not be underestimated. ^{99}Tc is a weak β^--emitter with a decay-energy of 292 keV and a half life time of 212'000 y. Waste products of nuclear fission of ^{235}U contain around 6% ^{99}Tc and its environmental chemistry therefore plays an important role for nuclear waste management.[7] Together with the extensive testing of nuclear weapons, an estimated 305 t of ^{99}Tc were produced or released worldwide, which further explains the interest in the environmental chemistry of ^{99}Tc.[10] Nonetheless, the main focus of this work lies on the application with ^{99m}Tc in nuclear medicine.

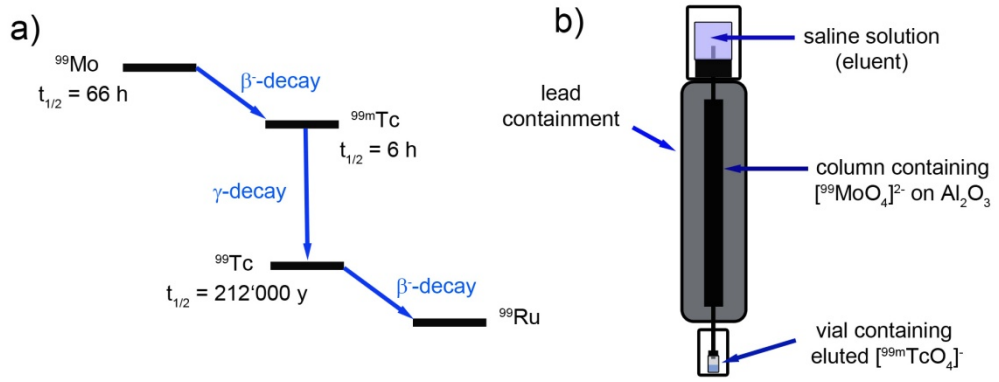

Figure 1: a) Decay pathway leading to ^{99m}Tc and ^{99}Tc. The energies and probabilities have been omitted. b) Schematic representation of the ^{99}Mo/^{99m}Tc generator.

^{99m}Tc is a nuclear isomer of ^{99}Tc and therefore, differences in chemistry are not expected. However, the different concentrations used in ^{99m}Tc- and ^{99}Tc chemistry often lead to different reaction patterns and products. ^{99m}Tc is eluted as $[^{99m}TcO_4]^-$ from the ^{99}Mo/^{99m}Tc generator in concentrations of 10^{-9} to 10^{-6} M,[7] while ^{99}Tc is available as $(NH_4)[^{99}TcO_4]$ in macroscopic quantities from the plutonium uranium redox extraction (PUREX) process.[11,12] The resulting difference in reagent stoichiometry has to be considered for the discussion of reactions of $^{99(m)}$Tc. In addition, the low concentration of ^{99m}Tc allows only reaction control by chromatographic methods such as high-performance liquid chromatography (HPLC) or thin-layer chromatography (TLC), in which the γ-radiation of the compounds is detected. For fundamental studies of $^{99(m)}$Tc chemistry, compounds are prepared with ^{99}Tc, where many of the commonly used analytical methods can be used for characterization, such as nuclear magnetic resonance- (NMR) and infrared (IR) spectroscopy, X-ray diffraction analysis of single crystals and determination of ^{99}Tc contents by liquid scintillation counting (LSC). The inherent radioactivity of probes containing ^{99}Tc does not allow the performance of elemental analyses other than the determination of the ^{99}Tc content and it also prohibits the use of mass spectrometry (MS). Therefore, the determination of X-ray structures is of great importance for an unambiguous identification of ^{99}Tc compounds. For the identification of ^{99m}Tc complexes, their HPLC retention times are compared with the corresponding ^{99}Tc or Re complexes. Therefore, the study of corresponding complexes with the higher homologue Re is not only a useful tool to further investigate the reactivity of the $^{99(m)}$Tc complexes, but also serves for the identification of ^{99m}Tc complexes if the ^{99}Tc complex is not available.

2.1.1 Core Structures of $^{99(m)}$Tc in the Focus of this Thesis

One reason for the success of ^{99m}Tc in nuclear medicine is its rich coordination chemistry.[7] $^{99(m)}$Tc complexes in many oxidation states are known, ranging from -I to VII.[13] $^{99(m)}$Tc chemistry evolves mainly around certain core structures, such as the *fac*-$\{^{99(m)}Tc(CO)_3\}^+$-, $\{^{99(m)}TcO\}^{3+}$- or *fac*-$\{^{99(m)}TcO_3\}^+$ core. These core structures are substitution inert and allow the derivatization with a large number of ligands, while the corresponding core structure also has an influence on the properties

of the overall complex. A core structure should ideally have a universal precursor, which is easily prepared and allows facile derivatization. The main focus in this thesis lies on the $\{^{99(m)}TcO\}^{3+}$- and the *fac*-$\{^{99(m)}Tc(CO)_3\}^{+}$ cores, which will be shortly presented in the next paragraphs.

2.1.1.1 Chemical Properties of the $\{^{99(m)}Tc^{V}O\}^{3+}$ Core

The $\{^{99(m)}TcO\}^{3+}$ core has a d^2 configuration and has been extensively studied.[13] The strong π-donation of the O^{2-} ligand stabilizes the high oxidation state, which is often further stabilized by strong polydentate chelating ligands. In ^{99}Tc chemistry, the generally used precursor for the $\{^{99}TcO\}^{3+}$ core is $[^{99}TcOCl_4]^-$, which is prepared by reaction of $[^{99}TcO_4]^-$ with conc. HCl (Scheme 1, a)). The Cl^- ligands in $[^{99}TcOCl_4]^-$ can be exchanged with a multitude of other ligands, which leads to five coordinate 14 e^- complexes with a distorted square pyramidal geometry. Depending on the total charge on the $^{99(m)}Tc$ and the properties of the ligands, the *trans*-position of the O^{2-} ligand can be coordinated by H_2O, which is subsequently deprotonated to form the corresponding octahedral 18 e^- complex containing the $\{^{99(m)}TcO_2\}^{+}$ core. In the case of anionic ligands, the $\{^{99(m)}TcO\}^{3+}$ core is usually favoured, while in the case of neutral ligands, formation of the $\{^{99(m)}TcO_2\}^{+}$ core is prevailing. In ^{99m}Tc chemistry, $\{^{99m}TcO\}^{3+}$ complexes are formed by reduction of $[^{99m}TcO_4]^-$ with $SnCl_2$ in the presence of the corresponding ligands (Scheme 1, b)) or by substitution reactions of ^{99m}Tc-glucoheptonate with the ligands of interest. The use of the commercially available ^{99m}Tc-glucoheptonate kit allows the facile formation of this $\{^{99m}TcO\}^{3+}$ precursor by addition of a saline solution containing $[^{99m}TcO_4]^-$ to a ^{99m}Tc-glucoheptonate kit. Among other components, this kit also contains $SnCl_2$, which underlines the importance of this reagent for the preparation of $\{^{99m}TcO\}^{3+}$ complexes.

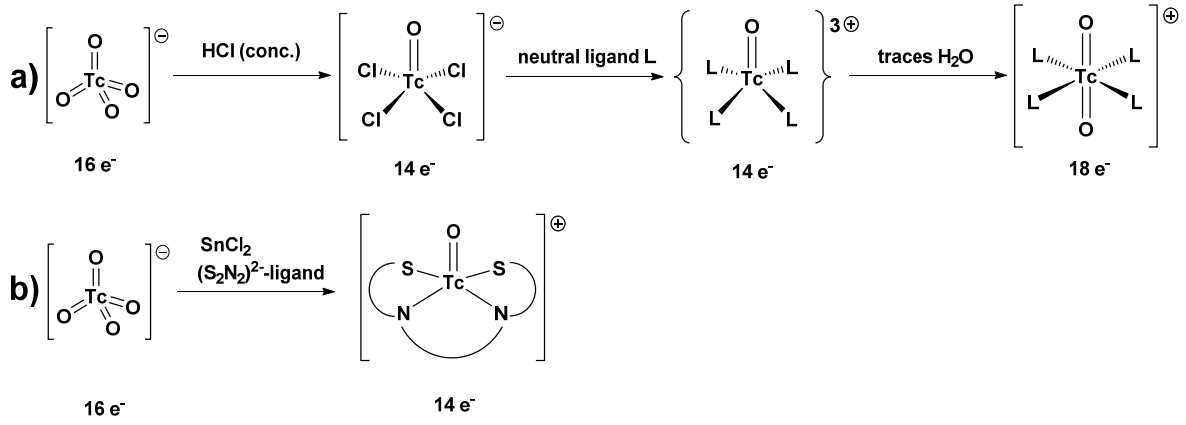

Scheme 1: Syntheses of $\{^{99(m)}TcO\}^{3+}$ complexes starting from $[^{99(m)}TcO_4]^-$. a) Reaction of $[^{99}TcO_4]^-$ with HCl leads to tetragonal pyramidal $[^{99}TcOCl_4]^-$, which can be derivatized with a multitude of ligands. As an example, the reaction of $[^{99}TcOCl_4]^-$ with a neutral monodentate ligand L leads to the formation of the intermediate $\{^{99}TcO(L)_4\}^{3+}$, which forms $[^{99}TcO_2(L)_4]^+$ by coordination and subsequent deprotonation of H_2O. b) Reaction of $[^{99m}TcO_4]^-$ with $SnCl_2$ in the presence of the ligand of interest, e.g. a tetradentate $(S_2N_2)^{2-}$ ligand, yields $[^{99m}TcO(S_2N_2)]^+$. Formation of the dioxo species is in this case unfavoured due to the dianionic ligand.

2.1.1.2 Chemical Properties of the *fac*-$\{^{99(m)}Tc^{I}(CO)_3\}^+$ Core

The *fac*-$\{^{99(m)}Tc(CO)_3\}^+$ core has a d^6 configuration and the resulting six coordinate octahedral complexes are highly stable. The *fac*-coordinating CO ligands give this core a lipophilic character, while the overall hydrophilicity/lipophilicity of the complex can be tuned by changing the remaining coordination sphere. Hieber *et al.* and Hileman *et al.* developed a high-pressure synthesis of $[^{99}Tc(CO)_{10}]$ in 1961, which is a precursor for *fac*-$\{^{99(m)}Tc(CO)_3\}^+$ complexes.[14,15] However, the high-pressure synthesis of $[^{99}Tc(CO)_{10}]$ is impractical and hazardous, which also impeded its applicability in ^{99m}Tc chemistry. Alberto *et al.* developed a low-pressure synthesis of *fac*-$[^{99}TcCl_3(CO)_3]^{2-}$ in the 1990s (Scheme 2, a)),[16] which led to the publication of a low-pressure synthesis of *fac*-$[^{99m}Tc(OH_2)_3(CO)_3]^+$ in 1998 (Scheme 2, b)).[17] In the following years, Alberto *et al.* developed a kit for the synthesis of *fac*-$[^{99m}Tc(OH_2)_3(CO)_3]^+$, which uses boranocarbonate (BH_3COO^{2-}) for the synthesis and was patented under the name IsoLink™ in 2001 (Scheme 2, c)).[18] This breakthrough for *fac*-$\{^{99(m)}Tc(CO)_3\}^+$ chemistry led to the preparation of a high number of complexes containing the *fac*-$\{^{99(m)}Tc(CO)_3\}^+$ core in the subsequent years. Besides its facile preparation, important factors for the success of *fac*-$[^{99m}Tc(OH_2)_3(CO)_3]^+$ as a precursor are its high stability in aqueous solution and the fact that all H_2O ligands are readily exchanged by a variety of ligands.[19]

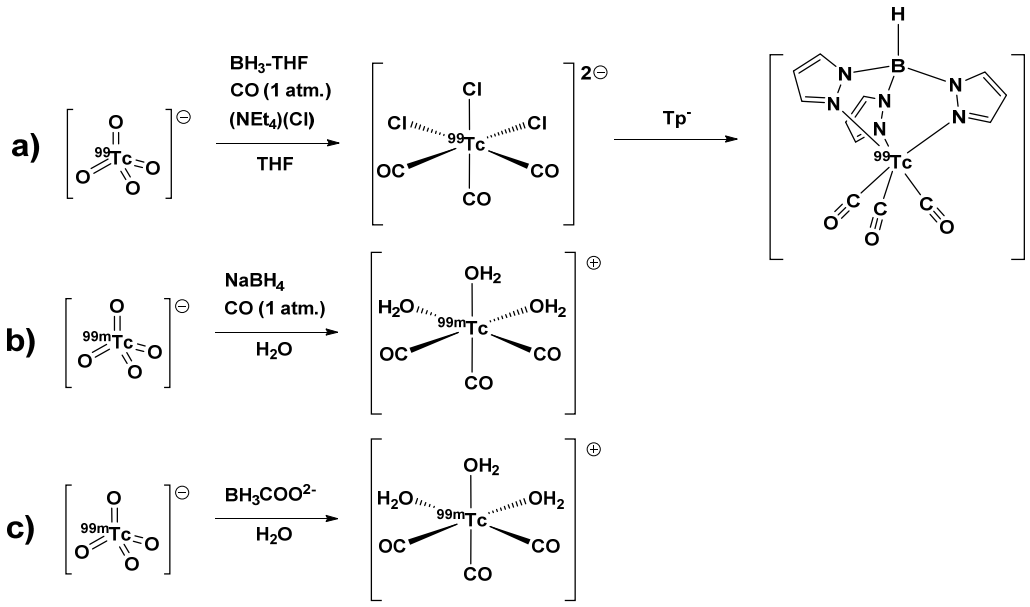

Scheme 2: Syntheses of *fac*-$\{^{99(m)}Tc(CO)_3\}^+$ complexes. a) Low-pressure synthesis of $[^{99}TcCl_3(CO)_3]^{2-}$ starting from $[^{99}TcO_4]^-$. As an example of a model chelating ligand, trispyrazolylborate (Tp^-) was chosen. The resulting complex $[^{99}Tc(Tp)(CO)_3]$ was described by Ziegler *et al.*, although it was prepared starting from $[^{99}Tc(CO)_5Br]$.[20] b) First low-pressure synthesis of $[^{99m}Tc(OH_2)_3(CO)_3]^+$ starting from $[^{99m}TcO_4]^-$. c) State of the art synthesis of $[^{99m}Tc(OH_2)_3(CO)_3]^+$ starting from $[^{99m}TcO_4]^-$.

2.2 Developments in $[^{99(m)}Tc(arene)_2]^+$ Chemistry

The first synthesis of a $[^{99}Tc(arene)_2]^+$ complex was published in 1961 by Baumgärtner *et al.*, who prepared $[^{99(m)}Tc(benzene)_2]^+$ by element transmutation using bombardment of a $[^{98}Mo(benzene)_2]$ target with thermal neutrons (Scheme 3, a)).[21] This exceptional reaction follows the same principle that is used for the generation of ^{99m}Tc in the $^{99}Mo/^{99m}Tc$ generator and consequently, only trace amounts of $[^{99(m)}Tc(benzene)_2]^+$ were obtained. Eventually, Fischer and Palm developed a synthetic method to $[^{99}Tc(arene)_2]^+$ (arene = benzene, hexamethylbenzene) by reaction of $[^{99}TcCl_4]$ with Al and $AlCl_3$ in the corresponding arene, which allowed the isolation of $[^{99}Tc(benzene)_2]^+$ in gram quantities (Scheme 3, b)).[22,23] In 1991, Wester *et al.* utilized this synthetic method to prepare $[^{99m}Tc(arene)_2]^+$ complexes with a variety of alkylated arenes starting from $[^{99m}TcO_4]^-$ and to study the biodistribution of these complexes (Scheme 3, c)).[24] Due to the incompatibility of the synthetic procedure with aqueous conditions, the synthesis of $[^{99m}Tc(arene)_2]^+$ required a time consuming evaporation of the saline solution obtained from the $^{99}Mo/^{99m}Tc$ generator. Besides this, the yields of the reactions were inconsistent and "varied from day to day and from arene to arene".[24] Due to this fact and the complicated synthetic procedure, $[^{99(m)}Tc(arene)_2]^+$ complexes were not further investigated in recent years. The lack of synthetic procedures to $[^{99(m)}Tc(arene)_2]^+$ complexes is surprising, considering their high stability and the various possibilities for derivatization and functionalization of such complexes. Furthermore, the impact of $\{Ru(arene)\}^{2+}$ complexes on the field of medicinal inorganic chemistry underlines the potential of $[^{99m}Tc(arene)_2]^+$ complexes in this important field.[1,2]

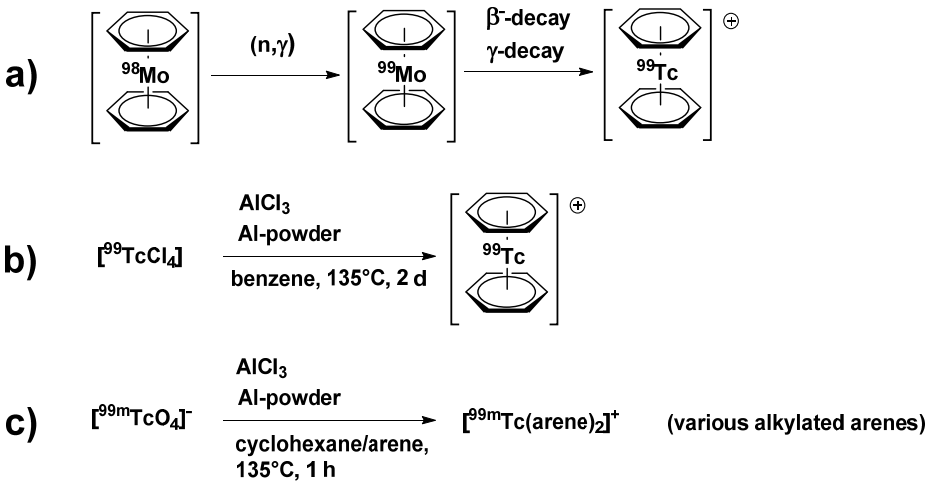

Scheme 3: Syntheses of $[^{99(m)}Tc(arene)_2]^+$ complexes. a) First synthesis of $[^{99(m)}Tc(benzene)_2]^+$ by element transmutation starting from $[^{98}Mo(benzene)_2]$. b) First chemical synthesis of $[^{99}Tc(benzene)_2]^+$ by reaction of $[^{99}TcCl_4]$ with $AlCl_3$ and Al in benzene. c) First chemical synthesis of $[^{99m}Tc(arene)_2]^+$ starting from $[^{99m}TcO_4]^-$.

2.3 State of the Art M-NHC Chemistry (M = Re, ^{99}Tc, Mn)

Since the first publication of N-heterocyclic carbene (NHC) complexes in 1968 by Öfele and Wanzlick,[25,26] NHCs have become more and more important as ligands in transition metal chemistry. NHCs have applications in a variety of fields, such as catalysis,[27-29] material science[30] and, more recently, NHC complexes have been investigated concerning their medicinal applications and as potential antitumor metallodrugs.[3,4] The increasing importance of NHC complexes in medicinal chemistry underlines the relevance of the $^{99(m)}$Tc-NHC chemistry described in this thesis. In general, NHCs are good σ-donors and have the potential to act as π-acceptors (Figure 2),[31,32] which enables NHCs to coordinate to metals in low and high oxidation states. The fact, that NHCs usually form strong bonds to metals is particularly interesting for $^{99(m)}$Tc chemistry, since the strong binding of a radio label to a targeting vector is a challenge for the development of new imaging probes. A wide variety of NHC ligands is known and therefore, a focus will be laid on NHCs of the type 1,3-dialkylimidazoline-5-ylidene.

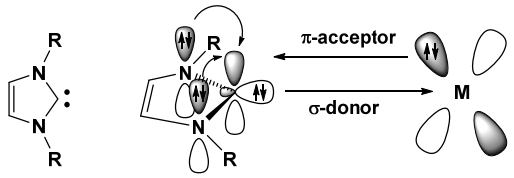

Figure 2: Bonding and resonance stabilization of a NHC ligand. The resonance-stabilized sp^2-hybridized C atom is a strong σ-donor and, due to the empty p-orbital, NHCs can also act as π-acceptors.

Publications on ^{99}Tc-NHC complexes are scarce, with only 3 publications until 2012.[33] The first synthesis of a ^{99}Tc-NHC complex, $[^{99}TcO_2(L^{iPr})_4][^{99}TcO_4]$ (L^{iPr} = 1,3-diisopropyl-4,5-dimethylimidazoline-2-ylidene), was published by Braband *et al.* in 2003 (Scheme 4).[34] $[^{99}TcO_2(L^{iPr})_4][^{99}TcO_4]$ was prepared by reaction of $(N^nBu_4)[^{99}TcOCl_4]$ with excess L^{iPr}, which was prepared in advance from the corresponding imidazole-2-thione by reaction with potassium.[35] Formation of the $\{^{99}TcO_2\}^+$ core is explained by the coordination and subsequent deprotonation of traces of H_2O. $[^{99}TcO_2(L^{iPr})_4][^{99}TcO_4]$ was reported to be stable as a solid in dry air, but unstable in solution, where it decomposes to $[^{99}TcO_4]^-$. X-ray diffraction analysis of $[^{99}TcO_2(L^{iPr})_4][^{99}TcO_4]$ showed the four NHC ligands in a paddle-wheel-like arrangement in the equatorial plane, with the O^{2-} ligands on the tetragonal axis. The stabilization of the high valent ^{99}Tc centre is explained by the strong donor properties of the NHC ligands and the effective shielding of the ^{99}Tc centre by the ^{i}Pr substituents. The corresponding Re complex, $[ReO_2(L^{iPr})_4](PF_6)$, was prepared in a similar procedure by reaction of $[ReOCl_3(PPh_3)_2]$ and excess L^{iPr} in the presence of KPF_6.[34] In contrast to $[^{99}TcO_2(L^{iPr})_4]^+$, $[ReO_2(L^{iPr})_4]^+$ is stable as a solid and in solution.

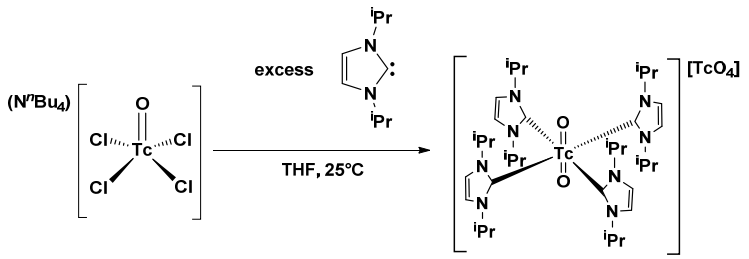

Scheme 4: Synthesis of the first ^{99}Tc-NHC complex, $[^{99}TcO_2(L^{iPr})_4][TcO_4]$, by reaction of $(N^nBu_4)[^{99}TcOCl_4]$ with excess L^{iPr}.

The syntheses of the first $\{^{99}TcN\}^{2+}$-NHC complexes were also published by Braband *et al.* in 2005 (Scheme 5).[36] Reaction of $[^{99}TcNCl_2(PR_2Ph)_3]$ (R = Me, Et) with excess L^{Et} (L^{Et} = 1,3-diethyl-4,5-dimethylimidazoline-2-ylidene) gave, depending on the reaction conditions, $[^{99}TcN(L^{Et})_4]Cl_2$, $[^{99}TcN(L^{Et})_2(OSiMe_2OSiMe_2O)]$ ($OSiMe_2OSiMe_2O$ = 1,1,3,3-tetramethyldisiloxane-1,3-diolato) or $[^{99}TcN(L^{Et})(PMe_2Ph)(OSiMe_2OSiMe_2O)]$. Formation of the $(OSiMe_2OSiMe_2O)^{2-}$ ligand was not expected and was explained by the activation of silicon grease by the highly nucleophilic NHC. $[^{99}TcN(L^{Et})_4]^{2+}$ has a similar stability as $[^{99}TcO_2(L^{iPr})_4]^+$ and also decomposes in solution. X-ray structure analysis of $[^{99}TcN(L^{Et})_4]^{2+}$ confirmed the expected distorted square pyramidal geometry of the complex and the NHC ligands have a paddle-wheel-like arrangement, as it was the case in $[^{99}TcO_2(L^{iPr})_4]^+$.

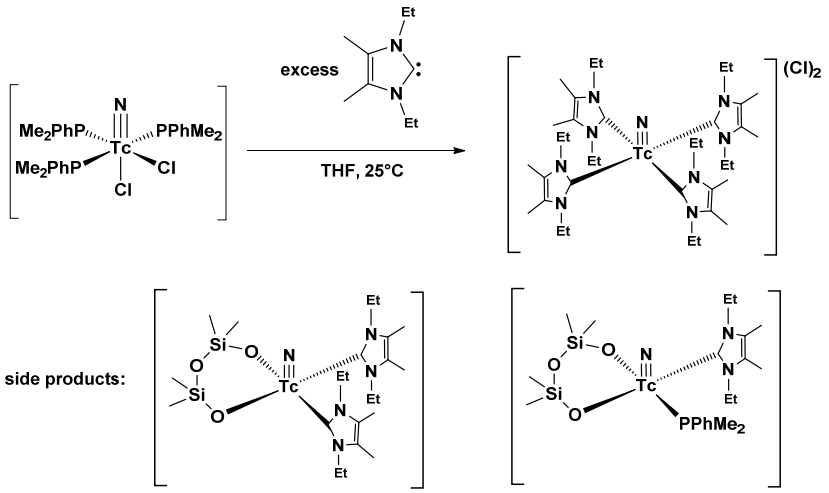

Scheme 5: Synthesis of $[^{99}TcN(L^{Et})_4]Cl_2$ by reaction of $[^{99}TcNCl_2(PMe_2Ph)_3]$ with excess L^{Et}. Formation of the side products $[^{99}TcN(L^{Et})_2(OSiMe_2OSiMe_2O)]$ and $[^{99}TcN(L^{Et})(PMe_2Ph)(OSiMe_2OSiMe_2O)]$ was also observed.

Recently, Oehlke *et al.* described the synthesis of $\{^{99}TcN\}^{2+}$ complexes comprised of aryl and NHC ligands (Scheme 6).[37] Reaction of $[^{99}TcNCl_4]$ with 3 eq. L^{Ph} (L^{Ph} = 1,3,4-triphenyl-1,2,4-triazoline-5-ylidene) led to the isolation of $[^{99}TcNCl_2(L^{Ph})_2]$, which can be further derivatized with excess PhLi or L^{Me} (L^{Me} = 1,3,4,5-tetramethylimidazoline-2-ylidene) to $[^{99}TcN(Ph)_2(L^{Ph})_2]$ or $[^{99}TcNCl(L^{Me})_4]^+$, respectively. While to former is a substitution reaction of the Cl^- ligands for Ph^-, the latter is a

substitution reaction of all four ligands in the equatorial plane for L^{Me} ligands. ^{99}Tc-NHC complexes comprised of monodentate ligands are only air-stable. Nonetheless, [$^{99}TcNCl_2(L^{Ph})_2$] is the first ^{99}Tc-NHC compound that can be derivatized with other ligands, which proves that $^{99}Tc^{V}$-NHC chemistry is not necessarily limited to compounds with four NHCs in the equatorial plane.

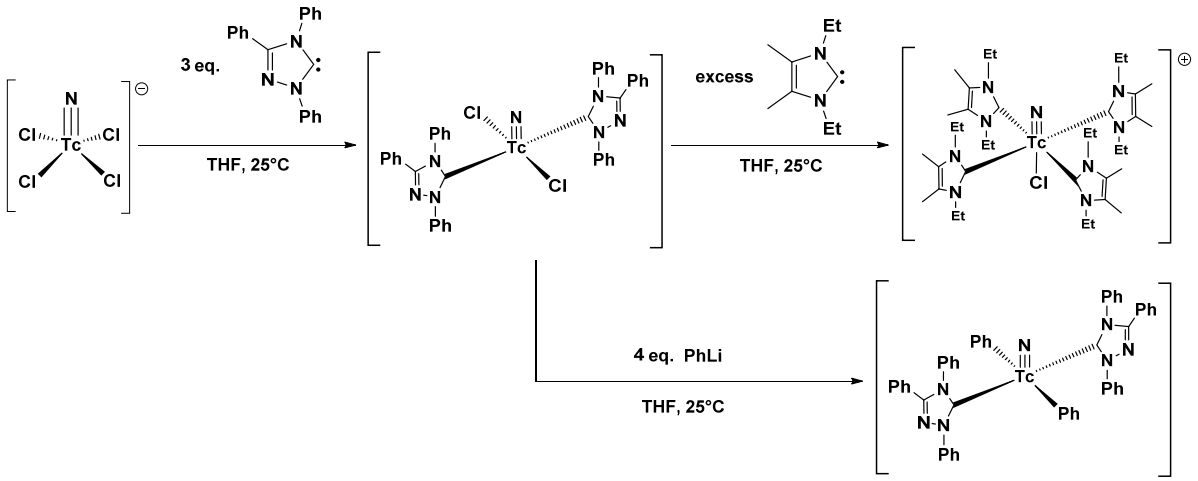

Scheme 6: Reaction of [$^{99}TcNCl_4$] with L^{Ph} yields [$^{99}TcNCl_2(L^{Ph})_2$], which is derivatized with PhLi or L^{Et} to [$^{99}TcN(Ph)_2(L^{Ph})_2$] or [$^{99}TcNCl(L^{Me})_4]^+$, respectively.

While ^{99}Tc-NHC complexes are comparably rare, Mn- and Re-NHC complexes have been extensively studied in the past decades.[33,38] Therefore, only selected examples of *fac*-{$M(CO)_3$}$^+$-NHC complexes will be discussed. Forshaw *et al.* recently published the preparation of *fac*-[$Mn(PhB(^{Me}Im)_3)(CO)_3$] by reaction of *fac*-[$MnBr(^{t}BuCN)(CO)_3]_2$ with $(PhB(^{Me}Im)_3)^-$, which is the first group 7 complex comprised of a tridentate NHC complex (Scheme 7, a)).[39] *Fac*-[$Mn(PhB(^{Me}Im)_3)(CO)_3$] is sensitive to O_2 and forms the homoleptic [$Mn(PhB(^{Me}Im)_3)_2$]$(OTf)_2$ within days in the presence of O_2. Only one *fac*-{$Re(CO)_3$}$^+$ complex with three NHC ligands is known. Flores-Figueroa *et al.* published the preparation of [$Re(SNHC)_3(CO)_3]^+$ (SNHC = saturated imidazoline-2-ylidene), which was obtained by stepwise cyclization reactions starting from [$ReBr(CO)_5$] (Scheme 7, b)).[40,41] Unfortunately, no details were given about the stability of [$Re(SNHC)_3(CO)_3]^+$.

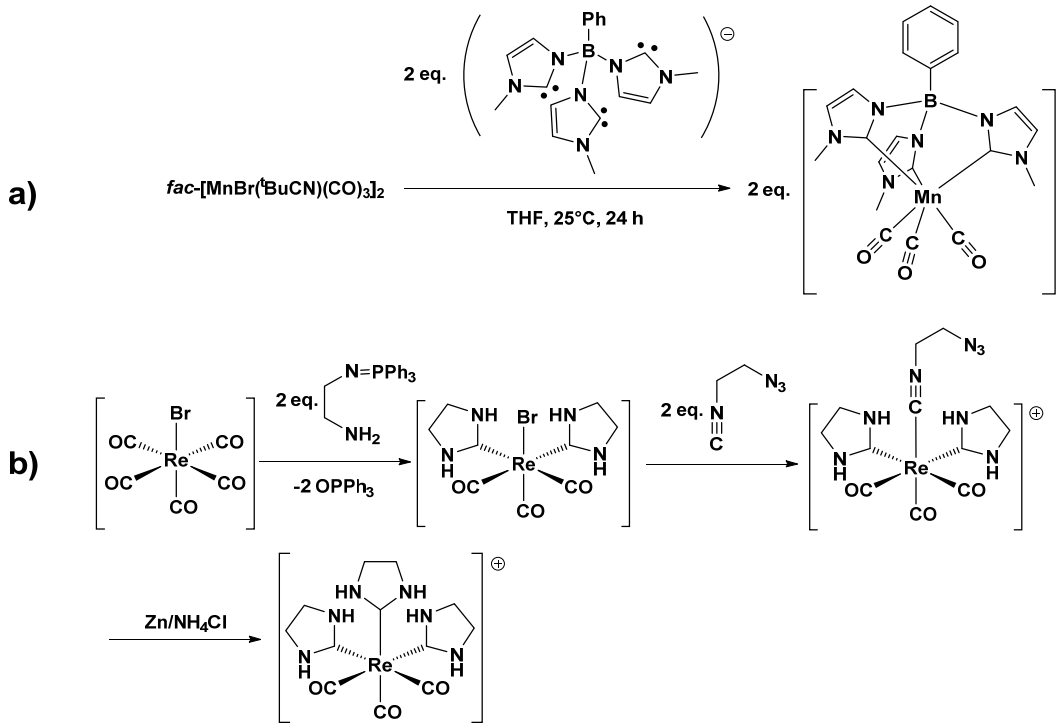

Scheme 7: Selected syntheses of *fac*-$\{M(CO)_3\}^+$ complexes (M = Mn, Re). a) *Fac*-$[Mn(PhB(^{Me}Im)_3)(CO)_3]$ is obtained by reaction of *fac*-$[MnBr(^tBuCN)(CO)_3]_2$ with $(PhB(^{Me}Im)_3)^-$. b) Stepwise cyclization from $[ReBr(CO)_5]$ yields $[Re(SNHC)_3(CO)_3]^+$ (SNHC = saturated imidazoline-2-ylidene).

Over the course of this thesis, two additional contributions to M-NHC chemistry were published that are related to the topics of this thesis. In 2013, Lum *et al.* published the preparation of $[ReO(OH)(L^R_B)_2]^{2+}$ (L^R_B = 1,1′-methylene-3,3′-dimethyl-4,4′-diimidazoline-2,2′-diylidene (R = Me), 1,1′-methylene-3,3′-diisopropyl-4,4′-diimidazoline-2,2′-diylidene (R = ^{i}Pr), 1,1′-methylene-3,3′-dibenzyl-4,4′-diimidazoline-2,2′-diylidene (R = Bz)) by a silver transmetalation reaction of the respective $[Ag_2(L^R_B)_2]^{2+}$ complexes with $[ReOCl_3(PPh_3)_2]$ (Scheme 8, a)).[42] As it was the case for $\{ReO\}^{3+}$-NHC complexes containing monodentate NHCs, the resulting complexes comprised of bidentate NHCs were stable in the presence of air and moisture. While the publication by Lum *et al.* did not serve as an inspiration for the synthesis of the water stable $\{^{99(m)}TcO_2\}^+$-NHC complexes discussed in this thesis, it complements the results obtained for the corresponding Re complexes described in this thesis. In 2014, Chan *et al* published the synthesis of the first ^{99m}Tc-NHC complex, *fac*-$[^{99m}Tc(CH_3CN)(L^{Py})(CO)_3]^+$ (L^{Py} = 1-(2-pyridyl)-3-methylimidazoline-2-ylidene), by reaction of *fac*-$[^{99m}Tc(OH_2)_3(CO)_3]^+$ with 1-(2-pyridyl)-3-methylimidazolium iodide (L^{Py}-H)(I) and Ag_2O (Scheme 8, b)).[43] The described *in situ* transmetalation reaction is very promising for the development of synthetic methods to ^{99m}Tc-NHC complexes.

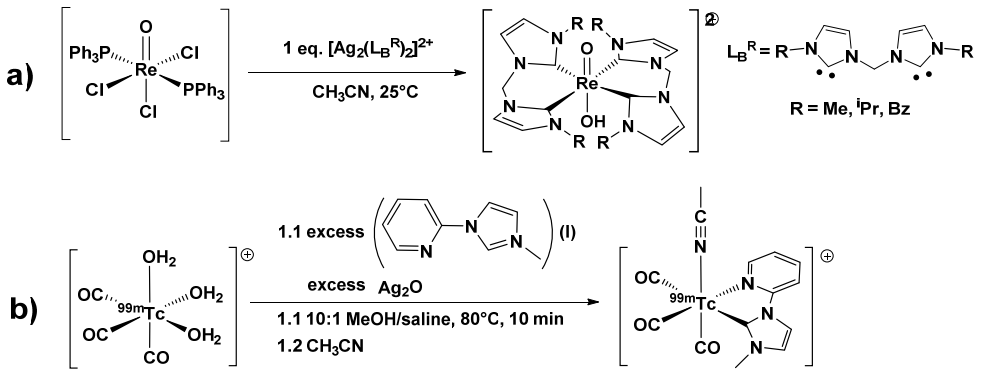

Scheme 8: Recently published syntheses that are related to this thesis. a) Synthesis of $[ReO(OH)(L_B^R)_2]^{2+}$ by transmetalation reaction of $[ReOCl_3(PPh_3)_2]$ with $[Ag_2(L_B^R)_2]^{2+}$. b) Synthesis of the first ^{99m}Tc-NHC complex, $[^{99m}Tc(CH_3CN)(L^{Py})(CO)_3]^+$, by reaction of $[^{99m}Tc(OH_2)_3(CO)_3]^+$ with $(L^{Py}$-H)(I) and Ag_2O.

3 Motivation and Goals

3.1 Facile Synthesis of $[^{99(m)}Tc^{I}(arene)_2]^+$ Complexes Starting from $[^{99(m)}Tc^{VII}O_4]^-$

The importance of the $\{M(arene)\}^{n+}$ fragment is underlined by the impact of the $\{Ru(p\text{-cymene})\}^{2+}$ fragment on medicinal chemistry.[1,2] In addition, phenyl groups are frequently found in pharmaceuticals and coordination of such a biologically active arene to ^{99m}Tc would be a novel and innovative labeling strategy. Furthermore, $[^{99(m)}Tc(arene)_2]^+$ complexes are very interesting for fundamental chemistry. Comparison to neighboring $\{M(arene)\}^{n+}$ complexes will reveal trends and differences in the periodic table. Thereby, gaps in fundamental knowledge will be closed. The lack of systematic investigations of $[^{99}Tc(arene)_2]^+$ complexes is mostly explained by the fact that they were only accessible starting from $[^{99}TcCl_4]$, which is impractical to use and difficult to prepare. Therefore, a synthetic procedure starting from the universal $^{99(m)}Tc$ starting material $[^{99(m)}TcO_4]^-$ is very desired for further investigations of $[^{99(m)}Tc(arene)_2]^+$ complexes. Wester *et al.* proved that the synthesis of $[^{99m}Tc(arene)_2]^+$ complexes is possible from $[^{99m}TcO_4]^-$,[24] however, this synthetic pathway is not suited for ^{99}Tc complexes. In 2013, Kudinov *et al.* published the preparation of $[Re(arene)_2]^+$ complexes directly from $[ReO_4]^-$.[44] One goal of this thesis is the translation of this work to $^{99(m)}Tc$ chemistry and the investigation of the fundamental chemistry of $[^{99}Tc(arene)_2]^+$ complexes with modern analytical tools.

3.2 Synthesis of Water Stable $^{99(m)}Tc$-NHC Complexes

Fundamental work on $^{99(m)}Tc$-NHC complexes is scarce, with very few structurally characterized ^{99}Tc-NHC complexes. This is mainly explained by their tendency to quickly hydrolyze in the presence of H_2O. The stability in water is a key factor for the application and synthesis of ^{99m}Tc-NHC complexes. Thus, the main goal of this thesis is to prepare water stable $^{99(m)}Tc$-NHC complexes. This goal should be achieved by the utilization of chelating NHCs. The two main core structures in the focus of this thesis are the *fac*-$\{^{99(m)}Tc(CO)_3\}^+$- and the $\{^{99(m)}TcO\}^{3+}$ core. All of the hitherto published ^{99}Tc-NHC complexes contain $^{99}Tc^{V}$, while there are no known *fac*-$\{^{99}Tc(CO)_3\}^+$-NHC complexes to date. Therefore, the main focus of this thesis lies on the expansion of $^{99}Tc^{V}$-NHC chemistry to multidentate NHC ligands and the synthesis of the first *fac*-$\{^{99}Tc(CO)_3\}^+$-NHC complexes. The gained knowledge from the synthesis of water stable ^{99}Tc-NHC complexes should then be used to prepare the first $^{99m}Tc^{V}$-NHC complexes. The corresponding Re chemistry will also be investigated in order to further elucidate the chemical properties of these complexes.

4 Results and Discussion

4.1 Synthesis of $[^{99(m)}Tc^{I}(arene)_2]^+$ Complexes

The syntheses of $[^{99}Tc(arene)_2]^+$ complexes (arene = benzene, toluene, mesitylene and tetralin) were adapted from a recently published synthesis of the corresponding Re complexes by Kudinov *et al.*.[44] In this publication, (K)[ReO_4] is reacted with an excess of $AlCl_3$ and Zn in the corresponding arene to form $[Re(arene)_2]^+$ in 30-50% yield (arene = benzene, toluene, *o*-xylene, *p*-xylene and mesitylene). Following the same reaction procedure, the synthesis of the naphthalene complex was also described, although only a yield of 5% was obtained. In the presence of ^{t}BuNC at 80°C, both naphthalene ligands in $[Re(naphthalene)_2]^+$ were replaced to form $[Re(^tBuNC)_6]^+$, while the synthesis of a mixed $[Re(naphthalene)(^tBuNC)_3]^+$ complex was not possible. Following the same strategy as for the synthesis of $[Re(arene)_2]^+$ complexes, $(NH_4)[^{99}TcO_4]$ was reacted with an excess $AlCl_3$ and Zn in the corresponding arene at 85°C (Scheme 9, **method a**). The resulting $[^{99}Tc(arene)_2]^+$ complexes were difficult to separate from black, colloidal material, which was removed by suspending the crude product in H_2O, followed by filtration. Precipitation from H_2O with NH_4PF_6 followed by filtration and drying *in vacuo* gave analytically pure $[^{99}Tc(arene)_2](PF_6)$ in yields of 7 – 12% (arene = benzene ([**1**](PF_6)), toluene ([**2**](PF_6)), mesitylene ([**3**](PF_6)) and tetralin ([**4**](PF_6))). While the yields were low, this is the first time that the synthesis of $[^{99}Tc(arene)_2]^+$ complexes was achieved directly from $[^{99}TcO_4]^-$.

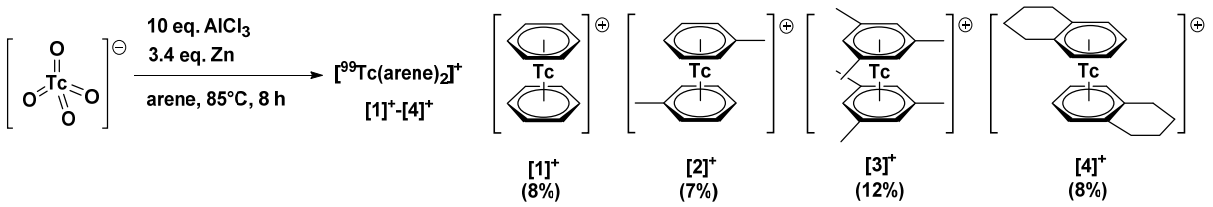

Scheme 9: Synthesis of $[^{99}Tc(arene)_2]^+$ complexes [**1**]$^+$ – [**4**]$^+$ starting from $[^{99}TcO_4]^-$ (**method a**).

It was speculated that the black, colloidal solid formed during the reaction was a reductive side product, which was likely formed due to the presence of excess Zn.[45] Consequently, the reactions were carried out without Zn. Reaction of (K)[TcO_4] with excess $AlCl_3$ in the corresponding arene for 4 h at 85°C gave a dark brown suspension (**method b**). The suspension was quenched with an equal volume of H_2O while still hot, leading to an immediate color change. After separation and filtration of the H_2O phase, the product was precipitated using NH_4PF_6. Filtration and drying *in vacuo* gave analytically pure $[^{99}Tc(arene)_2](PF_6)$ (arene = toluene, mesitylene, tetralin) in 69 – 90% yield. Interestingly, reaction without Zn and using benzene as a solvent only gave trace amounts of $[^{99}Tc(benzene)_2]^+$. The synthesis of [**2**]$^+$ – [**4**]$^+$ using only $AlCl_3$ was investigated further to gather information about the mechanism, while the activation of $[^{99}TcO_4]^-$ with strong Lewis acids has been studied before.[46-48] When $[^{99}TcOCl_4]^-$ was reacted with $AlCl_3$ in cyclohexane, formation of a yellow solid was observed.

The yellow solid was isolated, crystallized from DMF and the crystals were identified by X-ray crystallography as $[Al(DMF)_6][^{99}TcCl_6](Cl)\cdot DMF$ (Figure 3). $[Al(DMF)_6][^{99}TcCl_6](Cl)\cdot DMF$ crystallizes in the monoclinic space group $P2_1$. The ^{99}Tc and Al atoms are in the centre of an octahedron formed by the six coordinating ligands, with ^{99}Tc-Cl bond lengths in the range of 2.3523(7) – 2.3605(8) Å and Al-O bond lengths in the range of 1.862(2) – 1.892(2) Å (Table 1). These values are comparable to literature values.[49,50]

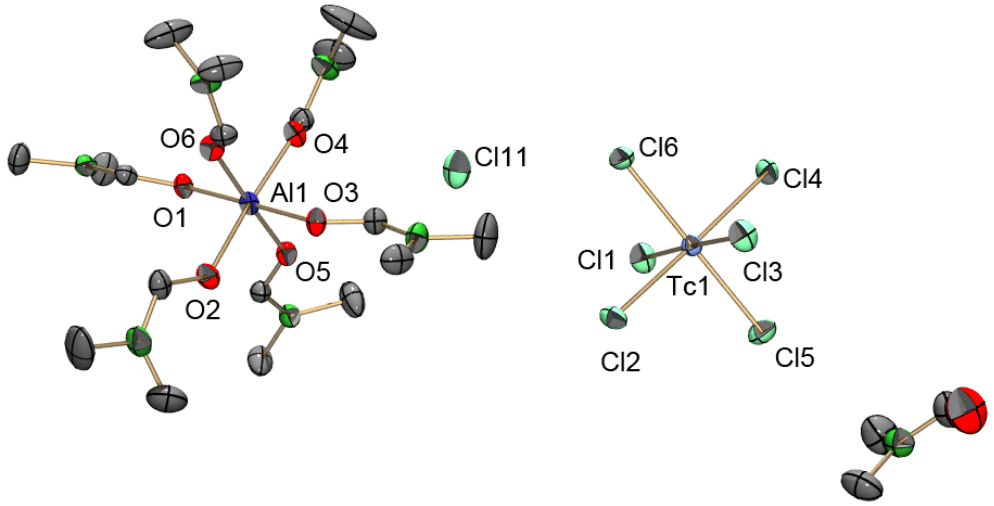

Figure 3: Oak Ridge thermal ellipsoid plot (ORTEP) representation[51] of the $[Al(DMF)_6][^{99}TcCl_6](Cl)\cdot DMF$ structure. Thermal ellipsoids are represented at the 50% probability level. Hydrogen atoms are omitted for clarity.

Table 1: Selected bond lengths and angles of $[Al(DMF)_6][^{99}TcCl_6](Cl)\cdot DMF$.

Selected bond lengths [Å]		Selected angles [°]	
Tc(1)-Cl(1)	2.3605(8)	Cl(1)-Tc(1)-Cl(2)	89.28(3)
Tc(1)-Cl(2)	2.3580(8)	Cl(1)-Tc(1)-Cl(3)	178.18(3)
Tc(1)-Cl(3)	2.3531(7)	Cl(1)-Tc(1)-Cl(4)	91.08(3)
Tc(1)-Cl(4)	2.3549(8)	Cl(1)-Tc(1)-Cl(5)	88.68(3)
Tc(1)-Cl(5)	2.3577(7)	Cl(1)-Tc(1)-Cl(6)	91.80(3)
Tc(1)-Cl(6)	2.3523(7)	Cl(2)-Tc(1)-Cl(3)	89.65(3)
Al(1)-O(1)	1.872(2)	O(1)-Al(1)-O(2)	92.83(9)
Al(1)-O(2)	1.890(2)	O(1)-Al(1)-O(3)	179.22(11)
Al(1)-O(3)	1.881(2)	O(1)-Al(1)-O(4)	90.18(10)
Al(1)-O(4)	1.892(2)	O(1)-Al(1)-O(5)	89.36(9)
Al(1)-O(5)	1.875(2)	O(1)-Al(1)-O(6)	88.90(9)
Al(1)-O(6)	1.862(2)	O(2)-Al(1)-O(3)	86.44(10)

Also, red crystals of $[^{99}Tc(benzene)_2][^{99}TcCl_5(OH_2)]$ were found by slow crystallization of the H_2O extract that was obtained according to **method b** and therefore, by starting from $[^{99}TcO_4]^-$. $[^{99}Tc(benzene)_2][^{99}TcCl_5(OH_2)]$ crystallizes as red blocks in the orthorhombic space group Pnma

(Figure 4). As in the previous case, $[^{99}TcCl_5(OH_2)]^-$ has an octahedral coordination environment with ^{99}Tc-Cl bond lengths in the range of 2.271(2) – 2.3341(12) Å and a ^{99}Tc-O bond length of 2.105(6) Å (Table 2). These values are in a similar range compared to values found in literature for $[^{99}TcCl_4(OH_2)_2]$, which has ^{99}Tc-Cl bond lengths of 2.283(3) and 2.331(2) Å and a ^{99}Tc-O bond length of 2.096(7) Å.[52] The ^{99}Tc-Cl bond length of the Cl^- ligand in *trans*-position to the OH_2 ligand is with 2.271(2) Å considerably shorter than the bond lengths of the Cl^- ligands in *cis*-position to the OH_2 ligand (^{99}Tc-Cl bond lengths of 2.3306(12) and 2.3341(12) Å), which is also observed in $[^{99}TcCl_4(OH_2)_2]$.[52] The structure of $[^{99}Tc(benzene)_2]^+$ will be discussed in detail later in this chapter.

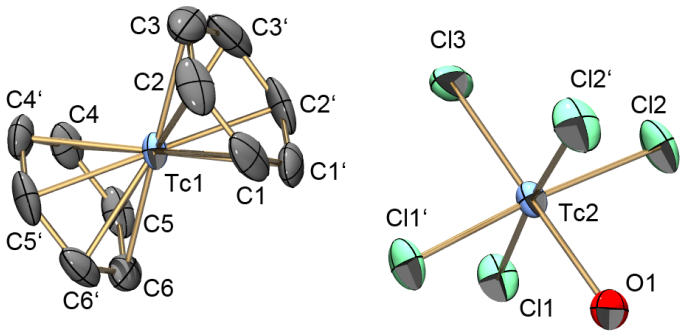

Figure 4: ORTEP representation[51] of the $[^{99}Tc(benzene)_2][^{99}TcCl_5(OH_2)]$ structure. Thermal ellipsoids are represented at the 50% probability level. Hydrogen atoms are omitted for clarity.

Table 2: Selected bond lengths and angles of $[^{99}Tc(benzene)_2][^{99}TcCl_5(OH_2)]$.

Selected bond lengths [Å]		Selected angles [°]	
Tc(1)-C(1)	2.228(5)	Cl(1)-Tc(2)-Cl(2)	91.49(5)
Tc(1)-C(2)	2.226(5)	Cl(2)-Tc(2)-Cl(3)	92.75(6)
Tc(1)-C(3)	2.232(5)	Cl(1)-Tc(2)-Cl(3)	92.13(5)
Tc(1)-C(4)	2.224(4)	Cl(1)-Tc(2)-Cl(2)#1	175.09(6)
Tc(1)-C(5)	2.229(5)	O(1)-Tc(2)-Cl(1)	88.34(12)
Tc(1)-C(6)	2.225(5)	O(1)-Tc(2)-Cl(2)	86.77(12)
Tc(2)-Cl(1)	2.3306(12)	O(1)-Tc(2)-Cl(3)	179.34(17)
Tc(2)-Cl(2)	2.3341(12)		
Tc(2)-Cl(3)	2.271(2)		
Tc(2)-O(1)	2.105(6)		

It becomes evident, that $AlCl_3$ is not only capable of activating $[^{99}TcO_4]^-$ due to its oxophilicity, but it also provides the Cl^- needed for the reduction of Tc^{VII} to Tc^{IV}. The synthesis of $[^{99}TcCl_6]^{2-}$ by reaction of $[^{99}TcO_4]^-$ in boiling conc. HCl follows a similar mechanism, in which the $[^{99}TcO_4]^-$ is activated by protonation, followed by reduction with Cl^-.[45] $(K)_2[^{99}TcCl_6]$ is a common starting material in ^{99}Tc chemistry and as stated before, it can be prepared from $(K)[^{99}TcO_4]$ in one step.[53] To confirm that $[^{99}TcCl_6]^{2-}$ is an intermediate in the reaction to $[^{99}Tc(arene)_2]^+$, $(K)_2[^{99}TcCl_6]$ was used as a starting

material. Reaction of $(K)_2[^{99}TcCl_6]$ and excess $AlCl_3$ in the corresponding arene with the same procedure as in **method b** gave $[^{99}Tc(arene)_2]^+$ in 60 – 63% yield (**method c**, arene = toluene, tetralin). Table 3 shows a comparison of the different reaction conditions used in **methods a** – **c** and summarizes the yields.

Table 3: Comparison of reaction conditions and yields for **methods a** – **c**.

Method	Starting compound	Eq. $AlCl_3$	Eq. Zn	Reaction temperature [°C]	Reaction time [h]	Yields [%]
Method a	$(NH_4)[^{99}TcO_4]$	10	3.4	85°C	8	$[\mathbf{1}]^+ = 8$ $[\mathbf{2}]^+ = 7$ $[\mathbf{3}]^+ = 12$ $[\mathbf{4}]^+ = 8$
Method b	$(K)[^{99}TcO_4]$	15	0	85°C	4	$[\mathbf{1}]^+$ = trace amount $[\mathbf{2}]^+ = 74$ $[\mathbf{3}]^+ = 90$ $[\mathbf{4}]^+ = 69$
Method c	$(K)_2[^{99}TcCl_6]$	10	0	85°C	4	$[\mathbf{1}]^+$ = not tested $[\mathbf{2}]^+ = 60$ $[\mathbf{3}]^+$ = not tested $[\mathbf{4}]^+ = 63$

$AlCl_3$ is still needed as a reagent even when starting from $(K)_2[^{99}TcCl_6]$, indicating that its role in the reaction goes beyond the activation of $[^{99}TcO_4]^-$ and being a source for Cl^-. No striking proof was found for the mechanism leading from Tc^{IV} to Tc^{I}, but the fact that the reaction without Zn does not work for benzene might be an important finding. Since the reaction does not work with benzene, it was concluded that either the enhanced donor properties of the alkyl substituted arenes are important for the stabilization of an intermediate, or that the alkyl substituents are important for the arenes to act as reductants for the reduction of Tc^{IV} to lower oxidation states under Friedel-Crafts conditions. However, further investigations are necessary to fully explain the mechanism leading to the formation of $[^{99}Tc(arene)_2]^+$.

The synthesis of $[^{99}Tc(biphenyl)_2]^+$ and $[^{99}Tc(naphthalene)_2]^+$ was also tested with similar conditions used in **method a**, but no products could be isolated and the crude product contained only $[^{99}TcO_4]^-$ and reduced ^{99}Tc side products according to ^{99}Tc-NMR and HPLC analysis. A challenging problem was the fact that biphenyl and naphthalene are solid at 25°C and thus, heating is required to melt these solid arenes. The neat reaction conditions required a minimal amount of 1 g solid arene in order to have enough solvent and the solid arene was difficult to remove upon workup, especially for naphthalene which has a tendency to sublime even at ambient conditions. The removal of the large excess of solid arene would presumably lead to large losses in yield, considering that typical batches contain only 0.05 – 0.10 mmol of $[^{99}TcO_4]^-$. Therefore, the use of organic solvents was thoroughly

tested to enable the synthesis of $[^{99}Tc(arene)_2]^+$ complexes with arenes that are solid at room temperature or with arenes that might be preferably used in low quantities due to toxicity or high cost. The reaction conditions were tested using toluene as a model ligand. Reactions using 7:1 dibutyl ether/toluene or cyclohexane/toluene mixtures according to **method b** did not lead to the formation of $[\mathbf{2}]^+$ and only $[^{99}TcO_4]^-$ and $^{99}TcO_2$ were observed in HPLC analysis after aqueous workup. While the low solubility of $AlCl_3$ in cyclohexane might be an issue in the case of cyclohexane as a solvent, the fact that dibutyl ether is presumably not chemically innocent when treated with $AlCl_3$ might prohibit the reaction in this case. The low functional group tolerance of $AlCl_3$ probably has also prevented the synthesis of $[^{99}Tc(anisole)_2]^+$ (**method c**), $[^{99}Tc(acetophenone)_2]^+$ (**method c**) and $[^{99}Tc(chlorobenzene)_2]^+$ (**method b**), since reactions in the corresponding arene under neat conditions did not result in the formation of product. $InCl_3$ was tested as a milder Lewis acid using toluene as a solvent according to **methods b** and **method c**, but also in this case, formation of $[\mathbf{2}]^+$ was not observed. A promising approach was found when mixtures of arenes with benzene were used, such as a 1:1 benzene/toluene mixture with synthesis according to **method b**. In this reaction, a mixture of products was found according to HPLC analysis and ^{99}Tc-NMR spectroscopy, with $[^{99}Tc(toluene)_2]^+$ as the main product and $[^{99}Tc(benzene)(toluene)]^+$ as the side product in an observed ratio of 2:1. This reaction utilizes the fact that $[^{99}Tc(benzene)_2]^+$ does not form without Zn in the reaction and, indeed, only trace amounts of $[^{99}Tc(benzene)_2]^+$ were observed in ^{99}Tc-NMR. However, the product mixture was difficult to purify and crystallization of the mixture gave only low quality single crystals. Using the same principle, the reaction was done in a 4:1 benzene/naphthalene mixture according to **method c**. Again, a mixture of products was found in the ^{99}Tc-NMR and in HPLC analysis, while presumably $[^{99}Tc(benzene)(naphthalene)]^+$ and $[^{99}Tc(naphthalene)_2]^+$ were the main products but could not be unambiguously identified due to the low crude yield and the unsuccessful crystallization of the product mixture. Despite the difficulties in the purification of the reaction products, these reactions are very important, because they could lead to the synthesis of a precursor complex for various complexes containing the $\{^{99}Tc(benzene)\}^+$ fragment. $[^{99}Tc(benzene)(naphthalene)]^+$ might be such a precursor complex, since Kudinov *et al.* already showed that the naphthalene ligands in $[Re(naphthalene)_2]^+$ can be replaced with ^{t}BuNC to give $[Re(^t BuNC)_6]^+$.[44]

$[^{99}Tc(arene)_2]^+$ complexes have been prepared and characterized before.[21,23] Due to the fact that these investigations have been done many years ago, a full characterization, including ^{99}Tc-NMR and cyclic voltammetry (CV), was done. Single-crystalline $[\mathbf{1}]^+$ – $[\mathbf{4}]^+$ was obtained by slow diffusion of Et_2O into an acetone solution of the complexes and the structures of $[\mathbf{1}]^+$ – $[\mathbf{4}]^+$ were analyzed.

$[\mathbf{1}](PF_6)$ crystallizes as colorless blocks in the monoclinic space group $P2_1/c$ (Figure 5). Measurement of the crystal was done at 253 K, because decomposition of the crystals was observed at 183 K (standard temperature for X-ray measurements). The structure contains two independent ^{99}Tc centres in the asymmetric unit that are very similar, except for a disorder on the benzene ligand of the Tc(2)

molecule. Due to their similarity, only the structure of the Tc(1) moiety will be discussed here. The ^{99}Tc-C bond lengths in [**1**]$^{+}$ are in the range of 2.210(3) – 2.225(3) Å (Table 4), which is in the expected range for ^{99}Tc-C single bonds. Compared to the ^{99}Tc-C bond lengths in [^{99}Tc(Cp*)(CO)$_3$] (Cp* = pentamethylcyclopentadienyl) of 2.285(5) – 2.302(5) Å,[54] the ^{99}Tc-C bond lengths of [**1**]$^{+}$ are significantly shorter. The bond lengths in [**1**]$^{+}$ are in a similar range as in the isoelectronic complex [Ru(benzene)$_2$]$^{2+}$ (2.202(2) Å).[55]

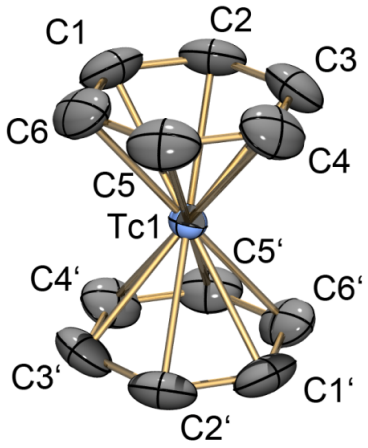

Figure 5: ORTEP representation[51] of the [^{99}Tc(benzene)$_2$]$^{+}$ ([**1**]$^{+}$) cation of the [**1**](PF$_6$) structure. Thermal ellipsoids are represented at the 50% probability level. Hydrogen atoms are omitted for clarity.

Table 4: Selected bond lengths and angles of [**1**]$^{+}$.

Selected bond lengths [Å]		Selected angles [°]	
Tc(1)-C(1)	2.217(3)	C(1)-Tc(1)-C(2)	36.23(15)
Tc(1)-C(2)	2.225(3)	C(2)-Tc(1)-C(3)	37.04(14)
Tc(1)-C(3)	2.215(3)	C(3)-Tc(1)-C(4)	37.04(13)
Tc(1)-C(4)	2.217(3)	C(4)-Tc(1)-C(5)	36.59(14)
Tc(1)-C(5)	2.216(3)	C(5)-Tc(1)-C(6)	36.73(13)
Tc(1)-C(6)	2.210(3)	C(6)-Tc(1)-C(1)	36.95(14)

[**2**](PF$_6$) crystallizes as colorless blocks in the monoclinic space group P2$_1$/n (Figure 6). The ^{99}Tc-C bond lengths in [**2**]$^{+}$ are in the range of 2.217(4) – 2.245(4) Å (Table 5). These values are in the same range as for [**1**]$^{+}$ and also in other regards, no major structural differences between these two complexes were found. The CH$_3$ groups in the two toluene ligands point in opposite directions in the solid state, while the ring atoms are eclipsed.

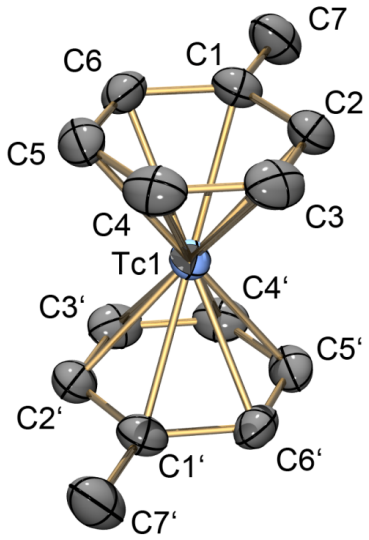

Figure 6: ORTEP representation[51] of the $[^{99}Tc(toluene)_2]^+$ ($[\mathbf{2}]^+$) cation of the $[\mathbf{2}](PF_6)$ structure. Thermal ellipsoids are represented at the 50% probability level. Hydrogen atoms are omitted for clarity.

Table 5: Selected bond lengths and angles of $[\mathbf{2}]^+$.

Selected bond lengths [Å]		Selected angles [°]	
Tc(1)-C(1)	2.245(4)	C(1)-Tc(1)-C(2)	36.83(14)
Tc(1)-C(2)	2.221(4)	C(2)-Tc(1)-C(3)	36.76(15)
Tc(1)-C(3)	2.225(4)	C(3)-Tc(1)-C(4)	36.76(14)
Tc(1)-C(4)	2.219(4)	C(4)-Tc(1)-C(5)	36.59(15)
Tc(1)-C(5)	2.217(4)	C(5)-Tc(1)-C(6)	36.83(14)
Tc(1)-C(6)	2.223(4)	C(6)-Tc(1)-C(1)	37.18(15)

$[\mathbf{3}](PF_6)$ crystallizes as colorless blocks in the orthorhombic space group $P2_12_12_1$ (Figure 7). The distances between the ^{99}Tc and the aromatic carbon atoms of the ligand were found to be in the range of 2.213(3) – 2.248(3) Å (Table 6) and no significant structural differences were found compared to the structure of $[\mathbf{1}]^+$ and $[\mathbf{2}]^+$. Interestingly, the conformation of the CH_3 groups in the two mesitylene ligands is almost eclipsed in the solid state.

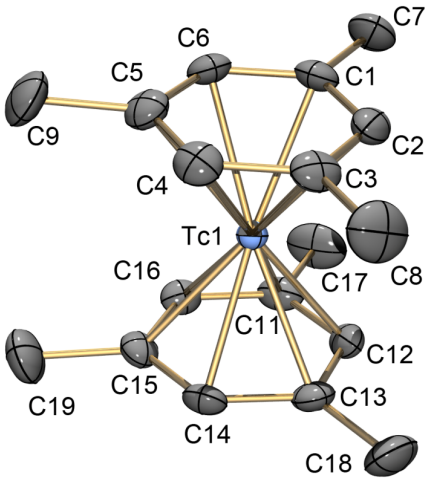

Figure 7: ORTEP representation[51] of the [^{99}Tc(mesitylene)$_2$]$^+$ ([**3**]$^+$) cation of the [**3**](PF$_6$) structure. Thermal ellipsoids are represented at the 50% probability level. Hydrogen atoms are omitted for clarity.

Table 6: Selected bond lengths and angles of [**3**]$^+$.

Selected bond lengths [Å]		Selected angles [°]	
Tc(1)-C(1)	2.245(3)	C(1)-Tc(1)-C(2)	37.14(10)
Tc(1)-C(2)	2.213(3)	C(2)-Tc(1)-C(3)	36.82(11)
Tc(1)-C(3)	2.243(3)	C(3)-Tc(1)-C(4)	36.83(10)
Tc(1)-C(4)	2.223(2)	C(4)-Tc(1)-C(5)	36.90(11)
Tc(1)-C(5)	2.248(3)	C(5)-Tc(1)-C(6)	36.49(10)
Tc(1)-C(6)	2.236(3)	C(6)-Tc(1)-C(1)	36.45(10)
Tc(1)-C(11)	2.250(2)	C(11)-Tc(1)-C(12)	37.01(11)
Tc(1)-C(12)	2.226(3)	C(12)-Tc(1)-C(13)	36.83(10)
Tc(1)-C(13)	2.237(3)	C(13)-Tc(1)-C(14)	37.05(11)
Tc(1)-C(14)	2.214(2)	C(14)-Tc(1)-C(15)	36.86(10)
Tc(1)-C(15)	2.241(3)	C(15)-Tc(1)-C(16)	36.88(10)
Tc(1)-C(16)	2.228(3)	C(16) Tc(1) C(11)	36.66(10)

[**4**](PF$_6$) crystallizes as pale yellow blocks in the monoclinic space group P2$_1$/n (Figure 8). No significant structural changes compared to [**1**]$^+$ – [**3**]$^+$ were found. The ^{99}Tc-C bond lengths are in the range of 2.219(2) – 2.250(2) Å (Table 7). As it was observed for [**2**]$^+$, the alkyl substituents in [**4**]$^+$ point in opposite directions, while the ring atoms are eclipsed in the solid state.

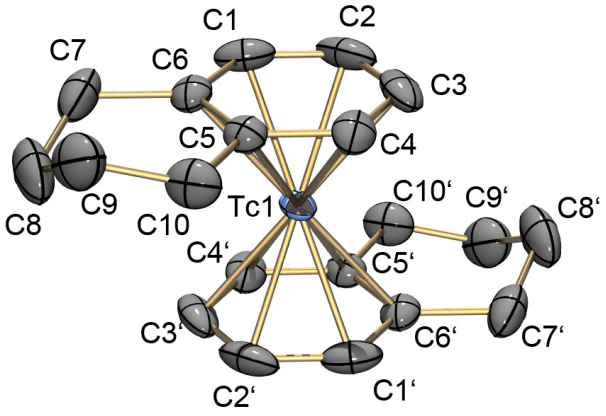

Figure 8: ORTEP representation[51] of the $[^{99}Tc(tetralin)_2]^+$ ($[\mathbf{4}]^+$) cation of the $[\mathbf{4}](PF_6)$ structure. Thermal ellipsoids are represented at the 50% probability level. Hydrogen atoms are omitted for clarity.

Table 7: Selected bond lengths and angles of $[\mathbf{4}]^+$.

Selected bond lengths [Å]		Selected angles [°]	
Tc(1)-C(1)	2.219(2)	C(1)-Tc(1)-C(2)	36.54(11)
Tc(1)-C(2)	2.228(2)	C(2)-Tc(1)-C(3)	36.29(12)
Tc(1)-C(3)	2.231(2)	C(3)-Tc(1)-C(4)	36.90(10)
Tc(1)-C(4)	2.227(2)	C(4)-Tc(1)-C(5)	37.03(9)
Tc(1)-C(5)	2.250(2)	C(5)-Tc(1)-C(6)	36.50(9)
Tc(1)-C(6)	2.250(2)	C(6)-Tc(1)-C(1)	37.31(9)

NMR spectroscopy of $[\mathbf{1}]^+$ – $[\mathbf{4}]^+$ measured in CD_3CN provides valuable insights. The ^{1}H-NMR spectra of $[\mathbf{1}]^+$ – $[\mathbf{4}]^+$ show CH signals in the range of 5.65 – 5.39 ppm, significantly shifted to higher field compared to the signals of the uncoordinated arenes at 7.37 – 6.78 ppm (Table 8).

Table 8: Comparison of ^{1}H-NMR shifts of the CH group for coordinated and uncoordinated arenes. A comparison of the ^{99}Tc-NMR shifts of $[\mathbf{1}]^+$ – $[\mathbf{4}]^+$ is also given.

Complex	^{1}H-NMR CH shift of uncoordinated arene [ppm]	^{1}H-NMR CH shift of coordinated arene [ppm]	^{99}Tc-NMR shift [ppm] and half line width
$[\mathbf{1}]^+$	7.37[a]	5.65[a]	-1859.71 ($\Delta\nu_{1/2}$ = 8 Hz)[a]
$[\mathbf{2}]^+$	7.30 – 7.10[a]	5.63 – 5.50[a]	-1743.92 ($\Delta\nu_{1/2}$ = 26 Hz)[a]
$[\mathbf{3}]^+$	6.78[b]	5.39[a]	-1532.37 ($\Delta\nu_{1/2}$ = 14 Hz)[a]
$[\mathbf{4}]^+$	7.08 – 7.06[b]	5.54 – 5.43[a]	-1585.94 ($\Delta\nu_{1/2}$ = 11 Hz)[a]

[a] measured in CD_3CN.[56] [b] measured in $CDCl_3$.[57]

While the trend in the ^{1}H-NMR of complexes $[\mathbf{1}]^+$ – $[\mathbf{4}]^+$ is clearly explained by the different substituents on the ring (increasing alkylation leads to shift to higher field), the trend observed in the chemical shifts in ^{99}Tc-NMR is exactly the opposite (Table 8). With increasing alkylation on the arene, the chemical shift of the ^{99}Tc nucleus shifts to lower field, which is presumably due to the fact that small differences in the first coordination sphere (e.g. longer bond distances) have a larger influence

on the chemical shift of the ^{99}Tc nucleus than the relatively small differences in donor properties of the arenes (Figure 9). The ^{99}Tc-NMR signals of $[\mathbf{1}]^+$ – $[\mathbf{4}]^+$ have comparably narrow half line widths $\Delta\nu_{1/2}$ of 8 – 26 Hz, which is due to the highly symmetrical first coordination sphere of the ^{99}Tc nucleus.

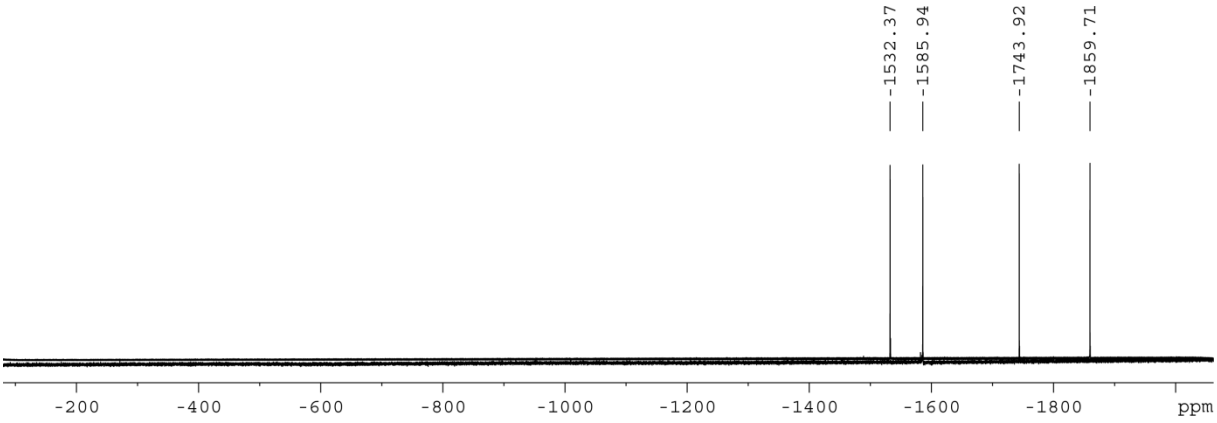

Figure 9: Comparison of the ^{99}Tc-NMR signals of $[\mathbf{1}]^+$ – $[\mathbf{4}]^+$.

In the ^{1}H-NMR spectrum, the CH signals in $[\mathbf{1}]^+$ are shifted to higher fields compared to isoelectronic complexes such as $[Re(benzene)_2]^+$ (CH shift = 6.14 ppm[44]) and $[M(benzene)_2]^{2+}$ (M = Fe, CH shift = 6.69 ppm;[58] M = Ru, CH shift = 6.90 ppm[59]). Compared to isoelectronic group 6 $[M(benzene)_2]$ complexes (M = Cr, CH shift = 4.21 ppm;[60] M = Mo, CH shift = 4.60 ppm;[61] M = W, CH shift = 5.00 ppm[61]), the CH signals in $[\mathbf{1}]^+$ are shifted to lower field, although comparison of the ^{1}H-NMR of $[\mathbf{1}]^+$ to these neutral complexes is difficult due to the fact that they were measured in perdeuterated benzene or toluene. Clear trends are visible, since going from left to right in a period leads to an increase of the positive charge and electronegativity on the metal, which leads to an increased chemical shift (shift to lower field) of the CH protons. Also, going down in a group leads to an increased chemical shift of the CH protons. ^{13}C-NMR spectroscopy of $[\mathbf{1}]^+$ – $[\mathbf{4}]^+$ in CD_3CN shows shifts for the CH groups between 87.94 – 81.43 ppm and therefore considerably shifted to higher field compared to the chemical shift of e.g. benzene in CD_3CN, which is found at 129.32 ppm. A relatively rare coupling to the ^{99}Tc nucleus (I = 9/2) is observed for the ^{99}Tc-C carbons of $[\mathbf{1}]^+$ – $[\mathbf{4}]^+$, which is poorly resolved due to the low natural abundance of the ^{13}C nucleus, leading to an observed block-shaped signal. Figure 10 shows the ^{13}C-NMR spectrum of $[\mathbf{3}]^+$ as an example.

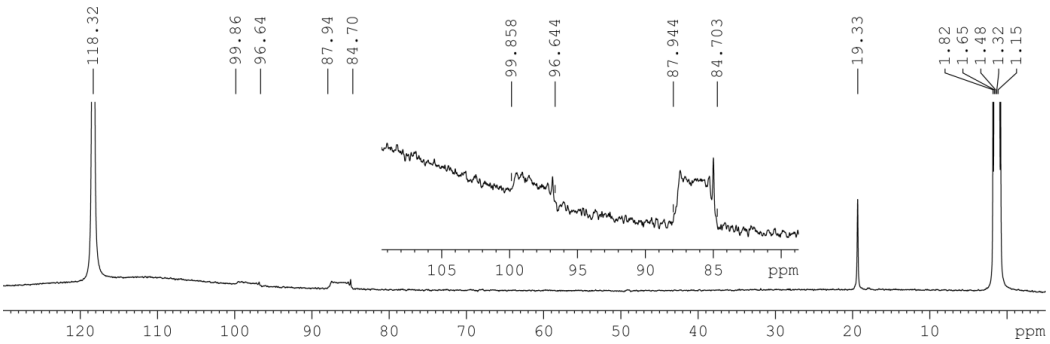

Figure 10: ^{13}C-NMR of $[\mathbf{3}]^+$ in CD_3CN with a detailed zoom on the block shaped signals of the ^{99}Tc-C coupling.

Formation of side products due to transalkylation reactions is often observed for reactions involving $AlCl_3$ and alkyl-substituted arenes. Due to the high sensitivity and the narrow signals, ^{99}Tc-NMR has proven to be an efficient analytical method for the observation of side products in the synthesis of $[\mathbf{2}]^+$ – $[\mathbf{4}]^+$. Due to the relatively low reaction temperature of 85°C and the comparably short reaction time of 4 h, only trace amounts of transmethylation products were found for $[\mathbf{2}]^+$ and $[\mathbf{3}]^+$. In the case of $[\mathbf{4}]^+$, a considerable amount of the transalkylation side product $[^{99}$Tc(tetralin)(OHPhen)$]^+$ (OHPhen = 1,2,3,4,5,6,7,8-octahydrophenanthrene, $[\mathbf{5}]^+$) was observed in ^{99}Tc-NMR and also in HPLC analysis. The ratio of $[\mathbf{4}]^+$:$[\mathbf{5}]^+$ was 4:1 according to HPLC analysis. $[\mathbf{5}](PF_6)$ was separated from $[\mathbf{4}](PF_6)$ by hand picking crystals from a mixture of single-crystalline $[\mathbf{4}](PF_6)$ and $[\mathbf{5}](PF_6)$, which was obtained by slow diffusion of Et_2O into an acetone solution containing both compounds. Crystals were separated based on their shape and, more importantly, their unit cell, which was determined by X-ray diffraction experiments. Unfortunately, X-ray structure analysis of $[\mathbf{5}]^+$ resulted in a low quality dataset and the structure could only be solved but not fully refined due to weak diffraction of the crystals (Figure 11). A small number of crystals of $[\mathbf{5}]^+$ were dissolved in CD_3CN and analyzed with ^{99}Tc-NMR (δ = -1470.34 ppm) and, in this exceptional case, ESI^+-MS (ESI = electrospray ionization) was done to unambiguously identify $[\mathbf{5}]^+$ as the side product of the reaction (observed m/z = 417.2, calculated m/z = 417.2). Due to the small amount of crystals isolated, no other analyses of $[\mathbf{5}]^+$ were performed.

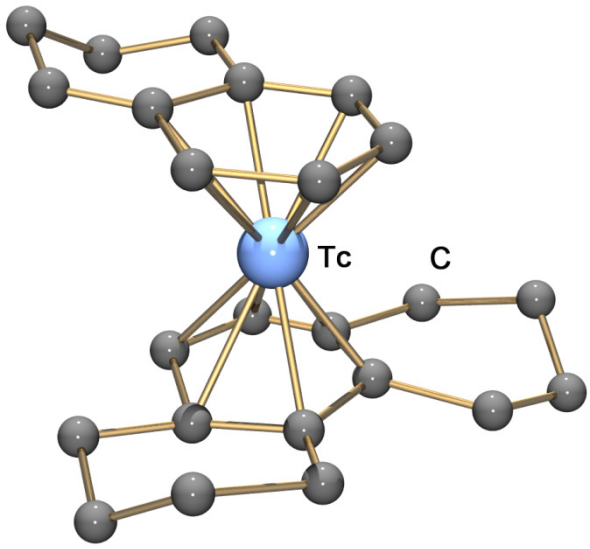

Figure 11: Representation[51] of the result of the structure solution of the $[^{99}$Tc(tetralin)(OHPhen)$]^+$ ($[\mathbf{5}]^+$) cation of the $[\mathbf{5}](PF_6)$ structure.

Complexes $[\mathbf{1}]^+$ – $[\mathbf{4}]^+$ were analyzed with CV experiments,[62,63] which showed a reversible oxidation wave for the $^{99}Tc^{I/II}$ couple and an irreversible reduction for the $^{99}Tc^{I/0}$ couple. The reversible oxidations of $[\mathbf{1}]^+$ – $[\mathbf{4}]^+$ were found at comparably high oxidation potentials $E^0_{1/2}$ > 1.4 V *vs.* Fc/Fc^+ at 0.45 V in CH_3CN and in general, increasing alkylation on the arenes leads to a shift of the oxidation

potentials to less positive values (Figure 12, table 9). The irreversible reduction of complexes $[\mathbf{1}]^+$ – $[\mathbf{4}]^+$ shows the same trend for increasing alkylation as the oxidation and the $Tc^{I/0}$ couples were found at values below -2 V *vs.* Fc/Fc^+ at 0.45 V in CH_3CN.

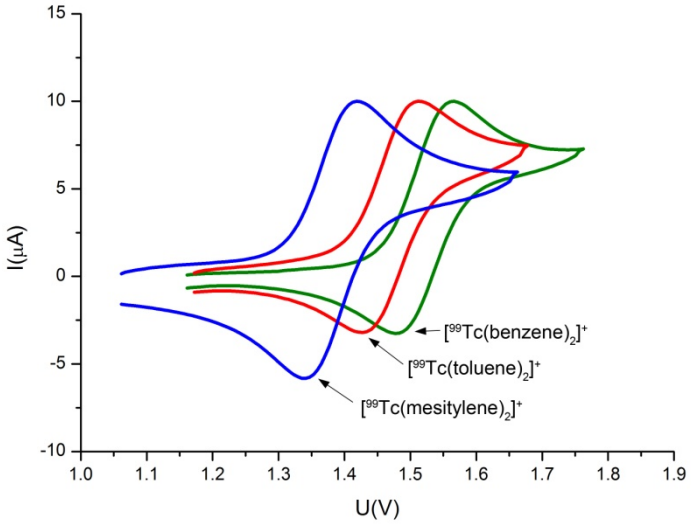

Figure 12: Cyclic voltammograms of the oxidation of $[\mathbf{1}]^+$ – $[\mathbf{3}]^+$. The CV of $[\mathbf{4}]^+$ was omitted for clarity.

Table 9: Overview on CV data of complexes $[\mathbf{1}]^+$ – $[\mathbf{4}]^+$. Measurements were done in 0.1 M $(N^nBu_4)(PF_6)$ electrolyte with a Ag/AgCl reference electrode and the potentials were referenced with Fc/Fc^+ at 0.45 V.

Compound (arene)	Reduction potential [V]	Oxidation potential [V]
$[\mathbf{1}]^+$ (benzene)	-2.04[a]	1.52[b]
$[\mathbf{2}]^+$ (toluene)	-2.12[a]	1.47[b]
$[\mathbf{3}]^+$ (mesitylene)	-2.27[a]	1.38[b]
$[\mathbf{4}]^+$ (tetralin)	-2.15[a]	1.39[b]

[a] irreversible reduction. [b] reversible oxidation.

Following general trends, the Re analogues of $[\mathbf{1}]^+$ – $[\mathbf{4}]^+$ are easier oxidized with oxidation potentials that are around 0.19 – 0.15 V shifted to less positive values.[62,63] General trends for transition metals are also followed when comparing the potentials of $[\mathbf{1}]^+$ to the neighbouring analogues, i.e. the reduction potential $E^0_{1/2}$ for the $[Ru(benzene)_2]^{2+/+}$ couple is found at -1.02 V, or almost 1 V more positive than observed for $[\mathbf{1}]^+$.[64] The oxidation potential for the $[Ru(benzene)_2]^{2+/3+}$ couple was not reported, presumably due to the fact that it cannot be observed in common solvents. The values for the $[Mo(benzene)_2]^{0/+}$ couple are not reported in literature, however, the values for the $[Cr(benzene)_2]^{0/+}$ couple are reported at +0.82 V *vs.* Ag/AgCl,[65] which suggests that the corresponding Mo analogue has an oxidation potential that is shifted to more negative values. The chemical stability of the $[^{99}Tc(arene)_2]^+$ complexes is in agreement with the electrochemical measurements, since $[\mathbf{1}]^+$ – $[\mathbf{4}]^+$ are

very stable at ambient conditions and also do not decompose over the whole pH-range even at elevated temperatures.

Following the successful and high yield synthesis of $[^{99}Tc(arene)_2]^+$ complexes, the synthesis was translated to ^{99m}Tc chemistry. The biggest challenge for the synthesis of the corresponding ^{99m}Tc complexes was the fact, that $[^{99m}TcO_4]^-$ is eluted from the $^{99}Mo/^{99m}Tc$ generator as a saline solution, which is not compatible with the reaction conditions used above. In the original preparation of $[^{99m}Tc(arene)_2]^+$ described by Wester *et al.*, this problem was solved by time consuming evaporation of the aqueous saline solution, followed by reaction in organic solvents.[24] The complicated multistep procedure essentially rendered the procedure impractical for application. In an effort to improve the synthesis of $[^{99m}Tc(arene)_2]^+$, a novel ionic liquid (IL)-based extraction of $[^{99m}TcO_4]^-$ was developed in our group. In this procedure, a vial was coated with IL by slow evaporation of a methyl *tert*-butyl ether (MTBE) solution of $[P(C_6H_{13})_3(C_{14}H_{29})]Br$, followed by addition of the generator eluate to the IL which led to an extraction of 80 – 97% of the $[^{99m}TcO_4]^-$ into the IL layer within 10 min by an anion exchange process. The saline phase was removed and the IL shortly dried in a stream of N_2, followed by addition of $AlCl_3$ and the corresponding arene. After heating on 100°C for 10 min in a microwave reactor, the organic phase was quenched with saline solution and the aqueous phase containing $[^{99m}\mathbf{1}]^+$ – $[^{99m}\mathbf{4}]^+$ in yields of 35 – 87% and radiochemical purities of >93% (except for $[^{99m}\mathbf{4}]^+$) was separated. The products were further purified by loading the aqueous solutions on a C_{18} SepPak column, followed by washing with saline solution. Elution with an aqueous EtOH solution gave the products in >96% radiochemical purity. The procedure was successfully applied for toluene and mesitylene, but as described above, the synthesis of $[^{99m}Tc(tetralin)_2]^+$ gave a mixture of products due to formation of $[^{99m}Tc(tetralin)(OHPhen)]^+$ ($[^{99m}\mathbf{5}]^+$), resulting in a low yield (Table 10). The ratio of $[^{99m}\mathbf{4}]^+$:$[^{99m}\mathbf{5}]^+$ for this reaction was 1:0.8. In the case of benzene, Zn is needed as a reducing agent, which is in agreement with results described above for the ^{99}Tc complexes. The prepared $[^{99m}Tc(arene)_2]^+$ complexes are highly stable and do not decompose to a measurable extent even when aqueous solutions are heated in a microwave at 180°C in the presence of air.

Table 10: Comparison of the yields and purities for the syntheses of $[^{99m}\mathbf{1}]^+$ – $[^{99m}\mathbf{4}]^+$.

Compound (arene)	Yield after reaction (radiochemical purity)	Yield after purification (radiochemical purity)
$[^{99m}\mathbf{1}]^+$ (benzene)	87% (99%)	67% (>99.9%)
$[^{99m}\mathbf{2}]^+$ (toluene)	80% (>99.9%)	58% (>99.9%)
$[^{99m}\mathbf{3}]^+$ (mesitylene)	53% (>93%)	43% (>96%)
$[^{99m}\mathbf{4}]^+$ (tetralin)	35% (21%)	15% (48%)

The presented syntheses to $[^{99(m)}Tc(arene)_2]^+$ complexes (arene = benzene, toluene, mesitylene, tetralin) starting from $[^{99(m)}TcO_4]^-$ provide an unprecedented access to these complexes. The synthetic limitations of the reaction are mostly due to the high Lewis acidity of $AlCl_3$, which is crucial for the activation and reduction of $[^{99(m)}TcO_4]^-$. This problem might be addressed by using a different Lewis acid and reductant for the reaction in the future. Another potential solution to broaden the scope of the reaction could be the use of arene combinations. For example, reaction of $[^{99(m)}TcO_4]^-$ with $AlCl_3$ in a mixture of benzene and the arene of interest will presumably lead to a mixture of $[^{99(m)}Tc(arene)_2]^+$ and $[^{99(m)}Tc(benzene)(arene)]^+$. Since the formation of $[^{99(m)}Tc(benzene)_2]^+$ was only observed in trace amounts without Zn in the reaction, the problem of purification is reduced to two products. A different approach is the derivatization of $[^{99(m)}Tc(arene)_2]^+$ complexes, either by substitution of the arene ligand or by derivatization of the coordinated arene. For the latter case, a broad scope of reactions has been described for other $\{M\text{-arene}\}^{n+}$ fragments,[66] which could lead to functionalized $[^{99(m)}Tc(arene)_2]^+$ complexes in the future.

4.2 Re- and $^{99(m)}$Tc Complexes with NHC Ligands

4.2.1 Synthesis of NHC Precursors

4.2.1.1 Imidazolium Salts for NHC Generation

A very convenient synthesis of NHCs involves the deprotonation of imidazolium salts. Therefore, a library of imidazolium salts was prepared for further use in the preparation of the various $^{99(m)}$Tc-, Ag- and Re-NHC complexes. This library contained mostly methyl-substituted imidazoles, with the exception of one bidentate NHC-precursor comprised of ethyl substituents.

The precursor imidazolium salt 1,3-dimethylimidazolium hexafluorophosphate (**L1**-H)(PF_6) for the preparation of the monodentate NHC 1,3-dimethylimidazoline-2-ylidene (**L1**), was prepared according to a literature procedure by Oertel *et al.* by methylation of 1-methylimidazole with MeI in toluene.[67] Following a procedure by Buitrago *et al.*, the obtained crude (**L1**-H)(I) was then treated with NH_4PF_6 in H_2O and extracted using CH_2Cl_2 to give (**L1**-H)(PF_6) in 41% yield (Scheme 10).[68] Due to its hygroscopicity, a stock solution of (**L1**-H)(PF_6) in dry CH_3CN was prepared and stored in a glovebox. For the preparation of the corresponding NHC, aliquots of the stock solution were evaporated *in vacuo* until the solvent was fully removed and (**L1**-H)(PF_6) was then suspended in tetrahydrofuran (THF). Deprotonation was achieved by addition of a solution of 1 eq. KO^{t}Bu in THF at 25°C and the resulting yellow clear solution containing **L1** was subsequently used for synthesis.

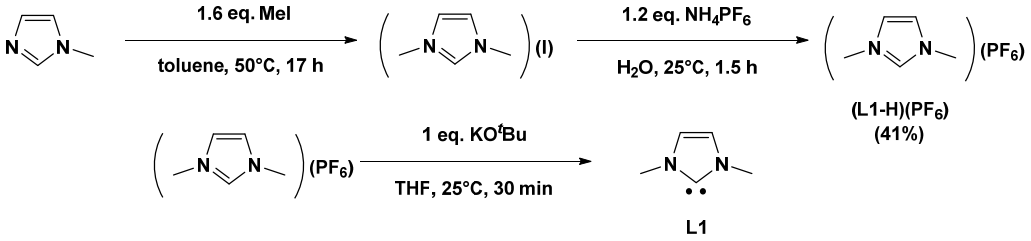

Scheme 10: Synthesis of (**L1**-H)(PF_6) from 1-methylimidazole and subsequent deprotonation reaction using KO^{t}Bu to give **L1**.

The preparations of the imidazolium salts 1,1'-methylene-3,3'-dimethyldiimidazolium dihexafluorophosphate ((**L2**-H_2)(PF_6)$_2$) and 1,1'-methylene-3,3'-diethyldiimidazolium dihexafluorophosphate ((**L3**-H_2)(PF_6)$_2$) for the preparation of bidentate NHCs 1,1′-methylene-3,3′-dimethyl-4,4′-diimidazoline-2,2′-diylidene (**L2)** and 1,1′-methylene-3,3′-diethyl-4,4′-diimidazoline-2,2′-diylidene (**L3**), respectively, were adapted from literature procedures by Cao *et al.* and In *et al.* (Scheme 11).[69,70] Preparation of (**L2**-H_2)(PF_6)$_2$ was achieved by nucleophilic substitution of CH_2Cl_2 with 1-methylimidazole in an autoclave at 110°C. The resulting crude solid containing the Cl^- salt was further purified by precipitation of the imidazolium salt with PF_6^- in H_2O. Following this procedure, an overall yield of 93% based on CH_2Cl_2 was achieved, which is a significant improvement compared to the reported yield of 33% for (**L2**-H_2)(Cl)$_2$.[69] For the preparation of (**L3**-H_2)(PF_6)$_2$, bisimidazol-1-

ylmethane (**L4**) had to be prepared in advance by nucleophilic substitution of CH_2Cl_2 with imidazole under basic conditions according to a procedure described by Díez-Barra *et al.* (Scheme 11).[71] Purification of **L4** was achieved by sublimation of the crude product with a yield of 82%. Losses in yield are explained by the high losses during sublimation due to deposition of **L4** at the wall of the flask instead of the sublimation finger and also by the solidification of the liquid mixture during the reaction, which prevented efficient stirring. To address this issue, the use of a mechanic stirrer is recommended. Alkylation of **L4** with EtBr using a procedure of In *et al.*, followed by precipitation with PF_6^- from H_2O gave (**L3**-H_2)$(PF_6)_2$ in 82% yield.[70] Both imidazolium salts, (**L2**-H_2)$(PF_6)_2$ and (**L3**-H_2)$(PF_6)_2$, were deprotonated by ^{n}BuLi in THF at -78°C. The low temperature is necessary due to the acidity of the protons of the CH_2-bridge, which prevents successful preparation of the NHC at ambient temperature.[72,73] Therefore, care has to be taken to let the solutions warm up from -78°C to 25°C very slowly during deprotonation.

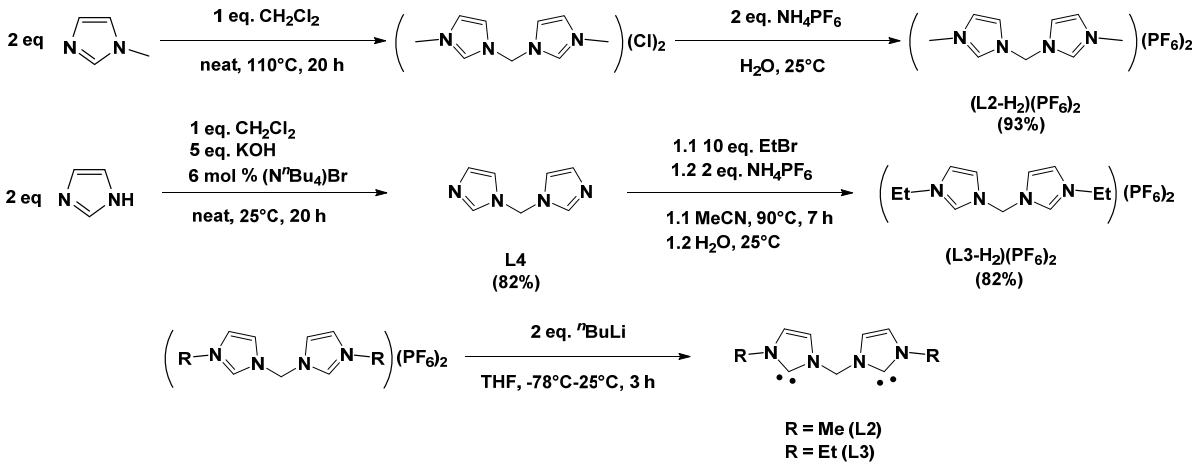

Scheme 11: Syntheses of (**L2**-H_2)$(PF_6)_2$, (**L3**-H_2)$(PF_6)_2$ and **L4**. (**L2**-H_2)$(PF_6)_2$ and (**L3**-H_2)$(PF_6)_2$ were deprotonated using ^{n}BuLi which gave the corresponding NHCs **L2** and **L3**.

Two precursors for tridentate NHCs were also prepared following literature procedures. Preparation of (PhB(^{Me}Im-H)$_3$)$(OTf)_2$ ((**L5**-H_3)$(OTf)_2$) was done following a procedure of Forshaw *et al.*, in which a 1:2:3 mixture of $PhBCl_2$, 1-methylimidazole and trimethylsilyl trifluoromethanesulfonate (TMSOTf) was heated on 80°C for 24 h (Scheme 12).[39] The yield of the reaction was with 89% slightly higher than the reported yield in the literature of 80%. (**L5**-H_3)$(OTf)_2$ was deprotonated in THF using lithium diisopropylamide (LDA) at 25°C. The NHC (Li)(**L5**) does not dissolve well in THF and, therefore, it has to be used in corresponding reactions as a suspension.

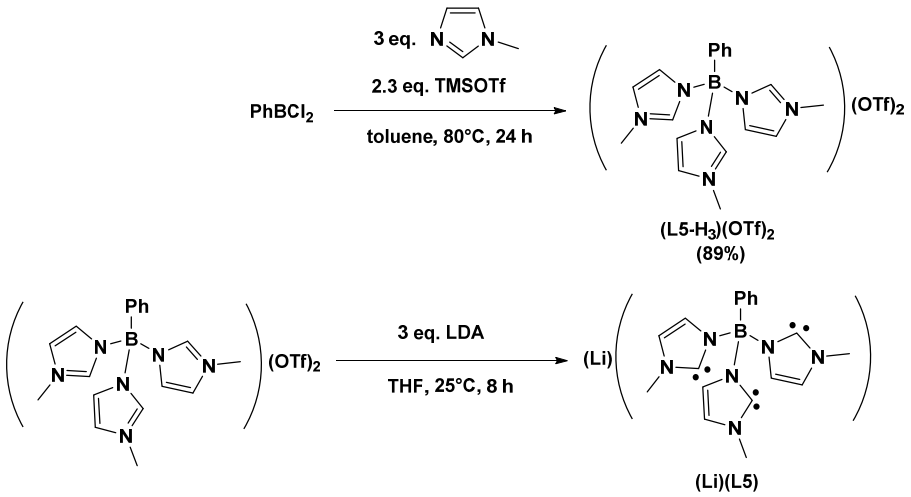

Scheme 12: Synthesis of the imidazolium salt (**L5**-H_3)$(OTf)_2$ and the corresponding deprotonation with LDA to give (Li)(**L5**).

With only one reaction step, the synthesis of (**L5**-H_3)$(OTf)_2$ is considerably shorter and more efficient than the synthesis of 1,1,1-tris[(3-methylimidazolium)-methyl]ethane trihexafluorophosphate ((**L6**-H_3)$(PF_6)_3$). The latter was prepared following a procedure described by Hu *et al.* (Scheme 13).[31] At first, 1,1,1-tris[(*p*-toluenesulfonato)methyl]ethane was prepared by reaction of 1,1,1-tris-(hydroxymethyl)ethane and *p*-toluenesulfonyl chloride in pyridine (py). Precipitation of the desired product was achieved by addition of the reaction solution to a 2:1 mixture of conc. HCl and MeOH. Recrystallization from MeOH gave 1,1,1-tris[(*p*-toluenesulfonato)methyl]ethane in 63% yield. Since *p*-toluenesulfonate is a much better leaving group than OH^-, it was now possible to easily obtain 1,1,1-tris(bromomethyl)ethane from the previously isolated 1,1,1-tris[(*p*-toluenesulfonato)methyl]ethane using NaBr. 1,1,1-Tris(bromomethyl)ethane was very effectively purified by bulb-to-bulb distillation with a yield of 84%. Care should be taken that the final product does not contain any CH_2Cl_2, since this can lead to the formation of (**L2**-H_2)$^{2+}$ as a side product in the following high-temperature reaction with 1-methylimidazole. Finally, (**L6**-H_3)$^{3+}$ was obtained by a neat reaction of 1,1,1-tris(bromomethyl)ethane with 1-methylimidazole. (**L6**-H_3)$(Br)_3$ was purified by recrystallization from MeOH with a yield of 45% and precipitation from H_2O using PF_6^- afforded (**L6**-H_3)$(PF_6)_3$ with 90% yield. Generation of the NHC **L6** was done by addition of a THF solution of 3 eq. KO^{t}Bu or LDA at 25°C. The uncharged **L6** is highly soluble in THF. Thus, the colorless suspension of (**L6**-H_3)$(PF_6)_3$ turns to a clear yellow solution within minutes and was used after 30 min of stirring at 25°C.

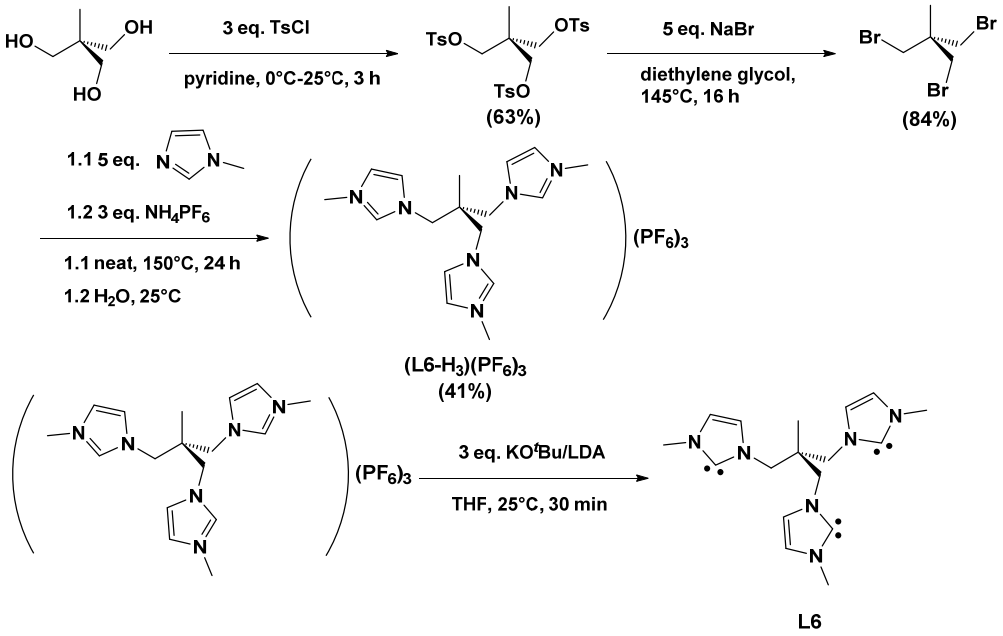

Scheme 13: Synthesis of (**L6**-H_3)$(PF_6)_3$ and the corresponding deprotonation reaction leading to **L6**.

As mentioned before, all the imidazolium salts were easily deprotonated to form the corresponding NHCs, which then were used *in situ*. Table 11 summarizes the conditions for the deprotonation reactions.

Table 11: Summary of conditions used for deprotonation of imidazolium salts to form corresponding NHCs *in situ*.

Imidazolium salt	NHC	Base for deprotonation	Temp. for deprotonation	Recommended time for deprotonation	Solubility of the NHC in THF
(**L1**-H)(PF_6)	**L1**	KO^{t}Bu	25°C	30 min	soluble
(**L2**/**L3**-H_2)$(PF_6)_2$	**L2**/**L3**	^{n}BuLi	-78°C	3 h	soluble
(**L5**-H_3)$(OTf)_2$	**L5**$^-$	LDA	25°C	8 h	insoluble
(**L6**-H_3)$(PF_6)_3$	**L6**	KO^{t}Bu/LDA	25°C	30 min	soluble

4.2.1.2 Ag^{I}-NHC Complexes for Transmetalation Reactions

Ag^{I}-NHC complexes were prepared for synthesis of Re- and $^{99(m)}$Tc-NHC complexes by transmetalation reactions. In particular, the formation of ^{99m}Tc complexes could considerably benefit from the use of Ag^{I}-NHC complexes due to the fact that ^{99m}Tc chemistry is often done in aqueous solutions or protic solvents and thus, the use of free NHCs has to be circumvented. Chan *et al.* demonstrated, that the rapid radiolabeling of *fac*-$[^{99m}Tc^{I}(OH_2)_3(CO)_3]^+$ with 1-(2-pyridyl)-3-methylimidazolium iodide using Ag_2O for transmetalation is in fact possible and gives ^{99m}Tc-NHC complexes with a high yield.[43]

Following a literature procedure by Quezada *et al.*, $[Ag_2(\mathbf{L2})_2](PF_6)_2$ ([**6**]$(PF_6)_2$) was prepared (Scheme 14).[74] At first, (**L2**-H_2)$(Cl)_2$ was prepared as previously described and the crude product was directly used for the reaction with Ag_2O in H_2O. This gave the corresponding $[Ag_2(\mathbf{L2})_2](Cl)_2$ complex, which was precipitated from an aqueous solution using PF_6^-. The overall yield for the formation of [**6**]$(PF_6)_2$ based on the initially used CH_2Cl_2 was 90%. In a similar reaction, the trinuclear complex $[Ag_3(\mathbf{L6})_2](PF_6)_3$ ([**7**]$(PF_6)_3$) was prepared (Scheme 14). In the literature procedure described by Hu *et al.*, the reaction of (**L6**-H_3)$(PF_6)_3$ with Ag_2O was done in dimethyl sulfoxide (DMSO) as a solvent and precipitation of [**7**]$(PF_6)_3$ was achieved by addition of H_2O.[31] This precipitation step could not be reproduced and thus, the reaction procedure was changed to using CH_3CN as a solvent and precipitation with Et_2O, which gave [**7**]$(PF_6)_3$ in 91% yield.

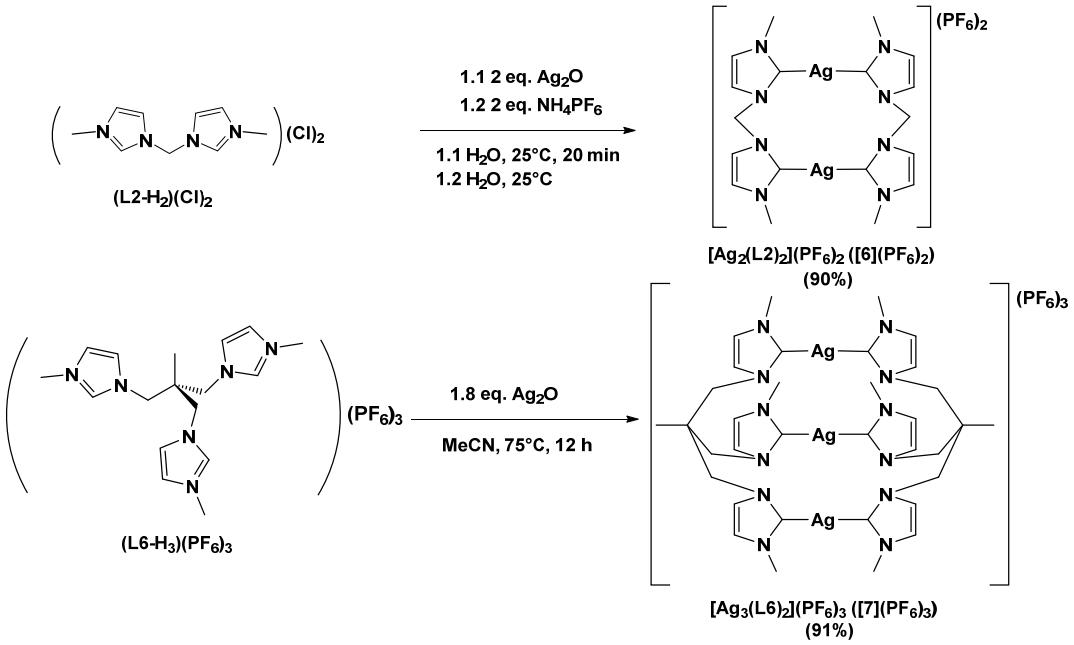

Scheme 14: Syntheses of [**6**]$(PF_6)_2$ and [**7**]$(PF_6)_3$ by reaction of the corresponding imidazolium salts with Ag_2O.

4.2.2 Synthesis of High-Valent M-NHC Complexes (M = Re, ^{99}Tc)

4.2.2.1 *Trans*-{^{99}Tc^{V}O$_2$}$^+$-NHC Complexes Comprised of Mono- and Bidentate NHC Ligands

Following the general preparation of $[^{99}TcO_2(NHC)_4]^+$ complexes, the preparation of $[^{99}TcO_2(\mathbf{L1})_4]^+$ and $[^{99}TcO_2(\mathbf{L2})_2]^+$ was tested starting from $(N^nBu_4)[^{99}TcOCl_4]$. Reactions were done in dry THF at 25°C under N_2 atmosphere by addition of the NHCs **L1** (4 eq.) or **L2** (2 eq.) that were previously prepared, as stated before, by addition of a strong base to the imidazolium salt in THF. The strong nucleophilicity of the NHCs often leads to decomposition of the $^{99}Tc^{V}$ starting material upon addition of the NHC, leading to a color change to brown, which indicates the formation of $Tc^{IV}O_2$. This decomposition reaction is commonly observed when $(N^nBu_4)[^{99}TcOCl_4]$ is reacted with strong or mild bases and can be suppressed by having an excess of a coordinating ligand present. For example, addition of excess NEt_3 to a solution of $(N^nBu_4)[^{99}TcOCl_4]$ in THF immediately leads to decomposition, whereas the same experiment with an excess of ethylene glycol (glyc-H_2) present leads to quantitative formation of $(N^nBu_4)[^{99}TcO(glyc)_2]$ ((N^nBu_4)[**8**]), as described by Davison *et al.*.[75] The increased stability of (N^nBu_4)[**8**] towards basic conditions makes it an important starting material for the synthesis of $[^{99}TcO(glyc)(tacn\text{-}R)]^+$ type complexes (tacn-R = 1,4,7-triazacyclononane and derivatives).[76,77] When solutions of the NHCs **L1** (4 eq.) and **L2** (2 eq.) were added to a solution of (N^nBu_4)[**8**], a color change to orange was observed, indicating formation of $[^{99}TcO_2(\mathbf{L1})_4]^+$ ([**9**]$^+$) and $[^{99}TcO_2(\mathbf{L2})_2]^+$ ([**10**]$^+$, scheme 15, **method a**).[78] Formation of the dioxo core is explained by the coordination of residual H_2O, followed by deprotonation under the basic conditions in the reaction solution.

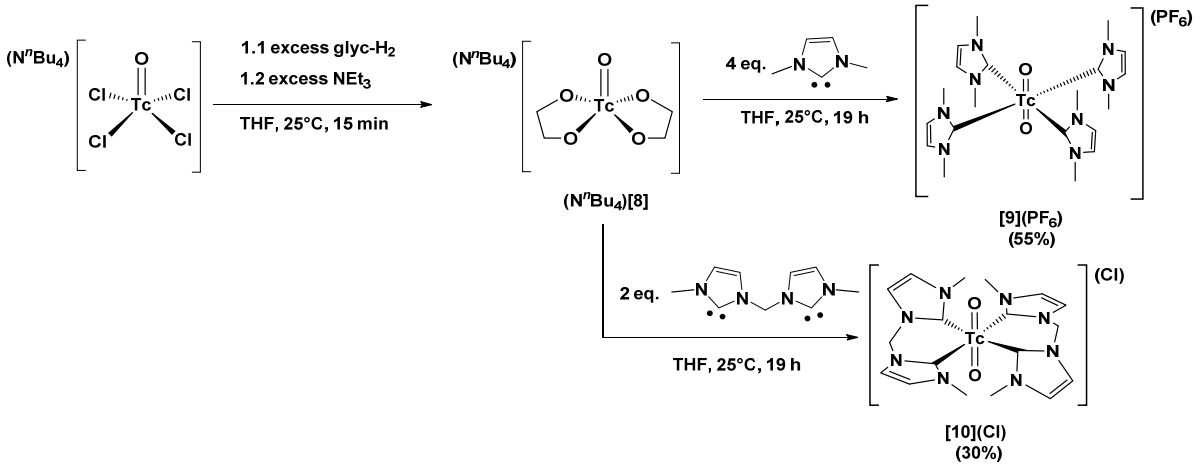

Scheme 15: Synthesis of [**9**]$^+$ and [**10**]$^+$ by reaction of the base-stable [**8**]$^-$ with the NHCs **L1** and **L2** (**method a**).

Isolation of [**9**](PF_6) was achieved by concentration of the crude solution followed by crystallization at -10°C and removal of the supernatant. A satisfying yield of 55% was achieved. [**9**]$^+$ is stable as a solid under inert atmosphere, but quickly decomposes at ambient conditions and thus, [**9**]$^+$ has a comparable stability to previously published ^{99}Tc-NHC complexes with monodentate NHC ligands.[34,36,37] The sensitivity towards air and moisture renders ^{99}Tc-NHC complexes comprised of monodentate NHC

ligands impractical for the application with ^{99m}Tc. Despite its sensitivity towards ambient conditions, a full analysis of [**9**](PF_6) was possible, including crystal structure analysis.

[**9**](PF_6) crystallizes as orange plates of the composition [**9**](PF_6)·glyc-H_2 in the monoclinic space group C2/c (Figure 13). The structure shows the four NHCs coordinated in the equatorial positions in a paddlewheel-like arrangement, which was also observed in previously reported structure of [$^{99}TcO_2(L^{iPr})_4$][$^{99}TcO_4$]·2.5THF (L^{iPr} = 1,3-diisopropyl-4,5-dimethylimidazoline-2-ylidene).[34] The ^{99}Tc-O bond length (1.759(2) Å, table 12) is similar to the ^{99}Tc-O bond lengths found in [$^{99}TcO_2(L^{iPr})_4$][$^{99}TcO_4$]·2.5THF (1.760(3) and 1.765(2) Å) and the Re-O bond lengths found in [$ReO_2(L^{Me})_4$](PF_6)$_{0.55}$[ReO_4]$_{0.45}$·2H_2O (L^{Me} = 1,3-dimethyl-4,5-dimethylimidazol-2-ylidene, 1.773(7) and 1.768(7) Å).[34,79] The ^{99}Tc-C bond lengths of [**9**]$^+$ (2.191(3) and 2.188(3) Å) are in the same range as in [$ReO_2(L^{Me})_4$](PF_6)$_{0.55}$[ReO_4]$_{0.45}$·2H_2O (2.19(1) – 2.21(1) Å),[79] but shorter than the ones found in [$^{99}TcO_2(L^{iPr})_4$][$^{99}TcO_4$]·2.5THF (2.220(3) – 2.232(3) Å).[34] This can be explained by the increased steric demand of the Li^{Pr} ligand compared to the L^{Me} ligand. The ^{99}Tc-centre has an almost ideal octahedral coordination environment, which is reflected in the almost linear O(1)-Tc(1)-O(1)' angle (179.68°), the O-^{99}Tc-C angles close to 90° (90.86(12) and 89.03(12)°) and the C(1)-Tc(1)-C(11) angle of 90.30(13)°.

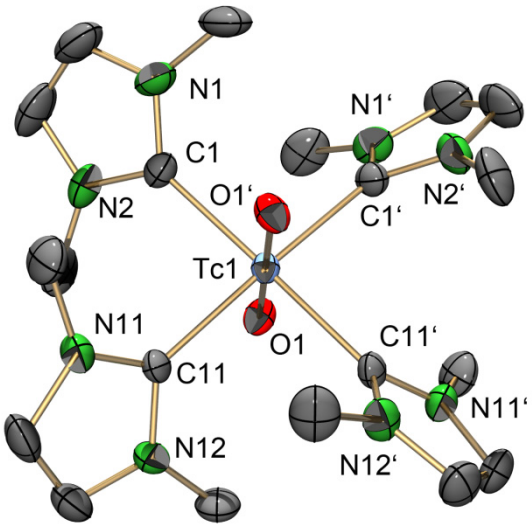

Figure 13: ORTEP representation[51] of the [$^{99}TcO_2$(**L1**)$_4$]$^+$ ([**9**]$^+$) cation of the [**9**](PF_6)·glyc-H_2 structure. Thermal ellipsoids are represented at the 50% probability level. Hydrogen atoms are omitted for clarity.

Table 12: Selected bond lengths and angles of [**9**]$^+$.

Selected bond lengths [Å]		Selected angles [°]	
Tc(1)-O(1)	1.759(2)	O(1) –Tc(1)-O(1)#1	179.68(15)
Tc(1)-C(1)	2.191(3)	C(11)-Tc(1)-C(1)#1	177.39(12)
Tc(1)-C(11)	2.188(3)	O(1)-Tc(1)-C(1)	90.86(12)
		O(1)-Tc(1)-C(11)	89.03(12)
		C(1)-Tc(1)-C(11)	90.30(13)

IR spectroscopy of [**9**](PF$_6$) shows besides a strong band at 844 cm^{-1} (PF$_6^-$) also the characteristic $\nu_{O=Tc=O}$ band at 780 cm^{-1}, which corresponds to the asymmetric stretching mode. Due to the almost linear O-^{99}Tc-O angle, the symmetric stretching frequency is IR-inactive. Compared to the $\nu_{O=Tc=O}$ band of [^{99}TcO$_2$(L^{iPr})$_4$] (783 cm^{-1}), the observed band is in the same range.[34] In contrast, the $\nu_{O=Re=O}$ band of [ReO$_2$(L^{Me})$_4$]$^+$ is observed at considerably lower wavenumbers, with a value of 768 cm^{-1}.[79] NMR spectroscopy of [**9**](PF$_6$) confirms that the complex has a high symmetry, since only one singlet for the CH$_3$ groups (3.42 ppm) and also only one singlet for the CH groups (7.34 ppm) was found in the ^{1}H NMR spectrum. This is also observed in the ^{13}C NMR spectrum, where only one signal was found for the CH groups (122.68 ppm) and the CH$_3$ groups (36.07 ppm).

As it was mentioned before, [**9**]$^+$ is not stable in the presence of H$_2$O and O$_2$. In contrast, the corresponding compound with the bidentate ligand **L2**, [**10**]$^+$, has an increased stability and is stable over days in H$_2$O at pH ≥ 7 and up to 50°C. This is presumably explained by the chelate effect. The stability and reactivity of [**10**]$^+$ at lower pH will be discussed in chapter 4.2.2.2. [**10**]$^+$ was purified by recrystallization. The stability of [**10**]$^+$ allows the crystallization of [**10**](Cl) directly from H$_2$O or the crystallization of [**10**](PF$_6$) from a 1:1 solution of acetone/H$_2$O, leading to high purity single-crystalline material. The yield achieved for the synthesis of [**10**](Cl) using **method a** was 30%, while the large losses are mostly explained by the used recrystallization purification. In addition, the increased stability of [**10**]$^+$ allowed the development of a one-pot synthesis in which the imidazolium salt (**L2**-H$_2$)(PF$_6$) was directly reacted with (N^{n}Bu$_4$)[**8**] in the presence of an excess of NEt$_3$ in refluxing CH$_2$Cl$_2$ (**method b**, scheme 16). This one-pot approach is especially convenient, since it avoids the need for extremely dry conditions and eliminates the step of the separate NHC generation by a strong base. Purification by recrystallization from acetone/H$_2$O afforded [**10**](PF$_6$) in 44% yield, which is slightly higher than the yield achieved in **method a**.

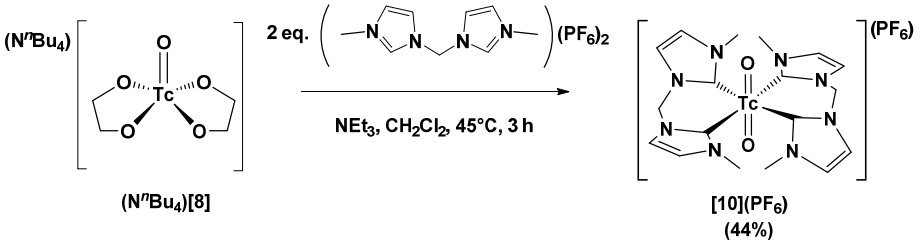

Scheme 16: One-pot synthesis of [**10**]$^+$ by reaction of the base-stable [**8**]$^-$ with the imidazolium salt (**L2**-H$_2$)(PF$_6$)$_2$ (**method b**).

The formation of M-NHC complexes by reaction of imidazolium salts with metal precursors has been described in literature before for various metals and a wide variety of imidazolium salts.[3,30,80-82] However, this is the first time that such an approach was successfully used for technetium and this alternative method opens up new perspectives for the synthesis of $^{99(m)}$Tc complexes. In order to better understand the mechanism of the one-pot reaction, it was studied in more detail. Interestingly,

(**L2**-H_2)$(PF_6)_2$ and [**8**]$^-$ form a purple salt of the composition (**L2**-H_2)$_2$[**8**]$(PF_6)_3$ which is not soluble in CH_2Cl_2. This salt was isolated and crystallized from acetone. In the structure, a pre-orientation of the imidazolium dication was observed, which might be crucial for the *in situ* deprotonation during the one-pot synthesis (Figure 14). Especially interesting is that the CH_2 group appears to also be involved in the pre-orientation, since H(2a)' of the CH_2 group points towards the O^{2-} ligand O(1) of the [**8**]$^-$ anion.

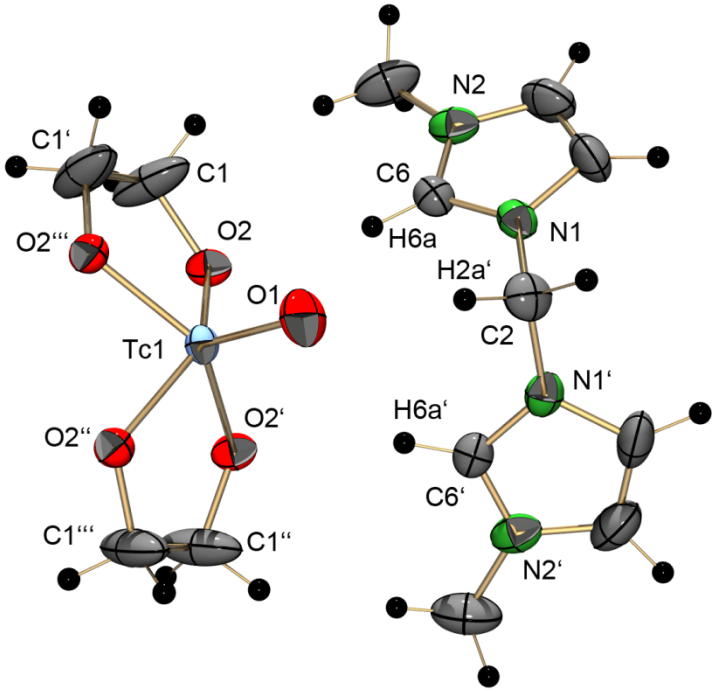

Figure 14: ORTEP representation[51] of the {(**L2**-H_2)[^{99}TcO(glyc)$_2$]}$^+$ fragment of the (**L2**-H_2)$_2$[^{99}TcO(glyc)$_2$]$(PF_6)_3$ structure. Thermal ellipsoids are represented at the 50% probability level.

Table 13: Selected bond lengths of [^{99}TcO(glyc)$_2$]$^-$ in the (**L2**-H_2)$_2$[^{99}TcO(glyc)$_2$]$(PF_6)_3$ structure.

Selected bond lengths [Å]		Selected angles [°]	
Tc(1)-O(1)	1.665(7)	O(1)-Tc(1)-O(2)	110.08(10)
Tc(1)-O(2)	1.932(3)	O(2)-Tc(1)-O(2)#3	82.82(17)
		O(2)-Tc(1)-O(2)#1	83.63(17)

Despite the pre-orientation of (**L2**-H_2)$^{2+}$, no significant changes in bond lengths or angles of the [**8**]$^-$ structure compared to the structure of (Li)[**8**] were found (Table 13).[78] Thus, there is no further structural evidence that this pre-orientation of the ligand is crucial for the coordination of the NHC. The exact mechanism of the reaction remains unknown, but it is expected that either [^{99}TcO(glyc)(**L2**)]$^+$, [^{99}TcOX(glyc)(**L2**)] or [^{99}TcOX_3(**L2**)] (X = Cl, glyc-H) forms as an intermediate after the coordination of the first **L2** (Figure 15). After the coordination of the second **L2**, formation of the intermediate [^{99}TcOX(**L2**)$_2$]$^{2+}$ (X = Cl, glyc-H) is expected before the dioxo core is formed. During the reaction leading to [**10**]$^+$, it was observed that the CH_2Cl_2 solution had a green color, indicating

formation of such a side product or intermediate. However, isolation or characterization of this green compound was not possible due to its sensitivity towards ambient conditions.

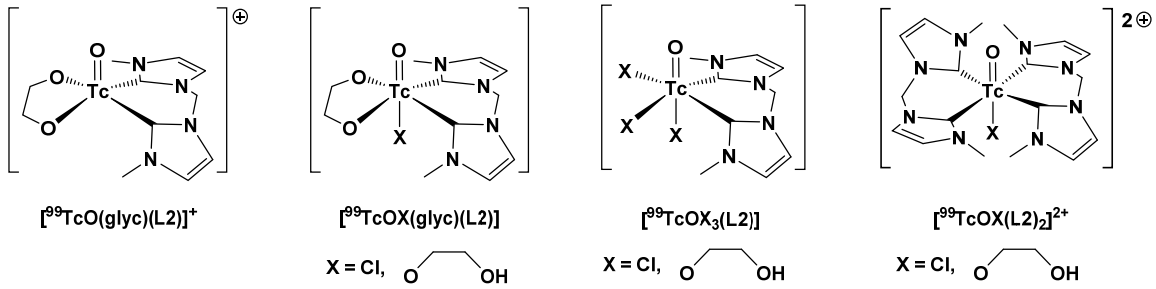

Figure 15: Potential intermediates in the formation of [**10**]$^{+}$ from [^{99}TcO(glyc)$_2$]$^{-}$.

[**10**](PF$_6$) crystallizes as yellow blocks of the composition [**10**](PF$_6$)·H$_2$O in the monoclinic space group P2/c (Figure 16). The structure shows that the NHCs coordinate in a more planar fashion compared to the paddle-wheel-like arrangement in [**9**]$^{+}$. The increased stability of [**10**]$^{+}$ implies a stronger binding of the **L2** ligand, which is reflected in the shorter ^{99}Tc-C bond lengths (2.170(4) and 2.166(4) Å, table 14) compared to [**9**]$^{+}$ (2.191(3) and 2.188(3) Å). However, the ^{99}Tc-O bond length (1.765(3) Å) is in the same range as in [**9**]$^{+}$ (1.759(2) Å). As it was the case in [**9**]$^{+}$, the O^{2-} ligands have a linear arrangement with a O(1)-Tc(1)-O(1)' angle of 180.00(9)° and the ^{99}Tc centre has a symmetrical octahedral coordination environment. The bite angle C(1)-Tc(1)-C(2) of **L2** (81.33(16)°) is similar to the bite angle found in the recently reported [ReO(OH)(**L2**)$_2$]$^{2+}$ (81.4(2)°).[42]

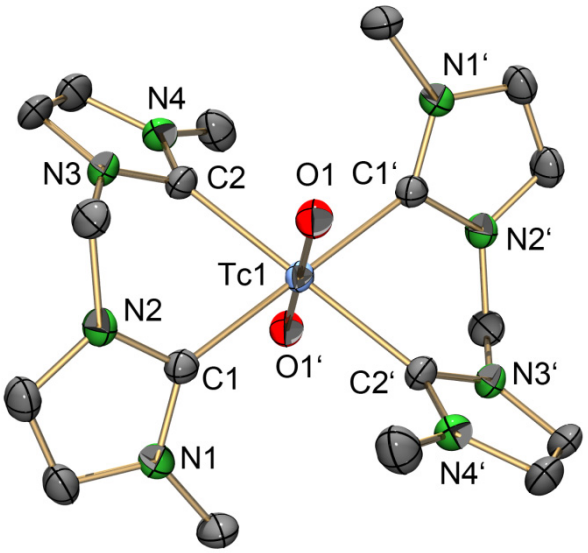

Figure 16: ORTEP representation[51] of the [^{99}TcO$_2$(**L2**)$_2$]$^{+}$ ([**10**]$^{+}$) cation of the [**10**](PF$_6$)·H$_2$O structure. Thermal ellipsoids are represented at the 50% probability level. Hydrogen atoms are omitted for clarity.

Table 14: Selected bond lengths and angles of [**10**]$^+$.

Selected bond lengths [Å]		Selected angles [°]	
Tc(1)-O(1)	1.765(3)	O(1)-Tc(1)-O(1)#1	180.00(9)
Tc(1)-C(1)	2.170(4)	O(1)-Tc(1)-C(1)	89.27(15)
Tc(1)-C(2)	2.166(4)	O(1)-Tc(1)-C(2)	89.24(15)
		C(1)-Tc(1)-C(2)	81.33(16)

IR spectroscopy of [**10**](PF_6) shows besides a strong band at 847 cm^{-1} (PF_6^-) the characteristic $\nu_{O=Tc=O}$ band of the asymmetric stretching mode at 765 cm^{-1}, which is at lower wavenumbers than the corresponding band of [**9**]$^+$ (780 cm^{-1}). This decrease in energy is presumably a consequence of the stronger binding of the **L2** ligand. NMR spectroscopy of [**10**](PF_6) in DMSO-D_6 confirms the high symmetry of the complex observed in the solid state. ^{1}H NMR spectroscopy shows two singlets for the backbone CH groups (7.71 and 7.43 ppm) and a singlet for the CH_3 groups (3.68 ppm). Only the CH_2 group is split into two doublets (6.92 and 6.44 ppm), which is due to the different chemical environments of the H atoms, pointing either towards or away from the O^{2-} ligand. The high symmetry of the complex is also confirmed by the ^{13}C NMR, with only 3 signals that correspond to the CH-, CH_2- and CH_3 groups of **L2** at 121.56, 62.00 and 36.16 ppm, respectively. The signals for the ^{99}Tc-C atoms are not observed, presumably due to the broadening of the signal caused by the ^{99}Tc nucleus. The observed chemical shifts in NMR spectroscopy are comparable to the chemical shifts found for [**9**]$^+$.

NHCs are highly versatile ligands and are easily derivatized with different alkyl substituents. In order to study the influence of the alkyl substituents on the formation and stability of the corresponding complexes, the synthetic methods described for **L2** were also tested with 1,1′-methylene-3,3′-diethyl-4,4′-diimidazoline-2,2′-diylidene (**L3**). Following the same reaction procedures as described for the synthesis of [**10**]$^+$, [$^{99}TcO_2$(**L3**)$_2$](PF_6) ([**11**](PF_6)) was prepared (Scheme 17).[78] For purification, the crude product was recrystallized from a 1:1 acetone/H_2O solution with yields of 33% (**method a**) and 26% (**method b**). While the yield for **method a** is comparable to the yield achieved in the synthesis of [**10**]$^+$ (30% yield), the yield for **method b** is considerably lower (46% yield for [**10**]$^+$). Apparently, the steric demand of the substituents has a larger influence on the reaction involving the metal-mediated *in situ* deprotonation of the imidazolium salt than on the reaction involving the highly reactive NHC. However, no change in the stability of [**11**]$^+$ compared to [**10**]$^+$ was found and no decomposition was observed during crystallization from 1:1 acetone/H_2O solutions, despite the more sterically demanding ethyl substituents of **L3**.

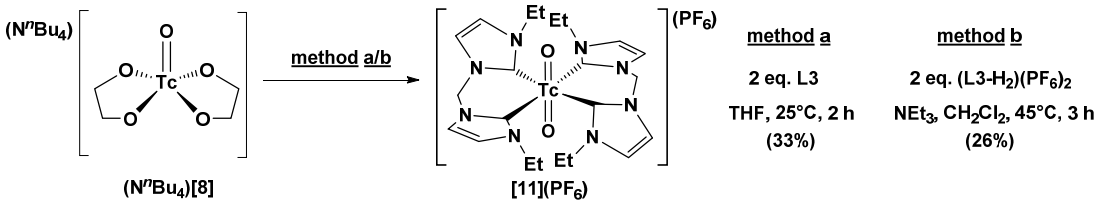

Scheme 17: Synthesis of [**11**](PF$_6$) starting from (N^{n}Bu$_4$)[**8**] following the same synthetic methods as for [**10**]$^+$.

[**11**](PF$_6$) crystallizes as yellow blocks of the composition [**11**](PF$_6$)·2.6H$_2$O in the triclinic space group P$\bar{1}$ (Figure 17). The structure contains two independent ^{99}Tc centres in the asymmetric unit that are very similar, except for a disorder that had to be considered in one ethyl substituent of one of the **L3** ligands of the Tc(2) molecule. Due to their similarity, only the structure of the Tc(1) moiety will be discussed here. The ^{99}Tc-O bond lengths of 1.762(2) Å is comparable with the corresponding bond length in [**10**]$^+$ (Table 15). In contrast to [**10**]$^+$, the ^{99}Tc-C bond lengths of [**11**]$^+$ (2.159(3) and 2.181(3) Å) are shortened and elongated. In [**10**]$^+$, both ^{99}Tc-C bond lengths are very similar (2.170(4) and 2.166(4) Å). This is presumably a consequence of the sterically demanding ethyl substituents. The C(1)-Tc(1)-C(2) bite angle of the **L3** ligand is with 80.47(12)° considerably smaller than for **L2** in [**10**]$^+$ (81.33(16)°), which is also due to the increased steric interactions between the equatorial ligands.

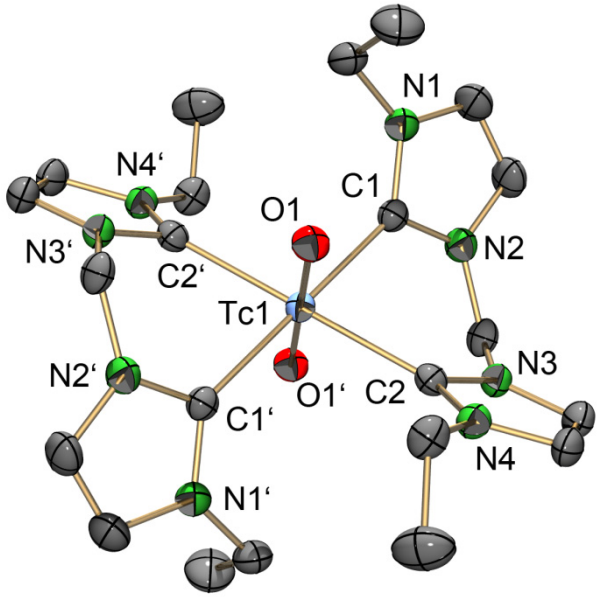

Figure 17: ORTEP representation[51] of the [^{99}TcO$_2$(**L3**)$_2$]$^+$ ([**11**]$^+$) cation of the [**11**](PF$_6$)·2.6H$_2$O structure. Thermal ellipsoids are represented at the 50% probability level. Hydrogen atoms are omitted for clarity.

Table 15: Selected bond lengths and angles of [**11**]$^+$.

Selected bond lengths [Å]		Selected angles [°]	
Tc(1)-O(1)	1.762(2)	O(1)-Tc(1)-O(1)#1	180.0
Tc(1)-C(1)	2.159(3)	O(1)-Tc(1)-C(1)	90.57(11)
Tc(1)-C(2)	2.181(3)	O(1)-Tc(1)-C(2)	90.51(11)
		C(1)-Tc(1)-C(2)	80.47(12)

IR spectroscopy of [**11**](PF_6) shows besides the strong band at 849 cm^{-1} (PF_6^-) also the characteristic $\nu_{O=Tc=O}$ band of the asymmetric stretching mode at 765 cm^{-1}. This value is identical with the value of the $\nu_{O=Tc=O}$ band found in [**10**]$^+$. ^{1}H NMR spectroscopy of [**11**](PF_6) in CD_3CN shows the expected set of signals, with two singlets for the CH groups (7.55 and 7.30 ppm), two doublets for the CH_2 bridge (7.15 and 6.14 ppm), a multiplet for the CH_2 groups of the ethyl substituents (4.29 – 4.09 ppm) and a triplet for the CH_3 groups of the ethyl substituents (1.21 ppm). A comparison to the chemical shifts of **L2** in [**10**]$^+$ is difficult due to the different solvents used, but no obvious trends for differences in the chemical shift were found. The introduction of ethyl groups causes different chemical shifts observed in the ^{13}C NMR for the carbons of the backbone CH groups (121.92 and 119.42 ppm) which were chemically equivalent in [**10**]$^+$. As it was the case before for [**9**]$^+$ and [**10**]$^+$, the ^{99}Tc-C signals were not observed in the ^{13}C NMR spectrum.

Following the successful preparation of the $^{99}Tc^{V}$-NHC complexes [**9**]$^+$ – [**11**]$^+$, reactions of (N^nBu_4)[**8**] with the tridentate ligands **L5**$^-$ and **L6** were also tested. Reactions of (N^nBu_4)[**8**] with **L5**$^-$ and **L6** in THF at 25°C did not lead to a color change as it was observed before and formation of [^{99}TcO(glyc)(**L**)]$^{n+}$ (**L** = **L5**$^-$, n = 0; **L** = **L6**, n = 1) was not observed (Scheme 18). The resulting purple crude product appeared to be the starting material [**8**]$^-$ according to analysis and no other products could be detected. Work under strict exclusion of air and moisture in a glovebox suitable for work with ^{99}Tc did not lead to formation of the corresponding ^{99}Tc-NHC complexes. Interestingly, bidentate coordination of **L5**$^-$ and **L6** to the ^{99}Tc centre to form [$^{99}TcO_2$(**L**-H)$_2$]$^{n+}$-type complexes (**L** = **L5**$^-$, n = 1; **L** = **L6**, n = 3) was also not observed, which is presumably explained by unfavourable steric interactions of the unbound imidazole with the O^{2-} ligands (Scheme 18). One-pot reactions of (N^nBu_4)[**8**] with (**L5**-H_3)$(OTf)_2$ or (**L6**-H_3)$(PF_6)_3$ with the same conditions as in **method b** used for the synthesis of [**10**]$^+$ and [**11**]$^+$ did also not lead to the formation of a product. Formation of product was also not observed with DMF instead of CH_2Cl_2 as a solvent for the reaction of (**L5**-H_3)$(OTf)_2$ with (N^nBu_4)[**8**] in the presence of NEt_3, despite heating to 90°C for several hours. The fact, that formation of $^{99}Tc^{V}$-NHC compounds containing **L5**$^-$ or **L6** is not possible is an important limitation of this reaction. The synthesis of [$^{99}Tc^{V}$O(glyc)(**L**)]$^{n+}$ (**L** = **L5**$^-$, n = 0; **L** = **L6**, n = 1) could have been important for the synthesis of the first $^{99}Tc^{VII}$-NHC complex, since corresponding [$^{99}Tc^{V}$O(glyc)(tacn-R)]$^+$-type complexes (tacn-R = 1,4,7-triazacyclononane and derivatives) have been reported as intermediates in the synthesis of *fac*-{$^{99}Tc^{VII}O_3$(tacn-R)}$^+$ complexes.[76,77]

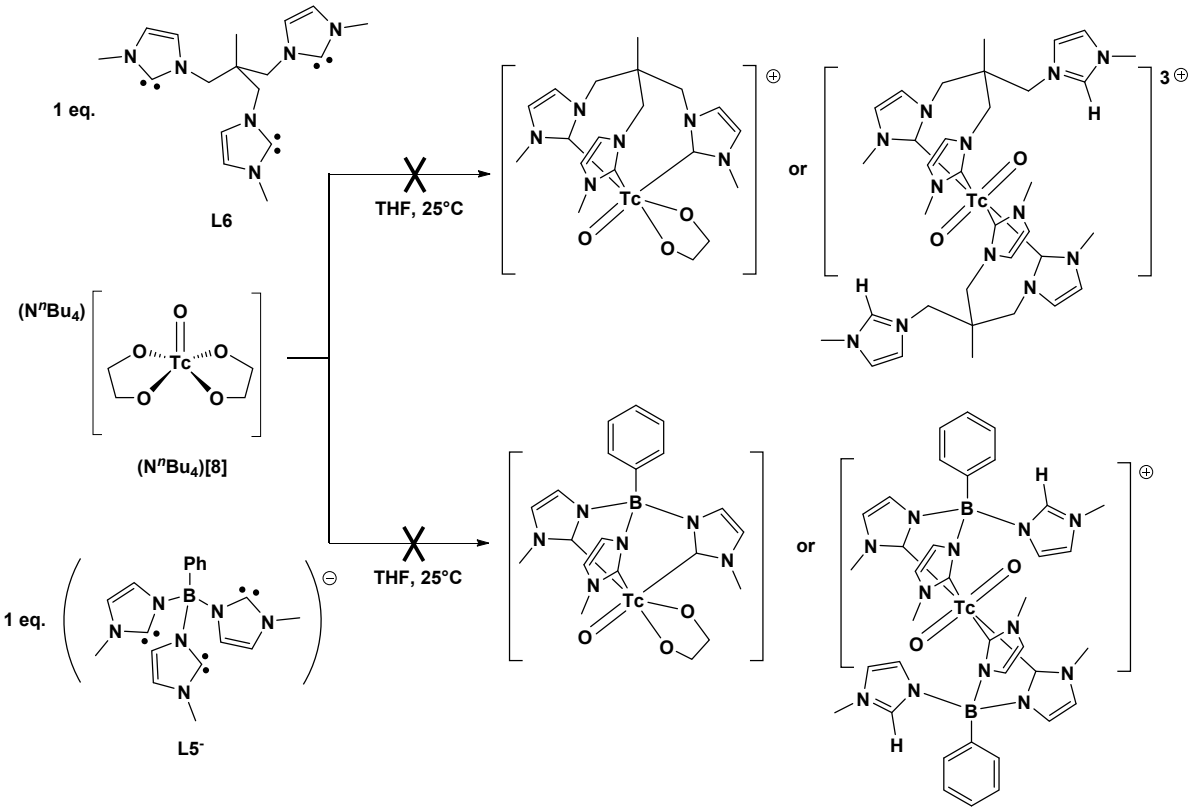

Scheme 18: Reaction of (N^{n}Bu$_4$)[**8**] with tridentate NHCs **L5**$^-$ and **L6** did not lead to formation of ^{99}Tc-NHC complexes. The reactions with the imidazolium salts (**L5**-H$_3$)(OTf)$_2$ and (**L6**-H$_3$)(PF$_6$)$_3$ have been omitted for clarity.

Despite a few limitations, the reaction of (N^{n}Bu$_4$)[**8**] with NHCs or imidazolium salts has proven to be a promising and very general route for the synthesis of ^{99}Tc^V-NHC complexes. So far, only bidentate NHCs with CH_2 bridges were tested, but further investigations of different alkyl bridges are necessary to unravel the synthetic possibilities provided by this reaction. In addition, the use of sterically more demanding substituents such as ^{i}Pr or ^{t}Bu on the bidentate ligand might provide additional information on the influence of the steric interactions between the two NHC ligands on the structure of the complex. The use of ^{i}Pr or ^{t}Bu substituents might also enable a synthetic route to monosubstituted $\{^{99}TcO_2\}^+$-NHC complexes due to the sterically unfavored disubstituted products. Complexes comprised of bidentate NHCs show a tremendous increase in stability and are the first water stable ^{99}Tc-NHC complexes. The water stability and pH-tolerance of [**10**]$^+$ and [**11**]$^+$ allow conversion of the $\{^{99}TcO_2\}^+$ core into the $\{^{99}TcO\}^{3+}$ core by treatment with HCl, which is the subject of the next chapter.

4.2.2.2 *Trans*-$\{^{99}Tc^{V}O(X)(L2)_2\}^{2+}$ Complexes (X = Cl, OMe, NCS)

The complexes $[^{99}TcO_2(\mathbf{L2}/\mathbf{L3})_2]^+$ ($[\mathbf{10}]^+/[\mathbf{11}]^+$) exhibit a high water stability at pH ≥ 7 even at elevated temperatures. When a 1:1 acetone/H_2O solution of $[\mathbf{10}]^+$ or $[\mathbf{11}]^+$ was acidified with excess 1 M HCl (pH = 1), a color change from yellow to green was observed, indicating formation of a new compound. The color change is due to the protonation and exchange of one of the O^{2-} ligands in $[\mathbf{10}]^+$ for a Cl^- ligand, leading to the formation of $[^{99}TcOCl(\mathbf{L2})_2]^{2+}$ ($[\mathbf{12}]^{2+}$).[78] This reactivity is remarkable, since the $\{^{99}TcO_2\}^+$ core is the thermodynamically most stable metal core for $^{99}Tc^{V}$- and Re^{V}-NHC complexes.[79,83] In addition, this metal core transformation shows the extraordinary and unprecedented stability of the ^{99}Tc-C bonds of ^{99}Tc-NHC complexes comprised of bidentate NHCs. NMR experiments in DMSO-D_6 showed that the reaction is reversible, since reaction of $[\mathbf{12}]^{2+}$ with excess NaOH gives again $[\mathbf{10}]^+$ (Figure 18). Formation of $[^{99}TcO_4]^-$ was not observed in the ^{99}Tc-NMR spectrum, indicating that no decomposition takes place. $[\mathbf{12}]^{2+}$ does not hydrolyze or form $[\mathbf{10}]^+$ at neutral or acidic pH, which was checked by NMR experiments over the course of 2 weeks. Purification of $[\mathbf{12}]^{2+}$ was achieved by crystallization from an acidic acetone/H_2O solution by slow evaporation of the acetone in the presence of NH_4PF_6, which gave green crystals of $[\mathbf{12}](PF_6)_2$ in 28% yield based on $(N^nBu_4)[^{99}Tc(glyc)_2]$ ($(N^nBu_4)[\mathbf{8}]$, **method a**).

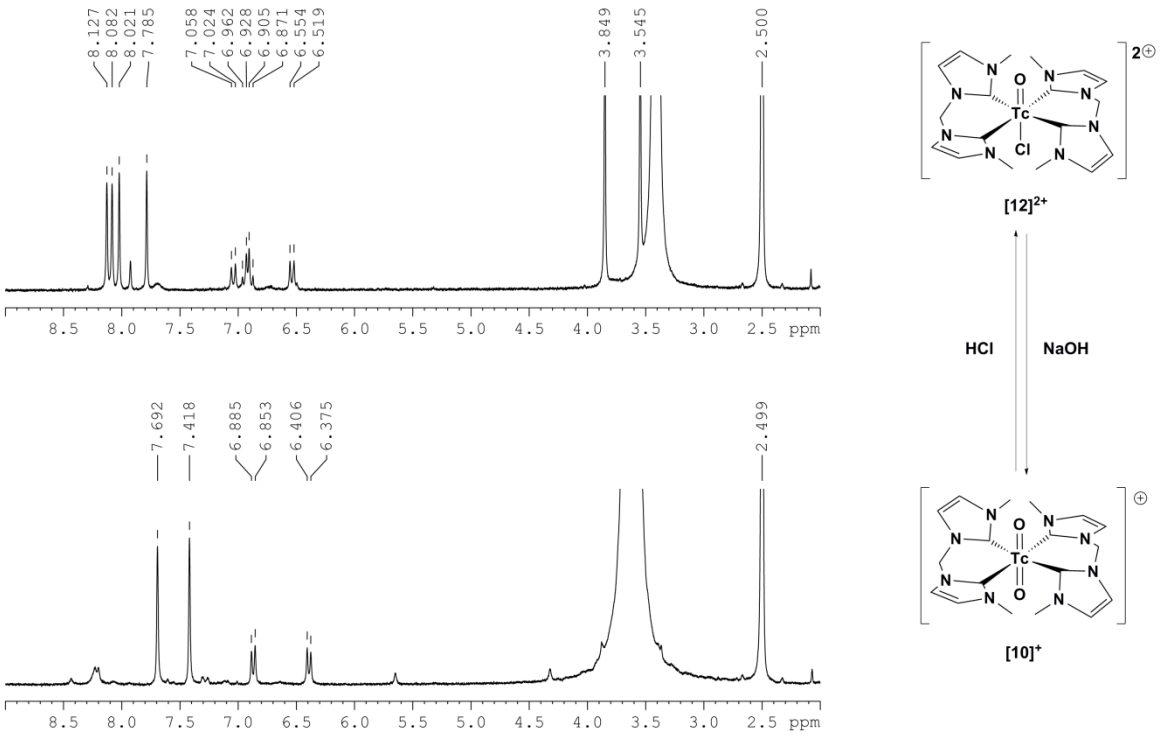

Figure 18: NMR experiment in DMSO-D_6 showing the pH controlled conversion of $[\mathbf{12}]^{2+}$ into $[\mathbf{10}]^+$ using excess NaOH. Formation of $[^{99}TcO_4]^-$ was not observed during this reaction.

The fact that $(\mathbf{L2}\text{-}H_2)_2[\mathbf{8}](PF_6)_3$ precipitates from CH_2Cl_2 was expected to lower the speed of the reaction that leads to formation of $[\mathbf{10}]^+$, which also has an influence on the total yield of $[\mathbf{12}]^{2+}$. In order to facilitate the reaction, DMF was tested as a solvent (**method b**). When $(N^nBu_4)[\mathbf{8}]$ was

dissolved in dry DMF and heated on 70°C in the presence of 2 eq. (**L2**-H_2)$(PF_6)_2$ and excess NEt_3, a color change to green was observed within the first 7.5 h. Reaction control with HPLC showed a conversion of >70% to the product after additional 15.5 h stirring at 25°C. The green color of the solution most likely originated from $[\mathbf{12}]^{2+}$, since the reaction was done in dry DMF and under exclusion of air and moisture which prevents formation of $[\mathbf{10}]^{+}$. Workup of the reaction was done by evaporation of the DMF with a stream of N_2, followed by washing of the crude with several solvents and recrystallization of the crude product from an acidic (1 M HCl) acetone/H_2O solution. A yield of 41% [**12**]$(PF_6)_2$ was achieved (based on (N^nBu_4)[**8**]), which is significantly higher than when CH_2Cl_2 was used as a solvent (**method a**). While the change to DMF as a solvent significantly improved the yield of the reaction, the use of CH_2Cl_2 as a solvent is still preferred due to the easier and faster workup of the reaction.

[**12**]$(PF_6)_2$ crystallizes as green plates in the triclinic space group P1 with two independent dications in the asymmetric unit (Figure 19). Both dications are systematically disordered along the O-^{99}Tc-Cl axis with a ratio of occupancy of 0.71:0.29 and 0.78:0.22. The difference in these occupancy-ratios is the reason for the lack of a centre of inversion in the whole structure, which leads to the observed rare non-centrosymmetric space group P1. Only the major species of one dication will be discussed here in detail. The disordered atoms O(1)/Cl(1b) and O(1b)/Cl(1) are located at the same positions, while the Tc(1a) and Tc(1b) are located above and below the C(1)C(2)C(11)C(12) plane. This leads to a distorted octahedral coordination sphere for the ^{99}Tc centre, which is also observed in the O-^{99}Tc-C angles that significantly differ from 90° (94.43(16) – 102.66(16)°, table 16). The C-^{99}Tc-C bite angles of the **L2** ligands are significantly different, with 81.04(17)° for C(1)-Tc(1a)-C(2) and 82.91(17)° for C(11)-Tc(1a)-C(12). The value for the C(1)-Tc(1a)-C(2) angle is in the same range as the C(1)-Tc(1)-C(1) angle found in $[\mathbf{10}]^{+}$ (81.33(16)°). The Tc(1a)-O(1) bond length is with 1.606(3) Å considerably shorter than in the structure of $[^{99}TcO(glyc)_2]^{-}$ (1.665(7) Å), but the values have to be interpreted with caution due to the disorder along the O-^{99}Tc-Cl axis. The same applies for the Tc(1a)-Cl bond length of 2.4103(15) Å. The ^{99}Tc-C bond lengths (2.131(5) – 2.201(5) Å) show no clear trend when compared to the ^{99}Tc-C bond lengths in $[\mathbf{10}]^{+}$ (2.166(4) and 2.170(4) Å).

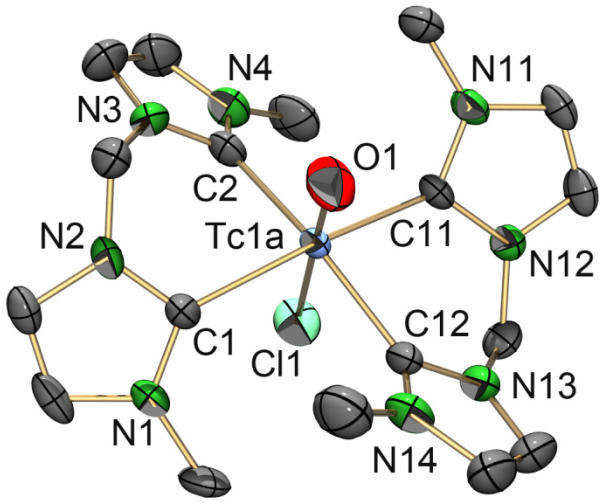

Figure 19: ORTEP representation[51] of the major species in the $[^{99}TcOCl(\mathbf{L2})_2]^{2+}$ ($[\mathbf{12}]^{2+}$) dication of the $[\mathbf{12}](PF_6)_2$ structure. Thermal ellipsoids are represented at the 50% probability level. Hydrogen atoms are omitted for clarity.

Table 16: Selected bond lengths and angles of the major species of $[\mathbf{12}]^{2+}$.

Selected bond lengths [Å]		Selected angles [°]	
Tc(1A)-O(1)	1.606(3)	O(1)-Tc(1A)-Cl(1)	178.52(12)
Tc(1A)-Cl(1)	2.4103(15)	O(1)-Tc(1A)-C(1)	102.66(16)
Tc(1A)-C(1)	2.155(4)	O(1)-Tc(1A)-C(2)	99.74(17)
Tc(1A)-C(2)	2.201(5)	O(1)-Tc(1A)-C(11)	94.43(15)
Tc(1A)-C(11)	2.159(4)	O(1)-Tc(1A)-C(12)	97.16(18)
Tc(1A)-C(12)	2.131(5)	C(1)-Tc(1A)-C(2)	81.04(17)
		C(11)-Tc(1A)-C(12)	82.91(17)

IR spectroscopy of $[\mathbf{12}](PF_6)_2$ shows a strong band at 839 cm^{-1} (PF_6^-) and a characteristic $\nu_{Tc=O}$ band with medium intensity at 985 cm^{-1}. This value is slightly lower than the value found for the comparable $[ReOCl(L^{Et})_4]^{2+}$ (L^{Et} = 1,3-diethyl-4,5-dimethylimidazol-2-ylidene), which has a $\nu_{Tc=O}$ band of 993 cm^{-1}.[79] The NMR spectra of $[\mathbf{12}](PF_6)_2$ are more complex than for $[\mathbf{10}]^+$ due to the loss in symmetry along the tetragonal axis (Figure 18). In the ^1H NMR spectrum, the backbone CH groups appear as four singlets (8.14, 8.09, 8.03 and 7.80 ppm) instead of two in the case of $[\mathbf{10}]^+$ (7.71 and 7.43 ppm). The CH_2 groups are split into two doublets (7.05 and 6.54 ppm) and a doublet of doublets (6.92 ppm) instead of only two doublets for the more symmetrical $[\mathbf{10}]^+$ (6.92 and 6.44 ppm). Due to their different chemical environments, the CH_3 groups pointing in opposite directions of the tetragonal axis have different chemical shifts (3.88 and 3.55 ppm). The protons in $[\mathbf{12}]^{2+}$ are significantly shifted to higher ppm values compared to $[\mathbf{10}]^+$, which is explained by the decreased electron density at the 16 electron ^{99}Tc centre. The ^{13}C NMR spectrum supports these findings, with four signals for the backbone CH groups (125.60, 125.22, 125.15 and 123.36 ppm), two signals for the CH_2 groups (64.16 and 62.38 ppm) and two signals for the CH_3 groups (38.15 and 36.81 ppm). A comparison with the ^{13}C

NMR spectrum of $[\mathbf{10}]^+$ (e.g. the CH groups at 121.56 ppm) again shows that the signals for $[\mathbf{12}]^{2+}$ are shifted to higher ppm values.

The Cl^- ligand in *trans*-position to the O^{2-} ligand enables the derivatization of $[\mathbf{12}]^{2+}$ with anionic ligands, which was demonstrated with MeO^- and SCN^-. Reaction of $[\mathbf{12}](PF_6)_2$ in a 1:1:4 $MeOH/NEt_3/CH_3CN$ solution gave $[^{99}TcO(OMe)(\mathbf{L2})_2]^{2+}$ ($[\mathbf{13}]^{2+}$, scheme 19). Purification of $[\mathbf{13}](PF_6)_2$ was done by precipitation from a CH_3CN solution with Et_2O, followed by washing of the purple solid with CH_2Cl_2, which gave $[\mathbf{13}](PF_6)_2$ with a yield of 97%. The reaction can be followed by a color change from green to purple, which, together with the high yield, suggests a quantitative conversion of $[\mathbf{12}]^{2+}$ to $[\mathbf{13}]^{2+}$. Crystallization of the purple product from a 1:1 MeOH/acetone solution gave purple single crystals of $[\mathbf{13}](PF_6)_2$.

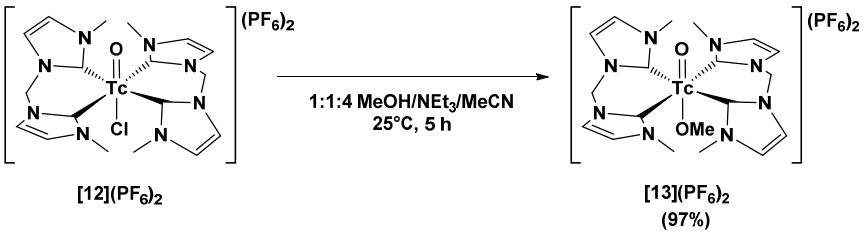

Scheme 19: Synthesis of $[^{99}TcO(OMe)(\mathbf{L2})_2](PF_6)_2$ ($[\mathbf{13}](PF_6)_2$) starting from $[^{99}TcOCl(\mathbf{L2})_2](PF_6)_2$ ($[\mathbf{12}](PF_6)_2$).

$[\mathbf{13}](PF_6)_2$ crystallizes as purple prisms of the composition $[\mathbf{13}](PF_6)_2 \cdot 0.67H_2O$ in the triclinic space group $P\bar{1}$ with two independent dications in the asymmetric unit. One of these dications is systematically disordered along the O-^{99}Tc-O axis with a ratio of occupancy of 0.50:0.50. The equal ratio of occupancy is the reason for the presence of an inversion centre in the structure, since an unequal ratio of occupancy would have resulted in the space group P1. Only the non-disordered dication will be discussed here in detail (Figure 20). In contrast to $[\mathbf{12}]^{2+}$, the ^{99}Tc centre in $[\mathbf{13}]^{2+}$ has a comparably symmetrical octahedral coordination environment, which is observed in the almost linear O-^{99}Tc-O angle (176.2(2)°) and O-^{99}Tc-C angles close to 90° (90.0(2) – 94.0(2)°, table 17). The ^{99}Tc-O bond length of the O^{2-} ligand in $[\mathbf{13}]^{2+}$ (1.659(4) Å) is considerably shorter than the ^{99}Tc-O bond length of $[\mathbf{10}]^+$ (1.765(3) Å), which is in agreement with general trends for $\{^{99}TcO_2\}^+$ and $\{^{99}TcO\}^{3+}$ complexes. Compared to $[\mathbf{12}]^{2+}$ (1.606(3) Å), the ^{99}Tc-O bond length of the O^{2-} ligand in $[\mathbf{13}]^{2+}$ is slightly elongated, while the values have to be interpreted with caution due to the disorder along the tetragonal axis in $[\mathbf{12}]^{2+}$ and $[\mathbf{13}]^{2+}$. The ^{99}Tc-C bond lengths in $[\mathbf{13}]^{2+}$ (2.150(7) – 2.174(6) Å) are in the same range as in $[\mathbf{10}]^+$ (2.166(4) – 2.170(4) Å) and in $[\mathbf{12}]^{2+}$ (2.131(5) – 2.201(5) Å). Consequently, the C-^{99}Tc-C bite angle of **L2** is also in the same range for $[\mathbf{10}]^+$ (81.33(16)°), $[\mathbf{12}]^{2+}$ (81.04(17) and 82.91(17)°) and $[\mathbf{13}]^{2+}$ (81.3(3) and 81.8(2)°). Structurally characterized $\{^{99}TcO(OMe)\}^{2+}$ complexes are rare, with the only two examples being $[^{99}TcO(OMe)(dppd)]$ (dppd-H_2 = N,N'-bis[2-(diphenylphosphino)phenyl]propane-1,3-diamine) and $[^{99}TcO(OMe)(o\text{-apdpp})_2]$ (*o*-apdpp-H = (*o*-aminophenyl)diphenylphosphine).[84,85] The ^{99}Tc-OMe bond length of $[\mathbf{13}]^{2+}$

(1.903(4) Å) is considerably shorter compared to the ^{99}Tc-OMe bond length of [^{99}TcO(OMe)(dppd)] (2.030(2) Å) and [^{99}TcO(OMe)(*o*-apdpp)$_2$] (1.999(8) Å), presumably due to the increased positive charge on the ^{99}Tc centre in [**13**]$^{2+}$. The ^{99}Tc-O-CH$_3$ angle in [**13**]$^{2+}$ (153.9(5)°) is considerably wider than the ^{99}Tc-O-CH$_3$ angle in [^{99}TcO(OMe)(dppd)] (123.1(3)°) and [^{99}TcO(OMe)(*o*-apdpp)$_2$] (124.57°).

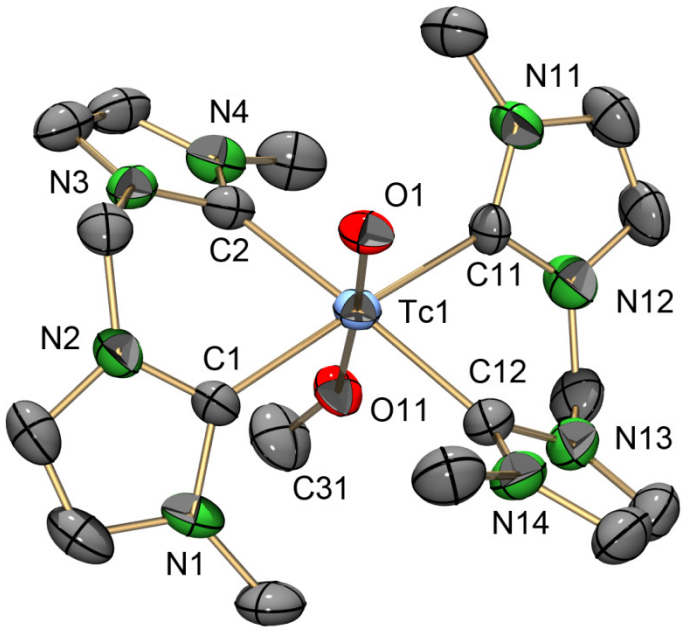

Figure 20: ORTEP representation[51] of the [^{99}TcO(OMe)(**L2**)$_2$]$^{2+}$ ([**13**]$^{2+}$) dication of the [**13**](PF$_6$)$_2$·0.67H$_2$O structure. Thermal ellipsoids are represented at the 50% probability level. Hydrogen atoms are omitted for clarity.

Table 17: Selected bond lengths and angles of [**13**]$^{2+}$.

Selected bond lengths [Å]		Selected angles [°]	
Tc(1)-O(1)	1.659(4)	O(1)-Tc(1)-O(11)	176.2(2)
Tc(1)-O(11)	1.903(4)	O(1)-Tc(1)-C(1)	90.9(2)
Tc(1)-C(1)	2.174(6)	O(1)-Tc(1)-C(2)	91.2(2)
Tc(1)-C(2)	2.170(7)	O(1)-Tc(1)-C(11)	94.0(2)
Tc(1)-C(11)	2.158(6)	O(1)-Tc(1)-C(12)	93.7(2)
Tc(1)-C(12)	2.150(7)	C(1)-Tc(1)-C(2)	81.8(2)
		C(11)-Tc(1)-C(12)	81.3(3)
		C(31)-O(11)-Tc(1)	153.9(5)

IR spectroscopy of [**13**](PF$_6$)$_2$ shows a strong band at 837 cm^{-1} (PF$_6^-$) and the characteristic $\nu_{Tc=O}$ band with medium intensity at 929 cm^{-1}. Compared to the $\nu_{Tc=O}$ band of [**12**](PF$_6$)$_2$ (985 cm^{-1}), this band is considerably shifted to lower wavenumbers, indicating a stronger donation of the OMe$^-$ ligand compared to the Cl$^-$ ligand, which leads to a weaker ^{99}Tc-O bond in [**13**](PF$_6$)$_2$. The shift to lower wavenumbers of the $\nu_{Tc=O}$ band in [**13**](PF$_6$)$_2$ is in agreement with the elongation of the ^{99}Tc-O bond of

the O^{2-} ligand described in the discussion of the X-ray structure. NMR spectroscopy of [**13**]$(PF_6)_2$ in DMF-D_7 gives similar spectra as for [**12**]$(PF_6)_2$. In the ^{1}H NMR spectrum, the backbone CH groups appear as four poorly resolved doublets (8.17, 8.14, 7.93 and 7.84 ppm). Four doublets are also observed for the CH_2 groups (7.14, 7.03, 6.81 and 6.55 ppm), while the NCH_3 groups are found as singlets at 4.00 and 3.78 ppm. These chemical shifts are very similar to the chemical shifts observed in the NMR spectrum of [**12**]$(PF_6)_2$. The signal of the OCH_3^- ligand is observed as a singlet at 2.70 ppm. The ^{13}C NMR also resembles the spectrum of [**12**]$(PF_6)_2$, with the exception of the OCH_3^- signal at 58.04 ppm. Compared to the chemical shift of MeOH in the ^{13}C NMR (48.59 ppm,[56] measured in DMSO-D_6), the observed signal of the MeO^- ligand is shifted to higher ppm values upon coordination to the ^{99}Tc.

Besides derivatization with MeO^-, reactions with SCN^- were also tested. Reaction of [$^{99}TcO_2$(**L2**)$_2$](PF_6) in 3:1 acetone/H_2O with 1 M HCl and an excess of NaSCN in the presence of NH_4PF_6 gave [^{99}TcO(NCS)(**L2**)$_2$]$(PF_6)_2$ ([**14**]$(PF_6)_2$, scheme 20). [**14**]$(PF_6)_2$ was obtained as green crystals that are suitable for X-ray diffraction analysis after slow evaporation of the acetone from the aqueous solution, with a yield of 58%. The use of HCl in the reaction is necessary to protonate one of the O^{2-} ligands, which then is exchanged for an NCS^-. With an approximately 18-fold excess of NCS^- over Cl^-, formation of $[\mathbf{12}]^{2+}$ as a side product was kinetically unfavored and not observed.

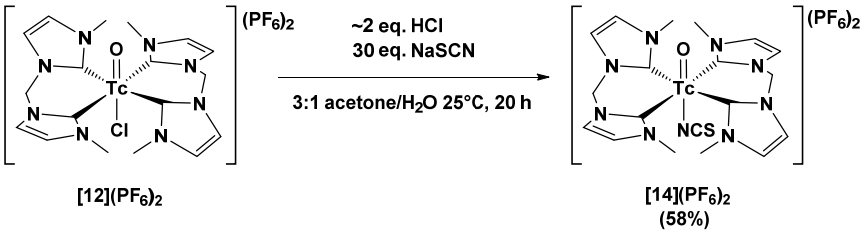

Scheme 20: Synthesis of [^{99}TcO(NCS)(**L2**)$_2$]$(PF_6)_2$ ([**14**]$(PF_6)_2$) starting from [^{99}TcOCl(**L2**)$_2$]$(PF_6)_2$ ([**12**]$(PF_6)_2$).

[**14**]$(PF_6)_2$ crystallizes as green blocks of the composition [**14**]$(PF_6)_2$·2acetone in the triclinic space group P1 (Figure 21). The dication is systematically disordered along the O-^{99}Tc-NCS axis with a ratio of occupancy of 0.91:0.09. This disorder is the reason for the lack of a centre of inversion, which leads to the observed rare non-centrosymmetric space group P1. Due to this crystallographic finding, only the major species of the O^{2-} and NCS^- ligands could be refined, while the disorder was fully refined for the ^{99}Tc centre. Only the major species will be discussed here in detail. The ^{99}Tc-O bond length (1.641(2) Å, table 18) is elongated compared to the corresponding bond length in $[\mathbf{12}]^{2+}$ (1.606(3) Å), although these values may be influenced by the refinement of the disorders. The ^{99}Tc-C bond lengths in $[\mathbf{14}]^{2+}$ (2.145(2) – 2.169(2) Å) are in a similar range as in $[\mathbf{12}]^{2+}$ (2.131(5) – 2.201(5) Å). The structure shows that the NCS^- ligand is bound over the nitrogen, which is explained within the Pearson acid base (hard and soft Lewis acid and base) theory by the hard Lewis acidity of the $^{99}Tc^V$ centre.[86] Since there are no published structurally characterized $\{M^VO\}^{3+}$-NHC (M = Re, ^{99}Tc) complexes

containing NCS^- ligands, a comparison to $[^{99}TcO(NCS)(CN)_4]^{2-}$ will be made.[86] $[^{99}TcO(NCS)(CN)_4]^{2-}$ has a ^{99}Tc-N bond length of 2.162(9) Å, which is in the same range as the corresponding bond in $[\mathbf{14}]^{2+}$ (2.155(2) Å). The ^{99}Tc-N-C angle in $[^{99}TcO(NCS)(CN)_4]^{2-}$ (169.5(12)°) is considerably different from the ^{99}Tc-N-C angle found in $[\mathbf{14}]^{2+}$ (159.2(2)°), which underlines the often observed variance in binding geometries of complexes containing thiocyanate ligands.[87,88] The N(41)-C(41) bond length (1.131(4) Å) and the almost linear N(41)-C(41)-S(41) angle (177.8°) in $[\mathbf{14}]^{2+}$ are in line with values reported in literature and show the general invariance of the thiocyanate ligand in terms of its own structural geometry.[87,88]

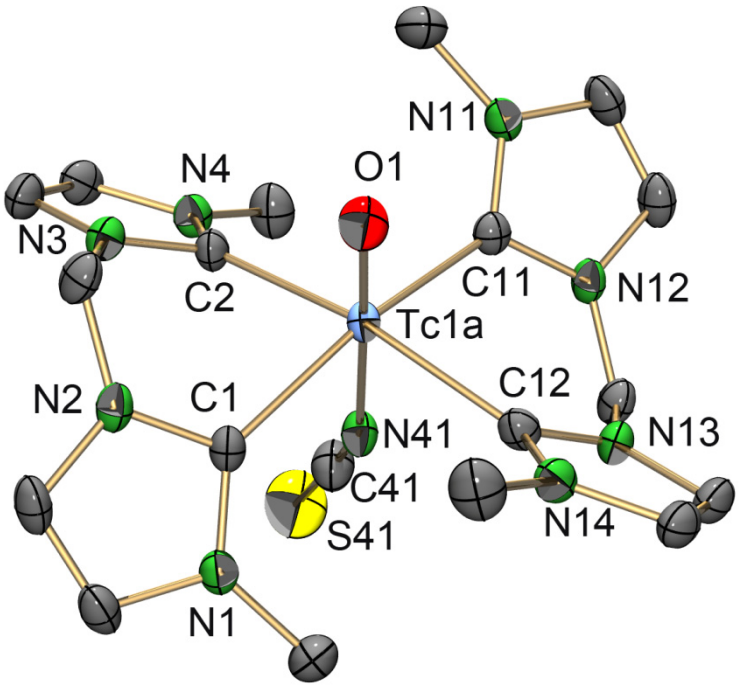

Figure 21: ORTEP representation[51] of the major species in the $[^{99}TcO(NCS)(\mathbf{L2})_2]^{2+}$ ($[\mathbf{14}]^{2+}$) dication of the $[\mathbf{14}](PF_6)_2 \cdot 2$acetone structure. Thermal ellipsoids are represented at the 50% probability level. Hydrogen atoms are omitted for clarity.

Table 18: Selected bond lengths and angles of the major species of $[\mathbf{14}]^{2+}$.

Selected bond lengths [Å]		Selected angles [°]	
Tc(1A)-O(1)	1.641(2)	O(1)-Tc(1A)-N(41)	177.29(10)
Tc(1A)-C(1)	2.158(2)	O(1)-Tc(1A)-C(1)	99.21(10)
Tc(1A)-C(2)	2.169(2)	O(1)-Tc(1A)-C(2)	96.17(10)
Tc(1A)-C(11)	2.145(2)	O(1)-Tc(1A)-C(11)	96.28(10)
Tc(1A)-C(12)	2.157(3)	O(1)-Tc(1A)-C(12)	98.16(10)
Tc(1A)-N(41)	2.155(2)	C(1)-Tc(1A)-C(2)	81.20(9)
N(41)-C(41)	1.131(4)	C(11)-Tc(1A)-C(12)	82.23(9)
		C(41)-N(41)-Tc(1A)	159.2(2)
		N(41)-C(41)-S(41)	177.8(3)

IR spectroscopy of [**14**]$(PF_6)_2$ shows several characteristic bands. The strong band at 844 cm^{-1} corresponds to the PF_6^- anion. Two bands were found in the characteristic range for the ν_{CN} band of the NCS^- ligand, a band with medium intensity at 2028 cm^{-1} and a band with strong intensity at 2067 cm^{-1}, respectively. In addition, two bands with medium intensities were found in the region characteristic for the $\nu_{Tc=O}$ band, at 984 and 997 cm^{-1}, respectively. The fact that two bands were observed in each of the characteristic regions makes an unambiguous assignment of the $\nu_{Tc=O}$ and ν_{CN} bands difficult. This fact also prompts questions about the purity of the sample. However, NMR studies of [**14**]$(PF_6)_2$ confirmed a high purity of the sample, since only one set of signals was found. In addition, crystal structure analysis of several crystals of the isolated [**14**]$(PF_6)_2$ showed only the observed unit cell for the [**14**]$(PF_6)_2$·2acetone structure described above. A comparison to $[^{99}TcO(NCS)(CN)_4]^{2-}$ (ν_{CN} band of NCS^- ligand = 2066 cm^{-1}, $\nu_{Tc=O}$ band =1004 cm^{-1}) suggests that the ν_{CN} band of [**14**]$(PF_6)_2$ is found at 2067 cm^{-1}, while the $\nu_{Tc=O}$ band of [**14**]$(PF_6)_2$ is presumably found at 984 cm^{-1}.[86] NMR spectroscopy of crystalline [**14**]$(PF_6)_2$ in DMF-D_7 confirmed that only one product is formed in the reaction. In the ^1H NMR spectrum, four poorly resolved doublets are observed for the CH groups (8.37, 8.33, 8.23 and 8.00 ppm). These signals are slightly shifted to higher ppm values compared to the CH signals of $[\mathbf{12}]^{2+}$ (8.14 – 7.80 ppm) and $[\mathbf{13}]^{2+}$ (8.17 – 7.84 ppm). As it was the case for $[\mathbf{12}]^{2+}$ and $[\mathbf{13}]^{2+}$, the CH_2 groups are observed as four doublets (7.43, 7.36, 6.89 and 6.51 ppm) and the CH_3 groups are observed as two singlets (4.09 and 3.71 ppm). In the ^{13}C NMR spectrum, the signal of the NCS^- ligand is observed at 144.54 ppm and in addition, a low intensity signal of unbound NCS^- is also observed at 130.96 ppm, which presumably is due to the fact that NCS^- is present as an anionic trace impurity ($(NH_4)(SCN)$: δ = 130.40 ppm in DMSO-D_6[57]). Unfortunately, the ^{13}C NMR spectrum of $[^{99}TcO(NCS)(CN)_4]^{2-}$ was not reported in literature and, to the best of the author's knowledge, no other ^{13}C NMR exists for ^{99}Tc-NCS complexes.[86] As it was described before, the ^{99}Tc-C signals of $[\mathbf{14}]^{2+}$ were poorly resolved and were thus not assigned in the spectrum.

In addition to the standard analysis of [**12**]$(PF_6)_2$ – [**14**]$(PF_6)_2$, ultraviolet–visible (UV-Vis) spectroscopy was done, including a comparison to [**10**](PF_6). Measurements were done in CH_3CN with different concentrations depending on the compound. For this comparison, 0.1 – 0.125 mM and 1.5 – 1.75 mM solutions of $[\mathbf{10}]^+$ and $[\mathbf{12}]^{2+}$ – $[\mathbf{14}]^{2+}$ were prepared by dilution of aliquots of stock solutions, while the concentrations of the stock solutions were determined using liquid scintillation counting. The results of the measurements at these concentrations are shown in figure 22.

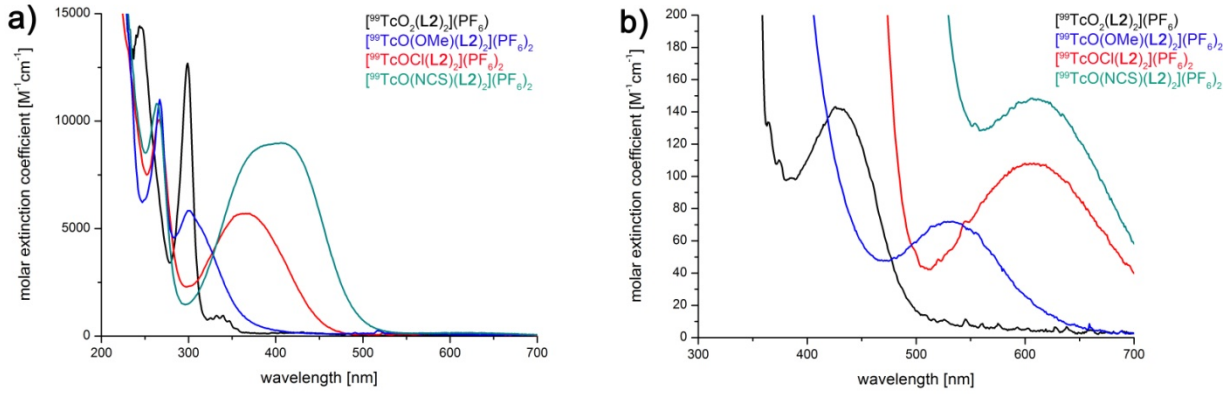

Figure 22: UV-Vis spectra of $[\mathbf{10}]^{+}$ and $[\mathbf{12}]^{2+}$ – $[\mathbf{14}]^{2+}$ at concentrations of 0.1 – 0.125 mM (a)) and 1.5 – 1.75 mM (b)).

The UV-Vis spectra at low concentrations show strong and broad absorption bands for $[\mathbf{12}]^{2+}$ – $[\mathbf{14}]^{2+}$ in the region of 300 – 500 nm and a strong and relatively narrow absorption band with a maximum at 298 nm for $[\mathbf{10}]^{+}$ (Figure 22, a)). These absorptions are most likely due to ligand-to-metal charge-transfer (LMCT) processes, since they have a high molar extinction coefficient (ε) and the ^{99}Tc is in a high oxidation state. In contrast, the measurements with higher concentrations showed weak absorptions between 500 – 700 nm for $[\mathbf{12}]^{2+}$ – $[\mathbf{14}]^{2+}$ and a band with absorption maximum at 426 nm for $[\mathbf{10}]^{+}$ (Figure 22 b)). Due to their low intensity, these absorptions are assigned to d – d transitions. The qualitative analysis with UV-Vis spectroscopy agrees well with the observed color and intensity of the crystalline samples. For example, $[\mathbf{10}]^{+}$ and $[\mathbf{13}]^{2+}$ have low intensity colors due to the strong LMCT band being outside of the visible spectrum, while $[\mathbf{12}]^{2+}$ and $[\mathbf{14}]^{2+}$ have very intense colors, which is in agreement with the observed intense and broad LMCT band of $[\mathbf{12}]^{2+}$ and $[\mathbf{14}]^{2+}$ in the visible region. Table 19 shows a comparison of the UV-Vis data of the studied complexes.

Table 19: Comparison of UV-Vis data of $[\mathbf{10}]^{+}$ and $[\mathbf{12}]^{2+}$ – $[\mathbf{14}]^{2+}$.

Compound	ε_{LMCT} [$M^{-1}cm^{-1}$] (λ_{max} [nm])	$\varepsilon_{d\text{-}d}$ [$M^{-1}cm^{-1}$] (λ_{max} [nm])
$[\mathbf{10}]^{+}$	12598 (298)	143 (426)
$[\mathbf{12}]^{2+}$	5701 (370)	108 (608)
$[\mathbf{13}]^{2+}$	5831 (301)	72 (529)
$[\mathbf{14}]^{2+}$	8995 (406)	148 (606)

While the exchange reactions starting from $[^{99}TcOCl(\mathbf{L2})_2]^{2+}$ were successful for MeO^- and NCS^-, this reaction has important limitations (Scheme 21). If coordination is expected to be slow, i.e. in the case of sterically demanding ligands, trace amounts of H_2O lead under basic conditions to the formation of $[^{99}TcO_2(\mathbf{L2})_2]^{+}$. This was observed when $[^{99}TcOCl(\mathbf{L2})_2]^{2+}$ was reacted with *L*-serine methyl ester hydrochloride in a 20:1 CH_3CN/NEt_3 solution, since only $[^{99}TcO_2(\mathbf{L2})_2]^{+}$ was found after the reaction. This problem was circumvented in the reaction with NCS^- described above, which was done in an

acidic aqueous solution. However, such an approach is only viable for anions that are not protonated under these conditions, which excludes many functional groups from this method. The stability of $[^{99}TcOX(\mathbf{L2})_2]^{2+}$ type complexes (X = anionic ligand) might be an additional problem, which became evident when thiophenol (PhSH) was reacted directly with $[^{99}TcO_2(\mathbf{L2})_2]^{+}$. The initially purple solution, which potentially contained $[^{99}TcO(SPh)(\mathbf{L2})_2]^{2+}$, slowly decomposed to a brown suspension containing colorless crystals within days and no product could be isolated. Decomposition might in this case have been caused by the oxidation of the thiolate ligands, leading to diphenyl disulfide and $^{99}Tc^{IV}O_2$. Besides being a suitable starting material for substitution reactions, $[^{99}TcOCl(\mathbf{L2})_2]^{2+}$ was also tested for its potential regarding the synthesis of the isoelectronic imine complex $[^{99}Tc(NPh)Cl(\mathbf{L2})_2]^{2+}$ using tetraphenylphosphine imide ($PhNPPh_3$). The reaction of $[^{99}TcOCl(\mathbf{L2})_2]^{2+}$ with excess $PhNPPh_3$ appeared to be very slow, since HPLC analysis showed complete conversion to product after approximately 5 days despite several 8 h intervals of heating to 90°C each day. Unfortunately, isolation and characterization of the supposedly formed $[^{99}Tc(NPh)Cl(\mathbf{L2})_2]^{2+}$ from the crude product was not possible due to lack of time for this side project. Another interesting reaction was done using N_3^- as a ligand for the position *trans* to the O^{2-} ligand. The reaction procedure was adapted from a literature procedure described by Abram *et al.*, in which [ReOCl(TSC)] (TSC = thiosemicarbazone derivative) was reacted with NaN_3 in a CH_2Cl_2/MeOH mixture.[89] The resulting $[ReO(N_3)(TSC)]$ was stable as a solid, but decomposed in solution to form the dimeric nitrido complex $[\{ReN(TSC\text{-}H)\}_2O]$ which is bridged by an O^{2-} ligand. Following this approach, $[^{99}TcOCl(\mathbf{L2})_2]^{2+}$ was reacted with 10 eq. NaN_3 in CH_3CN. Since no reaction was observed, MeOH was added to the reaction solution following the above described procedure for Re, leading to a color change from green to red-purple within 2 h at 25°C. However, IR and NMR spectroscopy after workup of this red-purple compound showed that $[^{99}TcO(OMe)(\mathbf{L2})_2]^{2+}$ had formed during the reaction. No evidence was found in the IR or NMR spectra that $[^{99}TcO(N_3)(\mathbf{L2})_2]^{2+}$ or a corresponding nitrido complex had formed. A second attempt of the reaction of $[^{99}TcOCl(\mathbf{L2})_2]^{2+}$ with NaN_3 in DMF was tested, but only $[^{99}TcOCl(\mathbf{L2})_2]^{2+}$ and $[^{99}TcO_2(\mathbf{L2})_2]^{+}$ were recovered from the solution. In a third attempt, the reaction principle of the preparation of $[^{99}TcO(NCS)(\mathbf{L2})_2]^{2+}$ was used. In this reaction, an aqueous solution of $[^{99}TcO_2(\mathbf{L2})_2]^{+}$ was acidified using HCl and an excess of NaN_3 was added. Again, only $[^{99}TcOCl(\mathbf{L2})_2]^{2+}$ could be isolated. These results indicate that the formation of $[^{99}TcO(N_3)(\mathbf{L2})_2]^{2+}$ is not favoured over the formation of $[^{99}TcOCl(\mathbf{L2})_2]^{2+}$ under the tested conditions. This also prohibited the formation of a corresponding nitrido complex, even if it would have formed from the corresponding azido complex.

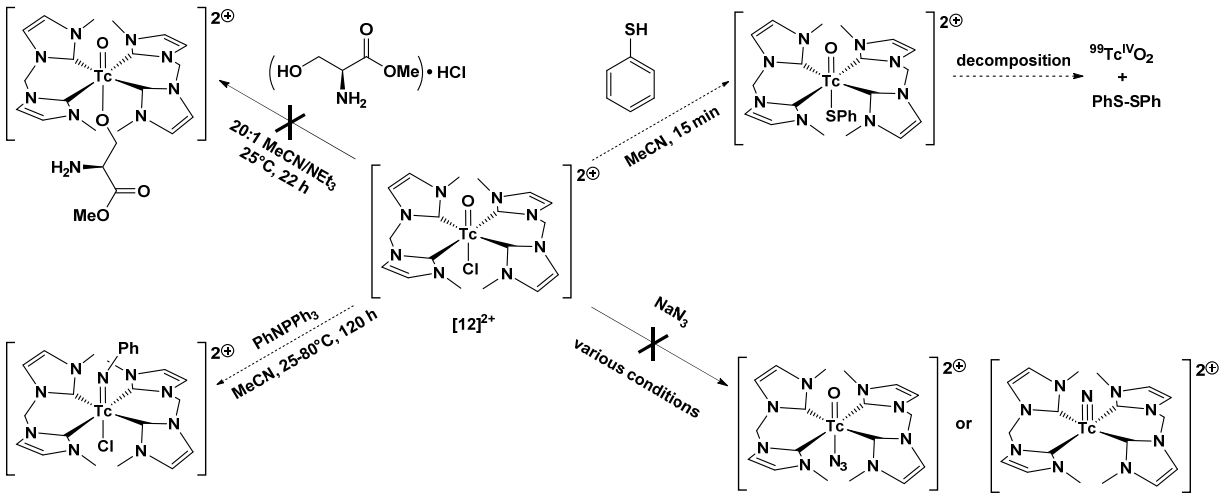

Scheme 21 Synthetic limitations of the derivatization of $[^{99}TcOCl(\mathbf{L2})_2]^{2+}$ ($[\mathbf{12}]^{2+}$) in the position *trans* to the O^{2-} ligand. Dashed arrows indicate tested reactions that produced promising results, but characterization and unambiguous identification of the compounds were not possible.

A particularly exotic product was found when the crude product of a reaction of $[^{99}TcOCl(\mathbf{L2})_2]^{2+}$ with boc-*L*-serine benzyl ester (boc-ser-OBz-H, boc = COO^tBu) was slowly crystallized. The reaction of $[^{99}TcOCl(\mathbf{L2})_2]^{2+}$ with boc-ser-OBz-H and NEt_3 was done in DMF, which was evaporated after the reaction using a stream of N_2. The crude product was then dissolved in CH_2Cl_2 and allowed to slowly evaporate over the course of several weeks, which resulted in the formation of single-crystalline red needles. X-ray analysis of these red needles confirmed that the product was not the desired $[^{99}TcO(\text{boc-ser-OBz})(\mathbf{L2})_2]^{2+}$. Instead, an unexpected trinuclear $\{^{99}TcO_2\}^+$-NHC complex of the composition $[^{99}Tc_3O_3(\mu\text{-}O)_3(\mu\text{-}CHO_2)(\mathbf{L2})_3(^{Me}Im)](PF_6)_2 \cdot 3CH_2Cl_2$ (^{Me}Im = 1-methylimidazole, CHO_2 = formate) had formed, which crystallized in the triclinic space group $P\bar{1}$ (Scheme 22).

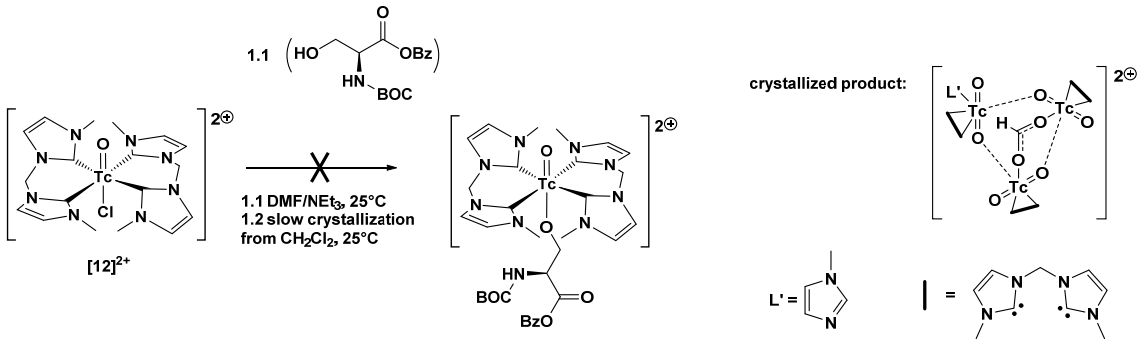

Scheme 22: Reaction of $[^{99}TcOCl(\mathbf{L2})_2]^{2+}$ with boc-*L*-serine benzyl ester resulted in the formation of the trinuclear complex $[^{99}Tc_3O_3(\mu\text{-}O)_3(\mu\text{-}CHO_2)(\mathbf{L2})_3(^{Me}Im)]^{2+}$. The given schematic representation of $[^{99}Tc_3O_3(\mu\text{-}O)_3(\mu\text{-}CHO_2)(\mathbf{L2})_3(^{Me}Im)]^{2+}$ is simplified to illustrate the observed differences in the ^{99}Tc-O bond lengths of the bridging O^{2-} ligands.

The structure of the dication contains three $\{^{99}TcO_2(\mathbf{L2})\}^+$ fragments, that contain one terminal and one bridging O^{2-} ligand (Figure 23). The remaining 3 coordination sites are occupied by a bridging formate ligand and a 1-methylimidazole ligand that is bound over the N atom. Formation of formate is explained by the hydrolysis of DMF in the presence of NEt_3,[90,91] while 1-methylimidazole is presumably formed by decomposition of **L2**.[72] The ^{99}Tc-O bond lengths of the terminal O^{2-} ligands (1.719(5) – 1.721(5) Å, table 20) are shorter than in $[^{99}TcO_2(\mathbf{L2})_2]^+$ (1.765(3) Å) and longer than in $[^{99}TcO(OMe)(\mathbf{L2})_2]^{2+}$ (1.659(4) Å). The O^{2-} ligands asymmetrically bridge the ^{99}Tc centres (1.795(5) – 1.807 Å and 2.090(5) – 2.131(5) Å). The trinuclear complex is therefore formally best represented by three $\{^{99}TcO_2(\mathbf{L2})\}^+$ units that are loosely connected over one of the O^{2-} ligands. The ^{99}Tc-C bond lengths (2.060(7) – 2.127(7) Å) are shorter than in $[^{99}TcO_2(\mathbf{L2})_2]^+$ (2.166(4) and 2.170(4) Å) and $[^{99}TcOX(\mathbf{L2})_2]^{2+}$ (X = Cl, OMe, NCS; 2.131(5) – 2.201(5) Å), which is explained by the reduced steric interactions of the methyl substituents of **L2** in the trinuclear complex. The ^{99}Tc centres have a distorted octahedral coordination environment. The O-^{99}Tc-O angles (168.0(2) – 175.4(2)°) are slightly bent, while the ^{99}Tc-O-^{99}Tc angles are considerably bent (139.7(3) – 154.1(3)°). A comparable trinuclear Re complex, $[Re_3O_3(\mu\text{-}O)_3Cl_3(DPMA\text{-}H_2)_3]$ (DPMA-H_2 = 2-(diphenylphosphinomethyl)-aniline)), is to the best of the author's knowledge the only comparable group 7 complex that has been structurally characterized.[92] The structure of $[Re_3O_3(\mu\text{-}O)_3Cl_3(DPMA\text{-}H_2)_3]$ resembles the structure of the presented trinuclear ^{99}Tc-NHC complex and the Re-O bond lengths of the terminal O^{2-} ligands (1.659(8) – 1.740(9) Å) are shorter than the Re-O bond lengths of the asymmetrically shared bridging O^{2-} ligands (1.817(8) – 1.952(8) Å and 2.050(8) – 2.133(8) Å). The Re-O-Re angles (138.7(4) – 160.1(4)°) are also comparable to the ^{99}Tc-O-^{99}Tc angles in the trinuclear ^{99}Tc-NHC complex (139.7(3) – 154.1(3)°).

The synthesis of $[^{99}TcOX(\mathbf{L2})_2]^{2+}$ complexes (X = Cl, OMe, NCS) starting from $[^{99}TcO_2(\mathbf{L2})_2]^+$ provides an interesting strategy for the derivatization of ^{99}Tc-NHC complexes. Unfortunately, the synthetic limitations of the presented reactions render these complexes impractical for an application with ^{99m}Tc due to their susceptibility to form $[^{99m}TcO_2(\mathbf{L2})_2]^+$ in the presence of large quantities of H_2O or trace amounts of OH^-. However, the reactions might have interesting implications for the *in vivo* chemistry of $[^{99m}TcO_2(\mathbf{L2})_2]^+$, since the dioxo core is not chemically innocent towards changes in pH and might react with many functional groups that are present *in vivo*. Besides this, the synthesis and derivatization of $[^{99}TcO_2(\mathbf{L2})_2]^+$ under neutral and acidic conditions are also relevant for high-valent Re-NHC chemistry and the corresponding reactions are presented in the next chapter.

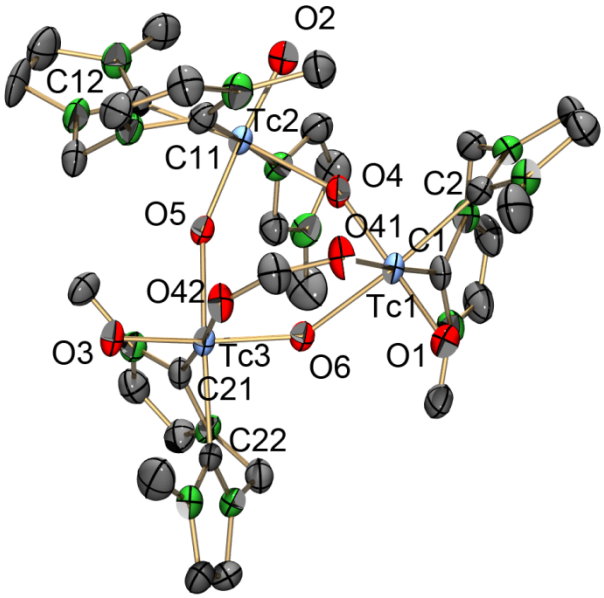

Figure 23: ORTEP representation[51] of the $[^{99}Tc_3O_3(\mu\text{-}O)_3(\mu\text{-}CHO_2)(\mathbf{L2})_3(^{Me}Im)]^{2+}$ dication of the $[^{99}Tc_3O_3(\mu\text{-}O)_3(\mu\text{-}CHO_2)(\mathbf{L2})_3(^{Me}Im)](PF_6)_2{\cdot}3CH_2Cl_2$ structure. Thermal ellipsoids are represented at the 50% probability level. Hydrogen atoms are omitted for clarity.

Table 20: Selected bond lengths and angles of $[^{99}Tc_3O_3(\mu\text{-}O)_3(\mu\text{-}CHO_2)(\mathbf{L2})_3(^{Me}Im)]^{2+}$.

Selected bond lengths [Å]		Selected angles [°]	
Tc(1)-O(1)	1.721(5)	O(1)-Tc(1)-O(4)	173.0(3)
Tc(2)-O(2)	1.721(5)	O(2)-Tc(2)-O(5)	175.4(2)
Tc(3)-O(3)	1.719(5)	O(3)-Tc(3)-O(6)	168.0(2)
Tc(1)-O(4)	1.795(5)	O(1)-Tc(1)-C(1)	95.2(3)
Tc(2)-O(5)	1.807(5)	O(1)-Tc(1)-C(2)	92.1(3)
Tc(3)-O(6)	1.799(4)	O(2)-Tc(2)-C(11)	93.6(3)
Tc(1)-O(6)	2.131(5)	O(2)-Tc(2)-C(12)	95.4(3)
Tc(2)-O(4)	2.090(5)	O(3)-Tc(3)-C(21)	93.1(3)
Tc(3)-O(5)	2.109(5)	O(3)-Tc(3)-C(22)	92.1(3)
Tc(1)-C(1)	2.085(8)	C(1)-Tc(1)-C(2)	83.8(3)
Tc(1)-C(2)	2.119(7)	C(11)-Tc(2)-C(12)	82.9(3)
Tc(2)-C(11)	2.090(7)	C(21)-Tc(3)-C(22)	83.7(3)
Tc(2)-C(12)	2.105(7)	Tc(1)-O(4)-Tc(2)	154.1(3)
Tc(3)-C(21)	2.060(7)	Tc(2)-O(5)-Tc(3)	153.7(3)
Tc(3)-C(22)	2.127(7)	Tc(3)-O(6)-Tc(1)	139.7(3)
Tc(1)-O(41)	2.212(5)		
Tc(3)-O(42)	2.247(5)		

4.2.2.3 Synthesis of $[ReO_2(L2)_2]^+$ and its Derivatives

Following the preparation of $[^{99}TcO_2(\mathbf{L2})_2](PF_6)$, the synthesis was translated to Re chemistry. The corresponding starting material, $(N^nBu_4)[ReO(glyc)_2]$ (glyc = ethylene glycolato, $(N^nBu_4)[\mathbf{15}]$), was prepared in analogy to the previously described $(N^nBu_4)[^{99}TcO(glyc)_2]$ ($(N^nBu_4)[\mathbf{8}]$).[75,93,94] Wieghardt *et al.* reported the formation of $[ReO(glyc)(tacn)]^+$ (tacn = 1,4,7-triazacyclononane) from $[ReOCl_3(PPh_3)_2]$ by reaction with glyc-H_2 and tacn in THF, which was described to presumably proceed via the intermediate $[ReOCl_2(tacn)]^+$.[94,95] However, Tisato *et al.* suggested formation of $(N^nBu_4)[\mathbf{15}]$ as an intermediate in the formation of [ReOCl(TSB)] (TSB = tetradentate N_2O_2 Schiff base) from $(N^nBu_4)[ReOCl_4]$ by reaction with glyc-H_2 and the corresponding TSB^{2-} ligand under basic conditions.[93]

Starting from $(N^nBu_4)[ReOCl_4]$, $(N^nBu_4)[\mathbf{15}]$ was prepared in analogy to the ^{99}Tc complex by addition of glyc-H_2 and NEt_3 in THF. At ambient conditions, the decomposition of $[\mathbf{15}]^-$ was observed, since solutions became colorless within 15 min, indicating formation of $[ReO_4]^-$. This is a major difference compared to $[\mathbf{8}]^-$, which is stable at the same conditions. Therefore, the synthesis of $(N^nBu_4)[\mathbf{15}]$ had to be done under exclusion of air and moisture and was done in a glovebox system. Furthermore, solutions containing $(N^nBu_4)[\mathbf{15}]$ were directly used after preparation, as it was the case for $(N^nBu_4)[\mathbf{8}]$. In order to confirm the structure of the starting material, it was crystallized from THF inside the glovebox. $(N^nBu_4)[\mathbf{15}]$ crystallizes in the triclinic space group $P\bar{1}$ and is isostructural to $[\mathbf{8}]^-$ (Figure 24). The Re(1)-O(1) bond length (1.685(6) Å, table 21) is slightly elongated compared to the $^{99}Tc(1)$-O(1) bond length in $[\mathbf{8}]^-$ (1.665(7) Å), which is also true for the M-O bond lengths to the glycolato ligands (M = Re: 1.943(6) – 1.956(5) Å, M = ^{99}Tc: 1.932(3) Å).

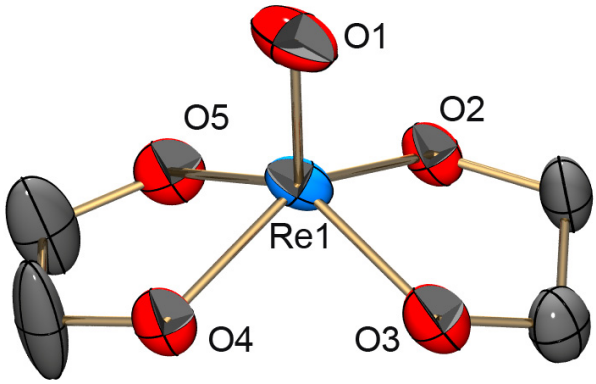

Figure 24: ORTEP representation[51] of the $[ReO(glyc)_2]^-$ ($[\mathbf{15}]^-$) anion of the $(N^nBu_4)[\mathbf{15}]$ structure. Thermal ellipsoids are represented at the 50% probability level. Hydrogen atoms are omitted for clarity.

Table 21: Selected bond lengths and angles of [**15**]$^-$.

Selected bond lengths [Å]		Selected angles [°]	
Re(1)-O(1)	1.685(6)	O(1)-Re(1)-O(2)	108.1(3)
Re(1)-O(2)	1.955(5)	O(1)-Re(1)-O(4)	110.0(3)
Re(1)-O(3)	1.943(6)	O(2)-Re(1)-O(5)	85.8(2)
Re(1)-O(4)	1.956(5)	O(3)-Re(1)-O(4)	83.8(2)
Re(1)-O(5)	1.948(6)	O(2)-Re(1)-O(3)	81.6(2)
		O(4)-Re(1)-O(5)	80.9(2)

Reaction of (N^nBu_4)[**15**] with 2 eq. **L2** in THF led to a color change to purple. This is a significant difference compared to the reaction with ^{99}Tc, in which a color change from purple to yellow-orange was observed. The purple compound did not retain its molecular structure at ambient conditions, which was observed when it was dissolved in non-dry CH_3CN and a color change from purple to orange occurred. HR-ESI$^+$ (HR = high resolution) measurements of this CH_3CN solution showed an intense peak at m/z = 571.15731, which corresponds to $[ReO_2(\mathbf{L2})_2]^+$ ([**16**]$^+$, calculated m/z = 571.15800). The fact that [**16**]$^+$ did not form directly after the addition of **L2** is explained by the strict exclusion of moisture due to the sensitivity of [**15**]$^-$, which prevents formation of the $\{ReO_2\}^+$ core from the $\{ReO\}^{3+}$ core by coordination and subsequent deprotonation of traces of H_2O. While the identity of the purple intermediate could not be revealed, it presumably has the composition $[ReO(X)(\mathbf{L2})_2]^{n+}$ (X = Cl, n = 2 or X = glyc, n = 1). Slow crystallization of crude purple compound at ambient conditions gave crystals of *cis*- and *trans*-[**16**]$^+$. Formation of the *cis*-product is unexpected, since *cis*-$\{ReO_2\}^+$ compounds are rare. Their rarity is explained by the fact that the *trans*-$\{ReO_2\}^+$ complexes are thermodynamically more stable. The only other structurally characterized hexacoordinate *cis*-$\{ReO_2\}^+$ compounds are $[ReO_2(OH_2)(Me_3tacn)]^+$ (Me_3tacn = 1,4,7-trimethyl-1,4,7-triazacyclononane),[96] $[ReO_2(dab\text{-}H)(py)_2]$ (dab-H_2 = 1,2-diaminobenzene, py = pyridine),[97] $[ReO_2(bipy)(py)_2]^+$ [98] (bipy = 2,2'-bipyridine) and $[ReO_2(cat)_2]^-$ (cat-H_2 = catechol).[99]

Cis-[**16**]$^+$ crystallizes as yellow blocks of the composition [**16**](Cl)·H_2O in the monoclinic space group C2. The crystal structure shows the Λ-enantiomer of *cis*-[**16**]$^+$ (Figure 25). *Cis*-[**16**]$^+$ has a distorted octahedral geometry and most angles between neighboring ligands deviate significantly from 90°, with the exception of the O(1)-Re(1)-C(1)' angle (89.8(3)°, table 22). The O-Re-O angle in this structure (84.0(4)°) is very small compared to $[ReO_2(OH_2)(Me_3tacn)]^+$ (106.7(5)°),[96] $[ReO_2(dab\text{-}H)(py)_2]$ (118.2(3)°),[97] $[ReO_2(bipy)(py)_2]^+$ (121.4(4)°)[98] and $[ReO_2(cat)_2]^-$ (99.4(5)°),[99] while a trend to smaller O-Re-O angles in complexes containing two bidentate ligands is evident. The Re-O bond length in *cis*-[**16**]$^+$ (1.790(6) Å) is elongated compared to $[ReO_2(dab\text{-}H)(py)_2]$ (1.716(6) and 1.723(7) Å),[97] $[ReO_2(bipy)(py)_2]^+$ (1.733(8) and 1.736(7) Å)[98] and $[ReO_2(cat)_2]^-$ (1.681(7) Å),[99] while it is in the same range as the Re-O bond lengths in $[ReO_2(OH_2)(Me_3tacn)]^+$ (1.82(1) and 1.78(1) Å).[96] The Re-C bond lengths in *cis*-[**16**]$^+$ (2.162(9) and 2.170(6) Å) are slightly elongated compared to the recently published structure of *trans*-$[ReO(OH)(\mathbf{L2})_2]^{2+}$ (2.155(5) and 2.154(4) Å).[42]

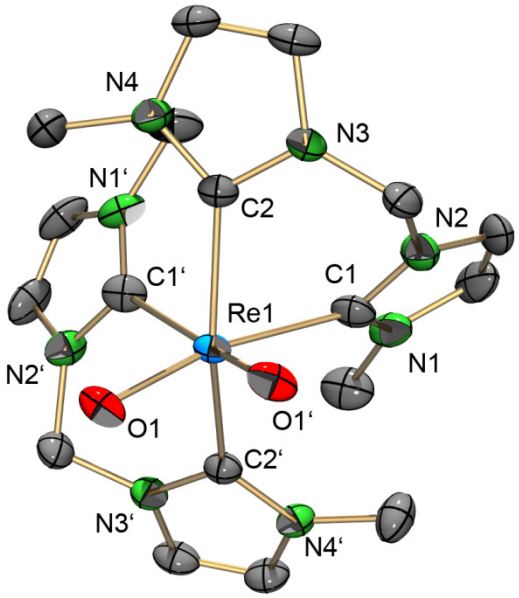

Figure 25: ORTEP representation[51] of the *cis*-$[ReO_2(\mathbf{L2})_2]^+$ ($[\mathbf{16}]^+$) cation of the $[\mathbf{16}](Cl)\cdot H_2O$ structure. Thermal ellipsoids are represented at the 50% probability level. Hydrogen atoms are omitted for clarity.

Table 22: Selected bond lengths and angles of *cis*-$[\mathbf{16}]^+$.

Selected bond lengths [Å]		Selected angles [°]	
Re(1)-O(1)	1.790(6)	O(1)-Re(1)-C(1)	167.6(3)
Re(1)-C(1)	2.162(9)	C(2)-Re(1)-C(2)#1	155.2(3)
Re(1)-C(2)	2.170(6)	O(1)-Re(1)-C(1)#1	89.8(3)
		O(1)-Re(1)-C(2)	109.7(3)
		O(1)-Re(1)-O(1)#1	84.0(4)
		C(1)-Re(1)-C(2)	80.9(3)
		C(1)-Re(1)-C(1)#1	98.2(5)

Trans-$[\mathbf{16}]^+$ crystallizes as yellow blocks of the composition $[\mathbf{16}](PF_6)\cdot 2H_2O\cdot 3THF\cdot LiPF_6$ in the monoclinic space group I2/a (Figure 26). The complex has a very symmetric octahedral coordination sphere, with an O-Re-O angle of 180° and O-Re-C angles that are close to 90° (89.56(14) and 89.35(15)°, table 23). The C-Re-C bite angle of **L2** (81.37(15)°) is comparable to *trans*-$[^{99}TcO_2(\mathbf{L2})_2]^+$ (81.33(16)°) and *trans*-$[ReO(OH)(\mathbf{L2})_2]^{2+}$ (81.4(2)°).[42] The Re-C bonds of *trans*-$[\mathbf{16}]^+$ are significantly different from each other (2.170(4) and 2.246(4) Å), which is not observed in the structures of *trans*-$[ReO(OH)(\mathbf{L2})_2]^{2+}$ (2.155(5) and 2.154(4) Å)[42] and *trans*-$[^{99}TcO_2(\mathbf{L2})_2]^+$ (2.170(4) and 2.166(4) Å). The Re-O bond lengths are considerably different in the structures of *cis*- and *trans*-$[\mathbf{16}]^+$, with values of 1.790(6) Å and 1.699(3) Å, respectively. The elongation of the Re-O bonds in *cis*-$[\mathbf{16}]^+$ presumably is due to the *trans*-influence of the strongly σ-donating NHC ligands in combination with the steric repulsion of the lone pairs of the O^{2-} ligands, which are in close proximity to each other.

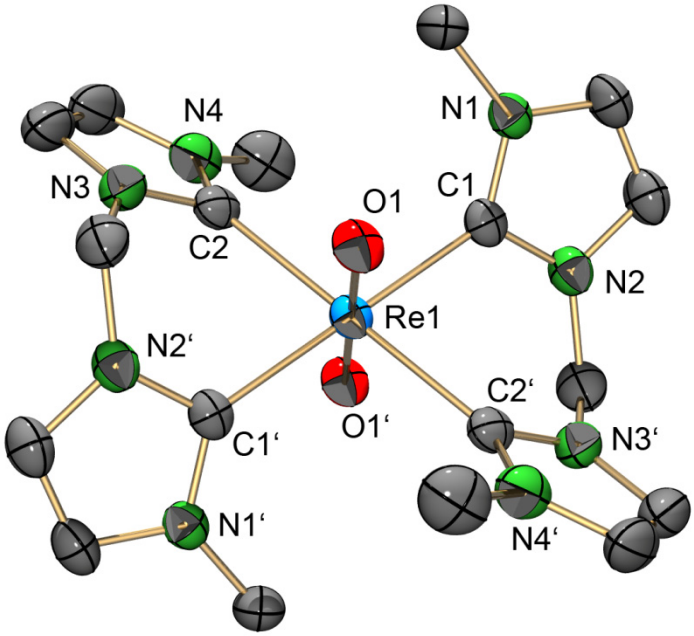

Figure 26: ORTEP representation[51] of the *trans*-$[ReO_2(\mathbf{L2})_2]^+$ ($[\mathbf{16}]^+$) cation of the $[\mathbf{16}](PF_6)\cdot 2H_2O\cdot 3THF\cdot LiPF_6$ structure. Thermal ellipsoids are represented at the 50% probability level. Hydrogen atoms are omitted for clarity.

Table 23: Selected bond lengths and angles of *trans*-$[\mathbf{16}]^+$.

Selected bond lengths [Å]		Selected angles [°]	
Re(1)-O(1)	1.699(3)	O(1)-Re(1)-O(1)#1	180.0
Re(1)-C(1)	2.170(4)	O(1)-Re(1)-C(1)	89.56(14)
Re(1)-C(2)	2.246(4)	O(1)-Re(1)-C(2)	89.35(16)
		C(1)-Re(1)-C(2)#1	81.37(15)

Besides ESI^+-MS and X-ray diffraction analysis, no other analytical data of *cis*- and *trans*-$[\mathbf{16}]^+$ were obtained from this reaction due to difficulties in the purification. Also, it remains unclear which conditions exactly lead to the formation of *cis*-$[\mathbf{16}]^+$. Presumably, the high reactivity of **L2** and the free coordination site in the *trans*-oxo position of $[ReO(glyc)_2]^-$ ($[\mathbf{15}]^-$) are important factors in the formation of the *cis*-product. A potential mechanism for the formation of *cis*- and *trans*-$[\mathbf{16}]^+$ is shown in scheme 23. Starting from $[\mathbf{15}]^-$, reaction with 1 eq. **L2** presumably leads to the formation of $[ReO(glyc)(\mathbf{L2})]^+$ (**intermediate 1**). A test reaction of $[\mathbf{15}]^-$ with only 1 eq. **L2** led to the formation of a blue compound, which is not stable at ambient conditions. Analysis with HR-ESI^+-MS confirmed formation of $[ReO(glyc)(\mathbf{L2})]^+$ (calculated m/z = 439.07803), since a peak at m/z = 439.07759 was observed. A peak at m/z = 477.11182 was also observed, but could not be assigned. The identity of **intermediate 1** is therefore not fully clear and formation of a $[ReO(X)(glyc)(\mathbf{L2})]^{n+}$-type complex (n = 0, 1; X = unknown ligand), that would fragment into $[ReO(glyc)(\mathbf{L2})]^+$ during the ESI^+-MS, cannot be excluded. Reaction of **intermediate 1** with a second eq. **L2** then leads to the *cis*- and *trans*-isomers of $[ReO(glyc)(\mathbf{L2})_2]^+$ (*cis*- and *trans*-**intermediate 2**), which was observed as a purple compound during

the reaction. Due to the monodentate binding of the glyc ligand, isomerisation of *cis*- and *trans*-**intermediate 2** might be possible at this point, while the *trans*-**intermediate 2** is thermodynamically favored. When **intermediate 2** is quenched with H_2O, coordination and deprotonation of the H_2O leads to the formation of *cis*- and *trans*-[**16**]$^+$. At this point, isomerisation presumably is no longer possible, unless the dioxo core is protonated again under acidic conditions.

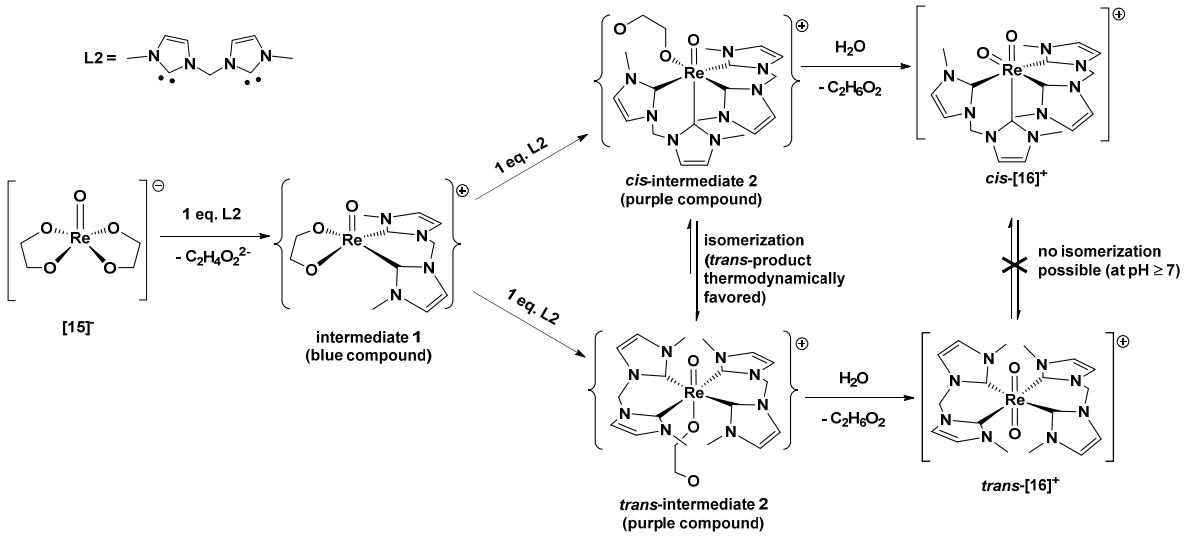

Scheme 23: Potential mechanism for the synthesis of *cis*- and *trans*-[**16**]$^+$.

In order to avoid formation of the kinetic product *cis*-[**16**]$^+$, the one-pot reaction of (N^nBu_4)[**15**] with 2 eq. (**L2**-H_2)$(PF_6)_2$ was tested with the same reaction conditions as in the corresponding synthesis of [$^{99}TcO_2$(**L2**)$_2$](PF_6) ([**10**]$^+$), with a prolonged refluxing of the CH_2Cl_2 reaction mixture of 22 h (Scheme 24). During the reaction, formation of a purple compound was again observed, which was converted to [**16**]$^+$ by basic workup in MeOH using 3 eq. NaOH. After further purification steps, analytically pure *trans*-[**16**](PF_6) was obtained in 47% yield. Formation of *cis*-[**16**]$^+$ was not observed, which is explained by the long refluxing of the CH_2Cl_2 reaction mixture that favors formation of the thermodynamic *trans*-product.

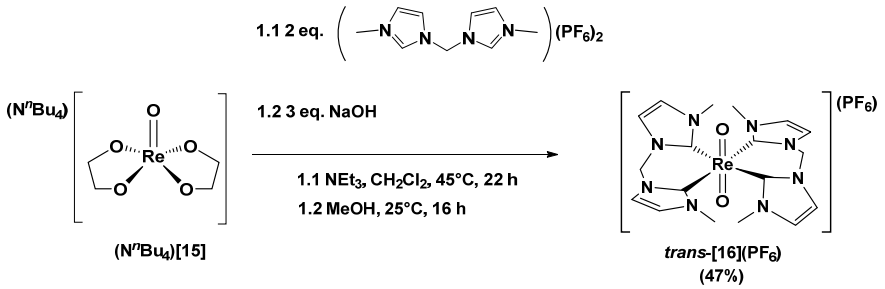

Scheme 24: Synthesis of *trans*-[**16**](PF_6) by reaction of (N^nBu_4)[**15**] with 2 eq. (**L2**-H_2)$(PF_6)_2$ under basic conditions, followed by workup with 3 eq. NaOH in MeOH.

IR spectroscopy of *trans*-[**16**](PF_6) shows the strong characteristic bands at 834 cm^{-1} (PF_6^-) and 734 cm^{-1} ($\nu_{O=Re=O}$ band of the asymmetric stretching mode), which is at considerably lower wave numbers than the corresponding bands in [**10**]$^+$ (765 cm^{-1}) or $[ReO_2(L^{Me})_4]^+$ (768 cm^{-1}, L^{Me} = 1,3-dimethyl-4,5-dimethylimidazol-2-ylidene).[79] Characterization of *trans*-[**16**](PF_6) with HR-ESI$^+$-MS in CH_3CN showed two peaks with the isotopic pattern of Re, the $[M]^+$ peak at m/z = 571.15710 (calculated m/z = 571.15800) and the peak of $[M+H]^{2+}$ at m/z 286.08277 (calculated m/z = 286.08235). ^{1}H NMR of *trans*-[**16**](PF_6) in CD_3CN shows a very similar spectrum as for [**10**](PF_6). The CH groups were observed as two doublets (7.51 and 7.23 ppm), which was also observed for the CH_2 groups (7.27 and 6.15 ppm). The CH_3 group appears as a singlet at 3.74 ppm, confirming the high symmetry of the compound. In the ^{13}C NMR, a signal for the Re-C carbons was observed at 176.83 ppm along with the expected signals for the H-containing groups. The chemical shift of the Re-C groups in *trans*-[**16**]$^+$ is slightly higher than the reported values of $[ReO(OH)(\mathbf{L2})_2]^{2+}$ (168.42 and 166.68 ppm, measured in DMSO-D_6) and $[ReO_2(L^{Me})_4]^+$ (173.72 ppm, measured in $CDCl_3$).[42,79]

Derivatization of *trans*-[**16**]$^+$ in *trans*-position was not as thoroughly studied as for [**10**]$^+$. One reason for this is that *trans*-$[ReOCl(\mathbf{L2})_2]^{2+}$ ([**17**]$^{2+}$) does not appear to be as easily accessible as the corresponding ^{99}Tc complex. When *trans*-[**16**]$^+$ was reacted with an excess of 1 M HCl in 3:1 acetone/H_2O, an expected color change to green was not observed. Instead, the solution remained orange and when the solvent of the reaction was removed with a stream of N_2, a purple crude product was obtained. Analysis by NMR showed a spectrum of higher order, which might indicate that *cis*-/*trans*-isomerization might have taken place. Crystallization of the crude product from DMF and X-ray diffraction analysis confirmed that one of the formed products indeed was *trans*-[**17**](PF_6)$_2$. *Trans*-[**17**](PF_6)$_2$ crystallizes as purple blocks in the monoclinic space group $P2_1$ with four independent dications in the asymmetric unit (Figure 27). As it was the case for the ^{99}Tc analogue, all four dications are systematically disordered along the O-Re-Cl axis with a ratio of occupancy of 0.52:0.48, 0.85:0.15, 0.76:0.24 and 0.64:0.36 The difference in these occupancy-ratios is the reason for the reduced symmetry of the space group. The structural features of *trans*-[**17**]$^{2+}$ have to be interpreted with caution due to these disorders. The Re-C bond lengths in *trans*-[**17**]$^{2+}$ (2.099(10) – 2.235(11) Å, table 24) are in the same range as in *trans*-[**16**]$^+$ (2.170(4) and 2.246(4) Å), while an expected trend to a shorter Re-O bond length in *trans*-[**17**]$^{2+}$ (1.711(5) Å) compared to *trans*-[**16**]$^+$ (1.699(3) Å) is not observed. The Re-Cl bond length of *trans*-[**17**]$^{2+}$ (2.413(4) Å) is in the expected range of Re-Cl bonds. The slightly bent O-Re-Cl angle (173.0(2)°) should not be overinterpreted, since it might be a result of the refinement of the O-Re-Cl disorder.

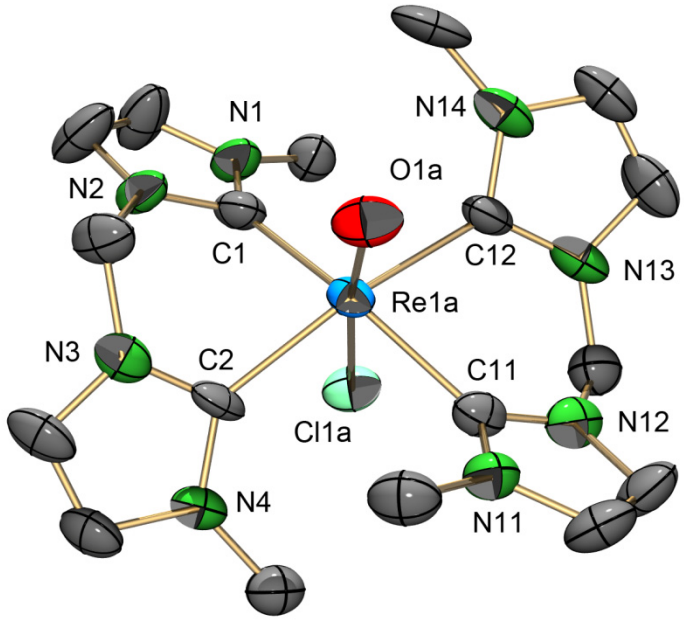

Figure 27: ORTEP representation[51] of the major species in the *trans*-$[ReOCl(\mathbf{L2})_2]^{2+}$ dication of the *trans*-$[ReOCl(\mathbf{L2})_2](PF_6)_2$ structure. Thermal ellipsoids are represented at the 50% probability level. Hydrogen atoms are omitted for clarity.

Table 24: Selected bond lengths and angles of the major species of *trans*-$[ReOCl(\mathbf{L2})_2]^{2+}$.

Selected bond lengths [Å]		Selected angles [°]	
Re(1A)-O(1A)	1.711(5)	O(1A)-Re(1A)-Cl(1A)	173.0(2)
Re(1A)-Cl(1A)	2.413(4)	O(1A)-Re(1A)-C(1)	103.8(4)
Re(1A)-C(1)	2.125(13)	O(1A)-Re(1A)-C(2)	107.0(3)
Re(1A)-C(2)	2.099(10)	O(1A)-Re(1A)-C(11)	95.2(3)
Re(1A)-C(11)	2.184(12)	O(1A)-Re(1A)-C(12)	90.5(3)
Re(1A)-C(12)	2.235(11)	C(1)-Re(1A)-C(2)	82.4(4)
		C(11)-Re(1A)-C(12)	80.0(4)

The synthesis and chemistry of $[ReO_2(\mathbf{L2})_2]^+$ is very comparable to $[^{99}TcO_2(\mathbf{L2})_2]^+$ and most of the differences encountered in its synthesis were caused by the rigid exclusion of air and moisture from the reaction. One key difference compared to its ^{99}Tc-analogue is the formation of *cis*-$[ReO_2(\mathbf{L2})_2]^+$ as a kinetic product of the reaction of $[ReO(glyc)_2]^-$ with **L2**. This problem can be circumvented, since the thermodynamic *trans*-product is the only product observed in the one-pot reaction of $[ReO(glyc)_2]^-$ with $(\mathbf{L2}\text{-}H_2)^{2+}$ in refluxing CH_2Cl_2. Due to their similar chemistry, $[ReO_2(\mathbf{L2})_2]^+$ and $[^{99}TcO_2(\mathbf{L2})_2]^+$ in principle represent a matched pair for "theranostic" approaches, in which $^{186/188}$Re is used for therapy and ^{99m}Tc is used for diagnosis.[100-102] Reaction of $[ReO(glyc)_2]^-$ with 1 eq. of **L2** gave a mono-substituted complex $[ReO(glyc)(\mathbf{L2})]^+$, which could not be isolated and purified. This asymmetric Re-NHC complex is synthetically very interesting and thus, a general route to complexes containing the $\{MO(\mathbf{L2})\}^{3+}$ fragment (M = Re, ^{99}Tc) will be discussed in the next chapter.

4.2.2.4 Synthesis and Derivatization of the $\{M^{V}O(L2)\}^{3+}$ Fragment via Acidic Cleavage of Novel M-Dimer Complexes (M = Re, ^{99}Tc)

Following the preparation of $[MO_2(\mathbf{L2})_2]^+$ (M = Re, ^{99}Tc) it was speculated that complexes of the corresponding monosubstituted $\{MO(\mathbf{L2})\}^{3+}$ fragment should also exist, since this fragment is part of the proposed intermediate in the reaction. The green color of the reaction solution during the preparation of $[^{99}TcO_2(\mathbf{L2})_2]^+$ was attributed to either be $[^{99}TcOCl(\mathbf{L2})_2]^{2+}$ or a desired monosubstituted complex such as $[^{99}TcO(glyc)(\mathbf{L2})]^+$. Unfortunately, the isolation of this green intermediate was not possible from the crude product. More evidence for the existence and possible synthesis of $\{MO(\mathbf{L2})\}^{3+}$-type complexes (M = Re, ^{99}Tc) was found with Re, where the reaction of $[ReO(glyc)_2]^-$ with only 1 eq. of **L2** gave a blue compound which was insoluble or only sparingly soluble in most tested solvents. HR-ESI$^+$-MS of this blue crude product confirmed the identity of the $\{ReO(\mathbf{L2})\}^{3+}$ fragment (Figure 28), since the isotopic pattern at m/z = 439.07759 corresponds to $[ReO(glyc)(\mathbf{L2})]^+$ (calculated m/z = 439.07803). The signal at m/z = 477.11182 also contains the isotopic pattern of Re, but it could not be assigned and does not fit to for example $[ReO(glyc)(\mathbf{L2})]^+$ + HCl (calculated m/z = 475.05471), $[ReO(glyc)(\mathbf{L2})]^+$ + LiCl (calculated m/z = 481.06289) or any possible solvent coordination in the remaining coordination site.

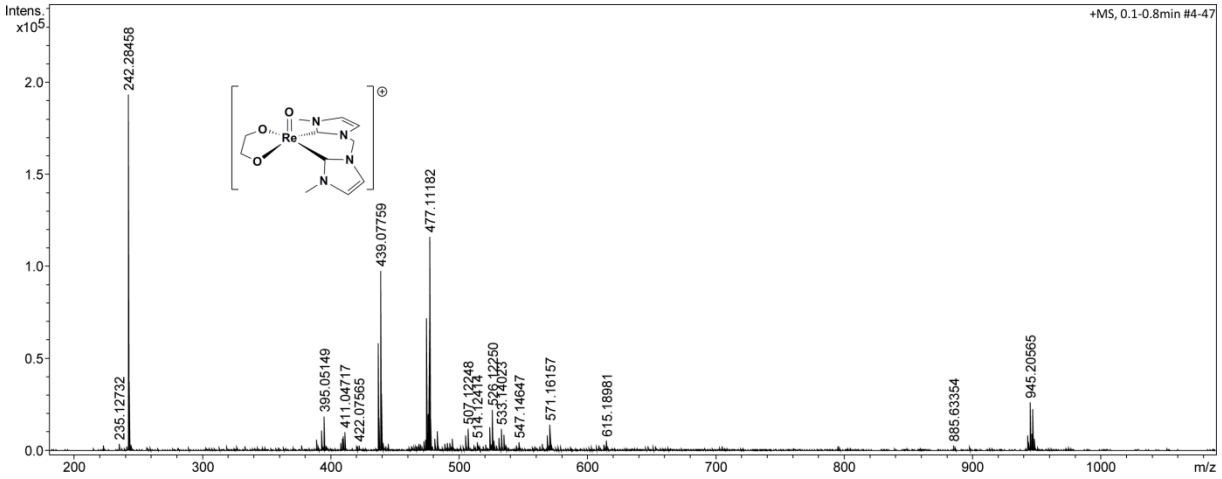

Figure 28: HR-ESI$^+$-MS confirming the possibility to prepare $\{Re^{V}O(\mathbf{L2})\}^{3+}$-type complexes.

As it is visible from the HR-ESI$^+$-MS, the purity of the sample was not satisfying. In addition, the blue crude product was exclusively soluble in MeOH and H_2O, and when dissolved in these solvents, it presumably did not retain its molecular structure, since a color change to purple (MeOH) or orange (H_2O) was observed. Unfortunately, this behaviour made it very difficult to isolate a pure product.

Another approach for the synthesis and isolation of $\{MO(\mathbf{L2})\}^{3+}$-type complexes was the *in situ* reaction with other ligands such as pyridine (py) to form $[MO_2(\mathbf{L2})(py)_2]^+$ (M = Re, ^{99}Tc). The main problem with this approach is the prevailing formation of $[MO_2(py)_4]^+$ (M = Re, ^{99}Tc), which has been first described by Kastner *et al.*.[103,104] A solution to this problem was found by use of bisimidazol-1-ylmethane (**L4**). When 2 eq. of **L4** were reacted with $[^{99}TcO(glyc)_2]^-$ in CH_2Cl_2, no reaction could be

observed. Therefore, 1 eq. **L4** and 1 eq. (**L2**-H_2)$(PF_6)_2$ were reacted with [^{99}TcO(glyc)$_2$]$^-$, which led to the formation of an orange solid that precipitated from the reaction solution. The orange solid was identified as [$^{99}TcO_2$(**L2**)(**L4**)]$_2(PF_6)_2$ ([**18**]$(PF_6)_2$), which represents a novel dimeric ^{99}Tc-NHC compound comprised of two {$^{99}TcO_2$(**L2**)}$^+$ fragments that are connected by two **L4** ligands (Scheme 25). Since [**18**]$(PF_6)_2$ precipitated from the reaction solution, it was filtered off and washed with CH_2Cl_2. For further purification, [**18**]$(PF_6)_2$ was dissolved in CH_3CN, filtered and precipitated with Et_2O with a yield of 67%. High purity crystalline [**18**]$(PF_6)_2$ was obtained from a 4:1 acetone/H_2O solution, in which the acetone was slowly allowed to evaporate, followed by filtration of the formed crystals. The decomposition of [**18**]$(PF_6)_2$ was not observed in the presence of H_2O at neutral or basic pH, while the chemistry of [**18**]$(PF_6)_2$ under acidic conditions will be discussed later in this chapter.

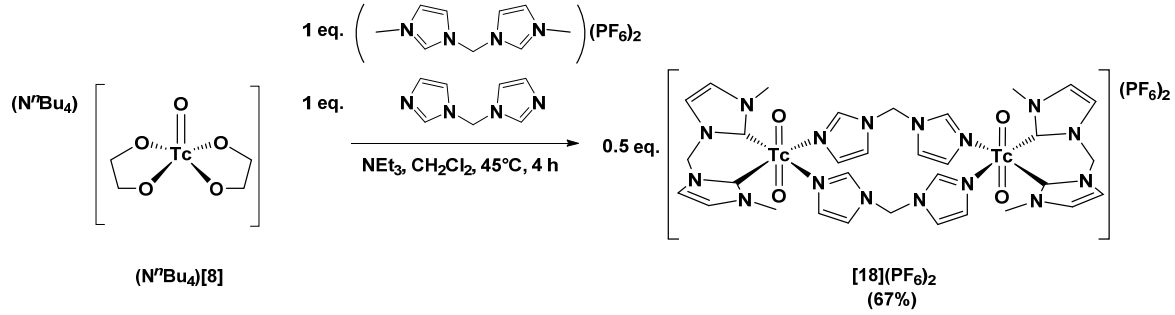

Scheme 25: Synthesis of [**18**]$(PF_6)_2$, a novel dimeric ^{99}Tc-NHC complex.

Depending on the method of crystallization, two different crystal structures were obtained. Crystallization of crude [**18**]$(PF_6)_2$ from DMF gave orange blocks of the composition [**18**]$(PF_6)_{1.5}(Cl)_{0.5}\cdot 3DMF\cdot 4H_2O$, while crystallization of crude [**18**]$(PF_6)_2$ from a 4:1 acetone/H_2O solution gave orange blocks of the composition [**18**]$(PF_6)_2\cdot 2H_2O$. Besides the different compositions of the crystals, the orientation of the bridging ligands **L4** is different in the two structures (Figure 29). In [**18**]$(PF_6)_{1.5}(Cl)_{0.5}\cdot 3DMF\cdot 4H_2O$, the imidazoles of the bridging ligands are oriented in the same direction leading to an overall more planar structure of [**18**]$^{2+}$ (**conformer 1**). On the other hand, the imidazoles of the **L4** ligands in [**18**]$(PF_6)_2\cdot 2H_2O$ are oriented in opposite directions, leading to a twisted structure (**conformer 2**).

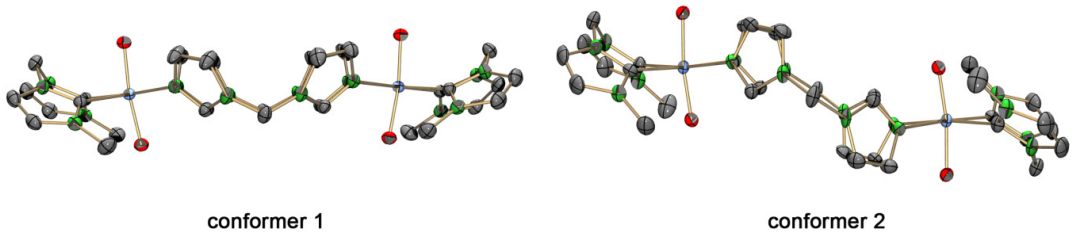

Figure 29: ORTEP representations[51] showing the conformational isomerism of [**18**]$^{2+}$. The two conformers are converted into each other by rotation of the imidazoles in the bridging ligand **L4**. Thermal ellipsoids are represented at the 50% probability level. Hydrogen atoms are omitted for clarity.

Conformer 1 of $[\mathbf{18}]^{2+}$ crystallizes as orange blocks of the composition $[\mathbf{18}](PF_6)_{1.5}(Cl)_{0.5}\cdot 3DMF\cdot 4H_2O$ in the monoclinic space group C2/c (Figure 30). Some disorders had to be considered during refinement, since 25% of the positions of the anions were found to be occupied by a Cl^- impurity. In addition, one of the DMF molecules was found to be disordered with a 50% occupancy. This DMF molecule presumably also has an important role in the crystallization of **conformer 1**, since all the NCHN groups of the **L4** ligands are oriented towards O(31) of the disordered DMF molecule. However, the interactions between the NCHN groups and O(31) presumably cannot be considered H-bonding interactions, since the donor-acceptor distances are comparably long (3.333(4) and 3.366(4) Å) and, more importantly, the donor-H-acceptor (DHA) angles are bent (144° and 145°). The ^{99}Tc-O bond lengths (1.755(2) Å, table 25) are slightly shorter than the ^{99}Tc-O bond lengths in $[^{99}TcO_2(\mathbf{L2})_2]^+$ ($[\mathbf{10}]^+$, 1.765(3) Å). A significant difference is found in the ^{99}Tc-C bond lengths, which are considerably shorter in this structure (2.109(3) Å and 2.107(3) Å) than in $[\mathbf{10}]^+$ (2.170(4) Å and 2.166(4) Å), which is presumably explained by the lack of steric interactions of the **L2** ligand with other ligands in $[\mathbf{18}]^{2+}$. The ^{99}Tc-N bond lengths (2.219(2) and 2.217(2) Å) are significantly elongated compared to the ^{99}Tc-N bond lengths in $[^{99}TcO_2(py)_4]^+$ (py = pyridine, 2.142(2) –2.161(2) Å).[103] The O(1)-Tc(1)-O(2) angle (172.16(9)°) is slightly bent and the ^{99}Tc centre has a distorted octahedral coordination environment. The shorter ^{99}Tc-C bond lengths and the reduced steric interactions between the equatorial ligands lead to a wider C(1)-Tc(1)-C(2) bite angle of **L2** (83.88(10)°) compared to the C(1)-Tc(1)-C(2) angle in $[\mathbf{10}]^+$ (81.33(16)°).

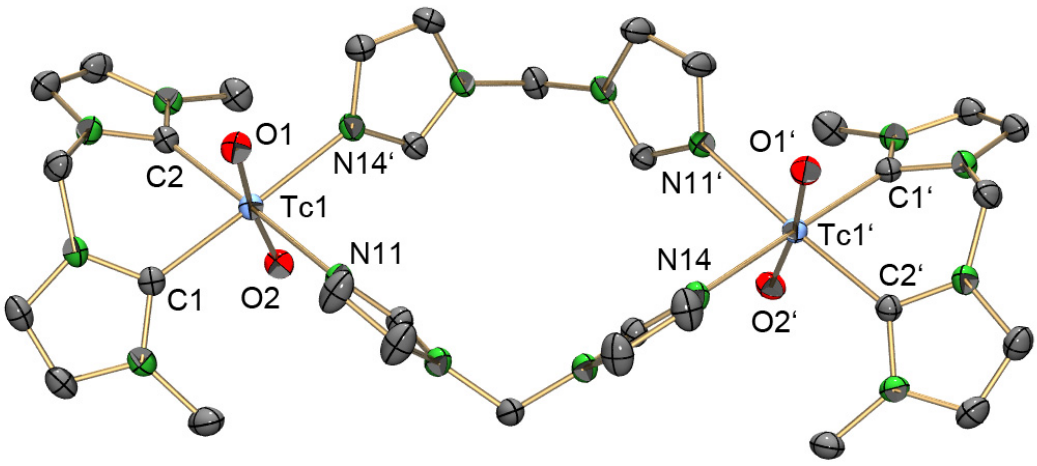

Figure 30: ORTEP representation[51] of the $[\mathbf{18}]^{2+}$ dication of the $[\mathbf{18}](PF_6)_{1.5}(Cl)_{0.5}\cdot 3DMF\cdot 4H_2O$ structure (**conformer 1**). Thermal ellipsoids are represented at the 50% probability level. Hydrogen atoms are omitted for clarity.

Table 25: Selected bond lengths and angles of **conformer 1** of $[\mathbf{18}]^{2+}$.

Selected bond lengths [Å]		Selected angles [°]	
Tc(1)-O(1)	1.755(2)	O(1)-Tc(1)-O(2)	172.16(9)
Tc(1)-O(2)	1.755(2)	O(1)-Tc(1)-C(1)	92.16(10)
Tc(1)-C(1)	2.109(3)	O(1)-Tc(1)-C(2)	90.58(10)
Tc(1)-C(2)	2.107(3)	O(1)-Tc(1)-N(11)	86.68(9)
Tc(1)-N(11)	2.219(2)	O(1)-Tc(1)-N(14)#1	87.11(9)
Tc(1)-N(14)#1	2.217(2)	N(11)-Tc(1)-N(14)#1	86.90(9)
		C(1)-Tc(1)-C(2)	83.88(10)
		C(1)-Tc(1)-N(11)	94.25(10)
		C(2)-Tc(1)-N(14)#1	94.93(10)

Conformer 2 of $[\mathbf{18}]^{2+}$ crystallizes as orange blocks of the composition $[\mathbf{18}](PF_6)_2 \cdot 2H_2O$ in the monoclinic space group $P2_1/n$ (Figure 31). The co-crystallized H_2O is H-bonded to the O(1) of $[\mathbf{18}]^{2+}$, with a donor-acceptor distance O(11)-O(1) of 2.737(5) Å and an almost linear DHA angle of 175(6)°. The ^{99}Tc-O bond lengths (1.738(3) and 1.767(3) Å, table 26) are comparable to **conformer 1** (1.755(2) Å). The ^{99}Tc-C bond lengths (2.103(4) and 2.106(4) Å) and ^{99}Tc-N bond lengths (2.225(4) and 2.231(3) Å) are also comparable to **conformer 1** (^{99}Tc-C bond lengths: 2.109(3) and 2.107(3) Å; ^{99}Tc-N bond lengths: 2.219(2) and 2.217(2) Å). The ^{99}Tc centre has a distorted octahedral coordination environment, which is observed e.g. in the O(1)-Tc(1)-O(2) angle (171.80(13)°). As it was the case in the structure of **conformer 1**, the C(1)-Tc(1)-C(2) bite angle of the **L2** ligand (82.62(16)°) is significantly larger than the bite angle observed in $[\mathbf{10}]^{+}$ (81.33(16)°).

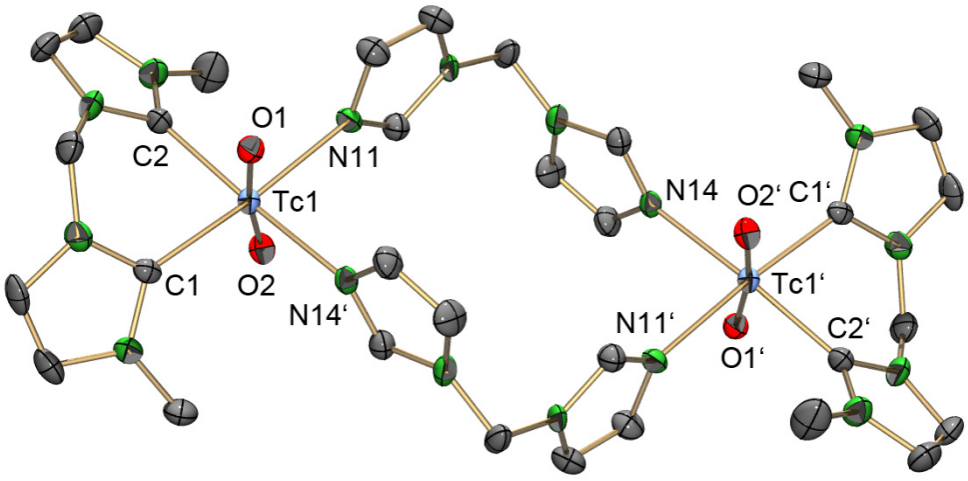

Figure 31: ORTEP representation[51] of the $[\mathbf{18}]^{2+}$ dication of the $[\mathbf{18}](PF_6)_2 \cdot 2H_2O$ structure (**conformer 2**). Thermal ellipsoids are represented at the 50% probability level. Hydrogen atoms are omitted for clarity.

Table 26: Selected bond lengths and angles of **conformer 2** of $[\mathbf{18}]^{2+}$.

Selected bond lengths [Å]		Selected angles [°]	
Tc(1)-O(1)	1.767(3)	O(1)-Tc(1)-O(2)	171.80(13)
Tc(1)-O(2)	1.738(3)	C(1)-Tc(1)-N(11)	175.54(14)
Tc(1)-C(1)	2.103(4)	C(2)-Tc(1)-N(14)#1	173.84(14)
Tc(1)-C(2)	2.106(4)	O(1)-Tc(1)-C(1)	91.38(15)
Tc(1)-N(11)	2.225(4)	O(1)-Tc(1)-C(2)	88.82(15)
Tc(1)-N(14)#1	2.231(3)	O(1)-Tc(1)-N(11)	85.75(13)
		O(1)-Tc(1)-N(14)#1	85.02(13)
		N(11)-Tc(1)-N(14)#1	85.39(13)
		C(1)-Tc(1)-C(2)	82.62(16)

IR-spectroscopy of $[\mathbf{18}](PF_6)_2$ shows besides the strong band at 848 and 837 cm^{-1} (PF_6^-) also strong $\nu_{O=Tc=O}$ bands at 795 cm^{-1} and 764 cm^{-1}. Comparison to the $\nu_{O=Tc=O}$ band of $[\mathbf{10}]^+$ (765 cm^{-1}) allows the assignment of the band at 764 cm^{-1} to the asymmetric stretch mode. The band at 795 cm^{-1} most certainly corresponds to the symmetric stretch mode, which is now IR-active because of the non-linear O-^{99}Tc-O arrangement. $[\mathbf{18}](PF_6)_2$ was investigated in detail with NMR spectroscopy in CD_3CN. ^{1}H-NMR spectroscopy of $[\mathbf{18}](PF_6)_2$ showed the expected signals for the imidazole-H atoms of **L2** as doublets with a chemical shift of 7.49 and 7.18 ppm (Figure 32, a)). Also, the CH_3 protons of **L2** are observed as a singlet with a chemical shift of 3.65 ppm. Interestingly, the CH_2 protons of **L2** are not fully resolved at 25°C and appear as two broad singlets with chemical shifts of 6.74 and 6.21 ppm. This is a notable difference compared to the ^{1}H NMR spectrum of $[\mathbf{10}]^+$, in which the CH_2 protons are observed as resolved doublets. The broadening is explained by a rapid movement of the CH_2 group in the **L2** ligand in axial direction, which is only possible due to the lack of steric interactions with other ligands (Scheme 26). This so-called "flapping wing" motion has also been described for other complexes containing **L2**, such as $[ReBr(\mathbf{L2})(CO)_3]$.[73] The ligand **L4** in $[\mathbf{18}](PF_6)_2$ has signals in the ^{1}H-NMR spectrum for the CH atoms at 8.33, 7.36 and 7.31 ppm and the signals for the CH_2 protons appear as a broad singlet at 6.12 ppm (Figure 32, a)). In addition to these findings, low-temperature NMR-spectroscopy of $[\mathbf{18}](PF_6)_2$ at -45°C confirmed the presence of two conformers of the dimeric complex, which as mentioned before, differ in the orientation of the bridging ligands **L4** (Scheme 26). At -45°C, the signals of the CH_2 protons in **L2** were resolved and showed a higher-order coupling pattern, which is attributed to the slowing or inhibition of the axial movement at lower temperatures (Figure 32, b)).

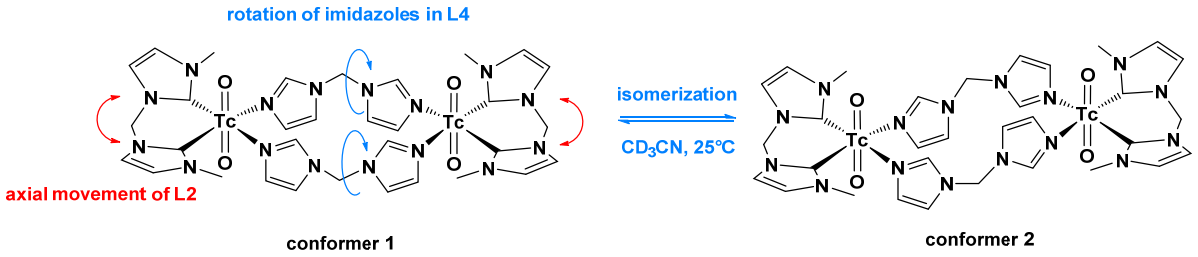

Scheme 26: Depiction of the two conformers of [**18**]$^{2+}$ that are the result of the rotation of imidazoles in **L4** (blue). The axial movement of **L2** is also shown (red), which leads to broad signals for the CH_2 group in the ^{1}H-NMR.

Nuclear overhauser effect (NOE) experiments at 25°C confirmed that the two conformers of [**18**]$(PF_6)_2$ are rapidly converted into each other by rotation of the imidazoles in **L4**, since the H atoms of the NCHN groups at 8.33 ppm appear to be in close proximity to the imidazole-H atoms at 7.36 and 7.31 ppm (Figure 32, c)). The ^{13}C-NMR also shows the expected signals for the equilibrium state at 25°C and a complex spectrum at -45°C. Notable is the absence of ^{99}Tc-C signals in the ^{13}C NMR, which are expected to be broadened due to the influence of the ^{99}Tc nucleus. All signals were assigned using a range of experiments, such as NOE- and various 2D-NMR measurements.

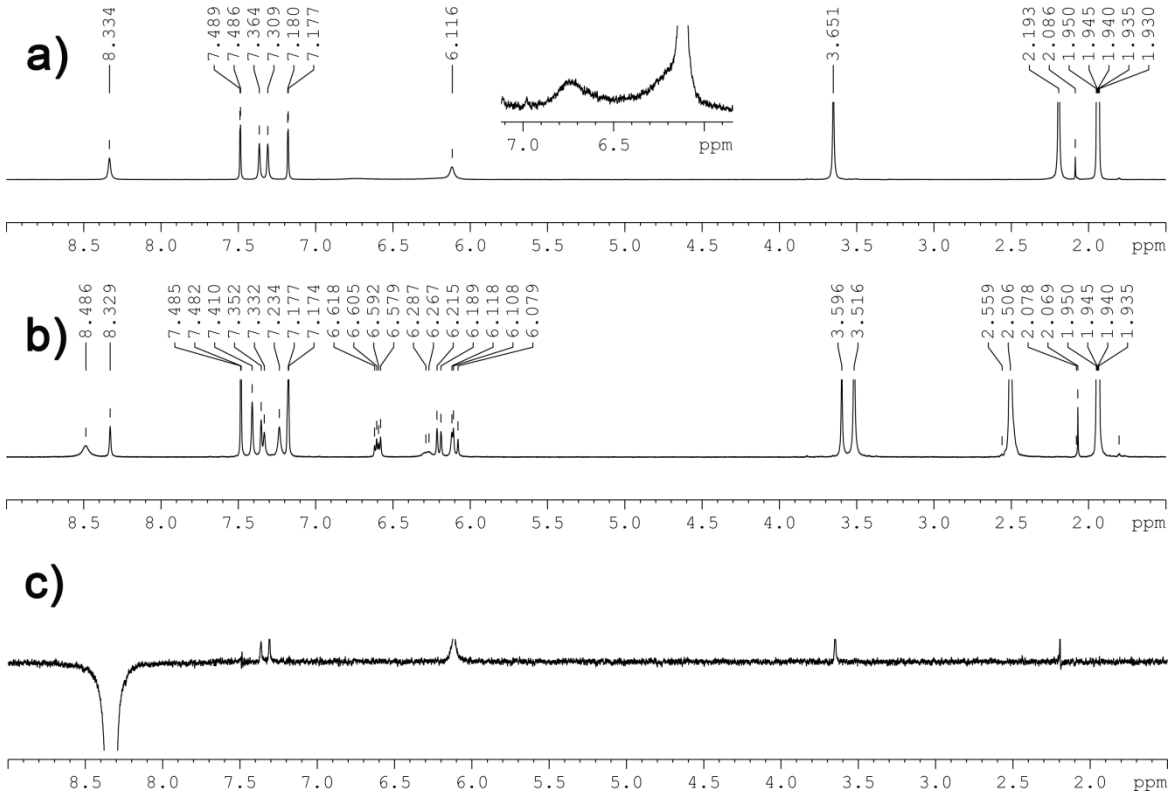

Figure 32: a) ^{1}H-NMR spectrum of [**18**]$(PF_6)_2$ in CD_3CN at 25°C, including a detailed zoom on the broadened signals of the CH_2 group in **L2**. b) ^{1}H-NMR spectrum of [**18**]$(PF_6)_2$ in CD_3CN at -45°C. c) NOE spectrum of [**18**]$(PF_6)_2$ in CD_3CN at 25°C.

The corresponding Re complex $[ReO_2(\mathbf{L2})(\mathbf{L4})]_2(PF_6)_2$ ($[\mathbf{19}](PF_6)_2$) was prepared in analogy to the ^{99}Tc complex $[\mathbf{18}](PF_6)_2$ (Scheme 27). As mentioned before, the reaction had to be performed under exclusion of air and moisture due to the sensitivity of $[ReO(glyc)_2]^-$. Besides this, minor changes in the workup procedure were made, since the purification of $[\mathbf{19}](PF_6)_2$ was not successful with the above described method for $[\mathbf{18}](PF_6)_2$. Recrystallization from MeOH proved to be a good method for purification and to obtain crystalline $[\mathbf{19}](PF_6)_2$ with a high purity. The isolated yield of 86% was slightly higher than the 67% isolated yield achieved in the case of $[\mathbf{18}](PF_6)_2$, which is presumably explained by to the longer reaction time and the different purification procedures used. $[\mathbf{19}](PF_6)_2$ has the same stability as the corresponding ^{99}Tc complex and hence is also stable in the presence of H_2O at neutral and basic conditions. As mentioned earlier, the stability of these dimeric complexes under acidic conditions will be discussed later in this chapter.

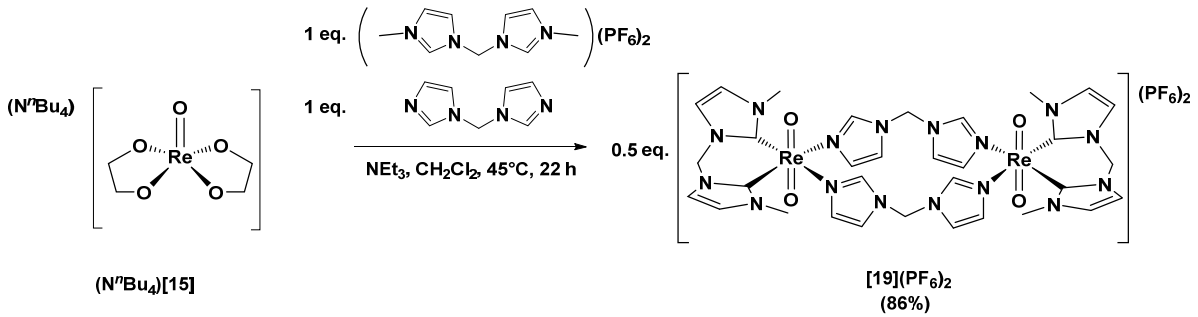

Scheme 27: Synthesis of $[\mathbf{19}](PF_6)_2$, which was prepared in analogy to the corresponding ^{99}Tc complex $[\mathbf{18}](PF_6)_2$.

$[\mathbf{19}](PF_6)_2$ crystallizes as orange needles of the composition $[\mathbf{19}](PF_6)_2 \cdot 2H_2O$ in the monoclinic space group $P2_1/n$ (Figure 33). The observed crystal structure is isostructural to **conformer 2** of $[\mathbf{18}]^{2+}$ and also contains co-crystallized H_2O. The co-crystallized H_2O is H-bonded to O(1), with a donor-acceptor distance O(11)-O(1) of 2.722(3) Å and a linear DHA angle (179(4)°). The Re-O bond lengths in $[\mathbf{19}]^{2+}$ (1.7840(19) and 1.7636(18) Å, table 27) are slightly elongated compared to the corresponding **conformer 2** of $[\mathbf{18}]^{2+}$ (1.767(3) and 1.738(3) Å). The Re-C bond lengths (2.104(3) and 2.097(3) Å) and the Re-N bond lengths (2.212(2) and 2.214(2) Å) are in the same range as for **conformer 2** of $[\mathbf{18}]^{2+}$. For comparison, the structure of $[ReO_2(\mathbf{L2})_2]^+$ ($[\mathbf{16}]^+$) has significantly shorter Re-O bond lengths (1.699(3) Å) and significantly longer Re-C bond lengths (2.170(4) and 2.246(4) Å). The Re centre in $[\mathbf{19}]^{2+}$ has a distorted octahedral coordination environment, with an O(1)-Re(1)-O(1) angle of 171.92(8)°, a C(1)-Re(1)-N(14) angle of 175.89(9)° and a C(2)-Re(1)-N(11) angle of 173.84(9)°. The bite angle C(1)-Re(1)-C(2) of the **L2** ligand (82.44(10)°) is larger than the corresponding angle in $[\mathbf{16}]^+$ (81.38(15)°).

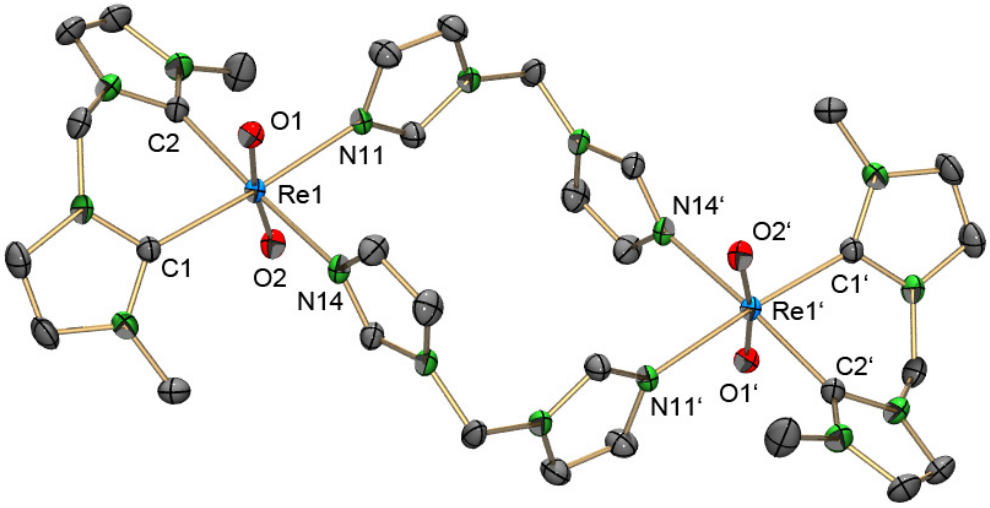

Figure 33: ORTEP representation[51] of the $[\mathbf{19}]^{2+}$ dication of the $[\mathbf{19}](PF_6)_2 \cdot 2H_2O$ structure (**conformer 2**). Thermal ellipsoids are represented at the 50% probability level. Hydrogen atoms are omitted for clarity.

Table 27: Selected bond lengths and angles of **conformer 2** of $[\mathbf{19}]^{2+}$.

Selected bond lengths [Å]		Selected angles [°]	
Re(1)-O(1)	1.7840(19)	O(1)-Re(1)-O(2)	171.92(8)
Re(1)-O(2)	1.7636(18)	C(1)-Re(1)-N(11)	175.89(9)
Re(1)-C(1)	2.104(3)	C(2)-Re(1)-N(14)	173.84(9)
Re(1)-C(2)	2.097(3)	O(1)-Re(1)-C(1)	90.90(9)
Re(1)-N(11)	2.214(2)	O(1)-Re(1)-C(2)	88.54(10)
Re(1)-N(14)	2.212(2)	O(1)-Re(1)-N(11)	86.26(8)
		O(1)-Re(1)-N(14)	85.35(8)
		N(11)-Re(1)-N(14)	84.34(8)
		C(1)-Re(1)-C(2)	82.44(10)

IR-spectroscopy of $[\mathbf{19}](PF_6)_2$ shows besides the strong band at 834 cm^{-1} (PF_6^-) also strong $\nu_{O=Re=O}$ bands at 782 and 761 cm^{-1}, which have almost the same intensities. As for $[\mathbf{18}](PF_6)_2$, it is concluded that the band at 782 cm^{-1} corresponds to the symmetric $\nu_{O=Re=O}$ stretching mode, while the band at 761 cm^{-1} is assigned to the asymmetric $\nu_{O=Re=O}$ stretching mode. Compared to $[\mathbf{18}](PF_6)_2$ (asymmetric $\nu_{O=Tc=O}$ band at 795 cm^{-1}), the band at 782 cm^{-1} is shifted to lower wavenumbers. The other bands in this region are in the same range, with 764 cm^{-1} for $[\mathbf{18}](PF_6)_2$ and 761 cm^{-1} for $[\mathbf{19}](PF_6)_2$. NMR spectroscopy of $[\mathbf{19}](PF_6)_2$ in CD_3CN gave very similar spectra as for $[\mathbf{18}](PF_6)_2$. The similarity of the NMR spectra of the ^{99}Tc and Re-dimers is evidence that there are also two conformers of $[\mathbf{19}]^{2+}$, even though only **conformer 2** could be crystallized. ^{1}H-NMR spectroscopy of $[\mathbf{19}](PF_6)_2$ showed an almost identical set of signals as found for $[\mathbf{18}](PF_6)_2$. As it was the case for $[\mathbf{18}](PF_6)_2$, the signals of the CH_2 group of **L2** are broadened due to the fast axial movement of the **L2** ligand by the “flapping wing” motion. The only notable difference in the ^{13}C-NMR spectrum is the presence of the Re-C

signal, which was observed at a chemical shift of 168.34 ppm. Compared to the chemical shift of the Re-C atoms in $[\mathbf{16}]^{+}$ (176.83 ppm, measured in CD_3CN), this signal is slightly shifted to a lower field. High-resolution ESI^{+}-MS of $[\mathbf{19}](PF_6)_2$ shows the $[M]^{2+}$ peak at m/z = 543.12672 (calculated m/z = 543.12670, figure 34). A molecular fragment corresponding to $\{ReO_2(\mathbf{L2})\}^{+}$ was also observed at m/z = 395.05143 (calculated m/z = 395.05181), which is explained by the loss of the **L4** ligands. This is especially interesting from a synthetic point of view, since the loss of the **L4** ligands in $[\mathbf{18}]^{2+}$ and $[\mathbf{19}]^{2+}$ in principle leads to the previously discussed $\{M^{V}O(\mathbf{L2})\}^{3+}$ fragment (M = Re, ^{99}Tc).

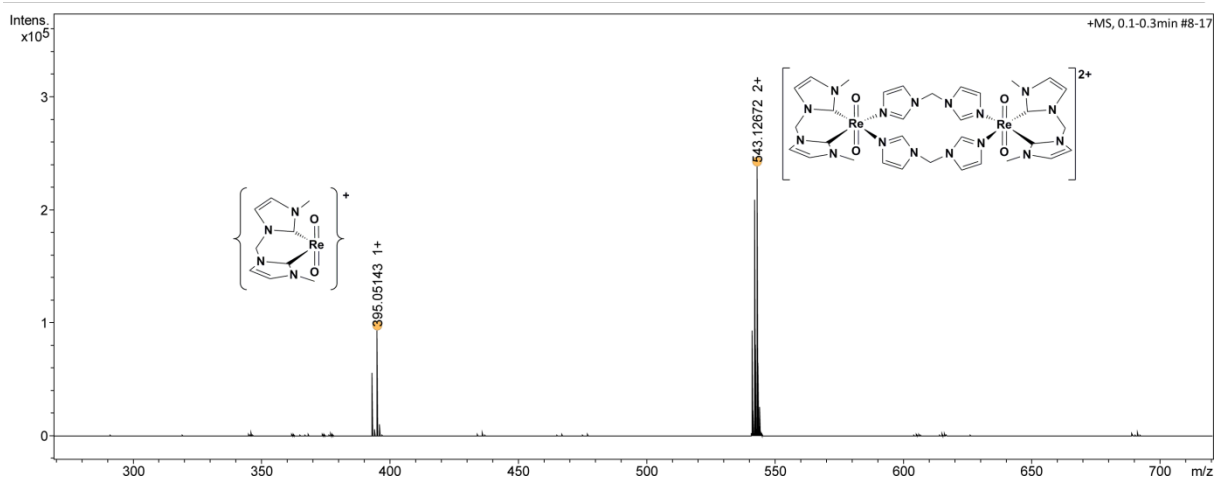

Figure 34: HR-ESI^{+}-MS of $[\mathbf{19}](PF_6)_2$, which shows the $[M]^{2+}$ peak and the peak of the $\{ReO2(\mathbf{L2})\}^{+}$ fragment.

The ligand **L4** has been used before for the preparation of similar structures as the dimeric complexes $[\mathbf{18}]^{2+}$ and $[\mathbf{19}]^{2+}$. For example, **L4** is a ligand in a large number of metal organic frameworks (MOFs) with various metals such as Zn,[105,106] Ni,[105,107] Cu,[106,107] Co,[107] Cd[106,108] and Hg.[109] However, to the best of the author's knowledge, this is the first time that such a dimeric structure with **L4** has been prepared with ^{99}Tc or Re and, especially, the first time **L4** was used as a ligand in combination with NHCs. As it was mentioned before, $[\mathbf{18}]^{2+}$ and $[\mathbf{19}]^{2+}$ are stable in H_2O at neutral and basic conditions. When $[\mathbf{18}]^{2+}$ and $[\mathbf{19}]^{2+}$ were dissolved in a mixture of H_2O and acetone and the orange solutions were acidified with 1 M HCl, a color change to green ($[\mathbf{18}]^{2+}$) or blue ($[\mathbf{19}]^{2+}$) was observed (Scheme 28).

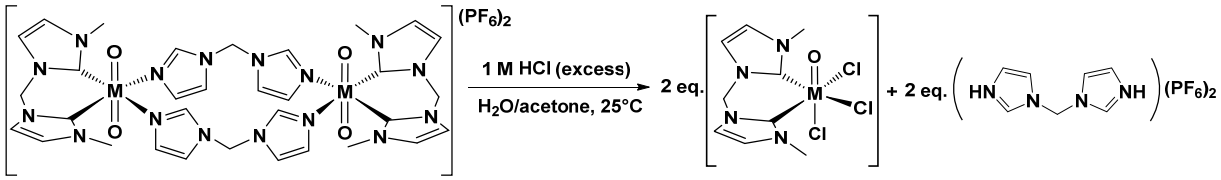

Scheme 28: Synthesis of $[MOCl_3(\mathbf{L2})]$ (M = ^{99}Tc ([**20**]), Re ([**21**])) by acidic cleavage of the corresponding dimeric complexes.

Slow evaporation of these solutions afforded a crude product containing crystalline [$MOCl_3$(**L2**)] (M = ^{99}Tc ([**20**]), Re ([**21**])), with (**L4**-H_2)$^{2+}$ as a colorless crystalline impurity present. NMR experiments of this reaction in DMSO-D_6 confirmed these findings, since the addition of excess 1 M HCl to a solution of [**18**]$(PF_6)_2$ led to a 1:1 mixture of [**20**] and (**L4**-H_2)$^{2+}$ (Figure 35).

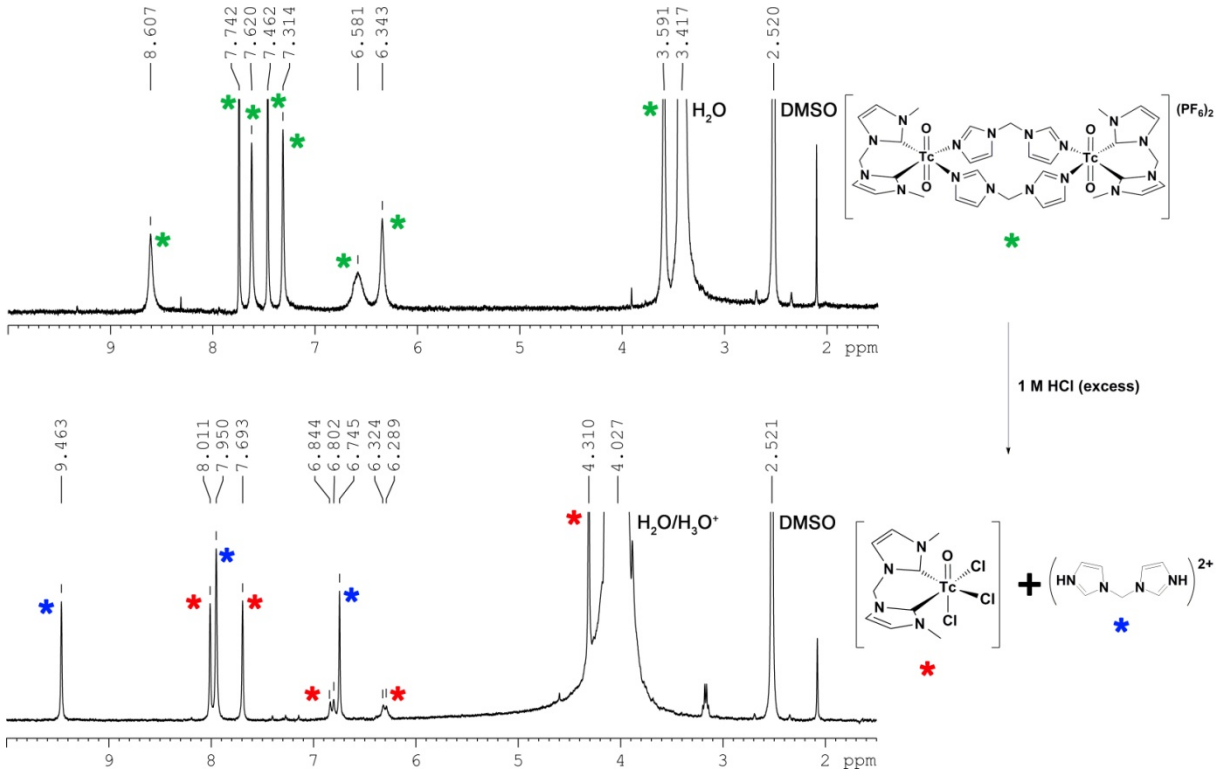

Figure 35: ^{1}H NMR experiment for the acidic cleavage of the ^{99}Tc-N bonds in [**18**]$(PF_6)_2$ using excess 1 M HCl, which leads to a 1:1 mixture of [**20**] and (**L4**-H_2)$^{2+}$.

Purification of [**20**] and [**21**] was done by loading acidic aqueous solutions on a C_{18} SepPak column, followed by washing with 1 M HCl to remove the polar (**L4**-H_2)$^{2+}$. The product was then eluted from the column using neutral H_2O, which presumably leads to exchange of at least one Cl^- ligand for a H_2O ligand. The change from neutral [**20**] and [**21**] to the corresponding charged aquo complexes leads to an increased polarity of the complexes, allowing elution from the C_{18} column. The combined aqueous solutions containing the aquo complex were then again acidified with HCl, followed by evaporation of the solvent with a stream of N_2 to give the analytically pure crystals of [**20**] (47% yield) and [**21**] (64% yield) that are suitable for X-ray diffraction experiments.

[**20**] crystallizes as green blocks in the orthorhombic space group $Pna2_1$. The structure of [**20**] was refined considering a systematic disorder along the O1-Tc1-Cl3 axis, with a ratio of occupancy of 0.60:0.40. The structural features of [**20**] have to be interpreted with caution due to these disorders. The disordered atoms O(1a)/Cl(3b) and O(1b)/Cl(3a) are located at the same positions, while Tc(1a) and Tc(1b) are located above and below the C(1)C(2)Cl(1)Cl(2) plane. Figure 36 shows an ORTEP representation[51] of the major species. The Tc(1a)-O(1a) bond length (1.7339(19) Å, table 28) is

considerably elongated compared to the Tc(1a)-O(1) bond length in $[^{99}TcOCl(\mathbf{L2})_2]^{2+}$ ($[\mathbf{12}]^{2+}$, 1.606(3) Å). The Tc(1a)-Cl bond lengths (2.4293(13) – 2.4587(10) Å) in [**20**] are slightly longer than the Tc(1a)-Cl(1) bond length of $[\mathbf{12}]^{2+}$ (2.4103(15) Å). The Tc(1a)-C bond lengths (2.105(3) and 2.105(4) Å) are significantly shorter than the ^{99}Tc-C bond lengths of $[^{99}TcO_2(\mathbf{L2})_2]^{+}$ ($[\mathbf{10}]^{+}$, 2.170(4) and 2.166(4) Å) and $[\mathbf{12}]^{2+}$ (2.131(5) – 2.201(5) Å). Compared to the ^{99}Tc-C bond lengths found in the structures of the ^{99}Tc-dimer $[\mathbf{18}]^{2+}$ (**conformer 1**: 2.109(3) and 2.107(3) Å, **conformer 2**: 2.103(4) and 2.106(4) Å), the values found in [**20**] are in the same range. The ^{99}Tc centre has a distorted octahedral coordination environment, which is observed e.g. in the Cl-^{99}Tc-Cl angles (82.43(5) – 84.42(5)°), the O(1a)-Tc(1a)-Cl(3a) angle (170.55(8)°) and the C(1)-Tc(1a)-Cl(1) angle (164.17(12)°). Due to the weak steric interactions between **L2** and the Cl^- ligands, the C(1)-Tc(1A)-C(2) bite angle of **L2** (84.80(14)°) is considerably wider than in the structures of $[\mathbf{10}]^{+}$ (81.33(16)°), $[\mathbf{12}]^{2+}$ (81.04(17) and 82.91(17)°) and also wider than the corresponding angle in the structures of $[\mathbf{18}]^{2+}$ (**conformer 1**: 83.88(10)°, **conformer 2**: 82.62(16)°).

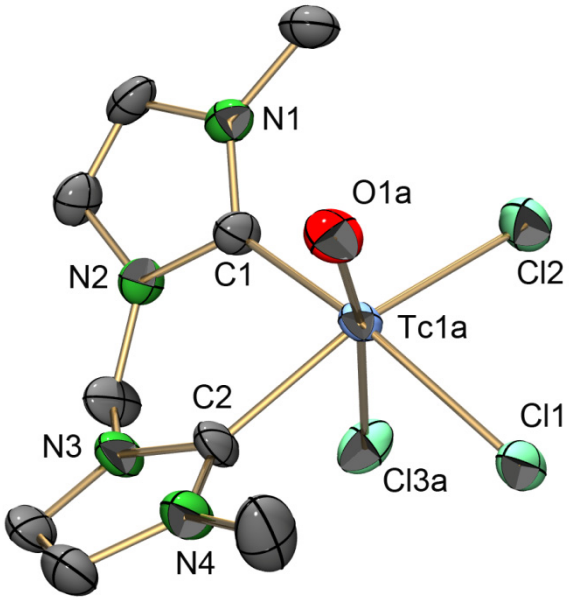

Figure 36: ORTEP representation[51] of the major species in the disordered structure of [**20**]. Thermal ellipsoids are represented at the 50% probability level. Hydrogen atoms are omitted for clarity.

Table 28: Selected bond lengths and angles of [**20**].

Selected bond lengths [Å]		Selected angles [°]	
Tc(1A)-O(1A)	1.7339(19)	O(1A)-Tc(1A)-Cl(3A)	170.55(8)
Tc(1A)-C(1)	2.105(3)	C(1)-Tc(1A)-Cl(1)	164.17(12)
Tc(1A)-C(2)	2.105(4)	O(1A)-Tc(1A)-C(1)	96.12(13)
Tc(1A)-Cl(1)	2.4587(10)	O(1A)-Tc(1A)-C(2)	93.20(14)
Tc(1A)-Cl(2)	2.4293(13)	O(1A)-Tc(1A)-Cl(1)	99.69(7)
Tc(1A)-Cl(3A)	2.4362(17)	O(1A)-Tc(1A)-Cl(2)	104.93(7)
		C(1)-Tc(1A)-C(2)	84.80(14)
		Cl(1)-Tc(1A)-Cl(2)	83.77(4)
		Cl(1)-Tc(1A)-Cl(3A)	82.43(5)
		Cl(2)-Tc(1A)-Cl(3A)	84.42(5)

In the IR spectrum of [**20**], a strong band is observed at 1007 cm^{-1} while no bands were found in the range of 900 – 1000 cm^{-1}. Due to the comparably long ^{99}Tc-O bond observed in the structure of [**20**] (1.7339(19) Å), a shift of the $\nu_{Tc=O}$ band to higher wavenumbers is not expected. However, the disorder along the O1-Tc1-Cl3 axis makes an assignment of the $\nu_{Tc=O}$ band based on structural features challenging. Compared to (N^nBu_4)[$^{99}TcOCl_4$] ($\nu_{Tc=O}$ = 1020 cm^{-1}) and [$^{99}TcOCl$(**L2**)$_2$](PF$_6$)$_2$ ($\nu_{Tc=O}$ = 985 cm^{-1}), the band at 1007 cm^{-1} of [**20**] is in a similar range.[110] Based on this comparison, the band at 1007 cm^{-1} was assigned to the asymmetric $\nu_{Tc=O}$ stretching mode. NMR spectroscopy of [**20**] was done in DMSO-D_6. ^{1}H NMR spectroscopy showed singlets for the CH (7.86 ppm) and CH_3 groups (4.27 ppm), while the CH_2 groups are observed as two doublets at 6.81 and 6.21 ppm. In the ^{13}C NMR spectrum, two signals for the CH groups (126.49 and 124.55 ppm), one signal for the CH_2 group (63.29 ppm) and a signal for the CH_3 group (38.72 ppm) were observed. As it was the case in previous ^{99}Tc-NHC complexes, the ^{99}Tc-C signal is not observed in the ^{13}C NMR due to the broadening of the signal. The chemical shifts of **L2** observed in the ^{1}H and ^{13}C NMR spectrum of [**20**] are comparable to the chemical shifts of **L2** observed in previously described complexes.

The corresponding Re complex, [$ReOCl_3$(**L2**)] ([**21**]), crystallizes as blue blocks in the orthorhombic space group $Pna2_1$. The structure of [**21**] is isostructural to the structure of [**20**] and also contains a disorder along the O1-Re1-Cl3 axis, although in this case the ratio of occupancy is 0.70:0.30. Figure 37 shows the major species of this disordered structure. The bond lengths in [**21**] do not significantly differ from [**20**], with a Re(1a)-O(1a) bond length of 1.748(3) Å, Re(1a)-C bond lengths of 2.092(6) and 2.104(4) Å and Re(1a)-Cl bond lengths in the range of 2.357(2) – 2.4409(12) Å (table 29). The structural similarity to [**20**] is also reflected in the bonding angles, i.e. the Re(1a)-Cl angles of [**21**] are in a range of 83.15(6) – 85.43(8)° compared to the Tc(1a)-Cl angles of [**20**] which are in the range of 82.43(5) – 84.42(5)°.

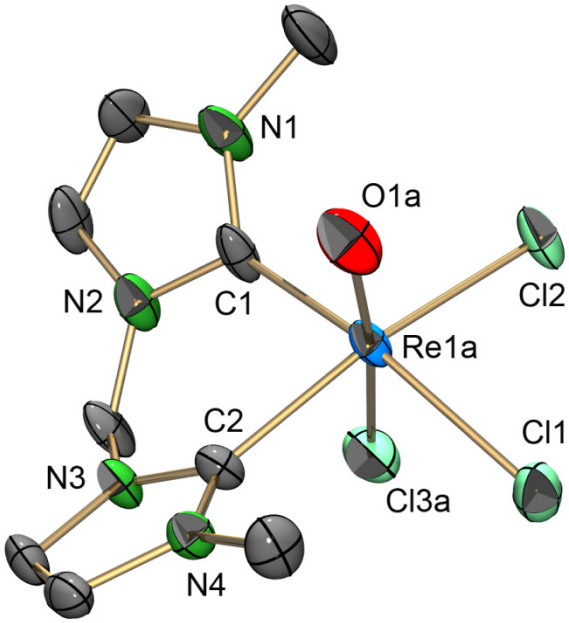

Figure 37: ORTEP representation[51] of the major species in the disordered structure of [**21**]. Thermal ellipsoids are represented at the 50% probability level. Hydrogen atoms are omitted for clarity.

Table 29: Selected bond lengths and angles of [**21**].

Selected bond lengths [Å]		Selected angles [°]	
Re(1A)-O(1A)	1.748(3)	O(1A)-Re(1A)-Cl(3A)	171.89(12)
Re(1A)-C(1)	2.092(6)	C(1)-Re(1A)-Cl(1)	164.14(18)
Re(1A)-C(2)	2.104(4)	O(1A)-Re(1A)-C(1)	93.3(2)
Re(1A)-Cl(1)	2.4292(17)	O(1A)-Re(1A)-C(2)	94.80(18)
Re(1A)-Cl(2)	2.4409(12)	O(1A)-Re(1A)-Cl(1)	102.52(11)
Re(1A)-Cl(3A)	2.357(2)	O(1A)-Re(1A)-Cl(2)	99.14(10)
		C(1)-Re(1A)-C(2)	84.4(2)
		Cl(1)-Re(1A)-Cl(2)	84.03(5)
		Cl(1)-Re(1A)-Cl(3A)	85.43(8)
		Cl(2)-Re(1A)-Cl(3A)	83.15(6)

IR spectroscopy of [**21**] shows a very similar spectrum compared to [**20**]. Between 900 and 1000 cm^{-1}, only a weak band at 962 cm^{-1} was found. A strong band at 1007 cm^{-1} was observed, which was also found in the IR spectrum of [**20**] and thus was assigned to the asymmetric $\nu_{Re=O}$ stretching mode.^{1}H NMR spectroscopy of [**21**] in DMSO-D_6 shows two doublets for the CH groups (7.75 and 7.72 ppm) which have very low coupling constants ($^{3}J(HH)$ = 1.8 Hz). This is a major difference compared to the corresponding ^{99}Tc complex [**20**], where the CH group was observed as one singlet (7.86 ppm). As it was the case in [**20**], the CH_2 groups were observed as two doublets (6.70 and 6.59 ppm) and the CH_3 groups were observed as a singlet with a chemical shift of 4.28 ppm. In the ^{13}C NMR spectrum of [**21**], the only major difference compared to [**20**] is the observed Re-C signal at

145.67 ppm, which is considerably shifted to lower ppm values compared to $[ReO_2(\mathbf{L2})_2]^+$ (176.83 ppm in CD_3CN) and the Re-dimer $[\mathbf{19}]^{2+}$ (168.34 ppm in CD_3CN).

$[MOCl_3(\mathbf{L2})]$ is an interesting starting material for the derivatization of the $\{MO(\mathbf{L2})\}^{3+}$ fragment (M = Re, ^{99}Tc). As mentioned before, dissolution of [**20**] and [**21**] in H_2O leads to a color change from green to orange-red (M = ^{99}Tc) and blue to purple (M = Re), indicating that at least one of the Cl^- ligands is exchanged for H_2O or OH^- in aqueous solution. Derivatization of the $\{MO(\mathbf{L2})\}^{3+}$ fragment with bidentate ligands was studied with 2,2'-bipyridine (bipy) as a model ligand. Addition of bipy to a solution of [**20**] and [**21**] in acetone/H_2O (1:1) did not visibly lead to a reaction. However, after addition of NEt_3 to the solution, a color change to yellow was observed, indicating formation of $[MO_2(\mathbf{L2})(bipy)]^+$ (Scheme 29, M = ^{99}Tc ($[\mathbf{22}]^+$), Re ($[\mathbf{23}]^+$)). $[\mathbf{22}]^+$ and $[\mathbf{23}]^+$ were isolated by precipitation from the aqueous solution using NH_4PF_6, with yields of 66% ($[\mathbf{22}](PF_6)$) and 20% ($[\mathbf{23}](PF_6)$). For high purity single-crystalline compounds, the complexes were crystallized from 1:1 acetone/H_2O solutions by slow evaporation of the acetone. The stability of $[\mathbf{22}](PF_6)$ and $[\mathbf{23}](PF_6)$ in aqueous solutions at pH ≥ 7 appears to be similar to the stability of $[^{99}TcO_2(\mathbf{L2})_2]^+$ ($[\mathbf{10}]^+$) and no decomposition was observed over days. Spectroscopic analysis of $[\mathbf{23}](PF_6)$ will be finished in the near future and thus only the crystal structure of this compound will be discussed in this thesis.

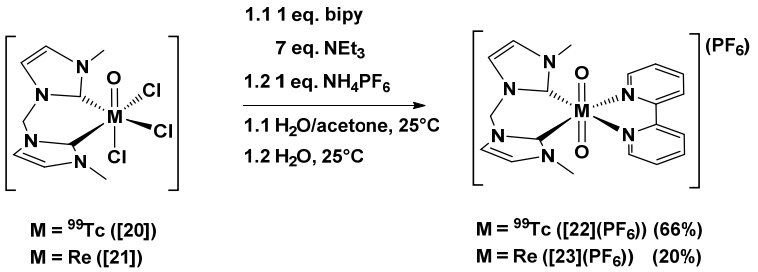

Scheme 29: Synthesis of $[MO_2(\mathbf{L2})(bipy)](PF_6)$ (M = ^{99}Tc ($[\mathbf{22}]^+$), Re ($[\mathbf{23}]^+$) under basic aqueous conditions.

$[\mathbf{22}](PF_6)$ crystallizes as yellow blocks of the composition $[\mathbf{22}](PF_6)\cdot H_2O$ in the orthorhombic space group Pbcm (Figure 38). The co-crystallized H_2O connects two molecules of $[\mathbf{22}]^+$ via H-bonds to linear chain structures in the solid state. The donor-acceptor distances of these H-bonding interactions are 2.713(3) and 2.716(3) Å and the DHA angles are almost linear (178(6)° and 174(6)°). The ^{99}Tc-O bond lengths (1.7506(19) and 1.7560(19) Å, table 30) are in the same range as the ^{99}Tc-O bond length in $[\mathbf{10}](PF_6)\cdot H_2O$ (1.765(3) Å). The ^{99}Tc-C bond length in $[\mathbf{22}]^+$ (2.1134(18) Å) is considerably shorter than in $[\mathbf{10}](PF_6)\cdot H_2O$ (2.170(4) and 2.166(4) Å) which is explained by the reduced steric interactions of the methyl substituents of the **L2** ligand in $[\mathbf{22}]^+$. Compared to the ^{99}Tc-C bond lengths in the structures of its precursor complexes $[\mathbf{18}]^{2+}$ (2.103(4) – 2.109(3) Å) and [**20**] (2.105(3) – 2.105(4) Å), the ^{99}Tc-C bonds in $[\mathbf{22}]^+$ are in the same range but slightly elongated, presumably due to the steric influence of the equatorial bipy ligand. Comparison of the ^{99}Tc-N bond lengths in $[\mathbf{22}]^+$ to $[^{99}TcO_2(bipy)_2]^+$ is not possible, since the steric interactions of the bipy ligands prohibit its formation.[13] Therefore, a comparison to the ^{99}Tc-N bond lengths in $[^{99}TcO_2(py)_4](Cl)\cdot 2H_2O$

(2.142(2) – 2.161(2) Å) and *cis*-[^{99}TcNBr(bipy)$_2$][^{99}TcBr$_4$]·MeOH (2.109(18) – 2.161(18) Å) is given,[103,111] which have significantly shorter ^{99}Tc-N bond lengths than [**22**]$^+$ (2.2125(16) Å). This elongation is presumably explained by the *trans*-influence of the strongly σ-donating NHC ligand in combination with the steric influence of the CH_3 substituents of **L2** on the bipy ligand. The O-^{99}Tc-O angle is considerably bent (171.69(9)°), which has already been observed in the structures of [**18**]$(PF_6)_{1.5}(Cl)_{0.5}$·3DMF·4H_2O (171.80(13)°) and [**18**]$(PF_6)_2$·2H_2O (172.16(9)°). The deviation from 180° might arise from the strong H-bonding interactions of the co-crystallized H_2O in combination with the steric interactions arising from the CH_2 group of **L2**. In comparison, the O-^{99}Tc-O angles in the structures of [**10**](PF_6)·H_2O (180.00(9)°) and its Re analogue *trans*-[**16**](PF_6)·2H_2O·3THF·$LiPF_6$ (180.0°) are linear. The C-^{99}Tc-C angle of [**22**]$^+$ (81.34(10)°) is similar as in [**10**](PF_6)·H_2O (81.33(16)°), but considerably smaller than in [**18**]$(PF_6)_{1.5}(Cl)_{0.5}$·3DMF·4H_2O (83.88(10)°), [**18**]$(PF_6)_2$·2H_2O (82.62(16)°) and [**20**] (84.80(14)°). This observation confirms previous conclusions that the steric interactions between the equatorial ligands have a significant influence on the bite angle of **L2**.

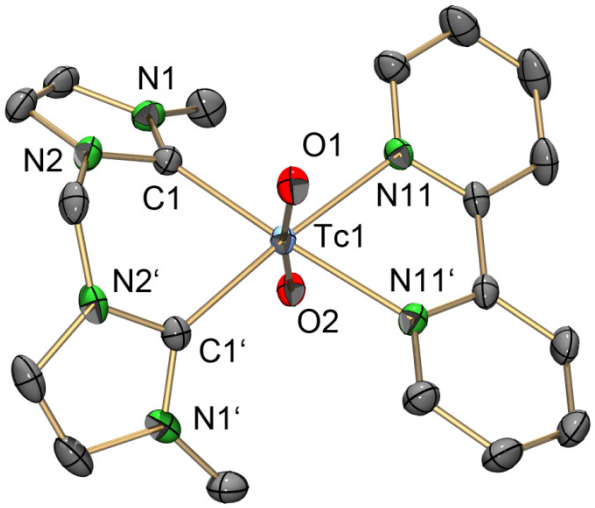

Figure 38: ORTEP representation[51] of the [^{99}TcO$_2$(**L2**)(bipy)]$^+$ ([**22**]$^+$) cation of the [**22**](PF_6)·H_2O structure. Thermal ellipsoids are represented at the 50% probability level. Hydrogen atoms are omitted for clarity.

Table 30: Selected bond lengths and angles of [**22**]$^+$.

Selected bond lengths [Å]		Selected angles [°]	
Tc(1)-O(1)	1.7506(19)	O(1)-Tc(1)-O(2)	171.69(9)
Tc(1)-O(2)	1.7560(19)	O(1)-Tc(1)-C(1)	93.06(7)
Tc(1)-C(1)	2.1134(18)	O(2)-Tc(1)-C(1)	93.24(7)
Tc(1)-N(11)	2.2125(16)	O(1)-Tc(1)-N(11)	88.54(6)
		O(2)-Tc(1)-N(11)	84.80(6)
		C(1)-Tc(1)-C(1)#1	81.34(10)
		N(11)-Tc(1)-N(11)#1	73.49(9)

IR spectroscopy of [**22**](PF_6) showed a strong band at 836 cm^{-1} (PF_6^-) and in addition two strong bands at 793 and 762 cm^{-1}. The band at 762 cm^{-1} was already observed in previous $\{^{99}Tc^{V}O_2\}^+$-NHC complexes and is assigned to the characteristic asymmetric $\nu_{O=Tc=O}$ stretching mode. The strong band at 793 cm^{-1} corresponds to the symmetric $\nu_{O=Tc=O}$ stretching mode, which is IR active due to the bent O-^{99}Tc-O angle. The same bands were observed for [**18**](PF_6)$_2$ (795 cm^{-1} and 764 cm^{-1}), which also has a non-linear O-^{99}Tc-O angle. The value of the asymmetric $\nu_{O=Tc=O}$ stretching mode is comparable to the corresponding band of [**10**](PF_6) (765 cm^{-1}). ^{1}H NMR spectroscopy of [**22**](PF_6) in acetone-D_6 shows four signals for the bipy-CH groups (9.5 – 7.8 ppm) that are shifted to significantly higher ppm values compared to uncoordinated 2,2'-bipyridine (8.59 – 7.12 ppm, measured in CCl_4).[57] To the best of the author's knowledge, $\{^{99}TcO_2\}^+$ complexes containing bipy as a ligand have not been reported before and therefore, a comparison to $\{^{99}TcO\}^{3+}$ complexes containing bipy will be made. The ^{1}H signals of the bipy-CH protons in [**22**](PF_6) are slightly shifted to higher ppm values compared to [^{99}TcO(*p*-$CH_3C_6H_4S)_3$(bipy)] (9.15 – 7.01 ppm, measured in $CDCl_3$) and [^{99}TcO(*p*-$CH_3OC_6H_4S)_3$(bipy)] (9.20 – 7.11 ppm, measured in $CDCl_3$).[112] The ligand **L2** has two signals for the CH protons (7.85 and 7.56 ppm), two doublets for the CH_2 protons (7.13 and 6.57 ppm) and a singlet for the CH_3 protons (4.17 ppm), which are comparable to values found for **L2** in [**10**](PF_6). In the ^{13}C NMR spectrum, all five signals of the carbon atoms of the bipy ligand were observed in the range of 155.85 – 124.84 ppm, along with the expected four signals for the **L2** ligand (124.41, 123.81, 62.94 and 37.80 ppm). As it was described before, the ^{99}Tc-C signal was not observed due to the broadening caused by the ^{99}Tc nucleus. The chemical shifts of **L2** observed in the ^{13}C NMR spectrum of [**22**](PF_6) are comparable to the chemical shifts of **L2** observed in [**10**](PF_6). The chemical shifts of the bipy ligand observed in the ^{13}C NMR spectrum of [**22**](PF_6) (155.85 – 124.84 ppm) are in agreement with the chemical shifts observed for [^{99}TcO(*p*-$CH_3C_6H_4S)_3$(bipy)] (151.95 – 120.81 ppm, measured in $CDCl_3$) and [^{99}TcO(*p*-$CH_3OC_6H_4S)_3$(bipy)] (151.92 – 120.73 ppm, measured in $CDCl_3$).[112]

The corresponding Re complex, [**23**](PF_6), crystallizes as yellow blocks of the composition [**23**](PF_6)·H_2O in the orthorhombic space group Pbcm (Figure 39). The structure is isostructural to [**22**](PF_6)·H_2O. The H-bonding of the co-crystallized H_2O and the O^{2-} ligands forms a linear chain structure in the solid state. The donor-acceptor distances (2.707(4) and 2.699(4) Å) and DHA angles (177(7) and 1.78(8)°) are very similar to those found in [**22**](PF_6)·H_2O. Following general trends, the Re-O bond lengths of [**23**]$^+$ (1.765(3) and 1.774(3) Å, table 31) are slightly longer than the corresponding bond lengths in [**22**](PF_6)·H_2O (1.7506(19) and 1.7560(19) Å). Compared to the Re-O bond lengths of the structure of the Re dimer [**19**](PF_6)$_2$·$2H_2O$ (1.7840(19) and 1.7636(18) Å) the values found for [**23**]$^+$ are in the same range, but they are significantly longer than in *trans*-[**16**](PF_6)·$2H_2O$·3THF·$LiPF_6$ (1.699(3) Å). This elongation of the Re-O bonds in [**23**]$^+$ might be due to the shorter Re-C bond length in [**23**]$^+$ (2.119(3) Å) compared to [**16**]$^+$ (2.170(4) and 2.246(4) Å) which presumably also leads to the bent O-Re-O angle (172.25(12)°) due to steric interactions of the CH_2 group of **L2** with the O^{2-} ligands. Besides this, the H-bonding interactions of the O^{2-} ligands with

the water of crystallization might also have an influence on the length of the Re-O bonds. The Re-N bond lengths of [**23**]$^{+}$ (2.206(2) Å) are comparable to the ^{99}Tc-N bond lengths found in [**22**]$^{+}$ (2.2125(16) Å). Other structural features such as the C-Re-C bite angle are in agreement with the values and trends described for the structure of [**22**]$^{+}$. Structurally characterized $\{Re^{V}O_2\}^{+}$ complexes with bipy ligands are rare, with *cis*-$[ReO_2(bipy)(py)_2](ClO_4)\cdot 0.33py\text{-}H\cdot 0.33ClO_4\cdot 0.33$acetone being the only other structurally characterized compound.[98] *Cis*-$[ReO_2(bipy)(py)_2](ClO_4)\cdot 0.33py\text{-}H\cdot 0.33ClO_4\cdot 0.33$acetone has slightly shorter Re-O bond lengths (1.733(8) and 1.736(7) Å) and comparable Re-N bond lengths (2.21(1) Å).

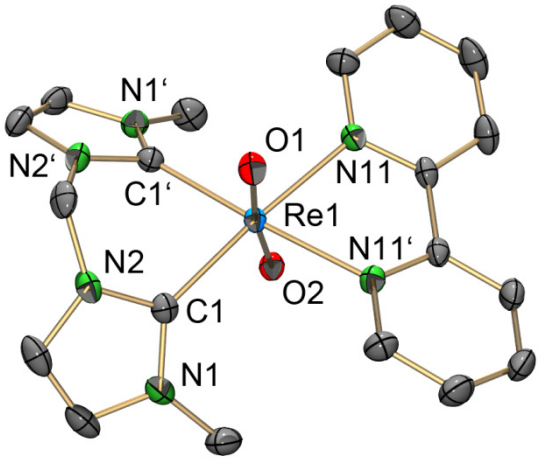

Figure 39: ORTEP representation[51] of the $[ReO_2(\mathbf{L2})(bipy)]^{+}$ ([**23**]$^{+}$) cation of the [**23**]$(PF_6)\cdot H_2O$ structure. Thermal ellipsoids are represented at the 50% probability level. Hydrogen atoms are omitted for clarity.

Table 31: Selected bond lengths and angles of [**23**]$^{+}$.

Selected bond lengths [Å]		Selected angles [°]	
Re(1)-O(1)	1.765(3)	O(1)-Re(1)-O(2)	172.25(12)
Re(1)-O(2)	1.774(3)	O(1)-Re(1)-C(1)	92.86(10)
Re(1)-C(1)	2.119(3)	O(2)-Re(1)-C(1)	93.02(10)
Re(1)-N(11)	2.206(2)	O(1)-Re(1)-N(11)	88.74(9)
		O(2)-Re(1)-N(11)	85.05(9)
		C(1)-Re(1)-C(1)#1	81.18(15)
		N(11)-Re(1)-N(11)#1	73.46(12)

The presented complexes containing the $\{MO(\mathbf{L2})\}^{3+}$ fragment (M = Re, ^{99}Tc) represent a new class of compounds in Re- and ^{99}Tc-NHC chemistry. While the synthetic route via the formation of the dimeric $[MO_2(\mathbf{L2})(\mathbf{L4})]_2(PF_6)_2$ complexes is presumably not suitable for application with ^{99m}Tc due to the low concentrations of $[^{99m}TcO_4]^{-}$ used, it still represents an important contribution to the fundamental chemistry of ^{99}Tc and Re. Furthermore, the acidic cleavage of the dimeric complexes led to the isolation of $[MOCl_3(\mathbf{L2})]$, which is an interesting starting material for the synthesis of complexes containing the $\{MO(\mathbf{L2})\}^{3+}$ fragment. The derivatization of $[MOCl_3(\mathbf{L2})]$ with bipy was

successfully tested and the resulting $[MO_2(\mathbf{L2})(bipy)]^+$ complexes are stable under aqueous conditions. The fact, that the synthesis of $[MO_2(\mathbf{L2})(bipy)]^+$ was done under aqueous conditions further underlines the stability of the $\{MO(\mathbf{L2})\}^{3+}$ fragment. $[MOCl_3(\mathbf{L2})]$ might also be a potential starting material for the synthesis of trimeric $[M_3O_3(\mu\text{-}O)_3X_3(\mathbf{L2})_3]^{n+}$ complexes (X = monodentate ligand), in the future. Following the synthesis of $[MO_2(\mathbf{L2})(bipy)]^+$, the synthesis of $[^{99m}TcO_2(\mathbf{L2})(bipy)]^+$ might also be possible, although not via the dimeric complex $[^{99m}TcO_2(\mathbf{L2})(\mathbf{L4})]_2(PF_6)_2$. While this was not tested in this thesis, a synthetic strategy using a mixture of $(\mathbf{L2}\text{-}H_2)^{2+}$ and bipy might lead to $[^{99m}TcO_2(\mathbf{L2})(bipy)]^+$, since its formation could be preferred over the formation of $[^{99m}TcO_2(\mathbf{L2})_2]^+$ due to the faster formation of the ^{99m}Tc-N bond. Also, the formation of *trans*-$[^{99m}TcO_2(bipy)_2]^+$ is prevented by the steric interaction of the coplanar bipy ligands.[13] However, the synthesis of $[^{99m}TcO_2(\mathbf{L2})_2]^+$, which is described in the next chapter, provides important limitations for the preparation of $^{99m}Tc^V$-NHC complexes, which presumably would also have an impact on a future synthesis of $[^{99m}TcO_2(\mathbf{L2})(bipy)]^+$.

4.2.2.5 Synthesis of $[^{99m}Tc^{V}O_2(L2)_2]^+$

The translation of the synthetic procedure used for the preparation of $[^{99}TcO_2(\mathbf{L2})_2]^+$ ($[\mathbf{10}]^+$) to ^{99m}Tc chemistry proved to be difficult, which was mainly due to the lack of a reliable synthesis of a $^{99m}Tc^{V}$ starting material and the fact that synthesis had to be done under exclusion of H_2O. As described before for the synthesis of $[^{99m}Tc(arene)_2]^+$ complexes, extraction of $[^{99m}TcO_4]^-$ from the saline solution into organic solvents using the ionic liquid $[P(C_6H_{13})_3(C_{14}H_{29})]Br$ (IL) proved to be a good method for the work under exclusion of H_2O (Figure 40).

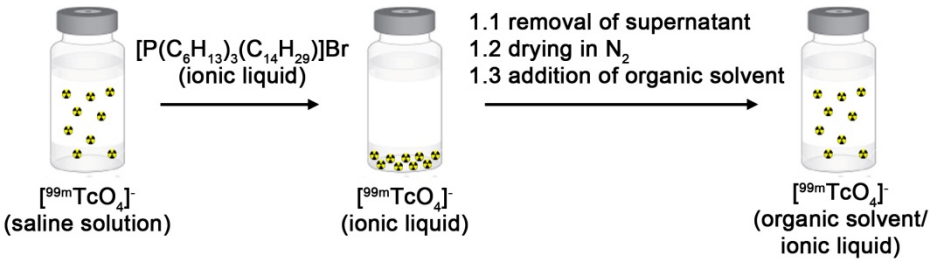

Figure 40: General procedure for the extraction of $[^{99m}TcO_4]^-$ into organic solvents using the ionic liquid $[P(C_6H_{13})_3(C_{14}H_{29})]Br$.

However, the use of IL has the drawback that it prevents the HPLC- or TLC analysis of the reaction solution and thus, reaction solutions containing IL have to be extracted using H_2O before analysis. This makes a systematic study of the synthesis of $[^{99m}\mathbf{10}]^+$ difficult, since reaction solutions that were extracted with H_2O for analysis cannot be used again for further synthesis. In addition to this problem, the synthesis of the $[^{99m}TcO(glyc)_2]^-$ ($[^{99m}\mathbf{8}]^-$, glyc-H_2 = ethylene glycol) starting material proved to be very challenging. Seifert *et al.* described a procedure for the preparation of $[^{99m}\mathbf{8}]^-$ from $[^{99m}TcO_4]^-$ using a very low amount of $SnCl_2$ in the presence of glyc-H_2, which was directly used for the synthesis of '3+1' mixed-ligand ^{99m}Tc complexes.[113] However, a method to control the formation of $[^{99m}\mathbf{8}]^-$ was not given. Treatment of $[^{99m}TcO_4]^-$ with $SnCl_2$ in the presence of a suitable ligand is a general method for the synthesis of Tc^{V} complexes, but the amount of $SnCl_2$ used in a reaction strongly depends on the present ligands and is by no means a fixed entity.[114,115] The fact that the amount of $SnCl_2$ needed for the synthesis of $[^{99m}\mathbf{10}]^+$ presumably cannot be derived from previously published syntheses further complicates the synthetic challenge. Scheme 30 shows the general approach for the synthesis of $[^{99m}\mathbf{10}]^+$ starting from $[^{99m}TcO_4]^-$.

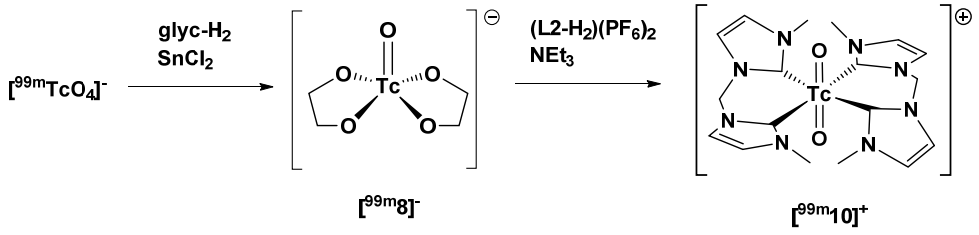

Scheme 30: General approach for the synthesis of $[^{99m}\mathbf{10}]^+$ starting from $[^{99m}TcO_4]^-$.

To compare the reaction to [^{99m}**8**]$^-$ with an established reaction, the ^{99m}Tc-glucoheptonate kit was tested, which is generally used for exchange reactions with ligands to form corresponding $^{99m}Tc^V$ complexes. Addition of [$^{99m}TcO_4$]$^-$ to the ^{99m}Tc-glucoheptonate kit followed by 10 min of stirring led to a broad peak at 4-6 min in the HPLC analysis with a triethylammonium phosphate (TEAP) buffer and no remaining [$^{99m}TcO_4$]$^-$ was detected. Testing the same solution with a trifluoroacetic acid (TFA) buffer reveals a comparably narrow peak at 3.9 min, which is at the same retention time as for [$^{99m}TcO_4$]$^-$ (3.8 min). A comparable experiment was done for the formation of [^{99m}**8**]$^-$, in which a vial was charged with 10 µl glyc-H_2 and the same amount of $SnCl_2$ as in the ^{99m}Tc-glucoheptonate kit, followed by addition of the [$^{99m}TcO_4$]$^-$ solution and stirring for 10 min. HPLC analysis of this solution showed again a broad peak at 4-6 min with the TEAP method, indicating that no [$^{99m}TcO_4$]$^-$ was left, and a narrow peak at 3.8 min with the TFA method, which is at the same retention time as [$^{99m}TcO_4$]$^-$. The results of these two tests indicate that all [$^{99m}TcO_4$]$^-$ was reduced, presumably to the corresponding $^{99m}Tc^V$ complexes. However, the tests also revealed that due to the similar retention time, the formed [^{99m}**8**]$^-$ cannot be distinguished from [$^{99m}TcO_4$]$^-$ with the TFA method. Due to the observation that [**10**]$^+$ is best analyzed with the TFA method, this is again a drawback.

Because of the difficulty in controlling the formation of [^{99m}**8**]$^-$, the synthesis of [^{99m}**10**]$^+$ was tested assuming full conversion of [$^{99m}TcO_4$]$^-$ to [^{99m}**8**]$^-$. Prior to the formation of [^{99m}**8**]$^-$, the [$^{99m}TcO_4$]$^-$ was extracted from the saline solution using the IL method described above, followed by removal of the supernatant saline solution. Glyc-H_2 dissolved in EtOH was added to the still wet IL containing [$^{99m}TcO_4$]$^-$, followed by a solution of $SnCl_2 \cdot 2H_2O$ in EtOH. At this point, full conversion of the [$^{99m}TcO_4$]$^-$ to the [^{99m}**8**]$^-$ was assumed. The EtOH was evaporated and the residue dried with a stream of N_2 for at least 45 min. Then, the reaction to [^{99m}**10**]$^+$ was done by addition of a CH_3CN solution containing NEt_3 and (**L2**-H_2)$(PF_6)_2$ to the vial containing [^{99m}**8**]$^-$ (Scheme 31, **method a**). After heating of the reaction on 70°C for 50 min, the solvent of the reaction was again evaporated using N_2 and the resulting residue was taken up in H_2O. At this point, HPLC analysis was done to see if product had formed, which was not possible before due to the presence of IL in the organic solvent. HPLC analysis with the TFA method showed a peak at 15.8 min, which corresponds to the retention time of [^{99}**10**]$^+$. A peak at 17.0 min was also present, indicating that a side product might have formed during the reaction. In order to purify the formed [^{99m}**10**]$^+$, it was loaded on a C_{18} SepPak column, washed with saline solution and eluted with MeOH. When a coinjection of the resulting MeOH solution with a CH_3CN solution of [^{99}**10**]$^+$ was done, a large peak at 4.0 min was also present, indicating formation of [$^{99m}TcO_4$]$^-$. Decomposition of [^{99m}**10**]$^+$ was not expected, since [^{99}**10**]$^+$ was stable in aqueous solutions for days. Therefore, the formation of [$^{99m}TcO_4$]$^-$ was presumably caused by the decomposition of the side product, either before or during purification with the C_{18} column. The overall yield of [^{99m}**10**]$^+$ for this reaction was 13% with a radiochemical purity of 42% (**method a**).

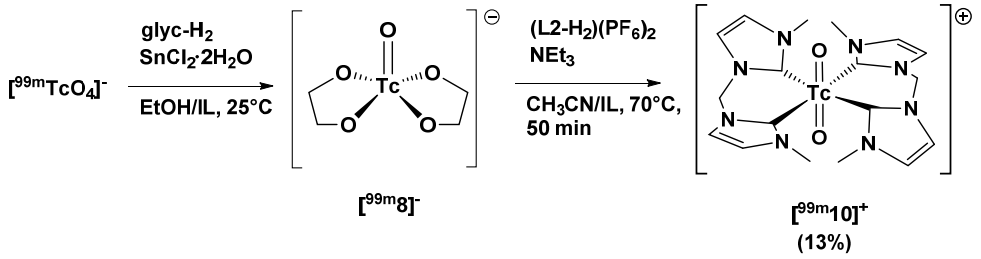

Scheme 31: Preparation of $[^{99m}\mathbf{10}]^+$ using (**L2**-H_2)$(PF_6)_2$ and NEt_3 in CH_3CN (**method a**).

In order to improve the reaction, the transmetalation complex $[Ag_2(\mathbf{L2})_2](PF_6)_2$ ($[\mathbf{6}](PF_6)_2$) was used instead of using the combination of NEt_3 and (**L2**-H_2)$(PF_6)_2$ (Scheme 32, **methods b** and **c**). Further changes were made by using exclusively reagents that were prepared and dissolved in a glovebox to avoid the presence of H_2O and O_2 in the reaction solution. For the formation of $[^{99m}\mathbf{8}]^-$, a stock solution of anhydrous $SnCl_2$ in dry 1:1 CH_3CN/DMF was prepared, while the solubility of $SnCl_2$ is best in DMF. After the extraction of $[^{99m}TcO_4]^-$, the IL was dried with a stream of N_2 for 1 h. A solution of glyc-H_2 in CH_3CN was added, followed by a solution of $SnCl_2$ in CH_3CN. The resulting solution containing $[^{99m}\mathbf{8}]^-$ was stirred for 15 min, a solution of $[\mathbf{6}](PF_6)_2$ was added and the resulting suspension was stirred for 1 h at 65°C. A colorless precipitate formed during the addition of $[\mathbf{6}](PF_6)_2$, which is explained by formation of AgX (X = Br, Cl) due to the present halides from the IL, the saline solution or the $SnCl_2$. After evaporation of the solvent with N_2, the residue was suspended in H_2O and centrifuged. The supernatant containing $[^{99m}\mathbf{10}]^+$ was separated and analyzed with HPLC, showing a peak at 15.8 min ($[^{99m}\mathbf{10}]^+$) and a peak at 3.7 min ($[^{99m}TcO_4]^-$ or $[^{99m}\mathbf{8}]^-$, figure 41, a)). In addition, a small peak at 17.4 min was also present, which is presumably caused by a side product of the reaction. In order to purify the formed $[^{99m}\mathbf{10}]^+$, it was loaded on a C_{18} SepPak column, washed with saline solution and eluted with MeOH (Figure 41, b)). Despite this purification step, a small peak at 3.7 min was still present in the following HPLC analysis. This is explained either by a retention of $[^{99m}\mathbf{8}]^-$ in the C_{18} column, or by a decomposition of the side product before or during the purification. The overall yield of this reaction was 5%, with a radiochemical purity of 72% (**method b**).

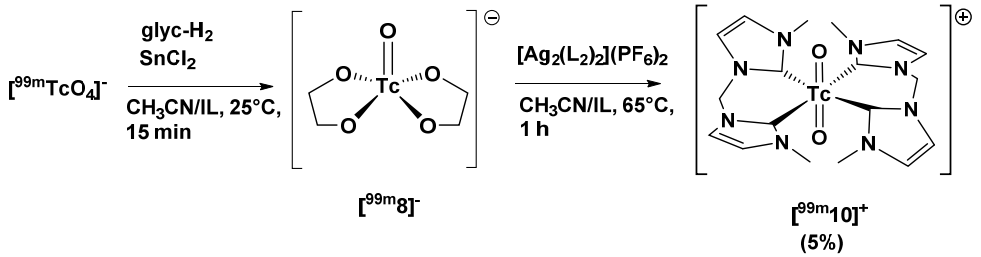

Scheme 32: Preparation of $[^{99m}\mathbf{10}]^+$ using $[Ag_2(\mathbf{L2})_2](PF_6)_2$ ($[\mathbf{6}](PF_6)_2$) in CH_3CN (**methods b** and **c**).

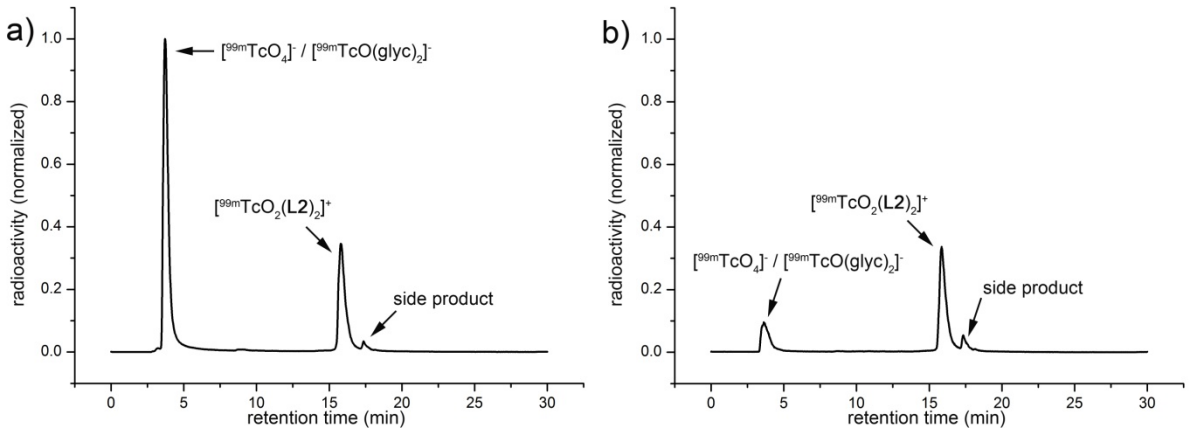

Figure 41: HPLC analysis of the preparation of $[^{99m}TcO_2(\mathbf{L2})_2]^+$ showing the formation of a side product during the reaction. a) Saline solution after extraction from the organic phase. b) MeOH solution after purification using a C_{18} SepPak column.

The stability of the formed $[^{99m}\mathbf{10}]^+$ was further investigated in neutral- (pH = 7), acidic- (pH = 1) and basic saline (pH = 11). For the stability measurements, the MeOH solution containing $[^{99m}\mathbf{10}]^+$ was evaporated with a stream of N_2 and the residue was dissolved in saline solution. The pH of the saline solution was then adjusted using 1 M HCl or NaOH solutions. $[^{99m}\mathbf{10}]^+$ is stable in saline solution at neutral pH for at least 120 min at 40°C (Figure 42). When the same solution was acidified with 1 M HCl and heated on 40°C for 30 min, no decomposition was observed as well. The observed side product appears to slightly decompose under acidic conditions, since a decrease in the intensity of the peak was observed when the solution was acidified.

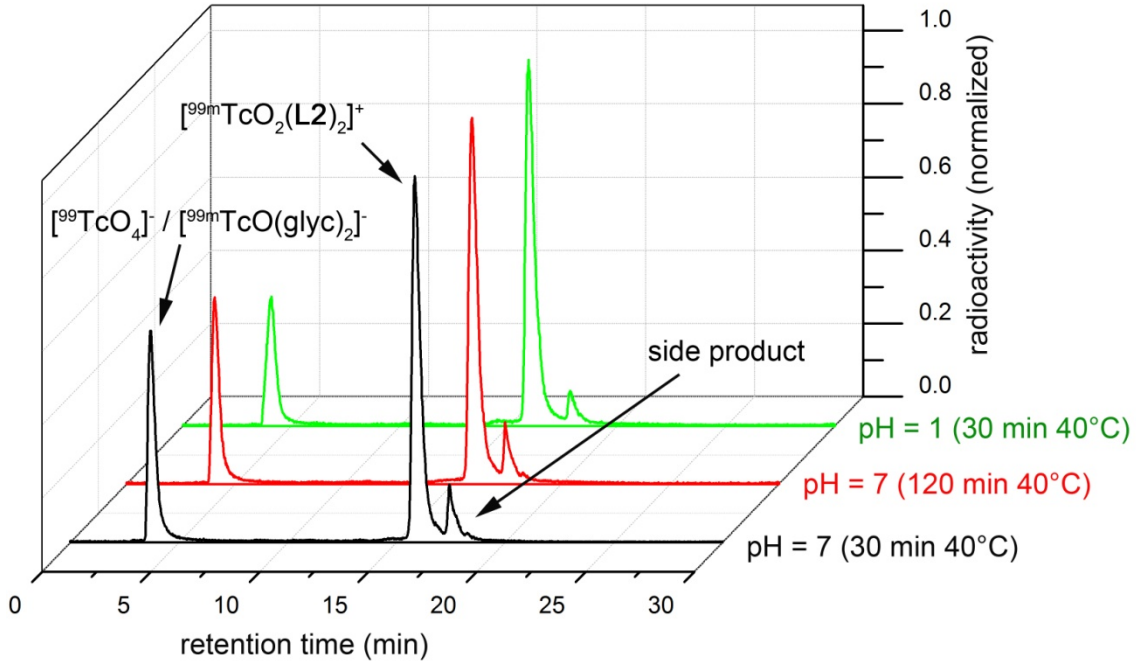

Figure 42: Stability analysis of the isolated $[^{99m}TcO_2(\mathbf{L2})_2]^+$ in saline solution at pH = 7 and pH = 1 at 40°C. No significant decomposition of $[^{99m}TcO_2(\mathbf{L2})_2]^+$ was observed.

The stability at basic pH was tested with a different solution of [^{99m}**10**]$^+$, which had been prepared using four times the amount of $SnCl_2$ stock solution (**method c**). HPLC analysis directly after the reaction showed a considerably higher amount of side product formed, which presumably decomposed before or during purification with the C_{18} SepPak since it was not observed anymore in the stability analysis. As it was the case before, a peak at 3.7 min ([^{99m}TcO$_4$]/[^{99m}**8**]$^-$) was still present after the purification, but in this case the amount observed was considerably larger (Figure 43). This could be explained by the increased amount of $SnCl_2$ present in the reaction, which leads to a larger amount of [^{99m}**8**]$^-$ that might have been retained on the C_{18} column. On the other hand, an increase of the 3.7 min peak might also be caused by the decomposition of the side product to [^{99m}TcO$_4$]$^-$ during or before the purification. The isolated [^{99m}**10**]$^+$ showed no significant decomposition under basic aqueous conditions for at least 90 min when heated on 40°C (Figure 43). The results of the stability analysis of [^{99m}**10**]$^+$ are in agreement with the experimentally determined stability of its ^{99}Tc analogue. The higher amount of $SnCl_2$ used in this reaction had a negative impact on the amount of product obtained, with an overall yield of only 2% and a radiochemical purity of 28%.

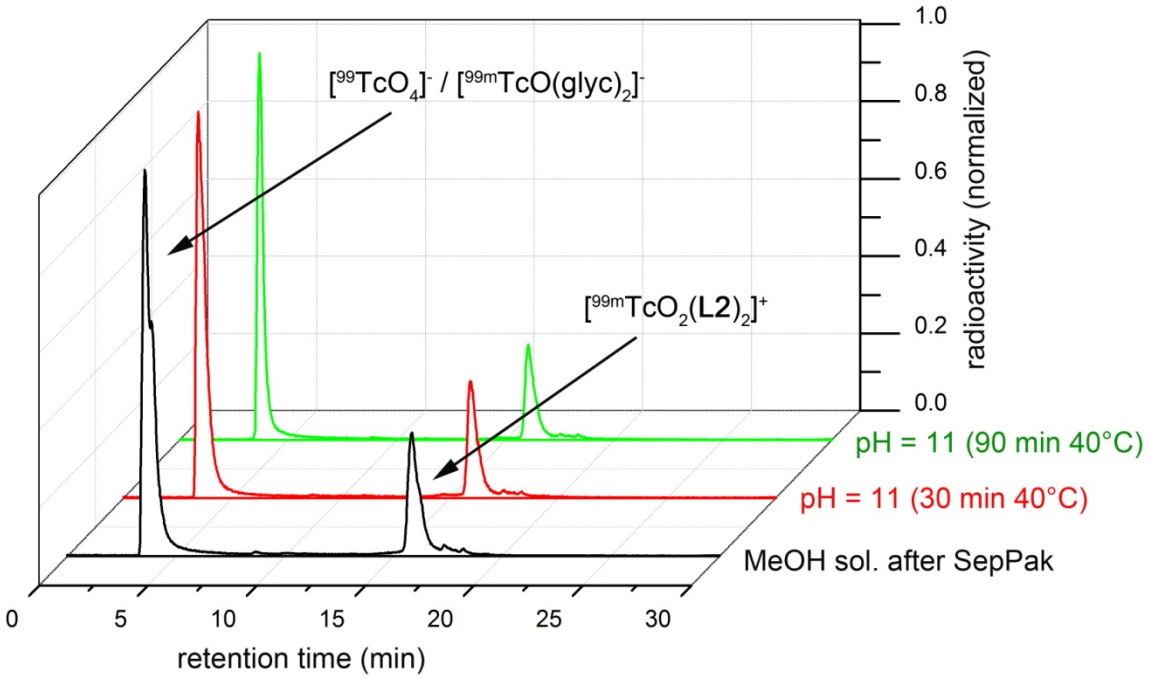

Figure 43: Stability analysis of the isolated [^{99m}TcO$_2$(**L2**)$_2$]$^+$ in saline solution at pH = 11 at 40°C. No significant decomposition of [^{99m}TcO$_2$(**L2**)$_2$]$^+$ was observed.

The observation that a side product formed during the synthesis of [^{99m}**10**]$^+$ made further investigations of the stability of [^{99}**10**]$^+$ necessary. Therefore, a solution of [^{99}**10**](PF$_6$) in 1:1 CH_3CN/saline solution was prepared and analyzed at neutral- (pH = 7), basic- (pH = 11) and acidic (pH = 1) conditions. At pH = 7, the slow formation of a small peak at 16.0 min (UV trace) was observed within 24 h at 25°C. This peak corresponds to the observed side product in the preparation of [^{99m}**10**]$^+$. When 1 M NaOH was added to the solution, the peak at 16.0 min disappeared in the HPLC analysis and formation of

[$^{99}TcO_4$]$^-$ was observed, indicating decomposition of the side product. The amount of [$^{99}TcO_4$]$^-$ remained constant for the duration of the rest of the experiment, even when the solution was acidified with 1 M HCl to pH = 1. From these results it is concluded that formation of the side product is exclusively observed at neutral pH and the side product decomposes immediately under basic aqueous conditions. This might be an explanation why formation of the side product is not always observed during the preparation of [^{99m}**10**]$^+$, since the side product presumably decomposes upon aqueous extraction of [^{99m}**10**]$^+$ from a basic reaction solution.

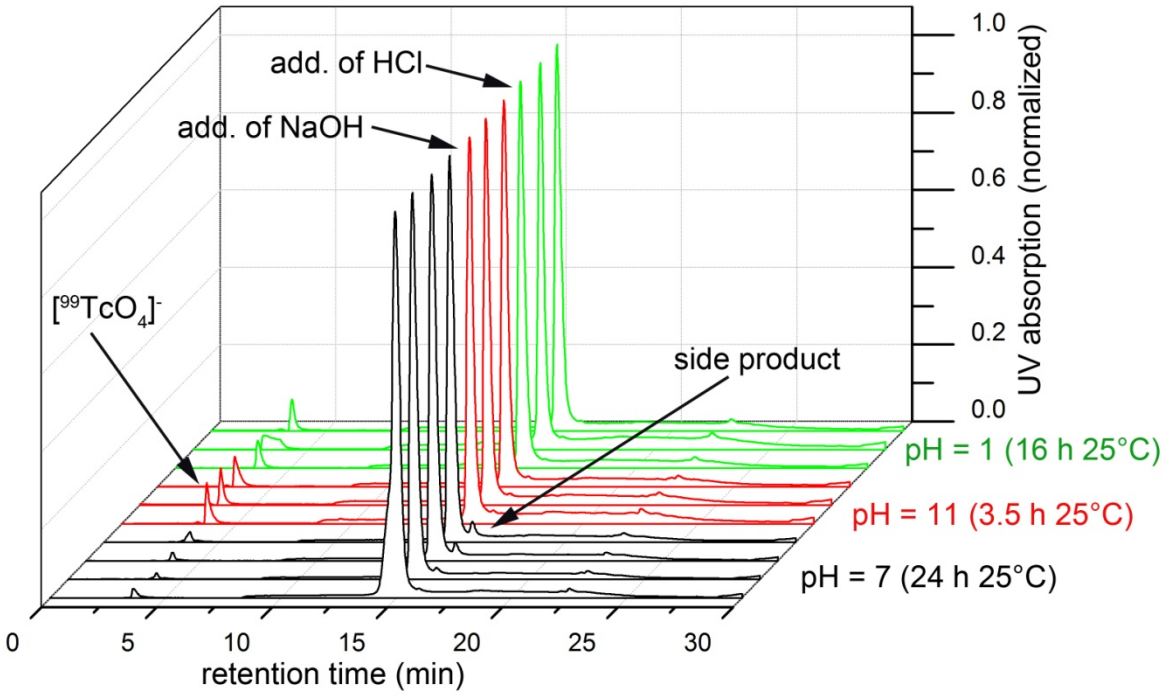

Figure 44: Stability investigation of [$^{99}TcO_2$(**L2**)$_2$](PF$_6$) in a 1:1 CH_3CN/saline solution at different pH values.

It was speculated that the formed side product of the reaction might be a reduced $^{99(m)}$Tc compound, which then decomposes at basic aqueous conditions by hydrolysis. Due to the presence of excess Cl^- in a saline solution, a reduction with Cl^- at neutral pH is plausible but certainly not favourable and hence, the formation of the side product appears to be slow. A more probable cause for the formation of the side product by reduction is found in the presence of excess $SnCl_2$ in the reaction leading to [^{99m}**10**]$^+$. The excess of $SnCl_2$ might be responsible for the reduction of [^{99m}**10**]$^+$ to the undesired side product, which then presumably decomposes during the isolation and purification process. Therefore, the reaction of [^{99}**10**]$^+$ with excess $SnCl_2$ was studied for further insight. When a solution of [^{99}**10**](PF$_6$) in DMF was treated with 8 eq. of $SnCl_2$ in DMF, a color change to red was observed within 1 h (Scheme 33). HPLC analysis showed a shift of the peak from 15.0 min to 16.1 min in the UV trace, which agreed well with the previously observed retention time of the side product in the synthesis of [^{99m}**10**]$^+$. Purification of the red compound was attempted by evaporation of the DMF and washing of the crude product with THF, followed by dissolution in CH_3CN and filtration. Very few red single crystals of

the composition *cis*-[^{99}TcCl$_2$(**L2**)$_2$](PF$_6$)$_2$·THF (*cis*-[**24**](PF$_6$)$_2$·THF) were obtained by slow evaporation of the CH$_3$CN solution containing the red crude product and traces of THF. Due to the difficulties in the removal of Sn-containing impurities, the isolation of analytically pure *cis*-[**24**](PF$_6$)$_2$ was not successful. IR spectroscopy of crude [**24**](PF$_6$)$_2$ confirmed complete consumption of [^{99}TcO$_2$(**L2**)$_2$](PF$_6$), since the characteristic $\nu_{O=Tc=O}$ band was not present.

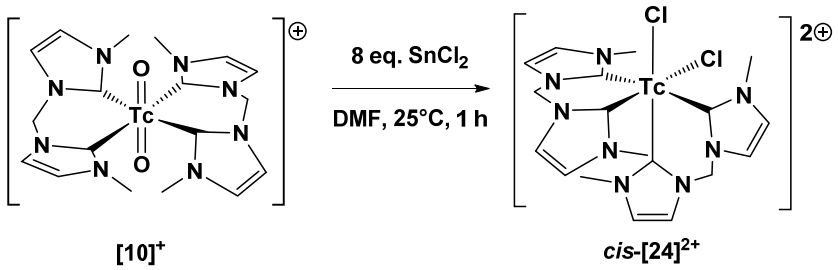

Scheme 33: Synthesis of *cis*-[^{99}TcCl$_2$(**L2**)$_2$]$^{2+}$) (*cis*-[**24**]$^{2+}$) by reaction of [^{99}TcO$_2$(**L2**)$_2$]$^+$ ([**10**]$^+$) with 8 eq. of SnCl$_2$ in DMF.

Cis-[**24**](PF$_6$)$_2$·THF crystallizes as red blocks in the monoclinic space group P2$_1$/n (Figure 45). The structure shows the Δ-enantiomer of *cis*-[**24**](PF$_6$)$_2$. The ^{99}Tc-C bond lengths of *cis*-[**24**]$^{2+}$ (2.144(5) – 2.168(5) Å, table 32) are in a similar range as in the structure of [^{99}TcO$_2$(**L2**)$_2$]$^+$ (2.170(4) and 2.166(4) Å) and also in the same range as in other ^{99}Tc-NHC complexes comprised of two **L2** ligands. The bite angles of the **L2** ligands of *cis*-[**24**]$^{2+}$ (81.8(2) and 81.7(2)°) are also comparable to [^{99}TcO$_2$(**L2**)$_2$]$^+$ (81.33(16)°) and other ^{99}Tc-NHC complexes containing two **L2** ligands. The ^{99}Tc centre has a distorted octahedral coordination sphere, which is observed in the slightly bent Cl-^{99}Tc-C angles (174.91(16) and 174.36(15)°) and the considerably bent C(1)-Tc(1)-C(11) angle (170.1(2)°). *Cis*-[**24**]$^{2+}$ is the first isolated ^{99}Tc^{IV}-NHC complex, while structurally characterized ^{99}Tc^{IV} complexes are rare in general. This rarity is explained by the tendency of ^{99}Tc^{IV} complexes to hydrolyze and form polymeric complexes such as ^{99}Tc^{IV}O$_2$.[13,116-119] The electronic configuration of the 4d^3 ^{99}Tc^{IV} complexes suggests that they are in a position between complexes that are stabilized by π-donors and π-acceptors and, consequently, ^{99}Tc^{IV} complexes comprised of carbonyl ligands or terminal oxo or nitrido ligands are not known.[13,50] Abram *et al.* described the formation of a series of [^{99}TcCl$_4$(L)$_2$] complexes (L = THF, CH$_3$CN, DMSO, thioxane, PMe$_2$Ph, PPh$_3$, OPPh$_3$, OH$_2$) starting from polymeric [^{99}TcCl4].[50,52] Comparison of the ^{99}Tc-Cl bond lengths of *cis*-[**24**](PF$_6$)$_2$·THF (2.2660(18) and 2.2924(17) Å) with the ^{99}Tc-Cl bond lengths found in *cis*-[^{99}TcCl$_4$(THF)$_2$] (2.283(1) – 2.320(1) Å),[50] *cis*-[^{99}TcCl$_4$(CH$_3$CN)$_2$]·CH$_3$CN (2.279(2) – 2.323(2) Å)[52] and *cis*-[^{99}TcCl$_4$(OH$_2$)$_2$]·2dioxane (2.283(3) and 2.331(2) Å)[52] reveals that the ^{99}Tc-Cl bond lengths in *cis*-[**24**](PF$_6$)$_2$·THF are slightly shorter. This is explained by the higher nuclear charge in the 2+ charged complex, which leads to a stronger binding of the Cl$^-$ ligands.

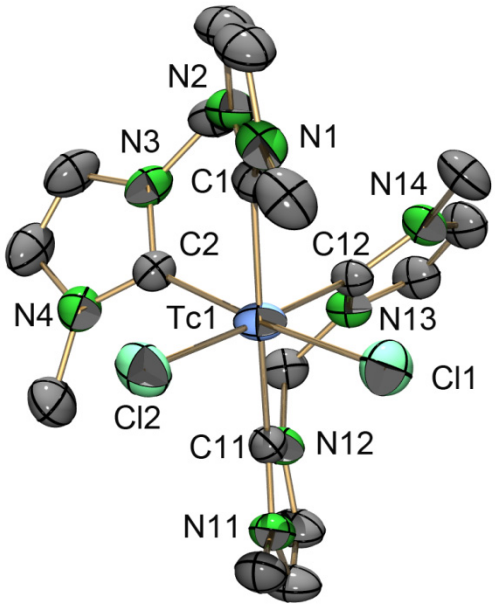

Figure 45: ORTEP representation[51] of the $[\mathbf{24}]^{2+}$ dication of the $[\mathbf{24}](PF_6)_2 \cdot THF$ structure. Thermal ellipsoids are represented at the 50% probability level. Hydrogen atoms are omitted for clarity.

Table 32: Selected bond lengths and angles of $[\mathbf{24}]^{2+}$.

Selected bond lengths [Å]		Selected angles [°]	
Tc(1)-Cl(1)	2.2660(18)	Cl(1)-Tc(1)-C(2)	174.91(16)
Tc(1)-Cl(2)	2.2924(17)	Cl(2)-Tc(1)-C(12)	174.36(15)
Tc(1)-C(1)	2.144(5)	C(1)-Tc(1)-C(11)	170.1(2)
Tc(1)-C(2)	2.168(5)	Cl(1)-Tc(1)-Cl(2)	96.87(7)
Tc(1)-C(11)	2.154(5)	C(1)-Tc(1)-C(12)	90.3(2)
Tc(1)-C(12)	2.156(5)	C(2)-Tc(1)-C(12)	86.9(2)
		C(1)-Tc(1)-C(2)	81.8(2)
		C(11)-Tc(1)-C(12)	81.7(2)

Further investigations with $[^{99}TcO_2(\mathbf{L2})_2](PF_6)$ were done using differential pulse- and cyclic voltammetry (DPV and CV). The CV showed a reversible oxidation at a potential $E^0_{1/2}$ of 1.16 V and an irreversible reduction at a potential of -1.58 V (measured *vs.* Fc/Fc^+ at 0.45 V, figure 46). The width of the DPV signals shows that the oxidation and the reduction of $[^{99}TcO_2(\mathbf{L2})_2]^+$ are one electron processes. Therefore, the reversible oxidation is assigned to the $[^{99}Tc^{V}O_2(\mathbf{L2})_2]^+/[^{99}Tc^{VI}O_2(\mathbf{L2})_2]^{2+}$ couple, while the irreversible reduction is assigned to the decomposition of $[^{99}Tc^{V}O_2(\mathbf{L2})_2]^+$ to $^{99}Tc^{IV}O_2$.

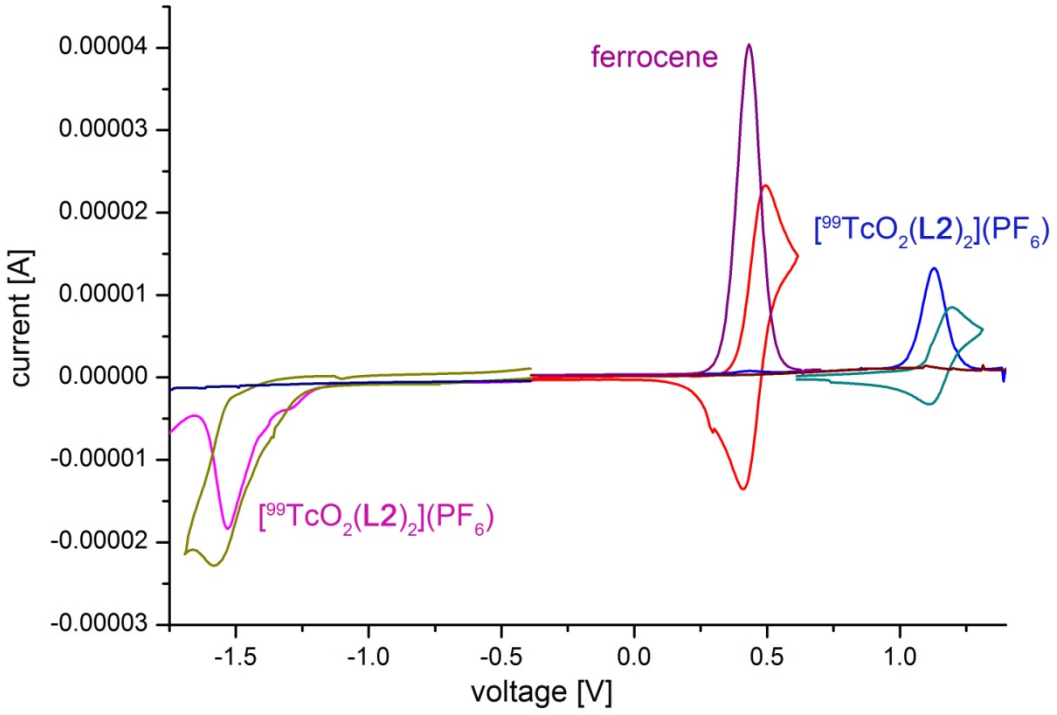

Figure 46: Electrochemical studies showing the differential pulse- and cyclic voltammograms of $[^{99}TcO_2(\mathbf{L2})_2](PF_6)$. Measurements were done in 0.1 M $(N^nBu_4)(PF_6)$ electrolyte with a Ag/AgCl reference electrode. The potentials were referenced with Fc/Fc^+ at 0.45 V, which is also shown in this figure.

While the electrochemical measurements give interesting insights into the properties of $[^{99}TcO_2(\mathbf{L2})_2]^+$, they also give some information about the mechanism that leads to the formation of *cis*-$[\mathbf{24}]^{2+}$. The chemical reduction of $[^{99}TcO_2(\mathbf{L2})_2]^+$ with $SnCl_2$ presumably follows a similar mechanism as the activation of $[^{99}TcO_4]^-$ by $AlCl_3$ that leads to the formation of $[^{99}TcCl_6]^{2-}$ (chapter 4.1). As it was the case for $AlCl_3$, the oxophilicity of the $SnCl_2$ allows the removal of the O^{2-} ligands. A reduction without removal of the oxo ligands would presumably result in the formation of $^{99}Tc^{IV}O_2$, as observed in the electrochemical experiments. A key difference in the formation of *cis*-$[\mathbf{24}]^{2+}$ compared to the reaction of $[^{99}TcO_4]^-$ with $AlCl_3$ is that the reducing agent is Sn^{2+} (Sn^{2+}/Sn^{4+} couple at -0.15 V *vs.* standard hydrogen electrode (SHE)[120,121]) and not Cl^- (Cl^-/Cl^0 couple at -1.36 V *vs.* SHE[120,122]).

Due to the insufficient purification of $[\mathbf{24}]^{2+}$ it is not clear if the *cis*-isomer is exclusively formed during the reduction. In addition, the potential formation of Λ- and Δ-enantiomers of *cis*-$[\mathbf{24}]^{2+}$ further complicates the challenge of purification and characterization of this compound. While HPLC analysis only showed formation of one product during the reduction of $[^{99}\mathbf{10}]^+$ with $SnCl_2$, it is questionable whether the different isomers could be separated with reversed-phase HPLC analysis. Further investigations are necessary to resolve these problems, while an investigation of different reducing agents might be necessary to improve the reaction. In this regard, the reduction of $[^{99}\mathbf{10}]^+$ with Zn in combination with HCl or $AlCl_3$ might lead to an alternative procedure for this reaction. The stability of

[**24**]$^{2+}$ was not further studied due to the insufficient purification. However, the previously discussed results already give good insights. The stability tests of [^{99m}**10**]$^{+}$ showed that [^{99m}**24**]$^{2+}$ is stable at 40°C in saline solution at pH = 7 and slowly decomposes at pH = 1 (Figure 42). The increased stability at these conditions is presumably due to the presence of a large excess of Cl^-. Under basic aqueous conditions, [^{99}**24**]$^{2+}$ immediately hydrolyzes at 25°C even in saline solution, as it was observed in the stability investigations of [^{99}**10**]$^{+}$ (Figure 44).

While it was proven that the synthesis of [^{99m}**10**]$^{+}$ starting from [^{99m}TcO$_4$]$^-$/[^{99m}**8**]$^-$ is possible, the excess $SnCl_2$ present in the reaction leads to the decomposition of the product. It was shown that the reaction of [$^{99(m)}$**10**]$^{+}$ with $SnCl_2$ leads to the formation of [^{99m}**24**]$^{2+}$, which is hydrolytically unstable under basic and acidic conditions in saline solution. This decomposition pathway presumably also leads to the low yields observed in the reactions, while the uncertainties in the preparation of [^{99m}**8**]$^-$ could also have an influence on the yield. A possible solution to this decomposition reaction would presumably be the synthesis and purification of a different $^{99m}Tc^{V}$ precursor complex, which should be isolated and separated from the $SnCl_2$ prior to the reaction with [Ag$_2$(**L2**)$_2$](PF$_6$)$_2$ or (**L2**-H$_2$)(PF$_6$)$_2$. It was tested if ^{99m}Tc-glucoheptonate or [^{99m}**8**]$^-$ could be purified by C_{18} column chromatography using a SepPak, but the high polarity of these compounds prevented a separation from residual $SnCl_2$. It is concluded that the synthesis of a new $^{99m}Tc^{V}$ starting material that can be separated from $SnCl_2$ and is suitable for substitution with NHCs is presumably the key to the successful synthesis of $^{99m}Tc^{V}$-NHC complexes, in the future.

4.2.3 Synthesis of Low-Valent *fac*-$\{M^{I}(CO)_3\}^{+}$-NHC Complexes (M = Re, ^{99}Tc)

So far, it has been shown that NHCs are capable of stabilizing high-valent ^{99}Tc and Re. As it was described before, only mono- and bidentate NHCs were successfully coordinated to high-valent ^{99}Tc and Re. Reactions with tridentate ligands did not lead to new products. It became clear, that the facially coordinating NHCs $(PhB(^{Me}Im)_3)^-$ (**L5**$^-$) and 1,1,1-tris[(3-methylimidazoline-2-ylidene)-methyl]ethane (**L6**) are much more suited for the synthesis of *fac*-$\{M(CO)_3\}^{+}$-NHC complexes (M = Re, ^{99}Tc), since the strong σ-Donor properties of the NHCs complement the strong π-acceptor properties of the CO ligands. The ligand **L5**$^-$ was selected due to the fact that it is negatively charged and tightly chelating, which renders it a strong σ-donor ligand.[39] In addition, the negative charge leads to the synthesis of neutral *fac*-$\{M(CO)_3\}^{+}$-NHC complexes, which makes these complexes interesting for brain perfusion. In contrast to **L5**$^-$, the ligand **L6** is neutral and more flexible, which should give further information on the influence of the donating properties and the flexibility on the structure and reactivity of the resulting complexes. Due to the faster synthetic accessibility of $(NEt_4)_2[ReBr_3(CO)_3]$ compared to $(NEt_4)_2[^{99}TcCl_3(CO)_3]$,[123,124] reactions were first optimized with Re before they were tested with ^{99}Tc. The synthesis was adapted from a recently published procedure to [Mn(**L5**)$(CO)_3$], which is the first group 7 complex comprised of a tridentate NHC ligand.[39]

Reaction of 1 eq. **L5**$^-$ with $(NEt_4)_2[ReBr_3(CO)_3]$ in THF at 25°C led to the formation of [Re(**L5**)$(CO)_3$] ([**25**], **method a**). After evaporation of the solvent, an orange sticky crude product was left which was chromatographed over SiO_2 with 10:1 hexane/EtOAc to give [**25**] as a colorless solid in an isolated yield of up to 10% (Scheme 34).

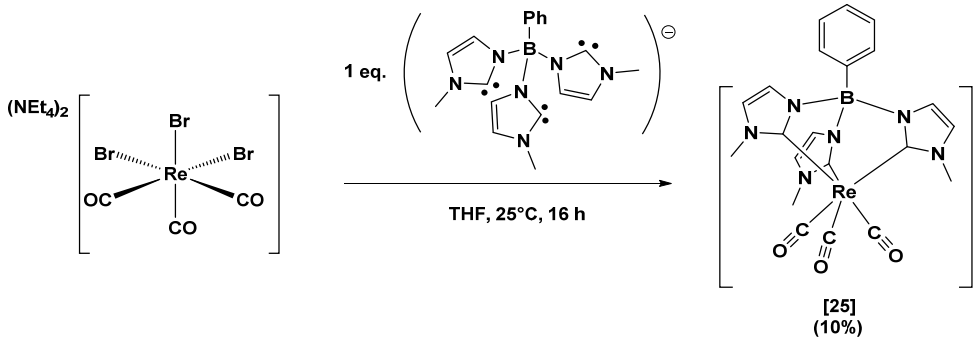

Scheme 34: Synthesis of the *fac*-$\{Re^{I}(CO)_3\}^{+}$-NHC complex [**25**].

Due to the low yield, a number of changes to the procedure were tested, which were based on anticipated problems either during NHC formation, complex formation, or complex isolation. At first, the use of AgOTf for precipitation of the Br^- in $(NEt_4)_2[ReBr_3(CO)_3]$ was tested (**method b**), since the formation of [ReBr(**L5**-H)$(CO)_3$] as a side product was expected. Evidence for the formation of this side product was found in ESI^+-MS measurements of the crude product of **method a**, since a low intensity peak with the correct isotopic pattern at m/z = 683.3 (calculated m/z of [ReBr(**L5**-H)$(CO)_3$] + H^+ = 683.1) was also present. However, the precipitation of the Br^- ligands with

AgOTf did not increase the yield of the reaction. The precipitation of the Br^- ligands with AgOTf still proved to be useful, since it increased the solubility of the Re starting complex in THF. This is important, because both compounds used in **method a**, the NHC **L5**$^-$ and $(NEt_4)_2[ReBr_3(CO)_3]$, are not soluble in THF. The reaction procedure was further varied by increasing the amount of LDA used for the formation of **L5**$^-$ from (**L5**-H_3)$(OTf)_2$ from 3 eq. to 5 eq. (**method c**), since it was assumed that incomplete NHC generation could be the problem. Unfortunately, this did not lead to an increase of the yield of the reaction. Interestingly, it did also not decrease the yield and it appears that the use of excess LDA does not lead to side reactions. Furthermore, the procedure was changed to include cooling to -78°C using acetone/dry ice during the addition of the Re complex to the **L5**$^-$ (**method d**), anticipating that the highly nucleophilic NHC might not be compatible with the CO ligands at 25°C. This change also did not lead to an improvement of the yield. In addition to the changes in the reaction procedure also changes in the workup procedure were made by changing the column material from SiO_2 to neutral Al_2O_3. However, also this change did not lead to an increased yield. Table 33 summarizes all the conditions used in **methods a-d**.

Table 33: Comparison of different reaction conditions for **methods a-d** for the synthesis of [**25**].

Method	Eq. LDA	Eq. AgOTf	Temperature [°C]	Yield [%]
Method a	3	0	25	8
Method b	3	3	25	10
Method c	5	3	25	8
Method d	3	3	-78	10

While the reason for the low yield could not be fully identified, it can be assumed that the low yield is due to the stability of [**25**]. [**25**] is stable when suspended in H_2O and no immediate decomposition was observed when [**25**] was dissolved in organic solvents with trace amounts of H_2O present. However, the initially colorless NMR solutions in CD_3CN gradually turned orange within days, indicating a decomposition reaction. The ^1H NMR showed several new peaks, confirming decomposition of [**25**] in solution. Interestingly, the orange colour was also observed in the crude product of the reaction, indicating that decomposition is most likely the main cause for the low yield. However, the exact mechanism of the decomposition reaction remains unknown. It is speculated that the B-Ph or the B-N bond might be cleaved during decomposition, or that one of the NHCs is protonated and exchanged. Due to the tight chelation of the **L5**$^-$ ligand, the latter case appears to be unlikely and decomposition of [**25**] was not observed when it was suspended in H_2O. A stability experiment in CH_3CN was done, in which [**25**] was treated with an excess of 1 M HCl. The solutions were analyzed with ESI^+-MS for potential decomposition products. The reference solution of [**25**] (calculated m/z = 602.1) in CH_3CN showed almost no decomposition within 72 h at 25°C (Figure 47, a)). When [**25**] was dissolved in CH_3CN and excess 1 M HCl was added, immediate formation of $[Re(\mathbf{L5}\text{-}H)(CO)_3]^+$ (calculated m/z = 603.1) was observed due to the protonation of one NHC ligand

(Figure 47, b)). After 72 h, decomposition had progressed to various *fac*-$\{Re(CO)_3\}^+$ complexes (Figure 47, c)), such as $[Re(CH_3CN)_3(CO)_3]^+$ (calculated m/z = 394.0) and $[Re(CH_3CN)_2(OH_2)(CO)_3]^+$ (calculated m/z = 371.0). Interestingly, peaks for $[Re(CH_3CN)_2(L)(CO)_3]^+$ (L = 1-methyl-3*H*-imidazoline-2-ylidene or 1-methylimidazole, calculated m/z = 435.0) and $[Re(CH_3CN)(L)_2(CO)_3]^+$ (calculated m/z = 476.1) were also found, while it is unclear if the remaining L binds via N (1-methylimidazole) or C (1-methyl-3*H*-imidazoline-2-ylidene). This indicates that the decomposition of [Re(**L5**-H)$(CO)_3]^+$ might proceed via the cleavage of the B-N bonds by HCl or H_2O. The stability experiments confirm that the protonation of one of the NHC ligands presumably initiates the decomposition of [**25**], while it cannot be excluded that the cleavage of the B-Ph or B-N bond also plays an important role in the subsequent decomposition reactions.

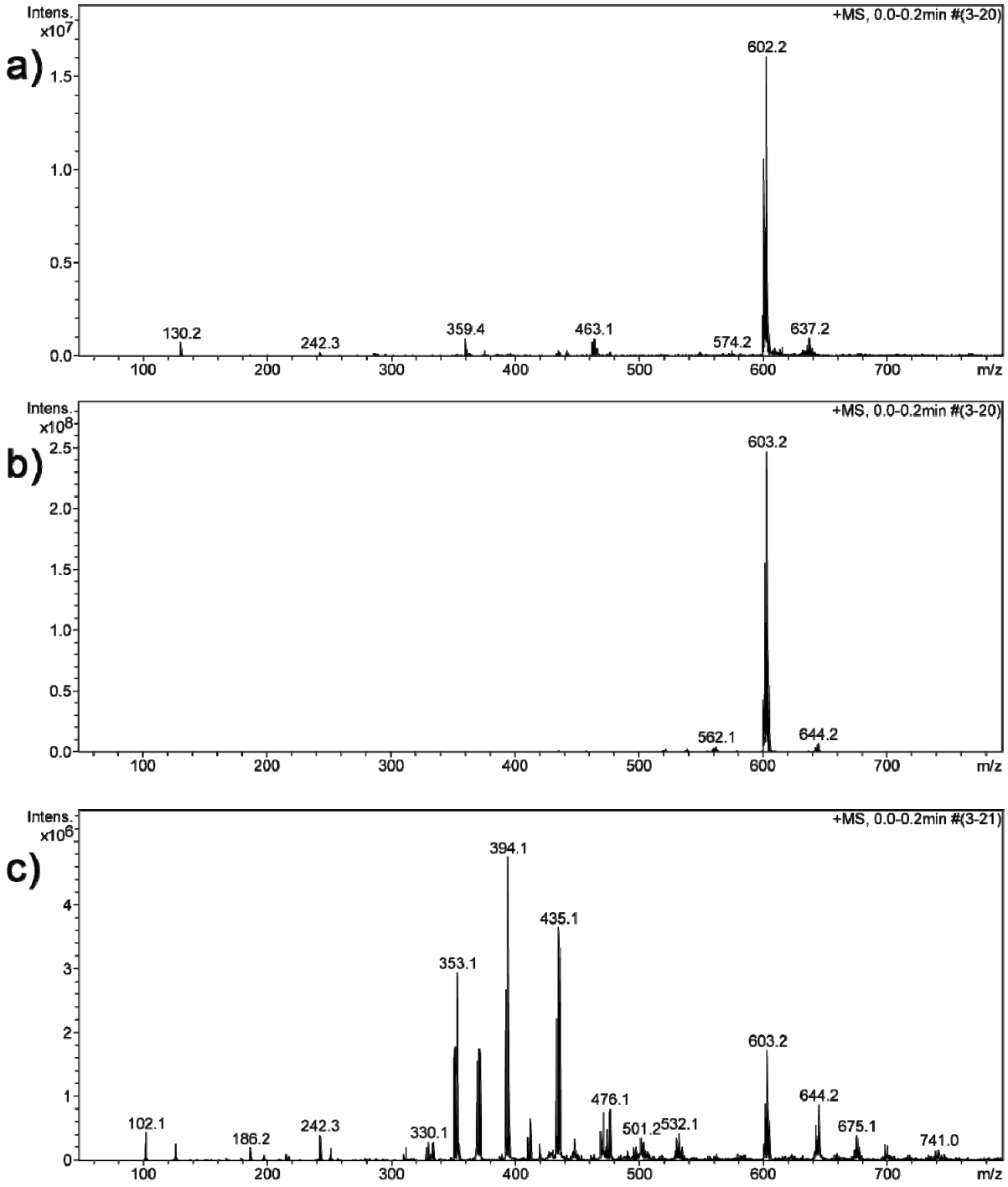

Figure 47: Stability measurements of [Re(**L5**)$(CO)_3$] ([**25**]) in CH_3CN. a) Reference solution of [**25**] after 72 h at 25°C. b) Solution of [**25**] 5 min after addition of excess 1 M HCl, showing immediate formation of [Re(**L5**-H)$(CO)_3]^+$. Solution of [**25**] 72 h after addition of excess 1 M HCl, showing decomposition to various *fac*-$\{Re(CO)_3\}^+$ complexes.

Crystals of [**25**] suitable for X-ray diffraction analysis were obtained by slow evaporation from CH_3CN. [**25**] crystallizes as colorless blocks in the orthorhombic space group $Cmc2_1$ (Figure 48). The Re-CO bond lengths (1.923(10) and 1.950(6) Å, table 34) are in the same range as the Re-C bond lengths found in $[ReBr_3(CO)]^{2-}$ (1.880(10) – 1.964(13) Å).[16] The only other tris(NHC) *fac*-$\{Re(CO)_3\}^+$ complex, $[Re(SNHC)_3(CO)_3]^+$ (SNHC = saturated imidazoline-2-ylidene), has a Re-CO bond length in a similar range (1.950(2) Å).[40] The Re-C bond lengths to the NHC ligand are 2.169(5) and 2.144(8) Å, which is shorter than in $[Re(SNHC)_3(CO)_3]^+$ (2.183(2) Å).[40] The C-Re-C bite angles of the NHC ligand (82.4(2) and 81.2(3)°) are considerably smaller than the corresponding angles in the homoleptic $[Mn(\mathbf{L5})_2]^{2+}$ (86.83(11) – 86.98(11)°).[39]

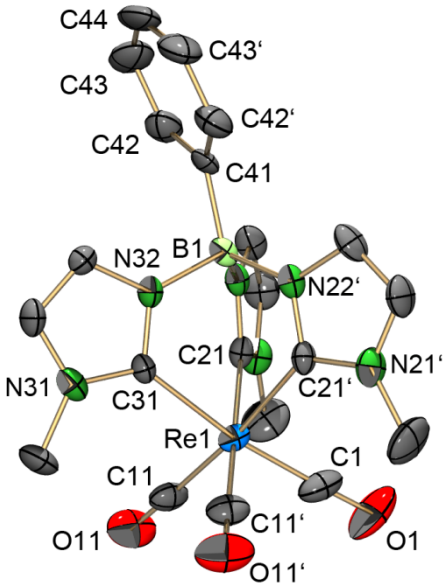

Figure 48: ORTEP representation[51] of [**25**]. Thermal ellipsoids are represented at the 50% probability level. Hydrogen atoms are omitted for clarity.

Table 34: Selected bond lengths and angles of [**25**]

Selected bond lengths [Å]		Selected angles [°]	
Re(1)-C(1)	1.923(10)	C(1)-Re(1)-C(11)	92.0(3)
Re(1)-C(11)	1.950(6)	C(11)-Re(1)-C(11)#1	92.7(3)
Re(1)-C(21)	2.169(5)	C(1)-Re(1)-C(21)	91.7(3)
Re(1)-C(31)	2.144(8)	C(11)-Re(1)-C(21)	92.9(2)
C(1)-O(1)	1.162(11)	C(21)-Re(1)-C(31)	82.4(2)
C(11)-O(11)	1.135(7)	C(21)-Re(1)-C(21)#1	81.2(3)
B(1)-N(22)	1.545(9)	N(22)-B(1)-N(32)	107.3(7)
B(1)-N(32)	1.566(10)	N(22)-B(1)-N(22)#1	106.0(9)
B(1)-C(41)	1.646(16)	N(22)-B(1)-C(41)	115.8(6)
		N(32)-B(1)-C(41)	104.1(9)

For comparison with the structure of [**25**], the imidazolium salt (**L5**-H_3)$(OTf)_2$ was crystallized (Figure 49). The B-N bond lengths in the structures of [**25**] (1.545(9) and 1.566(10) Å) and $(\mathbf{L5}\text{-}H_3)^{2+}$ (1.558(4) – 1.565(4) Å) are in the same range, while the B-C bond length in [**25**] (1.646(16) Å) is slightly elongated compared to $(\mathbf{L5}\text{-}H_3)^{2+}$ (1.606(4) Å, table 35). In addition, the phenyl ring in the structure of [**25**] is considerably bent (torsion angle B(1)-C(41)-C(42)-C(43) = 163.5(6)°) compared to the phenyl ring in $(\mathbf{L5}\text{-}H_3)^{2+}$ (torsion angle B(1)-C(31)-C(32)-C(33) = 175.5(2)°).

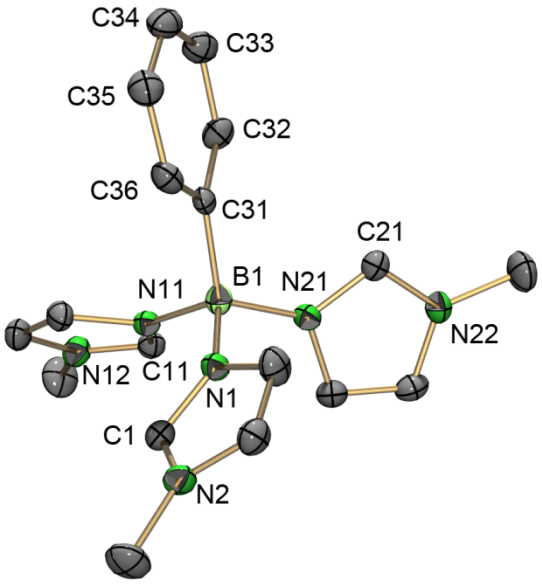

Figure 49: ORTEP representation[51] of the $(\mathbf{L5}\text{-}H_3)^{2+}$ dication of the (**L5**-H_3)$(OTf)_2$ structure. Thermal ellipsoids are represented at the 50% probability level. Hydrogen atoms are omitted for clarity.

Table 35: Selected bond lengths and angles of $(\mathbf{L5}\text{-}H_3)^{2+}$.

Selected bond lengths [Å]		Selected angles [°]	
B(1)-N(1)	1.564(4)	N(1)-B(1)-N(11)	107.9(2)
B(1)-N(11)	1.558(4)	N(11)-B(1)-N(21)	109.2(2)
B(1)-N(21)	1.565(4)	N(1)-B(1)-N(21)	104.5(2)
B(1)-C(31)	1.606(4)	N(1)-B(1)-C(31)	112.0(2)
		N(11)-B(1)-C(31)	108.4(2)
		N(21)-B(1)-C(31)	114.6(2)

IR spectroscopy of [**25**] shows the high intensity ν_{CO} bands at 1988 and 1867 cm^{-1}. These values are comparable to the observed ν_{CO} bands of the corresponding [Mn(**L5**)$(CO)_3$] complex (1990 and 1889 cm^{-1}). Compared to structurally similar $[Re(Tp)(CO)_3]^+$ complexes (Tp = tris-pyrazolylborate), such as $[Re(p\text{-}BrC_6H_4Tp^{Me})(CO)_3]$ (Tp^{Me} = tris(3-methylpyrazolyl)borate, ν_{CO} = 2013 and 1914 cm^{1}),[39] these bands are very much shifted to lower frequencies, which is explained by the strong σ-donor properties of the NHC ligands. For comparison, the only other tris(NHC) *fac*-$\{Re^{I}(CO)_3\}^+$ complex, $[Re(SNHC)_3(CO)_3]^+$, has ν_{CO} bands at 1999 and 1914 cm^{-1}, which are at considerably higher

frequencies.[40] ^{1}H-NMR spectroscopy of [**25**] in DMF-D_7 shows the expected Ph-H signals as multiplets at 8.01 – 7.99, 7.64 – 7.60 and 7.57 – 7.53 ppm. The imidazole-H atoms were observed as 2 doublets at 7.20 and 7.00 ppm and the CH_3 protons were observed at 3.88 ppm. Besides the other expected signals, the ^{13}C-NMR spectrum also shows the CO carbons at 199.28 ppm and the Re-C NHC carbons at 177.09 ppm. Compared to the chemical shift of the Re-C carbons in $[ReO_2(\mathbf{L2})_2]^+$ (176.83 ppm, measured in CD_3CN), this signal has an almost identical chemical shift. In comparison to the Re-C NHC carbons of $[Re(SNHC)_3(CO)_3]^+$ (204.2 ppm, measured in CD_3OD), the signals of [**25**] are found at considerably lower ppm values, while the Re-CO signals of $[Re(SNHC)_3(CO)_3]^+$ (198.2 and 194.7 ppm, measured in CD_3OD) are reported in a similar range.[40] The shift of the Re-C NHC carbons of [**25**] to higher field compared to $[Re(SNHC)_3(CO)_3]^+$ is presumably explained by the electron-rich boron central atom of the **L5**$^-$ ligand. High-resolution electron ionization mass spectrometry (HR-EI-MS) of [**25**] in the positive detection mode shows the $[M]^+$ isotopic pattern at m/z = 602.12420 (36% intensity, calculated m/z = 602.12478, figure 50). Also, the fragmentation of the CO ligands is visible, with an $[M\text{-}CO]^+$ peak at m/z = 574.12949 (44% intensity, calculated m/z = 574.12986) and an $[M\text{-}2CO]^+$ peak at m/z = 546.13428 (100% intensity, calculated m/z = 546.13494).

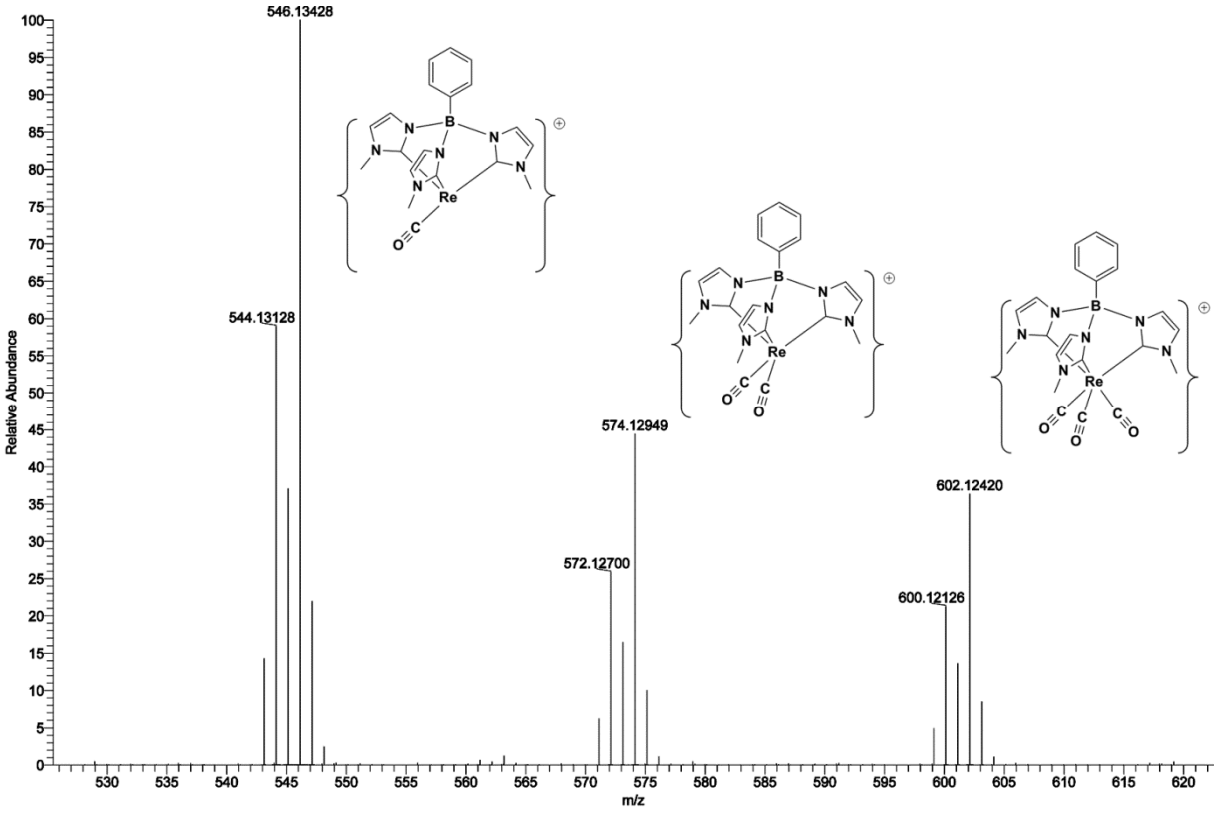

Figure 50: HR-EI-MS of [**25**] in the positive mode shows the $[M]^+$ peak and two peaks corresponding to the loss of one or two CO ligands.

To study the influence of the donor properties and the flexibility of the NHC ligand on the structure of the *fac*-$\{Re(CO)_3\}^+$-NHC complex, the ligand **L6** was tested. The complex $[Re(\mathbf{L6})(CO)_3]^+$ ($[\mathbf{26}]^+$) was prepared in analogy to [**25**], by reaction of $(NEt_4)_2[ReBr_3(CO)_3]$ with **L6** in THF at 25°C (Scheme 35). Analysis of the THF reaction solution with ESI^+-MS revealed that not only $[\mathbf{26}]^+$ was formed, but also the corresponding disubstituted complex $[ReBr(\mathbf{L6}\text{-H})(CO)_3]^+$ ($[\mathbf{27}]^+$). Formation of the disubstituted product $[\mathbf{27}]^+$ appears to be more prevalent with **L6** than with $\mathbf{L5}^-$, which is explained by the more flexible structure of **L6**. The disubstituted product $[\mathbf{27}]^+$ was initially purified by precipitation from THF using Et_2O and this precipitate contained mostly $[\mathbf{27}]^+$ according to ESI^+-MS.

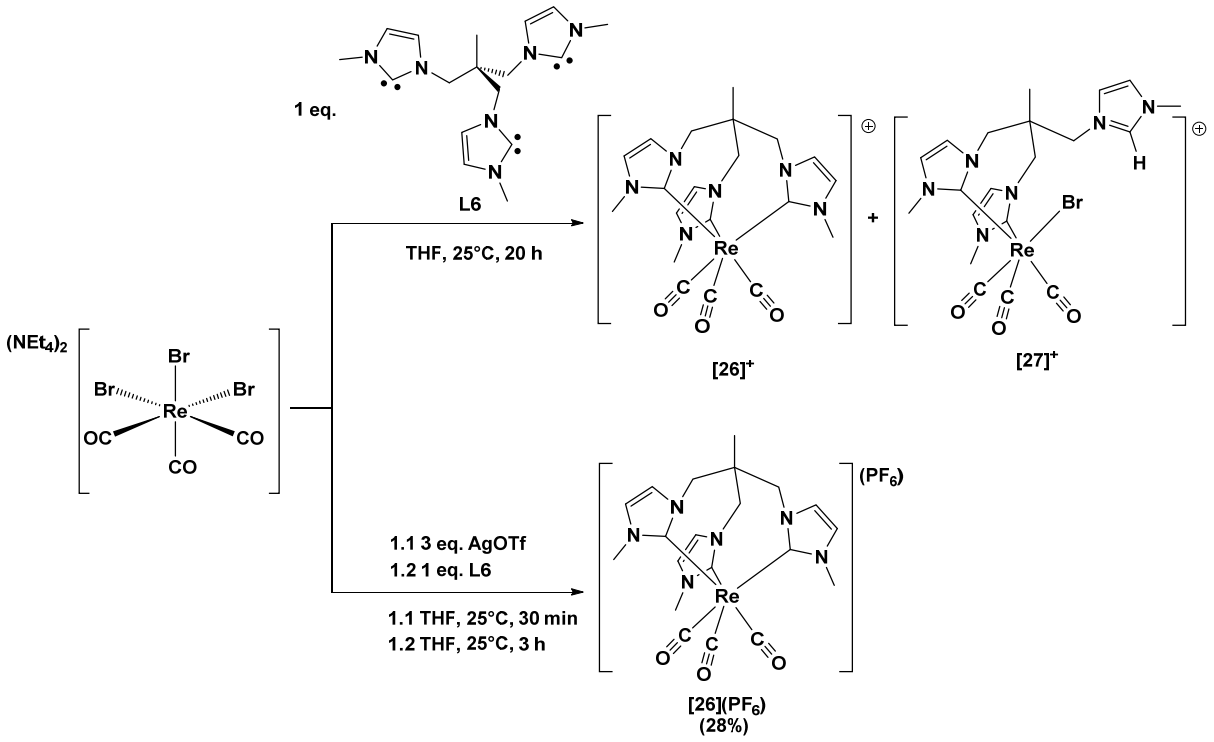

Scheme 35: Synthesis of [**26**](PF_6). Without precipitation of Br^- with AgOTf, the disubstituted side product $[\mathbf{27}]^+$ is also formed.

Crystallization of crude [**27**](Br) from CH_3CN by slow evaporation of the solvent gave crystals suitable for X-ray diffraction. [**27**](Br) crystallizes as colorless blocks of the composition $[\mathbf{27}](Br)\cdot H_2O\cdot CH_3CN$ in the space group $P\bar{1}$. The asymmetric unit contains two independent cations, which are both systematically disordered along the Br-Re-CO axis with a ratio of occupancy of 0.90:0.10 and 0.84:0.16. The difference in these occupancy-ratios decreases the overall symmetry of the structure, leading to $P\bar{1}$ as the observed space group. Due to the onesided occupancy-ratios, only the major species of the CO ligands could be refined, while the disorder was fully refined for the Br^- ligands. Only the major species of one cation will be discussed here in detail (Figure 51). The structure of $[\mathbf{27}]^+$ gives important details on the orientation of the ligand **L6**. **L6** coordinates in a bidentate way due to the fact that one Br^- ligand is still bound and, according to the structure, **L6** binds with one of the NHC ligands pointing away from the Re centre. Upon workup of the reaction, the unbound NHC

presumably is protonated to give [**27**]$^+$. Interestingly, no side products with bridging **L6** ligands were observed in the ESI$^+$-MS, despite the fact that the unbound NHC is highly reactive. The Re-CO bond lengths of [**27**]$^+$ (1.944(7) – 1.968(13) Å, table 36) are in a similar range as in [**25**] (1.923(10) and 1.950(6)), while the Re-C bond lengths to the NHC ligands are elongated in [**27**]$^+$ (2.219(7) and 2.212(7) Å) compared to the corresponding bond lengths in [**25**] (2.169(5) and 2.144(8) Å). The Re(1)-Br(1a) bond length of [**27**]$^+$ (2.6378(9) Å) is in the same range as in $[ReBr_3(CO)_3]^+$ (2.6328(1) – 2.6619(14) Å).[16] The C(4)-Re(1)-C(5) bite angle of the **L6** ligand is 97.9(2)°, which is considerably wider than in corresponding angles in [**25**] (82.4(2) and 81.2(3)°)). This is certainly a consequence of the more flexible structure of **L6** and the fact that the ligand forms an eight-membered ring including the Re centre.

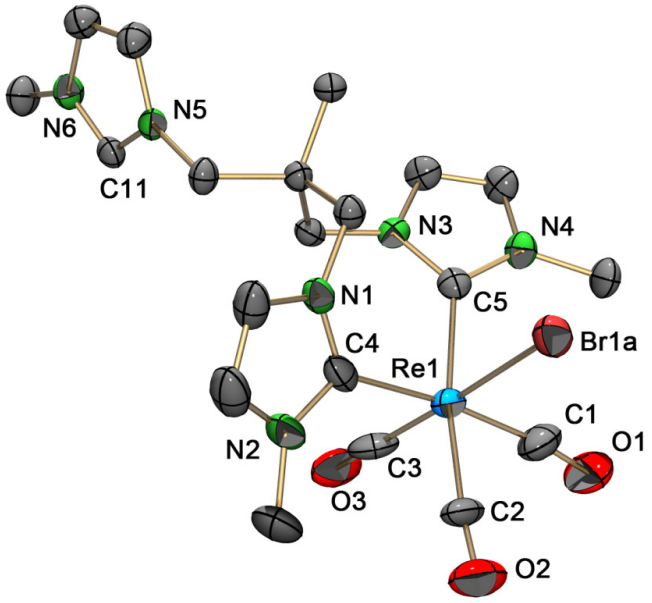

Figure 51: ORTEP representation[51] of the major species in the disordered structure of the [**27**]$^+$ cation of the [**27**](Br)·H_2O·CH_3CN structure. Thermal ellipsoids are represented at the 50% probability level. Hydrogen atoms are omitted for clarity.

Table 36: Selected bond lengths and angles of [**27**]$^+$.

Selected bond lengths [Å]		Selected angles [°]	
Re(1)-C(1)	1.954(9)	C(1)-Re(1)-C(2)	83.7(4)
Re(1)-C(2)	1.944(7)	C(2)-Re(1)-C(3)	94.2(3)
Re(1)-C(3)	1.968(13)	C(1)-Re(1)-C(3)	88.8(5)
Re(1)-C(4)	2.219(7)	C(1)-Re(1)-C(5)	90.1(3)
Re(1)-C(5)	2.212(7)	C(2)-Re(1)-C(4)	88.3(3)
Re(1)-Br(1A)	2.6378(9)	C(3)-Re(1)-C(4)	91.8(4)
C(1)-O(1)	1.134(10)	C(4)-Re(1)-C(5)	97.9(2)
C(2)-O(2)	1.135(9)	C(1)-Re(1)-Br(1A)	93.3(3)
C(3)-O(3)	1.028(14)	C(5)-Re(1)-Br(1A)	87.11(16)

As for [**25**], the procedure for the synthesis of [**26**]$^+$ was altered to include the precipitation of the Br^- ligands with 3 eq. AgOTf, which prevented the formation of [**27**]$^+$ according to ESI$^+$-MS of the reaction solution (Scheme 35). A crucial point to prevent the formation of [**27**]$^+$ was also, that (**L6**-H_3)$(PF_6)_3$ instead of (**L6**-H_3)$(Br)_3$ was used for the formation of **L6**. As an alternative, the use of 1 eq. transmetalation complex $[Ag_3(\mathbf{L6})_2](PF_6)_3$ also prevents formation of [**27**]$^+$ according to ESI$^+$-MS. However, using $[Ag_3(\mathbf{L6})_2](PF_6)_3$ has no advantage over the precipitation of the Br^- ligands with 3 eq. AgOTf. The use of 1 eq. $[Ag_3(\mathbf{L6})_2](PF_6)_3$ in the reaction with $[ReBr_3(CO)_3]^{2-}$ has the disadvantage that 2 eq. **L6** are present, with a 1:1 Ag:Br ratio. The reaction with 0.5 eq. $[Ag_3(\mathbf{L6})_2](PF_6)_3$ leads to the formation of 1 eq. of **L6**, with a 1:2 Ag:Br ratio. Both cases are not ideal, since the former case leads to an impurity of **L6** or (**L6**-H_3)$^{3+}$ after workup, while the latter case may lead to the formation of [**27**]$^+$ due to the presence of Br^-. Purification of [**26**](PF_6) was achieved by addition of an equal volume of Et_2O to the THF reaction solution, followed by removal of the precipitated impurities by filtration. The observation that [**26**]$^+$ does not entirely precipitate from THF by addition of Et_2O is in agreement with the procedure used above to initially purify [**27**]$^+$ from the reaction mixture. The solvent of the THF/Et_2O solution containing [**26**](PF_6) was removed and the resulting colorless [**26**](PF_6) was washed with H_2O, filtered and dried *in vacuo*. The isolated yield of 28% was rather low, which is due to the fact that the solubility of [**26**](PF_6) in the THF/Et_2O mixture is not very high. [**26**](PF_6) is stable when suspended in H_2O and also when dissolved in mixtures of CH_3CN and H_2O. However, acidified solutions of [**26**]$^+$ decompose rapidly. Surprisingly, solutions of [**26**](PF_6) in CH_2Cl_2 quickly change their color from colorless to orange-brown, indicating decomposition. This might be explained by the presence of traces of acid in CH_2Cl_2. Unfortunately, all attempts to grow single crystals of [**26**](PF_6) were not successful and the purity of the isolated product was not satisfying according to elemental analysis.

IR spectroscopy of [**26**](PF_6) shows the ν_{CO} bands at 2009 and 1870 cm^{-1} and, as expected, also a strong ν_{PF6} band at 843 cm^{-1}. Compared to [**25**], the ν_{CO} bands are shifted to higher wavelengths, indicating a weaker σ-donation of **L6** compared to **L5**$^-$. [**26**](PF_6) was characterized in detail with NMR-spectroscopy in DMF-D_7. ^{1}H-NMR spectroscopy shows the CH groups as doublets with shifts of 7.63 and 7.51 ppm (comparison with [**25**]: 7.20 and 7.00 ppm) and the NCH_3 groups at 4.02 ppm (comparison with [**25**]: 3.88 ppm). The signals of the CH_2 groups split into two doublets at 3.96 and 3.51 ppm, while the latter signal overlaps with the H_2O peak and was assigned by 2D-NMR experiments. The CCH_3 group is found at 1.57 ppm. Interestingly, the ^{13}C-NMR shows 2 signals for the CO groups at 202.01 and 200.71 ppm (1:2 intensity ratio), indicating a loss in symmetry compared to [**25**]. However, the difference in chemical shift of the CO ligands is very small and a loss of symmetry is not visible in the ^{1}H-NMR spectrum and also not in the IR spectrum. The Re-C NHC carbons were poorly resolved and have been assigned a shift of 169.90 ppm by a long range CH correlation experiment. High-resolution ESI$^+$-MS of [**26**](PF_6) shows the $[M]^+$ isotopic pattern at

m/z = 583.14545 (calculated m/z = 583.14677). A very low intensity peak for $[M\text{-}CO]^+$ at m/z = 555.15085 (calculated m/z = 555.15185) was also observed.

The knowledge gained from the synthesis of [**25**] and [**26**]$^+$ was used for the synthesis of the first *fac*-$\{^{99}Tc(CO)_3\}^+$-NHC complex. All manipulations for this reaction were done inside a glovebox system equipped for syntheses with ^{99}Tc, in case the resulting complex was sensitive towards ambient conditions. Following the same procedure as in the preparation of [**25**] according to **method b**, [^{99}Tc(**L5**)(CO)$_3$] ([**28**]) was prepared (Scheme 36). In this procedure, $(NEt_4)_2[^{99}TcCl_3(CO)_3]$ was first treated with 3 eq. AgOTf to precipitate the Cl^- ligands and **L5**$^-$ was then added to the solution containing the *fac*-$\{^{99}Tc^{I}(CO)_3\}^+$ precursor complex.

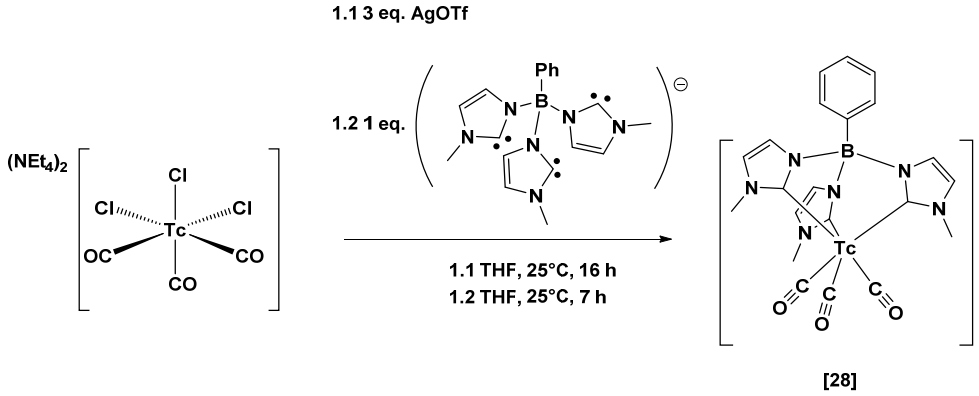

Scheme 36: Synthesis of the *fac*-$\{^{99}Tc^{I}(CO)_3\}^+$-NHC complex [**28**].

L5$^-$ had to be added to the ^{99}Tc solution and not *vice versa* due the fact that nonradioactive glassware was used for the preparation of **L5**$^-$. The resulting reaction solution containing [**28**] was analyzed after 4 h stirring at 25°C using ^{99}Tc-NMR, which showed a very intense peak at -764.42 ppm with a half line width ($\Delta\nu_{1/2}$) of 0.43 kHz, which was assigned to [**28**] (Figure 52, a)). The workup procedure was done at ambient conditions and was changed considerably due to the radioactivity involved. The solvent was removed with a stream of N_2 and the sticky orange crude product was washed with toluene and Et_2O. No radioactivity was found in these wash solutions. Thus it can be concluded that [**28**] is not soluble in toluene and Et_2O. Attempts to crystallize the orange crude from CH_2Cl_2 or CH_3CN failed. At this point, analysis of the crude solid with ^{99}Tc-NMR in DMF showed several peaks at -595.70, -750.92, -789.79 and -800.14 ppm, indicating decomposition of [**28**] during the workup procedure (Figure 52, b)). The peak at -750.92 ppm most likely corresponds to [**28**], since it has a half line width and a chemical shift that are in agreement with the previously observed signal. In an attempt to obtain at least some of the formed [**28**], the orange crude was washed with EtOH and a small amount of colorless precipitate formed. The precipitate was filtered off and washed with EtOH. Crystallization of this colorless solid from CH_3CN gave trace amounts of [**28**] as single-crystalline colorless plates that were suitable for X-ray diffraction analysis. Due to the low amount of crystals obtained, no bulk analysis could be performed.

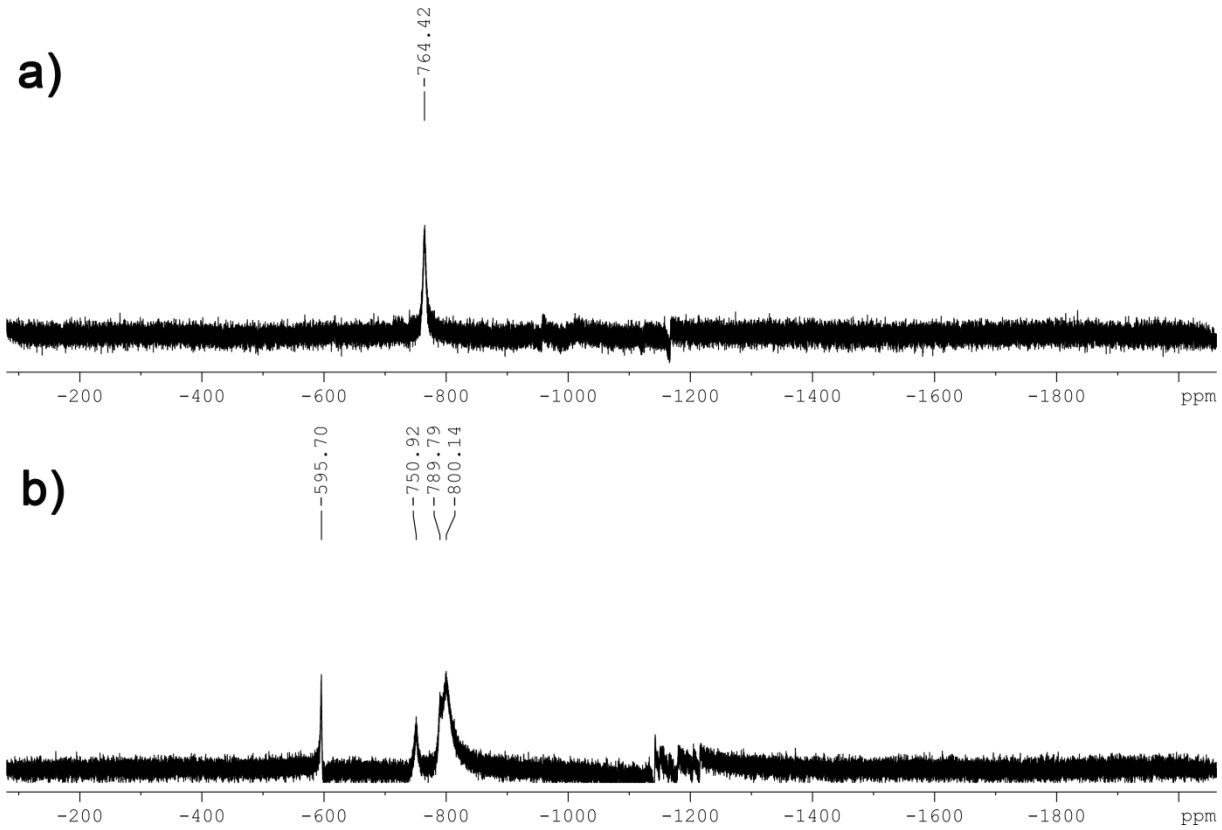

Figure 52: a) ^{99}Tc-NMR spectrum of the THF reaction solution 4 h after addition of **L5**$^-$ to the *fac*-$\{^{99}Tc^{I}(CO)_3\}^+$ precursor. b) ^{99}Tc-NMR spectrum of the crude product in DMF, showing decomposition of [**28**] during purification.

[**28**] crystallizes as colorless plates in the orthorhombic space group $Cmc2_1$ and is isostructural to the corresponding Re complex [**25**] (Figure 53). [**28**] has ^{99}Tc-CO bond lengths (1.948(4) and 1.940(3) Å, table 37), ^{99}Tc-C (NHC) bond lengths (2.169(3) and 2.137(3) Å) and C-O bond lengths (1.153(6) and 1.153(4) Å) that are similar to the corresponding bond lengths of [**25**] (Table 34). No significant differences in bond lengths were found in the B-N (1.557(4) and 1.585(4) Å) and B-C (1.625(5) Å) bond lengths in [**28**] compared to [**25**] or (**L5**-H_3)$^{2+}$. The C-Re-C bite angles of **L5**$^-$ (82.76(9) and 81.62(14)°) are also very similar compared to [**25**]. The phenyl ring in [**28**] is also considerably bent (Torsion angle B(1)-C(41)-C(42a)-C(43a) = 162.7(3)°) compared to (**L5**-H_3)$^{2+}$ (Torsion angle B(1)-C(31)-C(32)-C(33) = 175.5(2)°).

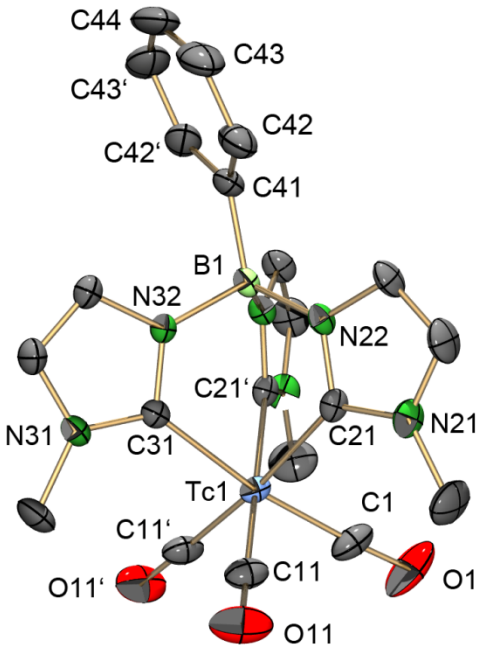

Figure 53: ORTEP representation[51] of [**28**]. Thermal ellipsoids are represented at the 50% probability level. Hydrogen atoms are omitted for clarity.

Table 37: Selected bond lengths and angles of [**28**].

Selected bond lengths [Å]		Selected angles [°]	
Tc(1)-C(1)	1.948(4)	C(1)-Tc(1)-C(11)	92.36(13)
Tc(1)-C(11)	1.940(3)	C(11)-Tc(1)-C(11)#1	92.66(18)
Tc(1)-C(21)	2.169(3)	C(1)-Tc(1)-C(21)	91.07(13)
Tc(1)-C(31)	2.137(3)	C(11)-Tc(1)-C(21)	92.75(12)
C(1)-O(1)	1.153(6)	C(21)-Tc(1)-C(31)	82.76(9)
C(11)-O(11)	1.153(4)	C(21)-Tc(1)-C(21)#1	81.62(14)
B(1)-N(22)	1.557(4)	N(22)-B(1)-N(32)	107.0(2)
B(1)-N(32)	1.585(4)	N(22)-B(1)-N(22)#1	105.5(3)
B(1)-C(41)	1.625(5)	N(22)-B(1)-C(41)	115.7(2)
		N(32)-B(1)-C(41)	105.4(3)

While the synthesis of *fac*-$\{M(CO)_3\}^+$ complexes (M = ^{99}Tc, Re) with tridentate NHC ligands was successful, some problems and limitations were discovered. [M(**L5**)$(CO)_3$] complexes appear to be unstable in solution, leading to low yields of the isolated compounds. A number of decomposition products of [^{99}Tc(**L5**)$(CO)_3$] were observed by ^{99}Tc-NMR, which could not be identified. Therefore, the exact decomposition mechanism remains unknown, but it is speculated that the increased bending of the phenyl group of the **L5**$^-$ ligand might be one potential reason for the decomposition. In addition, stability measurements of [Re(**L5**)$(CO)_3$] in CH_3CN showed an immediate formation of [Re(**L5**-H)$(CO)_3]^+$ when excess 1 M HCl was added, leading to several decomposition products within 72 h. This indicates that protonation of one of the NHC ligands might be an important starting point

for subsequent decomposition reactions. Similar problems were observed in the formation of $[Re(\mathbf{L6})(CO)_3]^+$, since **L6** has a tendency to coordinate bidentate due to its flexibility. The resulting $[ReBr(\mathbf{L6}\text{-}H)(CO)_3]^+$ was structurally characterized and its formation is prevented by precipitation of the Br^- ligands before reaction using AgOTf. $[^{99}Tc(\mathbf{L5})(CO)_3]$ is the first *fac*-$\{^{99}Tc(CO)_3\}^+$-NHC complex and its preparation is a proof of concept for the synthesis of stable *fac*-$\{^{99(m)}Tc(CO)_3\}^+$ complexes comprised of tridentate NHC ligands, in the future.

5 Conclusion and Outlook

In this thesis, the organometallic chemistry of $^{99(m)}$Tc with arene- and NHC ligand systems has been fundamentally studied. Thereby, a new synthetic pathway to the important class of $[^{99(m)}Tc(arene)_2]^+$ complexes was developed and the coordination chemistry of ^{99}Tc-NHC complexes has been significantly expanded and enhanced.

In the first part of this thesis, a facile synthesis of the highly stable $[^{99(m)}Tc(arene)_2]^+$ complexes starting from $[^{99(m)}TcO_4]^-$ was developed (Scheme 37). Remarkably, Zn is not needed as reducing agent for the formation of this class of complexes and the developed reactions give the target compounds in yields >60%. The reaction proceeds via the formation of $[^{99(m)}TcCl_6]^{2-}$ as an intermediate, as it was shown by the crystallization of the intermediates $[Al(DMF)_6][^{99}TcCl_6](Cl)\cdot DMF$ and $[^{99}Tc(benzene)_2][^{99}TcCl_5(OH_2)]$. Zn is only needed as a reducing agent in the case of benzene. Transalkylation, which is a common problem in the synthesis of $[Re(arene)_2]^+$ complexes, was exclusively observed in the preparation of $[^{99(m)}Tc(tetralin)_2]^+$, where $[^{99(m)}Tc(tetralin)(OHPhen)]^+$ (OHPhen = 1,2,3,4,5,6,7,8-octahydrophenanthrene) was unambiguously identified as a side product. While the reaction to $[^{99(m)}Tc(arene)_2]^+$ is currently limited to alkylated arenes that are liquid at 25°C, it represents a tremendous improvement over previously described procedures. One goal of future research is to broaden the scope of the reaction by the development of functional group tolerant reaction conditions. This would have a significant impact on the field of ^{99m}Tc chemistry, since functionalized $[^{99m}Tc(arene)_2]^+$ complexes represent a novel and unprecedented class of $^{99(m)}$Tc complexes. The preparation of functionalized $[^{99(m)}Tc(arene)_2]^+$ complexes might be achieved by using a combination of benzene and the arene of interest, since the formation of $[^{99(m)}Tc(benzene)_2]^+$ is only observed in trace quantities in the absence of Zn. Another approach for the synthesis of functionalized $[^{99(m)}Tc(arene)_2]^+$ complexes is the derivatization of coordinated arene ligands. In such a reaction, the benzene ligand in $[^{99(m)}Tc(benzene)_2]^+$ could be lithiated using LDA and then further derivatized, which is currently being investigated in our group for $[Re(benzene)_2]^+$.

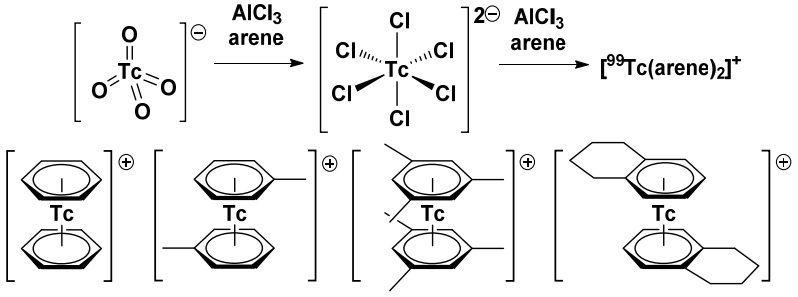

Scheme 37: Synthesized $[^{99}Tc(arene)_2]^+$ complexes.

In the second part of this thesis, NHCs have been introduced as unique ligands to further develop the organometallic chemistry of Re and $^{99(m)}$Tc. The synthesis of $\{^{99}TcO_2\}^+$-NHC complexes was significantly improved by using $[^{99}TcO(glyc)_2]^-$ instead of the base sensitive $[^{99}TcOCl_4]^-$ as a starting material (Scheme 38). Reaction of $[^{99}TcO(glyc)_2]^-$ with monodentate or bidentate NHCs led to the isolation of $\{^{99}TcO_2\}^+$-NHC complexes comprised of four NHC ligands in the equatorial plane. While complexes containing monodentate NHCs rapidly hydrolyze in the presence of H_2O, complexes comprised of bidentate NHCs are highly stable in the presence of H_2O. The unprecedented stability of these complexes confirms that water stable $^{99(m)}$Tc-NHC complexes exist and shows that chelation with multidentate NHCs is the key to the stability of these complexes. An alternative synthetic method was developed, in which the imidazolium salt is reacted with $[^{99}TcO(glyc)_2]^-$ and NEt_3 to give the water stable $\{^{99}TcO_2\}^+$-NHC complexes. This very convenient one-pot reaction avoids the preparation of the NHC before the reaction with $[^{99}TcO(glyc)_2]^-$ and thus simplifies the synthesis tremendously. When treated with HCl, $[^{99}TcO_2(\mathbf{L2})_2]^+$ undergoes a reversible core transformation in which one of the O^{2-} ligands is protonated and exchanged with Cl^- to give $[^{99}TcOCl(\mathbf{L2})_2]^{2+}$. This reaction further underlines the stability of these complexes. The Cl^- ligand in $[^{99}TcOCl(\mathbf{L2})_2]^{2+}$ was exchanged with MeO^- or SCN^-, which led to the isolation of $[^{99}TcOX(\mathbf{L2})_2]^{2+}$ (X = OMe, NCS). The chemistry of $[^{99}TcOX(\mathbf{L2})_2]^{2+}$ (X = Cl, OMe, NCS) is presumably relevant for the *in vivo* chemistry of $[^{99m}TcO_2(\mathbf{L2})_2]^+$, since it is proof that the $\{^{99m}TcO_2\}^+$ core in this complex is not chemically inert under acidic conditions. The corresponding chemistry with the higher homologue Re is very similar, although formation of *cis*- and *trans*-$[ReO_2(\mathbf{L2})_2]^+$ was observed in the reaction of $[ReO(glyc)_2]^-$ with **L2**. The exclusive formation of the thermodynamic product *trans*-$[ReO_2(\mathbf{L2})_2]^+$ was observed when the one-pot method was used, in which $[ReO(glyc)_2]^-$ was reacted with $(\mathbf{L2}\text{-}H_2)^{2+}$ and NEt_3 in refluxing CH_2Cl_2. Furthermore, the structure of *trans*-$[ReOCl(\mathbf{L2})_2]^{2+}$ was solved using X-ray diffraction experiment, which shows the feasibility of derivatization reactions in the position *trans* to the O^{2-} ligand. In the future, *trans*-$[ReOCl(\mathbf{L2})_2]^{2+}$ might be a useful starting material for further reactions and the investigation of the *cis*-/*trans*-isomerism in $[ReO_2(\mathbf{L2})_2]^+$ would presumably lead to a better understanding of the fundamental chemistry of the $\{ReO_2\}^+$ core.

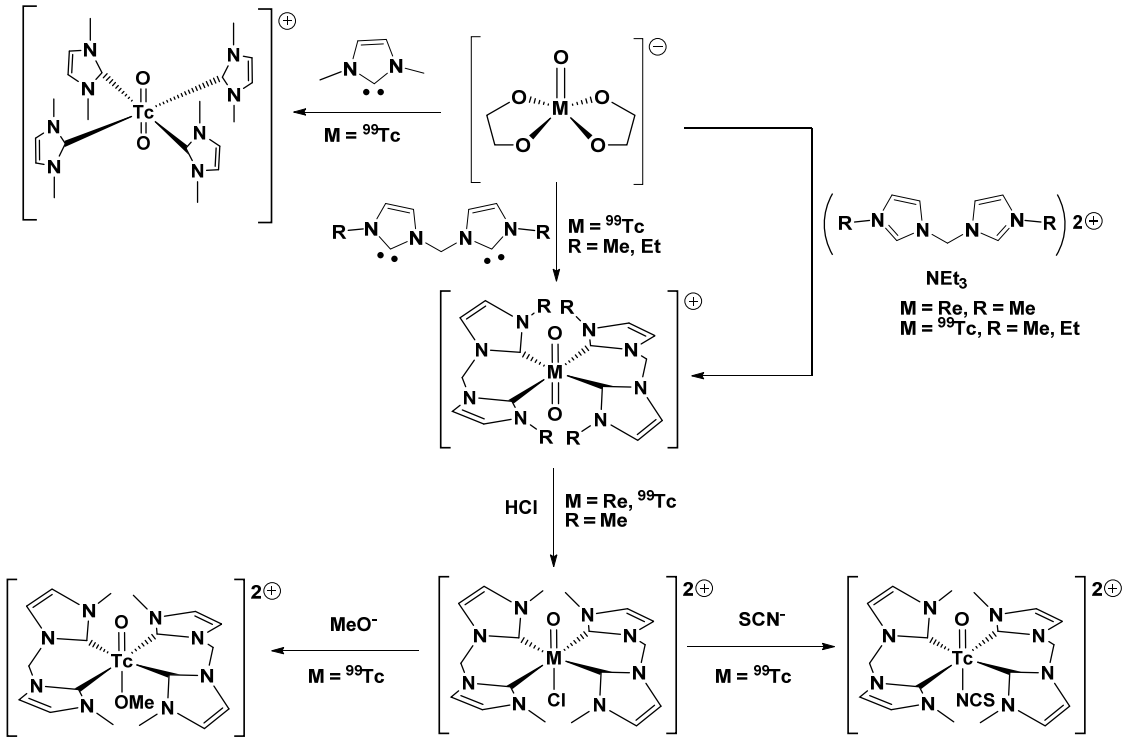

Scheme 38: Developed NHC chemistry, starting from $[MO(glyc)_2]^-$ (M = Re, ^{99}Tc).

Following a similar approach as in the preparation of $[MO_2(\mathbf{L2})_2]^+$, novel $[MO_2(\mathbf{L2})(\mathbf{L4})]_2^{2+}$ dimers were isolated (M = Re, ^{99}Tc). Reaction of $[MO(glyc)_2]^-$ with $(\mathbf{L2}\text{-}H_2)^{2+}$ and **L4** in the presence of NEt_3 afforded $[MO_2(\mathbf{L2})(\mathbf{L4})]_2^{2+}$ (Scheme 39). These dimeric complexes represent a new and unprecedented class of $\{MO_2\}^+$-NHC compounds and they are further evidence for the potential of NHCs to stabilize Re and $^{99(m)}$Tc in high oxidation states. Two conformers of $[MO_2(\mathbf{L2})(\mathbf{L4})]_2^{2+}$ were identified by X-ray diffraction experiments and studied by NMR experiments. Depending on the conditions during crystallization, the two conformers were selectively crystallized, which led to further insights into their structure. Reaction of $[MO_2(\mathbf{L2})(\mathbf{L4})]_2^{2+}$ with HCl resulted in cleavage of the dimers by protonation of **L4**, leading to the isolation of $[MOCl_3(\mathbf{L2})]$. These complexes showed an interesting chemistry in aqueous solution that should be further investigated, since at least one Cl^- is exchanged for an OH^- or H_2O ligand. Furthermore, reaction of $[MOCl_3(\mathbf{L2})]$ with 2,2'-bipyridine (bipy) in aqueous solution led to the isolation of $[MO_2(\mathbf{L2})(bipy)]^+$. The reactivity and stability of $[MOCl_3(\mathbf{L2})]$ makes it a unique and interesting starting material for further derivatization reactions, potentially leading to the synthesis of a large number of new Re- and $^{99(m)}$Tc-NHC complexes, in the future. The developed synthetic pathway to Re and ^{99}Tc complexes comprised of only two coordinated NHCs is remarkable, because high valent Re and ^{99}Tc complexes have a strong tendency to coordinate four NHCs in the equatorial plane. Therefore, this approach could be also of interest for the development of novel Re complexes for catalytic applications.

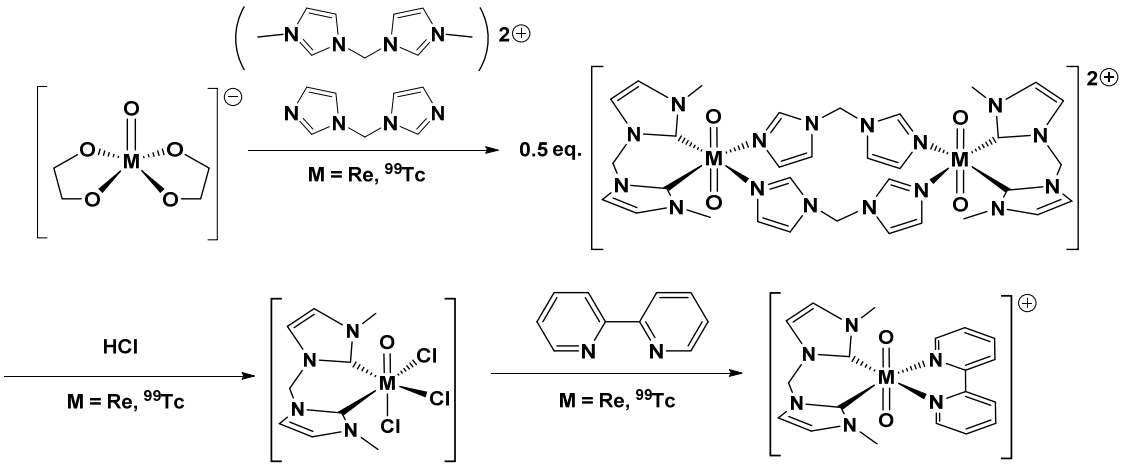

Scheme 39: General synthetic pathway to complexes containing the $\{MO(\mathbf{L2})\}^{3+}$ fragment (M = Re, ^{99}Tc).

The synthesis of $[^{99m}TcO_2(\mathbf{L2})_2]^+$ was developed starting from $[^{99m}TcO_4]^-$ (Scheme 40). To work under exclusion of H_2O, a novel phase transfer protocol was used, which utilizes the extraction of $[^{99m}TcO_4]^-$ from saline using the ionic liquid $[P(C_6H_{13})_3(C_{14}H_{29})]Br$. This method was also used for the preparation of $[^{99m}Tc(arene)_2]^+$ complexes and provides a great alternative to previously reported phase transfer protocols. Reaction of $[^{99m}TcO_4]^-$ with $SnCl_2$ in the presence of ethylene glycol led to $[^{99m}TcO(glyc)_2]^-$ as intermediate, which was further reacted with $(\mathbf{L2}\text{-}H_2)^{2+}$ and NEt_3 to give $[^{99m}TcO_2(\mathbf{L2})_2]^+$. An alternative method was developed, in which the *in situ* prepared $[^{99m}TcO(glyc)_2]^-$ was reacted with the transmetalation reagent $[Ag_2(\mathbf{L2})_2]^{2+}$. $[^{99m}TcO_2(\mathbf{L2})_2]^+$ is the first prepared $^{99m}Tc^V$-NHC complex, which proves that the synthesis of water stable ^{99m}Tc-NHC complexes is possible. Formation of a side product was observed during the synthesis of $[^{99m}TcO_2(\mathbf{L2})_2]^+$ regardless of the used procedure. The side product formed due to excess $SnCl_2$ present in the reaction and it was identified as $[^{99m}TcCl_2(\mathbf{L2})_2]^{2+}$. By reaction of $[^{99}TcO_2(\mathbf{L2})_2]^+$ with excess $SnCl_2$, *cis*-$[^{99}TcCl_2(\mathbf{L2})_2]^{2+}$ was synthesized in macroscopic amounts and characterized by X-ray diffraction experiments. The identification of *cis*-$[^{99}TcCl_2(\mathbf{L2})_2]^{2+}$ shows that NHCs are also capable of stabilizing oxidation states of $^{99(m)}$Tc other than +V and +I, leading to new possibilities for future investigations. Besides the interesting implications for fundamental $^{99(m)}$Tc chemistry, the elucidation of this side reaction in the preparation of $[^{99m}TcO_2(\mathbf{L2})_2]^+$ is important for the improvement of the reaction. In order to solve the problem of this side reaction, the $SnCl_2$ presumably needs to be removed from the $^{99m}Tc^V$ starting material before the reaction to $[^{99m}TcO_2(\mathbf{L2})_2]^+$. The development of such a $^{99m}Tc^V$ starting material, which can be separated from $SnCl_2$ by C_{18} SepPak column chromatography, would potentially improve the synthesis of $\{^{99m}TcO_2\}^+$-NHC complexes. However, a simple purification of the $^{99m}Tc^V$ starting material is not the only requirement. Ideally, the $^{99m}Tc^V$ starting material can be identified and quantified with HPLC analysis, while it also must be suitable for substitution reactions with the NHC-precursors.

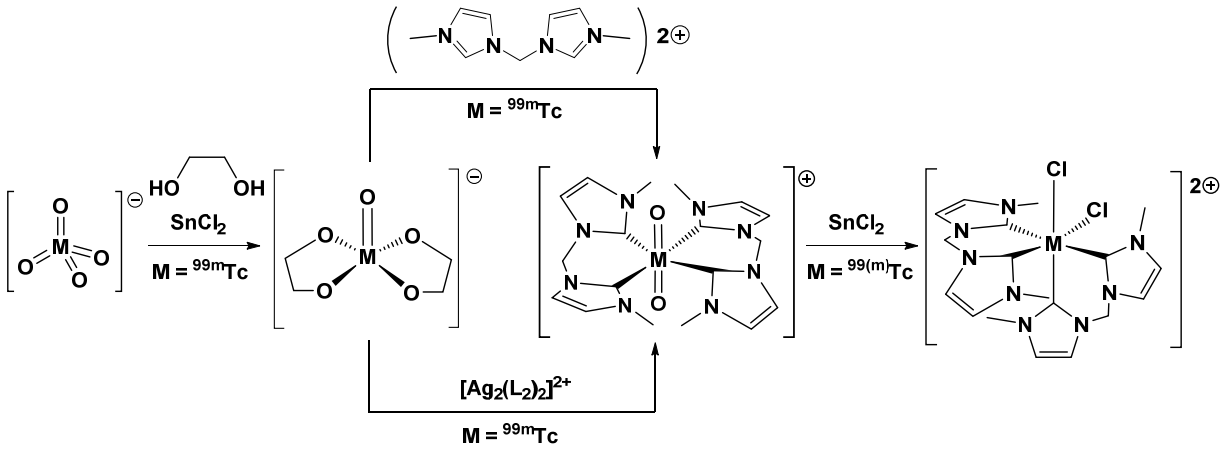

Scheme 40: Developed protocols for the synthesis of $[^{99m}TcO_2(\mathbf{L2})_2]^+$. The reduction of $[^{99(m)}TcO_2(\mathbf{L2})_2]^+$ leads to the formation of $[^{99(m)}TcCl_2(\mathbf{L2})_2]^{2+}$.

Finally, the first low-valent *fac*-$\{M(CO)_3\}^+$-NHC complexes (M = Re, ^{99}Tc) with tridentate NHCs were prepared (Scheme 41). Reaction of $[ReBr_3(CO)_3]^{2-}$ with the tridentate NHCs $(PhB(^{Me}Im)_3)^-$ (**L5**$^-$) or 1,1,1-tris[(3-methylimidazoline-2-ylidene)-methyl]ethane (**L6**) led to the isolation of [Re(**L5**)$(CO)_3$] and $[Re(\mathbf{L6})(CO)_3]^+$, respectively. Formation of disubstituted side products was also observed in the MS analysis of the crude products. Furthermore, $[ReBr(\mathbf{L6}\text{-H})(CO)_3]^+$ was identified as a side product of the reaction by X-ray diffraction experiments. The formation of disubstituted side products was successfully avoided by precipitation of the Br^- ligands using AgOTf. The knowledge gained from the Re chemistry has been applied for the synthesis of [^{99}Tc(**L5**)$(CO)_3$], which is the first *fac*-$\{^{99}Tc(CO)_3\}^+$-NHC complex. [M(**L5**)$(CO)_3$] complexes (M = Re, ^{99}Tc) showed a tendency to decompose in solution, although the exact mechanism of decomposition could not be identified. A stability experiment, in which [Re(**L5**)$(CO)_3$] was treated with HCl, indicated that decomposition might be initialized by protonation of one of the NHC ligands to form $[Re(\mathbf{L5}\text{-H})(CO)_3]^+$. However, further investigations are necessary to fully understand the decomposition reaction and improve the synthesis of these novel and unique complexes.

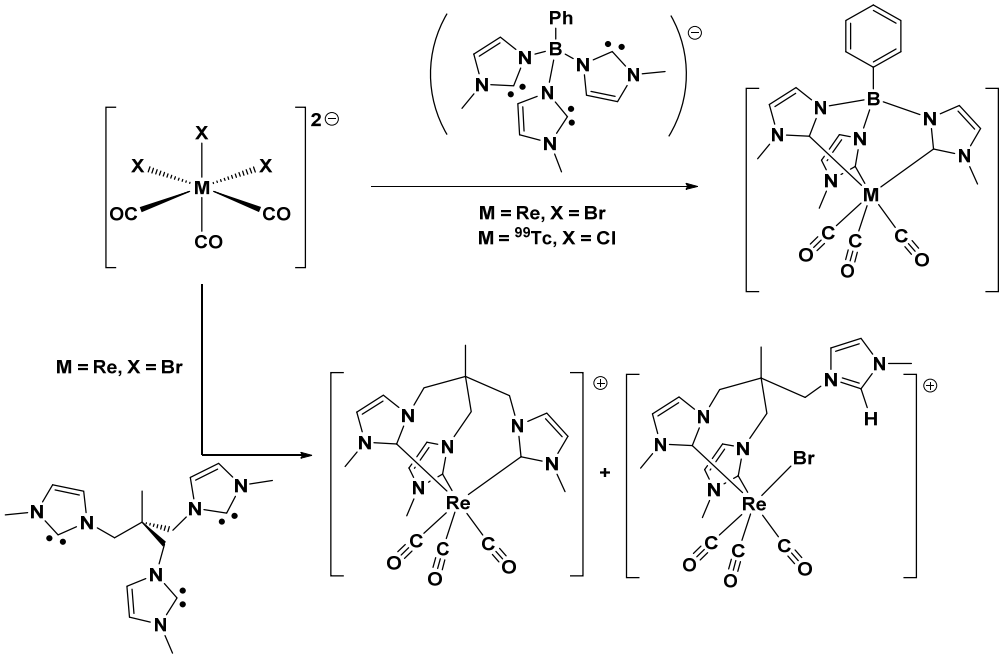

Scheme 41: Syntheses of the first *fac*-$\{M(CO)_3\}^+$-NHC complexes containing tridentate NHCs (M = Re, ^{99}Tc).

This thesis contributed significantly to the development of organometallic Re and $^{99(m)}$Tc chemistry. It broadens the scope of arene and NHC coordination chemistry of these two metals and thereby paves the way for new applications using these ligand systems.

6 Experimental Section

6.1 General Information

Caution: ^{99}Tc and ^{99m}Tc are weak β^-- and γ-emitters, respectively. All experiments have to be performed in laboratories approved for working with low-level radioactive materials.

All reactions were carried out under an inert N_2 atmosphere. $(NH_4)[^{99}TcO_4]$ (*Oak Ridge*) and all other chemicals were of reagent grade and used without further purification. $[^{99m}TcO_4]^-$ was eluted from a ^{99}Mo/^{99m}Tc *UltratechneKow FM* generator from *Mallinckrodt Schweiz AG*. The compounds $(K)[^{99}TcO_4]$,[125] $(K)_2[^{99}TcCl_6]$,[53] $(N^nBu_4)[^{99}TcOCl_4]$,[126] $(NEt_4)_2[^{99}TcCl_3(CO)_3]$,[124] $(N^nBu_4)[ReOCl_4]$[16,127] and $(NEt_4)_2[ReBr_3(CO)_3]$[123] were prepared according to published procedures. The preparations of the compounds (**L1**-H)(PF_6),[67,68] (**L2**-H_2)$(PF_6)_2$,[69] (**L3**-H_2)$(PF_6)_2$,[70] **L4**,[71] (**L5**-H_3)$(OTf)_2$,[39] (**L6**-H_3)$(PF_6)_3$,[31] [**6**]$(PF_6)_2$,[74] [**7**]$(PF_6)_3$,[31] (N^nBu_4)[**8**][75,77] and (N^nBu_4)[**15**][93,94] were adapted from standard literature procedures.

FT-IR spectra were measured as KBr pellets (^{99}Tc samples) or as neat samples, using a *Specac Golden Gate ATR* (attenuated total reflection) accessory, on a *Perkin Elmer Spectrum Two* spectrophotometer. ^{1}H and ^{13}C NMR spectra were recorded on a *Bruker DRX500* 500 MHz, a *Bruker AV-400* 400 MHz, a *Bruker AV-300* 300 MHz, a *Varian Gemini* 300 MHz, or a *Varian Mercury* 200 MHz spectrometer. ^{13}C NMR spectra were proton decoupled recorded. ^{99}Tc-NMR spectra were recorded on a *Bruker DRX500* 500 MHz or a *Bruker AV-400* 400 MHz spectrometer. ESI mass spectra were recorded with a *Bruker HCT Ultra*. HR-EI-MS was performed on *a Thermo DFS* (ThermoFisher Scientific, Bremen, Germany) double-focusing magnetic sector mass spectrometer (geometry BE). Mass spectra were measured in electron ionization (EI) mode at 45 eV, with solid probe inlet, a source temperature of 200°C, an acceleration voltage of 5 kV, and a resolution of 10'000. The instrument was scanned between e.g. m/z 300 und 350 at scan rate of 100-200 s / decade in the electric scan mode. Perfluorokerosene (PFK, Fluorochem, Derbyshire, UK) served for calibration. HR-ESI-MS was performed on a *Bruker maxis UHPLC-HR-MS* mass spectrometer. Samples were dissolved in an appropriate solvent at a concentration of around 1 µmol/ml and measured at continuous flow at 3 µl/min. The mass spectrometer was operated in the positive electrospray ionization mode at 4,000 V capillary voltage, -500 V endplate offset, with a N_2 nebulizer pressure of 0.8 bar and dry gas flow of 4 l/min at 180°C. MS acquisitions were performed in the mass range from m/z 50 to 2000 at 20,000 resolution (full width at half maximum) and 1.0 Hz spectra rate. Masses were calibrated between m/z 158 and 1450 or 2721 prior analysis below 2 ppm accuracy, with a 2 mM solution of sodium formate or with a *Fluka* (*Sigma Aldrich*) electrospray calibration solution that has been 100 times diluted with CH_3CN, respectively. UV-Vis spectra were measured using a *Cray 50* spectrometer with solution samples (CH_3CN) in 1 cm quartz cells. For ^{99}Tc content measurements, pure compounds were dissolved in the appropriate solvents. The measurements were carried out with a scintillation cocktail (*Packard Ultimate Gold XR*) and a liquid scintillation counter (*TRICARB 2200CA, Packard* or *Hidex 300 SL*). Elemental analyses were performed on a *Leco CHNS-932* and a *Leco TruSpec Micro*

elemental analyser. HPLC analyses were performed on *a Merck Hitachi LaChrom L 7100* pump coupled to a *Merck Hitachi LaChrom L7200* tunable UV detector and a radiodetector. The UV-Vis detection was performed at 250 nm. The detection of radioactive ^{99}Tc/^{99m}Tc complexes was performed with a *Berthold LB508* or a *Berthold LB513* radiodetector equipped with *YG/BGO* cells, respectively. Separations were achieved on a *Macherey-Nagel C_{18}* reversed-phase column (*Nucleosil* 10 µm, 250 × 4 mm) using a TEAP (CH_3CN/50 mM triethylammonium phosphate) or TFA (MeOH/0.1% CF_3COOH) gradient as eluent, and a flow rate of 0.5 ml/min. TEAP gradient: t = 0 – 3 min: 100% TEAP; 3 – 3.1 min: 100 – 75% TEAP; 3.1 – 9 min: 75% TEAP; 9 – 9.1 min: 75 – 66% TEAP; 9.1 – 12 min: 66% TEAP; 12 – 12.1 min: 66 – 0% TEAP; 15 – 15.1 min: 0 – 100% TEAP; 15.1 – 18min: 100% TEAP. TFA gradient: t = 0 – 3 min: 0% MeOH; 3 – 3.1 min: 0 – 25% MeOH; 3.1 – 9 min: 25% MeOH; 9 – 9.1 min: 25 – 34% MeOH; 9.1 – 18 min: 34 - 100% MeOH; 18 – 25 min: 100% MeOH, 25 – 25.1 min: 100 - 0% MeOH; 25.1 – 30 min: 0% MeOH. Comparison of the HPLC retention times for the ^{99m}Tc compounds with the corresponding ^{99}Tc and Re compounds confirmed identity. Electrochemical measurements were carried out in CH_3CN containing 0.1 M $N^nBu_4PF_6$ as a conducting electrolyte. For all measured ^{99}Tc-Complexes, a *Metrohm 757VA Computrace* electrochemical analyzer was used with a standard three-electrode setup of glassy carbon working electrode (i.d. = 3 mm), platinum auxiliary electrode and Ag/AgCl reference electrode. All potential are given *vs.* Ag/AgCl and are referenced with Fc/Fc^+ at 450 mV.

6.2 X-Ray Diffraction

Crystallographic data were collected at 183 K (except for [**1**](PF_6) which was measured at 253 K) on an *Oxford Diffraction Xcalibur* system with a *Ruby* detector using Mo K_α radiation (λ = 0.7107 Å) that was graphite-monochromated, a *Stoe IPDS* diffractometer using Mo K_α radiation (λ = 0.7107 Å) or an *Oxford Diffraction SuperNova* dual source system with an *Atlas* detector using Cu K_α (λ = 1.54184 Å) or Mo K_α radiation (λ = 0.7107 Å). Suitable crystals were covered with oil (*Infineum V8512*, formerly known as *Paratone N*), mounted on top of a glass fibre and immediately transferred to the diffractometer. In the case of the *Stoe IPDS*, a maximum of 8000 reflections distributed over the whole limiting sphere were selected by the program *SELECT* and used for unit cell parameter refinement with the program *CELL*.[128] Data were corrected for Lorentz and polarization effects as well as for absorption (numerical). In the case of the *Oxford* systems, the program suite *CrysAlisPro* was used for data collection, multi-scan absorption correction and data reduction.[129] Structures were solved with direct methods using *SIR97*[130] or SHELXS[131] and were refined by full-matrix least-squares methods on F^2 with *SHELXL-97* or *SHELXL-2014*.[131] The structures were checked for higher symmetry with help of the program *Platon*.[132] ORTEP representations were created by the program *ORTEP32*.[51]

6.3 Ligand Precursors

6.3.1 1,3-Dimethylimidazolium Hexafluorophosphate (L1-H)(PF_6)

1-Methylimidazole (0.8 ml, 10.0 mmol) and methyl iodide (1 ml, 16.1 mmol) were dissolved in toluene (30 ml) and heated on 50°C for 17 h. The reaction was allowed to cool to 25°C and the solvent was decanted. The remaining yellow crude solid was washed with Et_2O (2 × 10 ml) and dried *in vacuo*. The crude product was dissolved in H_2O (15 ml), NH_4PF_6 (1.954 g, 12.0 mmol) was added and the resulting yellow solution was stirred for 1.5 h. Extraction with CH_2Cl_2 (2 × 20 ml), followed by drying of the organic phase over $MgSO_4$, filtration and evaporation of the solvent *in vacuo*, afforded highly hygroscopic (**L1**-H)(PF_6). Yield: 1.00 g (41%). ^{1}H NMR (300 MHz, DMSO-D_6): δ = 9.01 (*s*, 1 H, N-*C*H-N), 7.67 (*s*, 2 H, Im-H), 3.84 (*s*, 6 H, *C*H_3) ppm.

6.3.2 1,1'-Methylene-3,3'-dimethyldiimidazolium Dihexafluorophosphate ((L2-H_2)(PF_6)$_2$)

In an autoclave equipped with a Teflon vessel, 1-methylimidazole (1 ml, 12.55 mmol) and CH_2Cl_2 (0.3 ml, 4.70 mmol) were heated on 110°C for 20 h. The resulting solid was washed with Et_2O (5 ml) and dried *in vacuo*. Afterwards, the solid was dissolved in H_2O (10 ml). A solution of NH_4PF_6 (1.55 g, 9.51 mmol) in H_2O (10 ml) was added, which led to the precipitation of a colorless solid. The solid was collected by filtration, washed with H_2O (5 ml) and dried *in vacuo*. Yield: 2.05 g (93%). ^{1}H NMR (200 MHz, DMSO-D_6): δ = 9.29 (*s*, 2 H, N-*C*H-N), 7.91 (*s*, 2 H, Im-H), 7.77 (*s*, 2 H, Im-H), 6.59 (*s*, 2 H, *C*H_2), 3.88 (*s*, 6 H, *C*H_3) ppm. Anal. calcd. for $C_9H_{14}F_{12}N_4P_2$ (%): C, 23.09; H, 3.01; N, 11.97. Found: C, 22.96; H, 2.94; N, 11.90.

6.3.3 Bisimidazol-1-ylmethane (L4)

Finely ground imidazole (1.49 g, 21.9 mmol), finely ground KOH (2.74 g, 48.8 mmol) and (N^nBu_4)Br (0.21 g, 0.65 mmol) were stirred for 30 min. CH_2Cl_2 (0.7 ml, 10.9 mmol) and H_2O (0.5 ml) were added and the mixture was left to react for 20 h. The now solid reaction mixture was purified by sublimation (0.93 mbar, 130°C-150°C) to afford **L4** as a colorless crystalline solid. Yield: 1.32 g (82%). ^{1}H NMR (300 MHz, $CDCl_3$): δ = 7.65 (*s*, N*C*HN, 2 H), 7.11 (*t*, ^{3}*J(HH)* = 2.1 Hz, Im-H, 2 H), 6.99 (*t*, ^{3}*J(HH)* = 2.7 Hz, Im-H, 2 H), 6.04 (*s*, *C*H_2, 2 H) ppm. Anal. calc. for $C_7H_8N_4$ (%): C, 56.75; H, 5.44; N, 37.81. Found: C, 56.18; H, 5.40; N, 37.59.

6.3.4 1,1'-Methylene-3,3'-diethyldiimidazolium Dihexafluorophosphate ((L3-H_2)(PF_6)$_2$)

Bisimidazol-1-ylmethane (200 mg, 1.35 mmol) was dissolved in CH_3CN (10 ml) and ethyl bromide (1 ml, 13.39 mmol) was added. The solution was heated on 90°C for 7 h. The resulting colorless precipitate was filtered, washed with CH_3CN (3 ml) and dried *in vacuo*. The solid was dissolved in H_2O (10 ml) and an aqueous solution of NH_4PF_6 (1 g, 6.13 mmol, dissolved in 10 ml H_2O) was added, which led to the precipitation of a colorless solid. The solid was collected by filtration, washed with H_2O (5 ml) and dried *in vacuo*. Yield: 550 mg (82%). ^{1}H NMR (200 MHz, CD_3CN): δ = 8.64 (*s*, 2 H, N-*C*H-N), 7.48 (*s*, 2 H, Im-H), 7.41 (*s*, 2 H, Im-H), 6.24 (*s*, 2 H, *C*H_2), 4.13 (*q*, ^{3}*J(HH)* = 7.4 Hz, 4 H,

CH_2CH$_3$), 1.38 (*t*, ^{3}*J(HH)* = 7.4 Hz, 6 H, CH$_2$*C*H$_3$) ppm. Anal. calcd. for $C_{11}H_{18}F_{12}N_4P_2$ (%): C, 26.63; H, 3.66; N, 11.29. Found: C, 26.59; H, 3.69; N, 11.31.

6.3.5 (PhB(^{Me}Im-H)$_3$)(OTf)$_2$ ((L5_H$_3$)(OTf)$_2$)

1-Methylimidazole (0.75 ml, 9.45 mmol) was added dropwise with a syringe to a solution of dichlorophenylborane (0.41 ml, 3.15 mmol) in toluene (9 ml). Immediately, the formation of a precipitate was observed and the suspension was stirred for 15 min at 25°C. A solution of trimethylsilyl trifluoromethanesulfonate (1.3 ml, 7.18 mmol) in toluene (10 ml) was added dropwise with a syringe, resulting in the formation of a colorless precipitate. The suspension was heated on 80°C for 24 h and was then slowly cooled to 25°C. Removal of the solvent *in vacuo* yielded a colorless solid, which was suspended in CH_2Cl_2 (60 ml), filtered, washed with CH_2Cl_2 (10 ml) and dried *in vacuo* to give (**L5**-H$_3$)(OTf)$_2$ as a colorless solid. Yield: 1.77 g (89%). ^{1}H NMR (200 MHz, DMSO-D$_6$): δ = 8.56 (*s*, 3 H, N-*C*H-N), 7.80 (*s*, 3 H, Im-H), 7.46-7.38 (*m*, 6 H, Im-H, Ph-H), 7.13-7.10 (*m*, 2 H, Ph-H), 3.85 (*s*, 9 H, *C*H$_3$) ppm. Anal. calcd. for $C_{20}H_{23}B_1F_6N_6O_6S_2$ (%): C, 37.99; H, 3.67; N, 13.29. Found: C, 38.08; H, 3.60; N, 13.21.

6.3.6 1,1,1-Tris[(3-methylimidazolium)-methyl]ethane Trihexafluorophosphate ((L6-H$_3$)(PF$_6$)$_3$)

6.3.6.1 1,1,1-Tris[(*p*-toluenesulfonato)methyl]ethane

1,1,1-Tris-(hydroxymethyl)ethane (3.04 g, 25.30 mmol) was dissolved in pyridine (9 ml) and cooled to 0°C. A solution of *p*-toluenesulfonyl chloride (14.50 g, 76.06 mmol) in pyridine (9 ml) was added in small portions over 15 min, ensuring that the temperature of the reaction solution did not exceed 20°C. The solution was stirred at 0°C for 1 h before it was allowed to warm to 25°C over the course of 2 h. The reaction mixture was added to a 0°C cold solution of conc. HCl (18 ml) and MeOH (9 ml). A colorless solid precipitated, was filtered off and washed with H_2O and MeOH. The colorless solid was recrystallized from MeOH and washed with cold MeOH. Drying *in vacuo* afforded 1,1,1-tris[(*p*-toluenesulfonato)methyl]ethane. Yield: 9.24 g (63%). ^{1}H-NMR (200 MHz, $CDCl_3$): δ 7.72 (*d*, ^{3}*J(HH)* = 8.4 Hz, 2 H, *C*H), 7.37 (*d*, ^{3}*J(HH)* = 9.2 Hz, 2 H, *C*H), 3.77 (*s*, 3 H, *C*H$_3$), 2.48 (*s*, 6 H, *C*H$_2$), 0.90 (*s*, 3 H, *C*H$_3$) ppm.

6.3.6.2 1,1,1-Tris(bromomethyl)ethane

1,1,1-Tris[(p-toluenesulfonato)methyl]ethane (9.24 g, 15.9 mmol) and NaBr (8.394 g, 81.6 mmol) were dissolved in diethylene glycol and heated on 145°C for 16 h. After the reaction had cooled to 25°C, H_2O (30 ml) was added and the product was extracted with CH_2Cl_2 (3 × 30 ml). The combined organic phases were dried over $MgSO_4$, filtered and the solvent removed under reduced pressure. The product was purified from the resulting crude oil by bulb-to-bulb distillation (10 mbar, 100-120°C). Yield: 4.14 g (84%).^{1}H-NMR (200 MHz, $CDCl_3$): δ 3.51 (*s*, 6 H, *C*H$_2$), 1.30 (*s*, 3 H, *C*H$_3$) ppm.

6.3.6.3 1,1,1-Tris[(3-methylimidazolium)-methyl]ethane Tribromide ((L6-H_3)$(Br)_3$)

1,1,1-Tris(bromomethyl)ethane (4.143 g, 13.4 mmol) and 1-methylimidazole (5.40 ml, 67.75 mmol) were heated on 150°C for 24 h. A colorless solid formed, which was washed with Et_2O and recrystallized from MeOH. Drying *in vacuo* afforded (**L6**-H_3)$(Br)_3$ as a colorless solid. Yield 3.37 g (45%). ^{1}H-NMR (200 MHz, DMSO-D_6): δ 9.16 (*s*, 3 H, N-*C*H-N), 7.80 (*s*, 3 H, Im-H), 7.70 (*s*, 3 H, Im-H), 4.29 (*s*, 6 H, *C*H_2), 3.89 (*s*, 9 H, *C*H_3), 0.94 (*s*, 3 H, *C*H_3) ppm. Anal. calcd. for $C_{17}H_{27}N_6Br_3$ (%): C, 36.78; H, 4.90; N, 15.14. Found: C, 36.00; H, 4.77; N, 14.12.

6.3.6.4 1,1,1-Tris[(3-methylimidazolium)-methyl]ethane Trihexafluorophosphate ((L6-H_3)$(PF_6)_3$)

(**L6**-H_3)$(Br)_3$ (331 mg, 0.60 mmol) was dissolved in MeOH (10 ml) and NH_4PF_6 (292 mg, 1.80 mmol) was added. (**L6**-H_3)$(PF_6)_3$ precipitated as a colorless solid which was filtered off, washed with MeOH (3 × 3 ml) and dried *in vacuo*. Yield: 404 mg (90%). ^{1}H-NMR (200 MHz, DMSO-D_6): δ 9.12 (*s*, 3 H, N-*C*H-N), 7.81 (*s*, 3 H, Im-H), 7.68 (*s*, 3 H, Im-H), 4.26 (*s*, 6 H, *C*H_2), 3.88 (*s*, 9 H, *C*H_3), 0.93 (*s*, 3 H, *C*H_3) ppm. Anal. calcd. for $C_{17}H_{27}F_{18}N_6P_3$ (%): C, 27.21; H, 3.63; N, 11.20. Found: C, 27.12; H, 3.56; N, 11.14.

6.3.7 $[Ag_2(L2)_2](PF_6)_2$ ([6]$(PF_6)_2$)

6.3.7.1 1,1'-Methylene-3,3'-dimethyldiimidazolium Dichloride ((L2-H_2)$(Cl)_2$)

In an autoclave with a Teflon vessel, 1-methylimidazole (1 ml, 12.55 mmol) and CH_2Cl_2 (0.3 ml, 4.70 mmol) were heated on 110°C for 20 h. The resulting colorless solid ((**L2**-H_2)$(Cl)_2$) was washed with Et_2O (5 ml), dried *in vacuo* and used for the formation of the Ag complex without further purification. Crude yield: 1.46 g.

6.3.7.2 $[Ag_2(L2)_2](PF_6)_2$ ([6]$(PF_6)_2$)

Crude (**L2**-H_2)$(Cl)_2$ (0.73 g) was dissolved in H_2O (25 ml) and Ag_2O (1.36 g, 5.87 mmol) was added. The solution was stirred for 20 min and then filtered through a pad of celite. A solution of NH_4PF_6 (768 mg, 4.71 mmol) in H_2O (2 ml) was added and the resulting suspension was stirred for 15 min. The colorless solid was filtered off, washed with H_2O (4 ml) and Et_2O (4 ml) and dried *in vacuo*. Yield: 910 mg (90% based on CH_2Cl_2). ^{1}H-NMR (400 MHz, DMSO-D_6): δ 7.89 (*d*, ^{3}*J(HH)* = 2.0 Hz, 4 H, Im-H), 7.56 (*d*, ^{3}*J(HH)* = 1.6 Hz, 4 H, Im-H), 6.64 (*br. s*, 4 H, *C*H_2), 3.88 (*s*, 12 H, *C*H_3) ppm. Anal. calcd. for $C_{18}H_{24}Ag_2F_{12}N_8P_2$ (%): C, 25.19; H, 2.82; N, 13.06. Found: C, 24.59; H, 2.66; N, 12.72.

6.3.8 $[Ag_3(L6)_2](PF_6)_3$ ([7]$(PF_6)_3$)

(**L6**-H_3)$(PF_6)_3$ (0.50 g, 0.67 mmol) was dissolved in CH_3CN (18 ml). A suspension of Ag_2O (0.27 g, 1.18 mmol) in CH_3CN (22 ml) was added and the resulting suspension was heated on 75°C for 12 h. The black suspension was then filtered through a pad of celite and the solvent partially evaporated under reduced pressure. Precipitation with Et_2O, followed by centrifugation of the suspension,

decanting of the supernatant and drying *in vacuo* afforded [**7**]$(PF_6)_3$.Yield: 423 mg (91% based on (**L6**-H_3)$(PF_6)_3$). ^{1}H-NMR (300 MHz, DMSO-D_6): δ 7.53 (*s*, 6 H, Im-H), 7.46 (*s*, 6 H, Im-H), 4.56-4.12 (*m*, 12 H, *C*H_2), 3.90 (*s*, 18 H, *C*H_3), 1.25 (*s*, 6 H, *C*H_3) ppm. Anal. calcd. for $C_{34}H_{48}Ag_3F_{18}N_{12}P_3$ (%): C, 29.52; H, 3.55; N, 12.15. Found: C, 29.33; H, 3.38; N, 12.03.

6.4 Technetium Complexes

6.4.1 General Procedures for the Preparation of [^{99}Tc(arene)$_2$](PF$_6$) (arene = benzene, toluene, mesitylene, tetralin, [1] – [4](PF$_6$)).

Method a. (NH$_4$)[^{99}TcO$_4$] (18 mg, 0.10 mmol), Zn-dust (22 mg, 0.34 mmol), AlCl$_3$ (134 mg, 1.00 mmol) and the corresponding arene (6 ml) were heated on 85°C. After 8 h, the solvent of the resulting dark brown suspension was removed with a stream of N$_2$. The residue was washed with Et$_2$O (3 × 2 ml). The remaining solid was extracted with H$_2$O (3 × 2 ml) and the aqueous solution filtered. NH$_4$PF$_6$ (150 mg, 0.92 mmol) in H$_2$O (1 ml) was added to the red-brown filtrate. The pale yellow precipitate was filtered off, washed with H$_2$O (2 × 0.5 ml) and Et$_2$O (2 × 0.5 ml) and dried *in vacuo* to give [^{99}Tc(arene)$_2$](PF$_6$) as a pale yellow powder. Alternatively, the precipitate can be extracted by CH$_2$Cl$_2$ from the aqueous suspension. Crystals suitable for X-ray diffraction analysis were grown by slow diffusion of Et$_2$O into an acetone solution of [**1**] – [**4**](PF$_6$).

Method b. (K)[^{99}TcO$_4$] (20 mg, 0.10 mmol), AlCl$_3$ (200 mg, 1.50 mmol) and the corresponding arene (8 ml) were heated on 85°C. After 4 h, H$_2$O (6 ml) was added to the hot dark brown solution and the aqueous phase was separated and filtered. The process was repeated with additional H$_2$O (2 × 2 ml). To the combined aqueous solutions was added a solution of NH$_4$PF$_6$ (150 mg, 0.92 mmol) in H$_2$O (1 ml). The formed pale yellow precipitate was filtered, washed with H$_2$O (2 × 0.5 ml) and dried *in vacuo* to give [^{99}Tc(arene)$_2$](PF$_6$) as a pale yellow powder.

Method c. (K)$_2$[^{99}TcCl$_6$] (37 mg, 0.10 mmol), AlCl$_3$ (134 mg, 1.00 mmol) and the corresponding arene (8 ml) were heated on 85°C for 4 h. H$_2$O (4 ml) was added to the dark brown hot solution and the aqueous phase was separated and filtered. The process was repeated with additional H$_2$O (2 × 2 ml) and to the combined aqueous solutions was added a solution of NH$_4$PF$_6$ (150 mg, 0.92 mmol) in H$_2$O (1 ml). The formed pale yellow precipitate was filtered, washed with H$_2$O (2 × 0.5 ml) and dried *in vacuo* to give [^{99}Tc(arene)$_2$](PF$_6$) as a pale yellow powder.

6.4.1.1 [^{99}Tc(benzene)$_2$](PF$_6$) ([1](PF$_6$))

Method a. Yield: 3 mg (8%).

IR (KBr): 3435 (*m*), 3095 (*w*), 2920 (*w*), 2851 (*w*), 1630 (*w*), 1441 (*m*), 1387 (*w*), 1156 (*w*), 1024 (*w*), 922 (*w*), 836 (*s*), 820 (*s*), 557 (*m*), 430 (*m*) cm^{-1}. ^{1}H NMR (400 MHz, CD$_3$CN): δ = 5.65 (*br. s*, 12 H, *C*H) ppm. ^{13}C NMR (125 MHz, CD$_3$CN): δ = 85.05-82.04 (*br. m*, ^{99}Tc-*C*H) ppm. ^{99}Tc NMR (90 MHz, CD$_3$CN): δ = -1859.71 (*s*, Δν$_{1/2}$ = 8 Hz) ppm. ^{99}Tc analysis calcd. for C$_{12}$H$_{12}$F$_6$PTc (%): 24.74; found: 24.23.

6.4.1.2 [^{99}Tc(toluene)$_2$](PF$_6$) ([2](PF$_6$))

Method a. Yield: 3 mg (7%).

Method b. Yield: 32 mg (74%).

Method c. Yield: 25 mg (60%).

IR (KBr): 3435 (*m*), 3090 (*w*), 2919 (*w*), 2851 (*w*), 1634 (*w*), 1574 (*w*), 1514 (*w*), 1455 (*m*), 1388 (*w*), 1043 (*w*), 835 (*s*), 777 (*w*), 558 (*m*), 441 (*w*), 410 (*w*) cm^{-1}. ^{1}H NMR (500 MHz, CD_3CN): δ = 5.63 (*br. s*, 4 H, CH), 5.55 (*br. s*, 4 H, CH), 5.50 (*br. s*, 2 H, CH), 2.12 (*br. s*, 6 H, CH_3) ppm. ^{13}C NMR (125 MHz, CD_3CN): δ = 87.26-81.43 (*br. m*, ^{99}Tc-*C*H, ^{99}Tc-^{t}*C*), 20.16 (*s*, *C*H_3) ppm. ^{99}Tc NMR (90 MHz, CD_3CN): δ = -1743.92 (*s*, $\Delta\nu_{1/2}$ = 26 Hz) ppm. ^{99}Tc analysis calcd. for $C_{14}H_{16}F_6PTc$ (%): 23.11; found: 22.71.

6.4.1.3 [^{99}Tc(mesitylene)$_2$](PF$_6$) ([3](PF$_6$))

Method a. Yield: 6 mg (12%).

Method b. Yield: 43 mg (90%).

IR (KBr): 3435 (*m*), 3086 (*w*), 2988 (*w*), 2967 (*w*), 2923 (*w*), 2847 (*w*), 1630 (*w*), 1540 (*w*), 1458 (*m*), 1384 (*w*), 1039 (*m*), 908 (*w*), 874 (*w*), 836 (*s*), 558 (*m*), 515 (*w*), 417 (*w*) cm^{-1}. ^{1}H NMR (400 MHz, CD_3CN): δ = 5.39 (*s*, 6 H, *C*H), 2.04 (*s*, 9 H, *C*H_3) ppm. ^{13}C NMR (125 MHz, CD_3CN): δ = 99.86-96.64 (*br. m*, ^{99}Tc-^{t}*C*), 87.94-84.70 (*br. m*, ^{99}Tc-*C*H), 19.33 (*s*, *C*H_3) ppm. ^{99}Tc NMR (90 MHz, CD_3CN): δ = -1532.37 (*s*, $\Delta\nu_{1/2}$ = 14 Hz) ppm. ^{99}Tc analysis calcd. for $C_{18}H_{24}F_6PTc$ (%): 20.44; found: 20.39.

6.4.1.4 [^{99}Tc(tetralin)$_2$](PF$_6$) ([4](PF$_6$))

Method a. Yield: 4 mg (8%).

Method b. Yield: 34 mg (69%).

Method c. Yield: 30 mg (63%).

IR (KBr): 3430 (*m*), 3086 (*w*), 2948 (*s*), 2869 (*m*), 1630 (*w*), 1484 (*w*), 1457 (*s*), 1435 (*s*), 1413 (*w*), 1357 (*w*), 1340 (*w*), 1282 (*w*), 1251 (*w*), 1152 (*w*), 1088 (*w*), 1071 (*w*), 1015 (*w*), 990 (*w*), 921 (*w*), 909 (*m*), 833 (*s*), 795 (*m*), 708 (*w*), 596 (*w*), 557 (*s*), 473 (*w*), 409 (*w*) cm^{-1}. ^{1}H NMR (500 MHz, CD_3CN): δ = 5.54 (*br. s*, 4 H, *C*H), 5.43 (*br. s*, 4 H, *C*H), 2.77-2.51 (*m*, *C*H_2), 1.73 (*br. s*, 4 H, *C*H_2) ppm. ^{13}C NMR (125 MHz, CD_3CN): δ = 103.12-100.16 (*br. m*, ^{99}Tc-^{t}C), 85.98-82.33 (*br. m*, ^{99}Tc-*C*H), 28.35 (*C*H_2), 22.96 (*C*H_2) ppm. ^{99}Tc NMR (90 MHz, CD_3CN): δ = -1585.94 (*s*, $\Delta\nu_{1/2}$ = 11 Hz) ppm. ^{99}Tc analysis calcd. for $C_{20}H_{24}F_6PTc$ (%): 19.47; found: 18.73.

6.4.1.5 [^{99}Tc(tetralin)(OHPhen)](PF$_6$) ([5](PF$_6$))

The isolated product [**4**](PF_6) contained considerable amounts of an unknown impurity. After crystallization of the product mixture, few crystals of different shapes could be identified, collected and analyzed. In this way the minor side product [^{99}Tc(tetralin)(OHPhen)]$^{+}$ (OHPhen = 1,2,3,4,5,6,7,8-octahydrophenanthrene) has been characterized by ^{99}Tc NMR, ESI-MS and X-ray diffraction. ^{99}Tc NMR (90 MHz, CD_3CN): δ = -1470.34 (*s*, $\Delta\nu_{1/2}$ = 21 Hz) ppm. ESI-MS (CD_3CN, pos. detection mode): m/z = 417.2 $[M]^{+}$.

6.4.2 (N^nBu_4)[$^{99}TcO(glyc)_2$] ((N^nBu_4)[8])

(N^nBu_4)[$^{99}TcOCl_4$] (24 mg, 0.05 mmol) was dissolved in THF (4 ml) and ethylene glycol (10 µl, 0.18 mmol) was added to the resulting green solution. Drop wise addition of NEt_3 (0.05 ml) led to a color change to purple and formation of a colorless precipitate, which was filtered off and washed with THF (1 ml). The purple solution of (N^nBu_4)[**8**] was directly used without further purification. If isolation of (Li)[**8**] is desired, a suspension of LiCl (2 mg, 0.05 mmol) in THF (1 ml) is added and the resulting pale purple solid is filtered off, washed with THF (1 ml) and dried in vacuo. The obtained crude product still contains small amounts of salts such as LiCl and $HNEt_3Cl$. Due to the high moisture sensitivity of (Li)[**8**] no further purification steps have been performed. Consequently, no yield (%) and technetium content can be given. Yield: 13 mg. IR (KBr): 3415 (*s*), 2935 (*m*), 2874 (*m*), 2857 (*m*), 2739 (*w*), 2678 (*w*), 2492 (*w*), 2025 (*w*), 1639 (*s*), 1618(*s*), 1457 (*w*), 1384 (*w*), 1338 (*w*), 1240 (*w*), 1170 (*w*), 1064 (*m*), 1046 (*s*), 1014 (*w*), 992 (*s*), 985 (*s*), 964 (*w*), 912 (*s*), 889 (*w*) cm^{-1}. ^1H NMR (200 MHz, DMF-D_7): δ = 4.22-4.00 (*m*, 8 H, *C*H_2) ppm. ^{13}C NMR (75 MHz, DMF-D_7): δ = 76.81 (*C*H_2) ppm. Crystals suitable for X-ray diffraction analysis were grown by slow evaporation of a DMF solution.

6.4.3 [$^{99}TcO_2$(L1)$_4$](PF_6) ([9](PF_6))

(**L1**-H)(PF_6) (61 mg, 0.25 mmol) was suspended in THF (2 ml) and a solution of KO^tBu (29 mg, 0.26 mmol) in THF (2 ml) was added. After 30 min, the resulting orange solution was added drop wise to a purple solution of (N^nBu_4)[**8**] (0.05 mmol) in THF (5 ml). The obtained yellow solution was stirred at 25°C for 1 h. The reaction mixture was filtered and the volume of the filtrate was reduced to 1 ml under reduced pressure. The solution was stored at -10°C for 1 week, which led to formation of orange crystals, suitable for X-ray diffraction analysis. Removal of the supernatant from the crystals and drying of the crystals *in vacuo* yielded analytically pure [**9**](PF_6)·glyc-H_2. Yield: 20 mg (55%). IR (KBr): 3549 (*m*), 3471 (*s*), 3415 (*s*), 3238 (*m*), 3179 (*w*), 3147 (*m*), 3035 (*w*), 2992 (*w*), 2948 (*m*), 2875 (*w*), 2816 (*w*), 1638 (*m*), 1618 (*m*), 1577 (*w*), 1460 (*m*), 1401 (*m*), 1384 (*w*), 1319 (*w*), 1231 (*m*), 1175 (*w*), 1136 (*w*), 1085 (*w*), 1022 (*w*), 878 (*m*), 844 (*s*), 780 (*s*), 733 (*m*), 688 (*m*), 662 (*w*), 625 (*w*), 558 (*m*), 470 (*w*) cm^{-1}. ^1H NMR (500 MHz, DMSO-D_6): δ = 7.34 (*s*, 8 H, Im-H), 3.42 (*s*, 24 H, *C*H_3) ppm. ^{13}C NMR (125 MHz, DMSO-D_6): δ = 122.68 (Im-C), 36.07 (*C*H_3) ppm. ^{99}Tc analysis calcd. for $C_{22}H_{38}F_6N_8O_4PTc$ (%): 13.70; found: 12.07.

6.4.4 [$^{99}TcO_2$(L2)$_2$](X) ([10](X), X = Cl, PF_6)

Method a. (**L2**-H_2)(PF_6)$_2$ (49 mg, 0.10 mmol) was suspended in THF (2 ml) and the suspension was cooled to -78°C. A solution of ^{n}BuLi (2.5 M in hexane, 0.09 ml, 0.22 mmol) was added and the solution was slowly warmed up to 25°C under stirring for 3 h. The orange solution was added drop wise to a solution of (N^nBu_4)[**8**] (0.05 mmol), resulting in a color change to yellow and formation of a precipitate. After 19 h, the solution was filtered, and the yellow solid was dissolved in DMF (1.5 ml) and filtered. The solvent was evaporated under a gentle stream of N_2 and the yellow residue was

dissolved in CH_3CN (2 ml). Addition of Et_2O (2 ml) and filtration gave [**10**](Cl) as a yellow solid, which was washed with Et_2O (2 ml) and dried *in vacuo*. Crystals suitable for X-ray diffraction analysis were obtained by storage of a DMF solution at -10°C. Yield: 8 mg (30%). IR (KBr): 3419 (*s*), 3239 (*s*), 3158 (*m*), 3086 (*m*), 3018 (*m*), 2954 (*m*), 2925 (*m*), 2857 (*m*), 1641 (*m*), 1566 (*w*), 1467 (*m*), 1403 (*m*), 1343 (*w*), 1314 (*m*), 1249 (*m*), 1221 (*m*), 1180 (*m*), 1108 (*w*), 1084 (*w*), 1056 (*w*), 1016 (*w*), 807 (*m*), 765 (*s*), 736 (*s*), 697 (*m*), 686 (*m*), 608 (*w*), 557 (*w*), 462 (*w*) cm^{-1}. ^1H NMR (500 MHz, DMSO-D_6): δ = 7.71 (*s*, 4 H, Im-H), 7.43 (s, 4 H, Im-H), 6.92 (*d*, $^2J(HH)$ = 12.5 Hz, 2 H, CH_2), 6.44 (*d*, $^2J(HH)$ = 12.5 Hz, 2 H, CH_2), 3.68 (*s*, 12 H, CH_3), ppm. ^{13}C NMR (125 MHz, DMSO-D_6): δ = 121.56 (Im-C), 62.00 (CH_2), 36.16 (CH_3) ppm.

Method b. A solution of (N^nBu_4)[**8**] (0.10 mmol) in THF (3 ml) was evaporated under reduced pressure and the purple residue dissolved in CH_2Cl_2 (10 ml). NEt_3 (1 ml) and [**L2**-H_2]$(PF_6)_2$ (95 mg, 0.20 mmol) were added and the solution was heated on 45°C for 5 h. After cooling to 25°C, the resulting green solution was filtered to give a pale yellow crude solid and a green filtrate. The solid was dissolved in a 2:1 acetone/H_2O solution (3 ml). Slow evaporation of the acetone resulted in formation of [**10**]$(PF_6)\cdot H_2O$ as yellow crystals (suitable for X-ray diffraction analysis) that were filtered, washed with H_2O (0.5 ml) and dried *in vacuo*. By concentration of the green filtrate and storage at -10°C a second batch of crystalline [**10**]$(PF_6)\cdot H_2O$ could be isolated. Yield: 29 mg (44%). IR (KBr): 847 cm^{-1} (*s*, $(PF_6)^-$). UV-Vis (CH_3CN): 298 (12598 $M^{-1}cm^{-1}$), 426 (143 $M^{-1}cm^{-1}$) nm. ^{99}Tc analysis calcd. for $C_{18}H_{26}F_6N_8O_3PTc$ (%): 15.32; found: 14.52. Other analytical data in accordance to [**10**](Cl).

6.4.5 [$^{99}TcO_2$(L3)$_2$](PF_6) ([11](PF_6))

Method a. (**L3**-H_2)$(PF_6)_2$ (50 mg, 0.10 mmol) was suspended in THF (6 ml) and the reaction mixture was cooled to -78°C. A solution of ^{n}BuLi (1.6 M in hexane, 0.13 ml, 0.21 mmol) was added and the solution was slowly warmed up to 25°C under stirring for 3 h. The colorless solution was added drop wise to a solution of (N^nBu_4)[**8**] (0.05 mmol), resulting in a color change to yellow and formation of a precipitate. After 2 h, the suspension was filtered and the yellow solid washed with THF (1 ml) and H_2O (1 ml). The crude solid was dissolved in a 1:1 acetone/H_2O solution (2 ml). Slow evaporation of the acetone resulted in formation of [**11**]$(PF_6)\cdot 2.6H_2O$ as yellow crystals which were analyzed by X-ray diffraction. The crystals were filtered, washed with H_2O (1 ml) and $CHCl_3$ (1 ml) and dried *in vacuo*. Yield: 12 mg (33%). IR (KBr): 3550 (*s*), 3413 (*s*), 3476 (*s*), 3236 (*m*), 2980 (*w*), 2942 (*w*), 2032 (*w*), 1638 (*m*), 1617 (*s*), 1564 (*w*), 1467 (*w*), 1420 (*w*), 1384 (*m*), 1342 (*w*), 1323 (*w*), 1263 (*w*), 1214 (*w*), 1175 (*w*), 1107 (*w*), 1059 (*w*), 1032 (*w*), 961 (*w*), 899 (*m*), 849 (*s*), 813 (*w*), 794 (*w*), 765 (*s*), 694 (*w*), 620 (*w*), 558 (*w*), 479 (*w*), 419 (*w*), 410 (*w*) cm^{-1}. ^1H NMR (400 MHz, CD_3CN): δ = 7.55 (*s*, 4 H, Im-H), 7.30 (*s*, 4 H, Im-H), 7.15 (*d*, $^2J(HH)$ = 12.4 Hz, 2 H, CH_2 bridge), 6.14 (*d*, $^2J(HH)$ = 12.4 Hz, 2 H, CH_2 bridge), 4.29-4.09 (*m*, 8 H, CH_3-CH_2-N), 1.21 (*t*, $^3J(HH)$ = 7.2 Hz, 12 H, CH_3-CH_2-N) ppm. ^{13}C NMR (100 MHz, CD_3CN): δ = 121.92 (Im-C), 119.42 (Im-C), 62.78 (CH_2 bridge), 44.77 (CH_3-CH_2-N), 15.07 (CH_3-CH_3-N) ppm. ^{99}Tc analysis calcd. for $C_{22}H_{37.20}F_6N_8O_{4.60}PTc$

(%): 13.54; found: 12.60.

Method b. A solution of (N^nBu_4)[**8**] (0.10 mmol) in THF was evaporated under reduced pressure and the purple residue dissolved in CH_2Cl_2 (5 ml). NEt_3 (1 ml) and (**L3**-H_2)(PF_6)$_2$ (97 mg, 0.20 mmol) were added and the solution was heated on 45°C for 3 h. After cooling to 25°C, the resulting green solution was filtered to give a pale yellow crude solid and a green filtrate. The crude was washed with cold CH_3CN (3x 0.5 ml) and the obtained yellow solid dried *in vacuo*. Yield: 18 mg (26%). ^{99}Tc analysis calcd. for $C_{22}H_{32}F_6N_8O_2PTc$ (%): 14.46; found 13.19. Other analytical data in accordance with **method a**.

6.4.6 [^{99}TcOCl(L2)$_2$](PF_6)$_2$ ([12](PF_6)$_2$)

Method a. A solution of (N^nBu_4)[**8**] (0.1 mmol) in THF was evaporated under reduced pressure and the purple residue dissolved in CH_2Cl_2 (10 ml). NEt_3 (0.5 ml) and (**L2**-H_2)(PF_6)$_2$ (92 mg, 0.2 mmol) were added and the solution was heated on 45°C for 7 h. After cooling to 25°C, the resulting green solution was filtered to give a pale yellow crude solid and a green filtrate. The crude was washed with CH_2Cl_2 (2 ml) and acetone (2 × 1 ml). The yellow residue was dissolved in a 1:1 acetone/H_2O solution (2 ml). Addition of HCl (1 M, 100 µl) resulted in a color change to green. Slow evaporation of the acetone yielded [**12**](PF_6)$_2$ as green crystals (suitable for X-ray diffraction analysis) that were filtered, washed with Et_2O (1 ml) and dried *in vacuo*. Yield (based on (N^nBu_4)[**8**]): 23 mg (28%). IR (KBr): 3454 (*s*), 3177 (*s*), 3151 (*m*), 3119 (*m*), 2964 (*w*), 2920 (*w*), 2853 (*w*), 2064 (*w*), 1635 (*s*), 1569 (*m*), 1475 (*m*), 1406 (*w*), 1384 (*w*), 1354(*w*), 1322 (*w*), 1259 (*w*), 1228 (*m*), 1192 (*w*), 1185 (*w*), 1121 (*w*), 1087 (*w*), 1065 (*w*), 985 (*m*), 839 (*s*), 755 (*m*), 741 (*m*) cm^{-1}. ^{1}H NMR (500 MHz, DMSO-D_6): δ = 8.14 (*s*, 2 H, Im-H), 8.09 (*s*, 2 H, Im-H), 8.03 (*s*, 2 H, Im-H), 7.80 (*s*, 2 H, Im-H), 7.05 (*d*, ^{2}*J(HH)* = 14.0 Hz, 1 H, *C*H_2), 6.92 (*dd*, ^{2}*J(HH)* = 13.5 Hz, 2 H, *C*H_2), 6.54 (*d*, ^{2}*J(HH)* = 14.0 Hz, 1 H, *C*H_2), 3.88 (*s*, 6 H, *C*H_3), 3.55 (*s*, 6 H, *C*H_3) ppm. ^{13}C NMR (125 MHz, DMSO-D_6): δ = 125.60 (Im-C), 125.22 (Im-C), 125.15 (Im-C), 123.36 (Im-C), 64.16 (CH_2), 62.38 (*C*H_2), 38.15 (*C*H_3), 36.81 (*C*H_3) ppm. UV-Vis (CH_3CN): 370 (5701 $M^{-1}cm^{-1}$), 608 (108 $M^{-1}cm^{-1}$) nm. ^{99}Tc analysis calcd. for $C_{18}H_{24}ClF_{12}N_8OP_2Tc$ (%): 12.49; found: 12.29.

Method b. A solution of (N^nBu_4)[**8**] (0.1 mmol) in THF was evaporated under reduced pressure and the purple residue dissolved in DMF (5 ml). NEt_3 (1 ml) and (**L2**-H_2)(PF_6)$_2$ (100 mg, 0.21 mmol) were added and the solution was heated on 70°C for 7.5 h. Afterwards it was stirred at 25°C for 15.5 h. The solvent of the resulting green solution was evaporated with a stream of N_2 and the oily red residue washed with Et_2O (3 × 2 ml). The red residue was dissolved in a 2:1 acetone/H_2O solution (2 ml) and 1 M HCl (0.5 ml) was added. Slow evaporation of the acetone yielded [**12**](PF_6)$_2$ as green crystals (suitable for X-ray diffraction analysis) that were filtered, washed with Et_2O (2 ml) and dried *in vacuo*. Yield (based on (N^nBu_4)[**8**]): 32 mg (41%). Other analytical data in accordance with **method a**.

6.4.7 [^{99}TcO(OMe)(L2)$_2$](PF$_6$)$_2$ ([13](PF$_6$)$_2$)

[^{99}TcOCl(**L2**)$_2$](PF$_6$)$_2$ (23 mg, 0.03 mmol) was dissolved in a mixture of MeOH (0.5 ml), NEt$_3$ (0.5 ml) and CH$_3$CN (2 ml). The resulting green solution was stirred for 5 h and the solvents of the resulting purple solution were evaporated with a stream of N$_2$. The remaining purple solid was dissolved in CH$_3$CN (0.5 ml) and Et$_2$O (5 ml) was added to precipitate the product. The purple solid was filtered off, washed with Et$_2$O (2 × 1 ml) and CH$_2$Cl$_2$ (2 × 1 ml) and dried *in vacuo* to give analytically pure [**13**](PF$_6$)$_2$ as a pale purple solid. Yield: 22 mg (97%). IR (KBr): 3553 (*s*), 3480 (*s*), 3414 (*s*), 3236 (*m*), 3176 (*m*), 3149 (*m*), 2962 (*w*), 2917 (*w*), 2810 (*w*), 2033 (*w*), 1638 (*m*), 1617 (*m*), 1570 (*w*), 1474 (*m*), 1406 (*w*), 1351 (*w*), 1318 (*w*), 1253 (*w*), 1226 (*w*), 1184 (*w*), 1112 (*m*), 1062 (*w*), 929 (*m*), 837 (*s*), 805 (*w*), 737 (*m*), 694 (*w*), 683 (*w*), 616 (*m*), 558 (*m*), 485 (*m*) cm^{-1}. ^{1}H NMR (500 MHz, DMF-D$_7$): δ = 8.17 (*d*, ^{3}*J(HH)* = 1.5 Hz, 2 H, *C*H), 8.14 (*d*, ^{3}*J(HH)* = 2.0 Hz, 2 H, *C*H), 7.93 (*d*, ^{3}*J(HH)* = 2.0 Hz, 2 H, *C*H), 7.84 (*d*, ^{3}*J(HH)* = 1.5 Hz, 2 H, *C*H), 7.14 (*d*, ^{2}*J(HH)* = 13.5 Hz, 1 H, *C*H$_2$), 7.03 (*d*, ^{2}*J(HH)* = 13.0 Hz, 1 H, *C*H$_2$), 6.81 (*d*, ^{2}*J(HH)* = 13.5 Hz, 1 H, *C*H$_2$), 6.55 (*d*, ^{2}*J(HH)* = 13.0 Hz, 1 H, *C*H$_2$), 4.00 (*s*, 6 H, N*C*H$_3$), 3.78 (*s*, 6 H, N*C*H$_3$), 2.70 (*s*, 3 H, O*C*H$_3$) ppm. ^{13}C NMR (125 MHz, DMF-D$_7$): δ = 123.92 (*C*H), 123.79 (*C*H), 123.75 (*C*H), 123.29 (*C*H), 63.23 (*C*H$_2$), 62.71 (*C*H$_2$), 58.04 (O*C*H$_3$), 37.13 (N*C*H$_3$), 36.18 (N*C*H$_3$) ppm. UV-Vis (CH$_3$CN): 301 (5831 M^{-1}cm^{-1}), 529 (72 M^{-1}cm^{-1}) nm. ^{99}Tc analysis calcd. for C$_{19}$H$_{27}$F$_{12}$N$_8$O$_2$P$_2$Tc (%): 12.56; found: 10.43.

6.4.8 [^{99}TcO(NCS)(L2)$_2$](PF$_6$)$_2$ ([14](PF$_6$)$_2$)

[^{99}TcO$_2$(**L2**)$_2$](PF$_6$) (35 mg, 0.06 mmol) was dissolved in a mixture of acetone (3 ml) and H$_2$O (1 ml). HCl (1 M, 100 µl) was added and to the resulting green solution was added a solution of NaSCN (145 mg, 1.79 mmol) and NH$_4$PF$_6$ (91 mg, 0.56 mmol) in H$_2$O (0.5 ml). The resulting dark solution was slowly reduced in volume over 20 h, following by filtration of dark green crystals. The crystals were washed with Et$_2$O (2 × 2 ml) and dried *in vacuo* to give analytically pure [**14**](PF$_6$)$_2$·2acetone. Yield: 30 mg (58%). IR (KBr): 3546 (*s*), 3473 (*s*), 3414 (*s*), 3238 (*m*), 3174 (*m*), 2957 (*w*), 2913 (*w*), 2845 (*w*), 2358 (*w*), 2067 (*s*), 2028 (*m*), 1706 (*w*), 1638 (*m*), 1618 (*m*), 1568 (*w*), 1479 (*m*), 1448 (*w*), 1405 (*w*), 1367 (*w*), 1353 (*w*), 1321 (*w*), 1257 (*w*), 1226 (*w*), 1188 (*w*), 1120 (*w*), 1088 (*w*), 1062 (*w*), 997 (*m*), 984 (*m*), 844 (*s*), 749 (*m*), 677 (*w*), 614 (*w*), 558 (*m*), 466 (*w*) cm^{-1}. ^{1}H NMR (500 MHz, DMF-D$_7$): δ = 8.37 (*d*, ^{3}*J(HH)* = 1.5 Hz, 2 H, *C*HNCH$_2$), 8.33 (*d*, ^{3}*J(HH)* = 1.5 Hz, 2 H, *C*HNCH$_2$), 8.23 (*d*, ^{3}*J(HH)* = 1.5 Hz, 2 H, *C*HNCH$_3$), 8.00 (*d*, ^{3}*J(HH)* = 1.5 Hz, 2 H, *C*HNCH$_3$), 7.43 (*d*, ^{2}*J(HH)* = 14.0 Hz, 1 H, *C*H$_2$), 7.36 (*d*, ^{2}*J(HH)* = 14.0 Hz, 1 H, *C*H$_2$), 6.89 (*d*, ^{2}*J(HH)* = 14.0 Hz, 1 H, *C*H$_2$), 6.51 (*d*, ^{2}*J(HH)* = 14.0 Hz, 1 H, *C*H$_2$), 4.09 (*s*, 6 H, *C*H$_3$), 3.71 (*s*, 6 H, *C*H$_3$) ppm. ^{13}C NMR (125 MHz, DMF-D$_7$): δ = 144.54 (N*C*S), 127.16 (*C*HNCH$_3$), 126.95 (*C*HNCH$_2$/*C*HNCH$_3$), 125.34 (*C*HNCH$_2$), 66.13 (*C*H$_2$), 64.32 (*C*H$_2$), 39.41 (*C*H$_3$), 37.64 (*C*H$_3$) ppm. UV-Vis (CH$_3$CN): 406 (8995 M^{-1}cm^{-1}), 606 (148 M^{-1}cm^{-1}) nm. ^{99}Tc analysis calcd. for C$_{25}$H$_{36}$F$_{12}$N$_9$O$_3$P$_2$STc (%): 10.63; found: 10.73.

6.4.9 [^{99}TcCl$_2$(L2)$_2$](PF$_6$)$_2$ ([24](PF$_6$)$_2$)

[^{99}TcO$_2$(**L2**)$_2$](PF$_6$) (16 mg, 0.03 mmol) was dissolved in DMF (3 ml) and a solution of $SnCl_2$ (47 mg, 0.25 mmol) in DMF (1 ml) was added. The solution was stirred for 1 h and the solvent was subsequently evaporated with a stream of N_2. The solid was suspended in THF (2 ml), filtered and washed with THF (2 × 1 ml). The remaining solid was dissolved in CH_3CN (4 ml) and filtered, followed by evaporation of the solvent under reduced pressure and drying of the red solid *in vacuo*. It has to be noted that the described purification procedure does not remove all Sn impurities. Consequently, no yield (%) and technetium content can be given. A trace amount of single crystalline [**24**](PF$_6$)$_2$·THF suitable for X-ray diffraction analysis was obtained by slow crystallization from a CH_3CN solution containing traces of THF. Yield: 15 mg. IR (KBr): 3430 (*s*), 3266 (*m*), 3167 (*m*), 3133 (*m*), 3035 (*m*), 2962 (*m*), 2924 (*m*), 2851 (*w*), 1652 (*s*), 1566 (*w*), 1468 (*m*), 1431 (*m*), 1404 (*w*), 1355 (*m*), 1318 (*w*), 1251 (*w*), 1225 (*w*), 1173 (*w*), 1124 (*w*), 1062 (*w*), 1015 (*w*), 989 (*w*), 955 (*w*), 845 (*s*), 741 (*w*), 695 (*w*), 622 (*w*), 558 (*m*), 417 (*w*) cm^{-1}.

6.4.10 [^{99}TcO$_2$(L2)(L4)]$_2$(PF$_6$)$_2$ ([18](PF$_6$)$_2$)

(N^{n}Bu$_4$)[^{99}TcOCl$_4$] (50 mg, 0.10 mmol) was dissolved in THF (2 ml) and ethylene glycol (22 µl, 0.39 mmol) was added to the resulting green solution. Addition of NEt_3 (100 µl) led to a color change to purple and the formation of a colorless precipitate, which was filtered off and washed with THF (2 × 1 ml). The purple solution of (N^{n}Bu$_4$)[**8**] was evaporated and the purple residue was dissolved in CH_2Cl_2 (10 ml). (**L2**-H$_2$)(PF$_6$)$_2$ (47 mg, 0.10 mmol), **L4** (15 mg, 0.10 mmol) and NEt_3 (1 ml) were added and the purple suspension was heated on 45°C for 4 h and then stirred at 25°C for 16 h. The formed orange solid was filtered off, washed with CH_2Cl_2 (2 × 2ml) and dried *in vacuo*. The orange crude was dissolved in CH_3CN (3 ml) and filtered. Addition of Et_2O (9 ml) to the orange solution led to precipitation of analytically pure [**18**](PF$_6$)$_2$, which was filtered off, washed with Et_2O (2 × 2 ml) and dried *in vacuo*. Yield: 40 mg (67%). IR (KBr): 3549 (*s*), 3475 (*s*), 3414 (*s*), 3237 (*m*), 3163 (*w*), 3128 (*m*), 3026 (*w*), 2961 (*w*), 2920 (*w*), 2856 (*w*), 2032 (*w*), 1638 (*m*), 1617 (*m*), 1568 (*w*), 1554 (*w*), 1527 (*w*), 1513 (*m*), 1466 (*m*), 1433 (*w*), 1405 (*w*), 1348 (*w*), 1317 (*w*), 1280 (*w*), 1252 (*w*), 1224 (*m*), 1185 (*m*), 1107 (*m*), 1091 (*m*), 1034 (*w*), 995 (*w*), 940 (*w*), 848 (*s*), 837 (*s*), 809 (*m*), 795 (*s*), 764 (*m*), 726 (*m*), 692 (*w*), 677 (*w*), 662 (*w*), 654 (*w*), 616 (*w*), 558 (*m*), 482 (*w*), 459 (*w*), 404 (*w*) cm^{-1}. ^{1}H NMR (500 MHz, CD_3CN): δ = 8.33 (*s*, 4 H, NC*H*N), 7.49 (*d*, ^{3}*J(HH)* = 1.5 Hz, 4 H, $CH_3NCHCHNCH_2$), 7.36 (s, 4 H, ^{99}TcNC*H*CHNCH$_2$), 7.31 (*s*, 4 H, ^{99}TcNCHC*H*NCH$_2$), 7.18 (*d*, ^{3}*J(HH)* = 1.5 Hz, 4 H, CH_3NC*H*CHNCH$_2$), 6.74 (*br. s*, 2 H, CH_3NCHCHNC*H*$_2$), 6.21 (*br. s*, 2 H, CH_3NCHCHNC*H*$_2$), 6.12 (*s*, 4 H, ^{99}TcNCHCHNC*H*$_2$), 3.65 (*s*, 12 H, *C*H$_3$) ppm. ^{13}C NMR (125 MHz, CD_3CN): δ = 137.04 (N*C*HN), 128.93 (^{99}TcN*C*H), 124.13 (CH_3N*C*H), 123.03 ($CH_3NCHCHNCH_2$), 120.90 (^{99}TcNCH*C*HNCH$_2$), 64.34 (CH_3NCHCHN*C*H$_2$), 57.72 (^{99}TcNCHCHN*C*H$_2$), 37.59 (*C*H$_3$) ppm. ^{99}Tc analysis calcd. for $C_{32}H_{40}F_{12}N_{16}O_4P_2Tc_2$ (%): 16.49; found: 16.10.

6.4.11 [^{99}TcOCl$_3$(L2)] ([20])

[^{99}TcO$_2$(**L2**)(**L4**)]$_2$(PF$_6$)$_2$ (32 mg, 0.08 mmol) was dissolved in H$_2$O (2 ml) and HCl was added (1 M, 0.5 ml). The green solution was stirred for 2.5 h at 25°C and then loaded on a C$_{18}$ SepPak column and washed with HCl (1 M, 1 ml). [**20**] was eluted from the column using H$_2$O. The resulting purple solution was acidified with HCl (conc., 50 µl) and the solvent was evaporated with a stream of N$_2$. Drying *in vacuo* gave analytically pure green [**20**]. Yield: 10 mg (47%). IR (KBr): 3547 (*s*), 3475 (*s*), 3413 (*s*), 3236 (*m*), 3159 (*m*), 3128 (*m*), 3108 (*m*), 2986 (*m*), 1638 (*m*), 1618 (*s*), 1568 (*w*), 1489 (*w*), 1454 (*w*), 1400 (*w*), 1385 (*m*), 1344 (*w*), 1315 (*w*), 1263 (*w*), 1220 (*w*), 1197 (*m*), 1122 (*w*), 1079 (*w*), 1007 (*s*), 964 (*w*), 842 (*w*), 807 (*w*), 763 (*m*), 736 (*m*), 665 (*m*), 654 (*m*), 618 (*m*), 558 (*w*), 481 (*w*), 463 (*m*), 443 (*w*), 404 (*w*) cm^{-1}. ^{1}H NMR (400 MHz, DMSO-D$_6$): δ = 7.86 (*s*, 4 H, *C*H), 6.81 (*d*, ^{2}*J(HH)* = 12.6 Hz, 1 H, *C*H$_2$), 6.21 (*d*, ^{2}*J(HH)* = 12.6 Hz, 1 H, *C*H$_2$), 4.27 (*s*, 6 H, *C*H$_3$) ppm. ^{13}C NMR (100 MHz, DMSO-D$_6$): 126.49 (*C*H), 124.55 (*C*H), 63.29 (*C*H$_2$), 38.72 (*C*H$_3$) ppm. ^{99}Tc analysis calcd. for C$_9$H$_{12}$Cl$_3$N$_4$OTc (%): 24.90; found: 24.45.

6.4.12 [^{99}TcO$_2$(L2)(bipy)](PF$_6$) ([22](PF$_6$))

[^{99}TcOCl$_3$(**L2**)] (20 mg, 0.05 mmol) was dissolved in H$_2$O (3 ml). A solution of bipy (8 mg, 0.05 mmol) in acetone (3 ml) was added, followed by the addition of NEt$_3$ (50 µl, 0.36 mmol). The solution was stirred for 24 h at 25°C and then the solvent was reduced with a stream of N$_2$ until 1 ml was left. Addition of a solution of NH$_4$PF$_6$ (8 mg, 0.05 mmol) in H$_2$O (0.5 ml) led to the precipitation of a yellow solid, which was filtered off and dried *in vacuo* to give analytically pure [**22**](PF$_6$). X-ray quality single-crystalline [**22**](PF$_6$)·H$_2$O was obtained by slow crystallization from a 1:1 acetone/H$_2$O solution. Yield: 20 mg (66%). IR (KBr): 3547 (*m*), 3402 (*s*), 3349 (*s*), 3257 (*m*), 3174 (*w*), 3146 (*w*), 3116 (*w*), 3029 (*w*), 2962 (*w*) 2219 (*w*), 1656 (*w*), 1638 (*w*), 1618 (*m*), 1599 (*m*), 1571 (*w*), 1473 (*m*), 1446 (*m*), 1404 (*w*), 1385 (*w*), 1316 (*w*), 1220 (*m*), 1187 (*w*), 1157 (*w*), 1026 (*w*), 876 (*m*), 856 (*s*), 836 (*s*), 793 (*s*), 762 (*s*), 738 (*m*), 697 (*w*), 654 (*w*), 616 (*w*), 557 (*m*), 454 (*w*) cm^{-1}. ^{1}H NMR (500 MHz, acetone-D$_6$): δ = 9.35 (*s*, 2 H, bipy-*C*H), 8.87-8.76 (*m*, 2 H, bipy-*C*H), 8.47-8.37 (*m*, 2 H, bipy-*C*H), 7.97-7.79 (*m*, 2 H, bipy-*C*H), 7.85 (*s*, 2 H, Im-*C*H), 7.56 (*s*, 2 H, Im-*C*H), 7.13 (*d*, ^{2}*J(HH)* = 12.5 Hz, 1 H, *C*H$_2$), 6.57 (*d*, 12.5 Hz, 1 H, *C*H$_2$), 4.17 (*s*, 6 H, *C*H$_3$) ppm. ^{13}C NMR (125 MHz, acetone-D$_6$): 155.85 (bipy-*C*), 154.09 (bipy-*C*H), 141.30 (bipy-*C*H), 127.54 (bipy-*C*H), 124.84 (bipy-*C*H), 124.41 (Im-*C*H), 123.81 (Im-*C*H), 64.94 (*C*H$_2$), 37.80 (*C*H$_3$) ppm. ^{99}Tc analysis calcd. for C$_{19}$H$_{22}$F$_6$N$_6$O$_3$PTc (%): 15.80; found: 15.02.

6.4.13 [^{99}Tc(L5)(CO)$_3$] ([28])

To a colorless suspension of (**L5**-H$_3$)(OTf)$_2$ (65 mg, 0.10 mmol) in THF (3 ml), a solution of LDA (1 M in hexane/THF 7:1, 0.30 ml, 0.30 mmol) was added with a syringe. The solution turned orange clear and after 5 min of stirring a colorless precipitate formed. The suspension was stirred at 25°C for 16 h. To a suspension of (NEt$_4$)$_2$[^{99}TcCl$_3$(CO)$_3$] (54 mg, 0.10 mmol) in THF (2 ml), a solution of AgOTf (77 mg, 0.30 mmol) in THF (3 ml) was added. A grey precipitate formed (AgCl), which was

filtered off over celite after stirring for 16 h and washed with THF (3 × 0.5 ml). To the pale yellow clear filtrate was added the solution containing the NHC and the resulting yellow solution was stirred for 7 h. The solvent was evaporated with a stream of N_2 and the resulting crude solid was washed with Et_2O and toluene. The orange crude solid was partially dissolved in CH_2Cl_2 (4 ml), filtered and the sticky orange solid washed with CH_2Cl_2 (2 × 1 ml). The resulting orange CH_2Cl_2 solution was left standing at ambient conditions to give an orange sticky solid. Slow evaporation from CH_3CN (1.5 ml) did not result in the formation of crystals. The orange sticky solid was partially dissolved in EtOH (2 ml) and an insoluble colorless solid was filtered off, washed with EtOH (0.5 ml), dried *in vacuo* and then dissolved in CH_3CN (2 ml). The solution containing [**28**] was left standing at ambient conditions to give a trace amount of crystals suitable for X-ray diffraction analysis. ^{99}Tc-NMR (90 MHz, THF): δ = -764.42 (*br. s*, $\Delta\nu_{1/2}$ = 0.43 kHz) ppm.

6.4.14 Preparation of $[^{99m}TcO_2(L2)_2]^+$ ($[^{99m}$**10**$]^+$)

Method a. A stock solution of trihexyl(tetradecyl)phosphonium bromide (35.2 mM in methyl *tert*-butyl ether, 0.1 ml, 3.52 µmol) was added to a capped vial. Under constant rotation of the vial, the solvent was evaporated by a stream of N_2. $[^{99m}TcO_4]^-$ eluate (1 ml) was added to this vial and it was gently shaken for 10 min. The aqueous solution was removed and a solution of ethylene glycol (10 µl, 0.18 mmol) in EtOH (0.3 ml) was added, followed by addition of a stock solution of $SnCl_2 \cdot 2H_2O$ (2.2 mM in EtOH, 0.2 ml, 0.44 µmol). The resulting solution was evaporated and dried with a stream of N_2 for 45 min. A solution of (**L2**-H_2)$(PF_6)_2$ (10 mg, 0.02 mmol) and NEt_3 (0.2 ml) in CH_3CN (0.5 ml) was added to the residue and the resulting solution was heated on 70°C for 50 min. The solvent of the reaction was evaporated with a stream of N_2, the residue suspended in saline solution (1 ml) and the solution filtered. At this point, formation of $[^{99m}$**10**$]^+$ was confirmed with HPLC analysis. Finally, the aqueous solution containing the product was loaded on a C_{18} SepPak column, washed with saline solution and eluted using MeOH. Yield: 13% (radiochemical purity: 42%). HPLC retention time (TFA method): 15.8 min.

Method b. A stock solution of trihexyl(tetradecyl)phosphonium bromide (35.2 mM in methyl *tert*-butyl ether, 0.1 ml, 3.52 µmol) dissolved in methyl *tert*-butyl ether (0.1 ml) was added to a capped vial. Under constant rotation of the vial, the solvent was evaporated by a stream of N_2. $[^{99m}TcO_4]^-$ eluate (1 ml) was added to this vial and it was gently shaken for 10 min. The aqueous solution was removed and the residue dried with a stream of N_2 for 1 h. A solution of ethylene glycol (10 µl, 0.18 mmol) in CH_3CN (0.2 ml) was added, followed by addition of a $SnCl_2$ stock solution (65.9 mM in 1:1 CH_3CN/DMF, 20 µl, 1.3 µmol) dissolved in CH_3CN (0.2 ml). The resulting solution was stirred for 15 min and then a solution of $[Ag_2($**L2**$)_2](PF_6)_2$ (9 mg, 0.01 mmol) in CH_3CN (0.2 ml) was added. The resulting suspension was heated on 65°C for 1 h. The solvent of the reaction was evaporated with a stream of N_2, the residue suspended in saline solution (1 ml) and the suspension centrifuged for 10 min. At this point, formation of $[^{99m}$**10**$]^+$ was confirmed with HPLC analysis. Finally, the aqueous solution containing the product was loaded on a C_{18} SepPak column, washed with saline solution and

eluted using MeOH. Yield: 5% (radiochemical purity: 72%). Other analytical data in accordance with **method a**. For stability measurements, the solvent of this solution was evaporated and the residue dissolved in saline solution. The pH of the solution was adjusted using NaOH (1 M) or HCl (1 M).

Method c. Performed analogous to **method b** using four times the amount of $SnCl_2$ stock solution (65.9 mM in 1:1 CH_3CN/DMF, 80 µl, 5.3 µmol). Yield: 2% (radiochemical purity: 28%). Other analytical data in accordance with **method a**. For stability measurements, the solvent of the solution obtained after the purification with a C_{18} SepPak column was evaporated and the residue dissolved in saline solution. The pH of the solution was adjusted using NaOH (1 M) or HCl (1 M).

6.5 Rhenium Complexes

6.5.1 $(N^nBu_4)[ReO(glyc)_2]$ ((N^nBu_4)[15])

$(N^nBu_4)[ReOCl_4]$ (30 mg, 0.05 mmol) was dissolved in THF (2 ml) and ethylene glycol (11 µl, 0.20 mmol) was added to the resulting green solution. Drop wise addition of NEt_3 (0.05 ml) led to the formation of a colorless precipitate, which was filtered off and washed with THF (1 ml). The solution of (N^nBu_4)[**15**] was directly used without further purification. Because of the sensitivity of (N^nBu_4)[**15**] to ambient conditions, no analysis was performed. Crystals suitable for X-ray diffraction analysis were grown by slow evaporation of a THF solution inside the glovebox.

6.5.2 *Trans*-$[ReO_2(L2)_2](PF_6)$ (*Trans*-[16](PF_6))

To a solution of $(N^nBu_4)[ReOCl_4]$ (60 mg, 0.10 mmol) and ethylene glycol (22 µl, 0.39 mmol) in THF (2 ml) was drop wise added NEt_3 (0.1 ml) and the resulting suspension was stirred for 15 min. The formed colorless solid was filtered off and washed with THF (2 × 1 ml). Evaporation of the solvent gave an oily residue, which was dissolved in CH_2Cl_2 (10 ml), followed by addition of (**L2**-H_2)$(PF_6)_2$ (97 mg, 0.21 mmol) and NEt_3 (1 ml). The resulting purple suspension was heated on 45°C for 22 h. The solvent was evaporated with a stream of N_2 and the residue was suspended in MeOH (10 ml) and stirred for 30 min. NaOH (1 M in H_2O, 0.3 ml, 0.30 mmol) was added and the solution was stirred for 16 h. The solvent of the orange solution was evaporated with a stream of N_2 and the residue was suspended in CH_2Cl_2 (6 ml). The yellow precipitate was filtered off, washed with CH_2Cl_2 (2 × 2 ml), H_2O (2 × 1 ml) and THF (2 × 1 ml) and dried *in vacuo* to give analytically pure *trans*-[**16**](PF_6). Yield: 34 mg (47%). IR (neat): 3436 (*w*), 3342 (*w*), 3245 (*w*), 3025 (*w*), 2955 (*w*), 2156 (*w*), 1647 (*w*), 1569 (*w*), 1472 (*m*), 1432 (*w*), 1409 (*w*), 1389 (*w*), 1362 (*w*), 1350 (*w*), 1315 (*m*), 1252 (*w*), 1222 (*m*), 1186 (*m*), 1107 (*w*), 1088 (*w*), 1060 (*w*), 1021 (*w*), 915 (*w*), 834 (*s*), 734 (*s*), 704 (*m*) cm^{-1}. HR-ESI-MS (CH_3CN, pos. detection mode): m/z = 286.08277 $[M+H]^{2+}$, 571.15710 $[M]^+$. ^1H NMR (400 MHz, CD_3CN): δ = 7.51 (*d*, $^3J(HH)$ = 2.0 Hz, 4 H, *C*H), 7.27 (*d*, $^2J(HH)$ = 12.4 Hz, 2 H, *C*H_2), 7.23 (*d*, $^3J(HH)$ = 2.0 Hz, 4 H, *C*H), 6.15 (*d*, $^2J(HH)$ = 12.4 Hz, 2 H,), 3.74 (*s*, 12 H, *C*H_3) ppm. ^{13}C NMR (100 MHz, CD_3CN): δ = 176.83 (Re-*C*), 121.54 (*C*H), 121.27 (*C*H), 63.94 (*C*H_2), 36.51 (*C*H_3) ppm. Anal. calcd. for $C_{18}H_{26}F_6N_8O_3PRe$ (%): C, 29.47; H, 3.57; N, 15.27. Found: C, 29.07; H, 3.68; N, 13.84.

6.5.3 $[ReOCl(L2)_2](PF_6)_2$ ([17]$(PF_6)_2$)

To a solution of *trans*-$[ReO_2$(**L2**$)_2](PF_6)$ (36 mg, 0.05 mmol) in 3:1 acetone/H_2O (4 ml) was added HCl (1 M, 200 µl). The resulting orange suspension was slowly allowed to evaporate at ambient conditions. Analysis of the resulting crude product with NMR showed a spectrum of higher order, indicating formation of more than one product, which could not be separated. As a consequence, no analyses are given. Crystals suitable for X-ray diffraction analysis of *trans*-[**17**]$(PF_6)_2$ were obtained by slow crystallization of the purple crude product from DMF.

6.5.4 $[ReO_2(L2)(L4)]_2(PF_6)_2$ ([19](PF$_6$)$_2$)

To a solution of (N^nBu_4)[$ReOCl_4$] (59 mg, 0.10 mmol) and ethylene glycol (22 µl, 0.39 mmol) in THF (2 ml) was drop wise added NEt_3 (0.1 ml) and the resulting suspension was stirred for 15 min. The formed colorless solid was filtered off and washed with THF (2 × 1 ml). Evaporation of the solvent gave an oily residue, which was dissolved in CH_2Cl_2 (10 ml), followed by addition of (**L2**-H_2)(PF_6)$_2$ (49 mg, 0.10 mmol) and **L4** (15 mg, 0.10 mmol) and NEt_3 (1 ml). The resulting purple suspension was heated on 45°C for 22 h. The solvent was evaporated with a stream of N_2 and the residue was suspended in MeOH (10 ml) and stirred for 30 min. The orange precipitate was filtered off, washed with MeOH (2 × 1 ml) and dried *in vacuo* to give analytically pure [**19**](PF$_6$)$_2$. Single crystals of [**19**](PF$_6$)$_2$·2H_2O suitable for X-ray diffraction analysis were obtained by recrystallization from MeOH. Yield: 60 mg (86%). IR (neat): 3143 (*w*), 3111 (*w*), 3029 (*w*), 1707 (*m*), 1569 (*w*), 1534 (*w*), 1510 (*w*), 1471 (*w*), 1436 (*w*), 1404 (*w*), 1361 (*m*), 1315 (*w*), 1287 (*w*), 1224 (*m*), 1189 (*w*), 1093 (*m*), 1029 (*w*), 947 (*w*), 834 (*s*), 782 (*s*), 761 (*s*), 731 (*s*) cm^{-1}. HR-ESI-MS (CH_3CN, pos. detection mode): m/z = 395.05143 $[C_9H_{12}N_4O_2Re]^+$, 543.12672 $[M]^{2+}$. ^{1}H NMR (500 MHz, CD_3CN): δ = 8.29 (*s*, 4 H, N*C*HN), 7.49 (*d*, ^{3}*J(HH)* = 1.5 Hz, 4 H, $CH_3NCHCHNCH_2$), 7.39 (*s*, 4 H, $ReNCHCHNCH_2$), 7.34 (*s*, 4 H, $ReNCHCHNCH_2$), 7.12 (*d*, ^{3}*J(HH)* = 1.5 Hz, 4 H, $CH_3NCHCHNCH_2$), 6.98 (*br. s*, 2 H, $CH_3NCHCHNCH_2$), 6.22 (*br. s*, 2 H, $CH_3NCHCHNCH_2$), 6.15 (*s*, 4 H, $ReNCHCHNCH_2$), 3.72 (*s*, 12 H, CH_3) ppm. ^{13}C NMR (125 MHz, CD_3CN): δ = 168.34 (Re-*C*), 135.54 (N*C*HN), 127.65 (ReN*C*H), 122.88 (CH_3NCH), 121.56 ($CH_3NCHCHNCH_2$), 119.75 ($ReNCHCHNCH_2$), 64.87 ($CH_3NCHCHNCH_2$), 56.69 ($ReNCHCHNCH_2$), 36.47 (CH_3) ppm. Anal. calcd. for $C_{32}H_{44}F_{12}N_{16}O_6P_2Re_2$ (%): C, 27.24; H, 3.14; N, 15.88. Found: C, 27.66; H, 3.14; N, 15.60.

6.5.5 $[ReOCl_3(L2)]$ ([21])

[ReO_2(**L2**)(**L4**)]$_2$(PF_6)$_2$ (44 mg, 0.03 mmol) was dissolved in H_2O (2 ml) and HCl (1 M, 1 ml) was added. The resulting blue solution was stirred for 3 h at 25°C and then loaded on a C_{18} SepPak column and washed with HCl (1 M, 1 ml). [**21**] was eluted from the column using H_2O. The resulting orange-red solution was acidified with HCl (conc., 50 µl) and the solvent was evaporated with a stream of N_2. Drying *in vacuo* gave analytically pure blue [**21**]. Yield: 20 mg (64%). IR (neat): 3413 (*s*), 3128 (*m*), 2986 (*m*), 1636 (*m*), 1618 (*s*), 1568 (*w*), 1454 (*w*), 1400 (*w*), 1385 (*m*), 1344 (*w*), 1315 (*w*), 1263 (*w*), 1220 (*w*), 1197 (*m*), 1119 (*w*), 1007 (*s*), 962 (*w*), 842 (*w*), 807 (*w*), 762 (*m*), 736 (*m*) cm^{-1}. ^{1}H NMR (400 MHz, DMSO-D_6): δ = 7.75 (*d*, ^{3}*J(HH)* = 1.8 Hz, 2 H, *C*H), 7.72 (*d*, ^{3}*J(HH)* = 1.8 Hz, 2 H, *C*H), 6.70 (*d*, ^{2}*J(HH)* = 13.1 Hz, 1 H, CH_2), 6.59 (*d*, ^{2}*J(HH)* = 13.1 Hz, 1 H, CH_2), 4.28 (*s*, 6 H, CH_3) ppm. ^{13}C NMR (100 MHz, DMSO-D_6): 145.67 (Re-*C*), 126.01 (*C*H), 124.24 (*C*H), 63.36 (CH_2), 38.07 (CH_3) ppm. Anal. calcd. for $C_9H_{12}N_4OCl_3Re$ (%): C, 22.30; H, 2.49; N, 11.56. Found: C, 22.38; H, 3.57; N, 9.03.

6.5.6 [ReO_2(L2)(bipy)](PF_6) ([23](PF_6))

[$ReOCl_3$(**L2**)] (20 mg, 0.04 mmol) was dissolved in DMSO (3 ml) and the resulting blue solution was stirred for 15 min. Bipy (8 mg, 0.05 mmol) was added, followed by the addition of NEt_3 (50 µl, 0.36 mmol). The resulting red solution was stirred for 16 h at 25°C and afterwards the solvent was removed with a stream of N_2. The orange residue was dissolved in H_2O (1 ml) and a solution of NH_4PF_6 (7 mg, 0.04 mmol) in H_2O (0.5 ml) was added, leading to precipitation of an orange solid. The orange solid was filtered off and dried *in vacuo* to give [**23**](PF_6). Yield: 6 mg (20%).

6.5.7 [Re(L5)$(CO)_3$] ([25])

Method a. To a colorless suspension of (**L5**-H_3)$(OTf)_2$ (66 mg, 0.10 mmol) in THF (4 ml), a solution of LDA (1 M in hexane/THF 7:1, 0.34 ml, 0.34 mmol) was added with a syringe. The solution turned orange clear. After 5 min of stirring a colorless precipitate formed. The suspension was stirred at 25°C for 8 h. A suspension of $(NEt_4)_2[ReBr_3(CO)_3]$ (77 mg, 0.10 mmol) in THF (2 ml) was added and the mixture was stirred for 20 h at 25°C. Filtration over celite of the orange suspension and evaporation of the orange filtrate *in vacuo* gave a crude product. The orange solid was chromatographed (4 g SiO_2, hexane/EtOAc 10:1) to give [**25**] as a colorless solid after evaporation of the solvent *in vacuo*. Yield: 5 mg (8%). IR (neat): 2924 (*w*), 2855 (*w*), 1988 (*s*), 1867 (*s*), 1714 (*w*), 1552 (*w*), 1441 (*m*), 1358 (*m*), 1294 (*m*), 1178 (*m*), 1074 (*w*), 1024 (*m*), 880 (*w*), 795 (*m*) cm^{-1}. HR-EI-MS (CH_3CN, pos. detection mode): m/z = 546.13428 $[M\text{-}2CO]^+$ (100%), 574.12949 $[M\text{-}CO]^+$ (44%), 602.12420 $[M]^+$ (36%). ^1H NMR (400 MHz, DMF-D_7): δ = 8.01-7.99 (*m*, 2 H, Ph-H), 7.64-7.60 (*m*, 2 H, Ph-H), 7.57-7.53 (*m*, 1 H, Ph-H), 7.20 (*d*, $^3J(HH)$ = 2.0 Hz, 3 H, Im-H), 7.00 (*d*, $^3J(HH)$ = 1.6 Hz, 3 H, Im-H), 3.88 (*s*, 9 H, CH_3) ppm. ^{13}C NMR (100 MHz, DMF-D_7): δ = 199.28 (*C*O), 177.09 (Re-*C*), 134.83 (Ph-*C*), 128.12 (Ph-*C*), 127.71 (Ph-*C*), 122.69 (Im-*C*), 120.79 (Im-*C*), 37.49 (CH_3) ppm. Anal. calcd. for $C_{21}H_{20}B_1N_6O_3Re$ (%): C, 41.94; H, 3.35; N, 13.97. Found: C, 41.72; H, 3.32; N, 13.89.

Method b. To a colorless suspension of (**L5**-H_3)$(OTf)_2$ (66 mg, 0.10 mmol) in THF (4 ml), a solution of LDA (1 M in hexane/THF 7:1, 0.34 ml, 0.34 mmol) was added with a syringe. The solution turned orange clear and after 5 min of stirring a colorless precipitate formed. The suspension was stirred at 25°C for 8 h. To a suspension of $(NEt_4)_2[ReBr_3(CO)_3]$ (77 mg, 0.10 mmol) in THF (2 ml), a solution of AgOTf (77 mg, 0.30 mmol) in THF (2 ml) was added. A grey precipitate formed, which was filtered off over celite after stirring for 15 min and washed with THF (3 × 0.5 ml). The clear colorless filtrate was added to the formed carbene and the solution was stirred for 20 h. Filtration of the orange suspension containing colorless solid over celite and evaporation of the orange filtrate *in vacuo* gave a crude product as an orange solid. The orange solid was chromatographed (4 g SiO_2, hexane/EtOAc 10:1) to give [**25**] as a colorless solid after evaporation of the solvent *in vacuo*. Yield: 6 mg (10%). Analytical data in accordance with **method a**.

Method c. Performed analogous to **method b** using 5 eq. of LDA for the formation of the NHC. The crude product was chromatographed (4 g SiO_2, hexane/EtOAc 10:1) to give [**25**] as a colorless solid

after evaporation of the solvent *in vacuo*. Yield: 5 mg (8%). Analytical data in accordance with **method a**.

Method d. To a colorless suspension of (**L5**-H_3)$(OTf)_2$ (66 mg, 0.10 mmol) in THF (4 ml), a solution of LDA (1 M in hexane/THF 7:1, 0.34 ml, 0.34 mmol) was added with a syringe. The solution turned orange clear and after 5 min of stirring a colorless precipitate formed. The suspension was stirred at 25°C for 8 h. To a suspension of $(NEt_4)_2[ReBr_3(CO)_3]$ (77 mg, 0.10 mmol) in THF (2 ml), a solution of AgOTf (77 mg, 0.30 mmol) in THF (2 ml) was added. A grey precipitate formed, which was filtered off over celite after stirring for 15 min and washed with THF (3 × 0.5 ml). The clear colorless filtrate was added to the formed carbene at –78°C and the solution was allowed to slowly warm up to 25°C and was stirred for 20 h. Filtration of the orange suspension containing colorless solid over celite and evaporation of the orange filtrate *in vacuo* gave a crude product as an orange solid. The orange solid was chromatographed (4 g SiO_2, hexane/EtOAc 10:1) to give [**25**] as a colorless solid after evaporation of the solvent *in vacuo*. Yield: 6 mg (10%). Analytical data in accordance with **method a**.

6.5.8 [ReBr(L6-H)$(CO)_3$](Br) ([27](Br))

(**L6**-H_3)$(Br)_3$ (53 mg, 0.01 mmol) was suspended in THF (4 ml) and a solution of LDA (1 M in hexane/THF 7:1, 0.30 ml, 0.30 mmol) was added. The suspension was stirred for 30 min. To the resulting orange clear solution was added a suspension of $(NEt_4)_2[ReBr_3(CO)_3]$ (75 mg, 0.01 mmol) in THF (3 ml). The suspension was stirred for 20 h before it was filtered. The solvent of the filtrate was fully evaporated under reduced pressure and the resulting orange solid was washed with toluene (3 ml) and Et_2O (3 × 2 ml). The remaining orange solid was dissolved in CH_3CN (2 ml) and precipitated by addition of Et_2O (4 ml). Filtration of the suspension afforded an orange solid, which was washed with Et_2O and dried *in vacuo*. Crystals suitable for X-ray diffraction analysis were obtained by slow evaporation of an CH_3CN solution. IR (neat): 3369 (*m*), 3097 (*w*), 2978 (*w*), 1998 (*s*), 1858 (*s*), 1578 (*w*), 1455 (*m*), 1403 (*m*), 1238 (*w*), 1222 (*w*), 1168 (*m*), 1132 (*w*), 1076 (*w*), 1024 (*w*), 886 (*w*), 740 (*m*) cm^{-1}. ESI-MS (CH_3CN, pos. detection mode): m/z = 663.3 $[M]^+$.

6.5.9 [Re(L6)$(CO)_3$](PF_6) ([26](PF_6))

(**L6**-H_3)$(PF_6)_3$ (77 mg, 0.10 mmol) was suspended in THF (2 ml) and a solution of LDA (1 M in hexane/THF 7:1, 0.30 ml, 0.30 mmol) was added. The resulting orange solution was stirred for 30 min. $(NEt_4)_2[ReBr_3(CO)_3]$ (76 mg, 0.10 mmol) was suspended in THF (2 ml) and a solution of AgOTf (79 mg, 0.31 mmol) in THF (4 ml) was added. A grey precipitate formed (AgBr), which was filtered off over celite after stirring for 30 min and washed with THF (2 × 1 ml). The clear colorless filtrate was added to the solution containing the NHC using THF (2 × 1 ml) for transfer. The resulting solution was stirred for 3 h. An equal volume of Et_2O (12 ml) was added to the solution, which led to precipitation of a pale yellow solid. The solid was filtered off, washed with Et_2O (2 × 1 ml) and the solvent of the filtrate was removed with a gentle stream of N_2. The resulting solid was suspended in H_2O (2 ml) for 15 min, followed by filtration, washing with H_2O (2 ml) and drying *in vacuo*.

Yield: 20 mg (28%). IR (neat): 2963 (*w*), 2924 (*w*), 2853 (*w*), 2009 (*s*), 1870 (*s*), 1581 (*w*), 1467 (*m*), 1443 (*m*), 1401 (*w*), 1358 (*w*), 1258 (*s*), 1167 (*m*), 1092 (*m*), 1030 (*s*), 911 (*w*), 843 (*s*), 801 (*s*), 736 (*m*) cm^{-1}. HR-ESI-MS (CH_3CN, pos. detection mode): m/z = 555.15085 $[M\text{-}CO]^+$, 583.14545 $[M]^+$. ^1H NMR (500 MHz, DMF-D_7): δ = 7.63 (*d*, $^3J(HH)$ = 2.0 Hz, 3 H, Im-H), 7.51 (*d*, $^3J(HH)$ = 1.5 Hz, 3 H, Im-H), 4.02 (*s*, 9 H, CH_3), 3.96 (*d*, $^2J(HH)$ = 16.0 Hz, 3 H, CH_2), 3.51 (*d*, $^2J(HH)$ = 16.2 Hz, 3 H, CH_2), 1.57 (*s*, 3 H, CH_3) ppm. ^{13}C NMR (125 MHz, DMF-D_7): δ = 202.01 (*C*O), 200.71 (*C*O), 169.90 (N*C*N), 125.79 (*C*H), 124.70 (*C*H), 56.66 (CH_2), 41.21 (NCH_3), 38.20 (CCH_3), 34.49 (CCH_3) ppm. Anal. calcd. for $C_{20}H_{24}F_6N_6O_3PRe$ (%): C, 33.01; H, 3.32; N, 11.55. Found: C, 28.30; H, 3.55; N, 4.31.

7 Acknowledgements

I would like to sincerely thank Prof. Dr. Roger Alberto for giving me the opportunity to work in his group and his constant support for this thesis. In addition to this, I would like to thank Prof. Dr. Roger Alberto for the possibility to attend the RheManTec II and TERACHEM 2014, which have been great and interesting experiences. Further I would like to sincerely thank Dr. Henrik Braband for the interesting projects and for the incredible daily support he provided during this PhD thesis, but also during the Master thesis before. I would like to thank Prof. Dr. Cristina Nevado for the helpful discussions and remarks that she provided as a member of my PhD committee.

I would like to thank Dr. Paul Schmutz and Giuseppe Meola for their work concerning the synthesis of $[Re(arene)_2]^+$ complexes, which contributed to the synthesis of $[^{99(m)}Tc(arene)_2]^+$ complexes described in this thesis. Furthermore, the enthusiastic and diligent work of several students is greatly acknowledged. Jonathan Halter studied the electrochemistry of the $[^{99}Tc(arene)_2]^+$ complexes described in this thesis during his Master thesis.[62] Dustin Bornemann worked on the synthesis of $[MO_2(\mathbf{L2})(\mathbf{L4})]_2^{2+}$ (M = Re, ^{99}Tc) and the corresponding derivatives during his practical research course. Mauro Schilling and Simona Müller worked on the synthesis of $[ReO_2(\mathbf{L2})_2]^+$ during a project in the practical course in inorganic chemistry. David Schmid worked on the synthesis of $[Re(\mathbf{L5})(CO)_3]$ during a project in the practical course in inorganic chemistry.

I would like to thank several people for their help concerning measurements and analyses. The help of PD Dr. Bernhard Spingler concerning X-ray diffraction analysis of single crystals is greatly appreciated, especially since many of the compounds in this thesis had systematic disorders. Concerning NMR analyses I would like to sincerely thank Dr. Thomas Fox for his great service and his help with NMR analyses in general. I would also like to thank the whole MS-service team for their great service. Furthermore I would like to thank Heinz Spring for elemental analyses and Hanspeter Stalder and his team for technical support.

I would like to thank the University of Zurich and the Graduate School of Chemical and Molecular Sciences in general for their administrative work. Financial support from the Swiss National Science Foundation (200021_140665/1) is greatly acknowledged.

I thank all the members of the Alberto group and the Department of Chemistry at University of Zurich for a friendly and productive working atmosphere. I would also like to sincerely thank my family and friends for their continuous support during my time at University of Zurich. In particular I want to thank my mother Prisca Benz and my two sisters Alexandra and Janine Benz. Last, but certainly not least, I would like to thank my wonderful girlfriend Nicole Kovacs for everything she has done for me during the past years.

8 Appendix

8.1 Crystallographic Details

Table 38: Data collection and structure calculation details.

	[^{99}Tc(benzene)$_2$](PF$_6$) [**1**](PF$_6$)	[^{99}Tc(toluene)$_2$](PF$_6$) [**2**](PF$_6$)	[^{99}Tc(mesitylene)$_2$](PF$_6$) [**3**](PF$_6$)
Dataset	MEB051213	MEB211113	MEB101213
Machine	Xcalibur	Xcalibur	Xcalibur
Formula	$C_{12}H_{12}F_6PTc$	$C_{14}H_{16}F_6PTc$	$C_{18}H_{24}F_6PTc$
M_w [g/mol]	400.19	428.25	484.35
Space group	$P2_1/c$	$P2_1/n$	$P2_12_12_1$
a [Å]	13.8831(7)	7.7559(8)	9.2697(5)
b [Å]	9.8745(5)	11.0030(8)	13.0695(16)
c [Å]	9.7190(6)	8.9353(8)	15.815(6)
α [°]	90	90	90
β [°]	94.232(5)	98.474(9)	90
γ [°]	90	90	90
μ [mm^{-1}]	1.260	1.116	0.890
Z	4	2	4
V [Å^3]	1328.74(13)	754.20(12)	1916.0(8)
ρ_{calc} / [g/cm^3]	1.995	1.881	1.676
R1[a, c]	0.0337	0.0408	0.0372
wR2[b, c]	0.0809	0.0876	0.0717
CCDC	1017765	1017766	1017767

[a] R1 = $|F_o - F_c|/|F_o|$; [b] wR2 = $[w(F_o^2 - F_c^2)^2/(wF_o^2)]^{1/2}$; [c] I > 2 sig(I)

	[^{99}Tc(tetralin)$_2$](PF$_6$) [**4**](PF$_6$)	[^{99}Tc(tetralin)(OHPhen)](PF$_6$)[d] [**5**](PF$_6$)	[Al(DMF)$_6$][^{99}TcCl$_6$](Cl)· DMF
Dataset	MEB120214	MEB300414	MEB310114
Machine	Xcalibur	Xcalibur	Xcalibur
Formula	$C_{20}H_{24}F_6PTc$	$C_{24}H_{30}F_6PTc$	$C_{21}H_{49}AlCl_7N_7O_7Tc$
M_w [g/mol]	508.37	562.47	885.81
Space group	$P2_1/n$	$Pna2_1$	$P2_1$
a [Å]	8.7563(6)	13.8364(3)	8.8724(3)
b [Å]	12.1899(11)	13.9152(5)	23.5963(7)
c [Å]	9.5187(15)	11.4229(5)	9.6318(3)
α [°]	90	90	90
β [°]	108.089(10)	90	96.888(3)
γ [°]	90	90	90
μ [mm^{-1}]	0.887	-	0.892
Z	2	-	2
V [Å^3]	965.80(19)	-	2001.92(11)
ρ_{calc} / [g/cm^3]	1.745	-	1.468
R1[a, c]	0.0464	-	0.0305
wR2[b, c]	0.1336	-	0.0651
CCDC	1017768	-	1017769

[a] R1 = $|F_o - F_c|/|F_o|$; [b] wR2 = $[w(F_o^2 - F_c^2)^2/(wF_o^2)]^{1/2}$; [c] I > 2 sig(I); [d] structure was not fully refined.

	$[^{99}Tc(benzene)_2][^{99}TcCl_5(OH_2)]$ [**1**][$^{99}TcCl_5(OH_2)$]	$(Li)[^{99}TcO(glyc)_2]\cdot DMF$ (Li)[**8**]·DMF
Dataset	MEB270514o	MEB051112
Machine	SuperNova	Stoe IPDS
Formula	$C_{12}H_{14}Cl_5OTc_2$	$C_7H_{15}LiNO_6Tc$
M_w [g/mol]	549.51	315.14
Space group	Pnma	$P2_1/c$
a [Å]	6.31521(12)	7.2092(7)
b [Å]	10.59360(19)	9.1767(6)
c [Å]	24.5539(4)	17.0327(16)
α [°]	90	90
β [°]	90	101.810(8)
γ [°]	90	90
μ [mm^{-1}]	21.086	1.315
Z	4	4
V [$Å^3$]	1642.68(5)	1102.97(17)
ρ_{calc} / [g/cm^3]	2.214	1.892
R1[a, c]	0.0365	0.0316
wR2[b, c]	0.0919	0.0861
CCDC	-	960942

[a] R1 = $|F_o - F_c|/|F_o|$; [b] wR2 = $[w(F_o^2 - F_c^2)^2/(wF_o^2)]^{1/2}$; [c] I > 2 sig(I)

	(**L2**-H_2)$_2$[$^{99}TcO(glyc)_2$]$(PF_6)_3$ (**L2**-H_2)$_2$[**8**]$(PF_6)_3$	[$^{99}TcO_2$(**L1**)$_4$](PF_6)·glyc-H_2 [**9**](PF_6)·glyc-H_2
Dataset	MEB100113	MEB210612
Machine	Stoe IPDS	Xcalibur
Formula	$C_{22}H_{36}F_{18}N_8O_5P_3Tc$	$C_{22}H_{38}F_6N_8O_4PTc$
M_w [g/mol]	1026.47	722.56
Space group	Pmmn	C2/c
a [Å]	12.350(3)	19.7741(15)
b [Å]	22.423(9)	10.2626(5)
c [Å]	6.907(13)	15.8185(11)
α [°]	90	90
β [°]	90	107.132(9)
γ [°]	90	90
μ [mm^{-1}]	0.635	0.600
Z	2	4
V [$Å^3$]	1913(4)	3067.7(4)
ρ_{calc} / [g/cm^3]	1.781	1.562
R1[a, c]	0.0607	0.0524
wR2[b, c]	0.1569	0.1238
CCDC	-	960943

[a] R1 = $|F_o - F_c|/|F_o|$; [b] wR2 = $[w(F_o^2 - F_c^2)^2/(wF_o^2)]^{1/2}$; [c] I > 2 sig(I)

	$[^{99}TcO_2(\mathbf{L2})_2](Cl)\cdot 2H_2O$ $[\mathbf{10}](Cl)\cdot 2H_2O$	$[^{99}TcO_2(\mathbf{L2})_2](PF_6)\cdot H_2O$ $[\mathbf{10}](PF_6)\cdot H_2O$	$[^{99}TcO_2(\mathbf{L3})_2](PF_6)\cdot 2.6H_2O$ $[\mathbf{11}](PF_6)\cdot 2.6H_2O$
Dataset	MEB130712	MEB031212	MEB150313
Machine	Stoe IPDS	Stoe IPDS	Xcalibur
Formula	$C_{18}H_{28}ClN_8O_4Tc$	$C_{18}H_{26}F_6N_8O_3PTc$	$C_{22}H_{37.20}F_6N_8O_{4.60}PTc$
M_w [g/mol]	554.92	646.42	731.35
Space group	C2/c	P2/c	$P\bar{1}$
a [Å]	12.8951(7)	9.7640(10)	8.6324(2)
b [Å]	10.5795(4)	8.2135(6)	9.6076(3)
c [Å]	18.3405(9)	15.6688(15)	18.6505(5)
α [°]	90	90	86.566(2)
β [°]	106.496(4)	90.694(8)	80.875(2)
γ [°]	90	90	88.031(2)
μ [mm^{-1}]	0.752	0.719	0.606
Z	4	2	2
V [$Å^3$]	2399.1(2)	1256.5(2)	1524.01(7)
ρ_{calc} / [g/cm^3]	1.534	1.706	1.592
R1[a, c]	0.0328	0.0496	0.0490
wR2[b, c]	0.0888	0.1201	0.1139
CCDC	960944	960945	960947

[a] $R1 = |F_o - F_c|/|F_o|$; [b] $wR2 = [w(F_o^2 - F_c^2)^2/(wF_o^2)]^{1/2}$; [c] I > 2 sig(I)

	$[^{99}TcOCl(\mathbf{L2})_2](PF_6)_2$ $[\mathbf{12}](PF_6)_2$	$[^{99}TcO(OMe)(\mathbf{L2})_2](PF_6)_2\cdot 0.67H_2O$ $[\mathbf{13}](PF_6)_2\cdot 0.67H_2O$
Dataset	MEB300613	MEB291014o
Machine	Xcalibur	SuperNova
Formula	$C_{18}H_{24}ClF_{12}N_8OP_2Tc$	$C_{19}H_{28.33}F_{12}N_8O_{2.67}P_2Tc$
M_w [g/mol]	792.82	800.47
Space group	P1	$P\bar{1}$
a [Å]	10.9223(5)	12.1331(4)
b [Å]	11.4201(4)	12.1336(3)
c [Å]	12.9602(6)	15.5009(4)
α [°]	83.541(3)	92.686(2)
β [°]	87.715(4)	91.644(2)
γ [°]	62.811(4)	104.659(2)
μ [mm^{-1}]	0.819	6.080
Z	2	3
V [$Å^3$]	1428.70(10)	2203.37(10)
ρ_{calc} / [g/cm^3]	1.841	1.807
R1[a, c]	0.0447	0.0744
wR2[b, c]	0.0945	0.1787
CCDC	960946	-

[a] $R1 = |F_o - F_c|/|F_o|$; [b] $wR2 = [w(F_o^2 - F_c^2)^2/(wF_o^2)]^{1/2}$; [c] I > 2 sig(I)

	$[^{99}TcO(NCS)(\mathbf{L2})_2](PF_6)_{1.4}(SCN)_{0.6}\cdot H_2O$ $[\mathbf{14}](PF_6)_{1.4}(SCN)_{0.6}\cdot H_2O$	$[^{99}TcO(NCS)(\mathbf{L2})_2](PF_6)_2\cdot 2acetone$ $[\mathbf{14}](PF_6)_2\cdot 2acetone$
Dataset	MEB131014o	MEB290115
Machine	SuperNova	Xcalibur
Formula	$C_{19.6}H_{26}F_{8.4}N_{9.6}O_2P_{1.4}S_{1.6}Tc$	$C_{25}H_{36}F_{12}N_9O_3P_2STc$
M_w [g/mol]	781.33	931.61
Space group	C2/c	P1
a [Å]	26.4347(4)	9.2280(5)
b [Å]	11.22620(17)	9.8789(5)
c [Å]	19.8367(3)	11.5941(7)
α [°]	90	114.809(6)
β [°]	90.5606(14)	101.083(5)
γ [°]	90	95.855(5)
μ [mm^{-1}]	6.610	0.637
Z	8	1
V [$Å^3$]	5886.48(16)	921.50(9)
ρ_{calc} / [g/cm^3]	1.762	1.677
R1[a, c]	0.0273	0.0381
wR2[b, c]	0.0682	0.0864
CCDC	-	-

[a] R1 = $|F_o - F_c|/|F_o|$; [b] wR2 = $[w(F_o^2 - F_c^2)^2/(wF_o^2)]^{1/2}$; [c] I > 2 sig(I)

	$(N^nBu_4)[ReO(glyc)_2]$ $(N^nBu_4)[\mathbf{15}]$	*cis*-$[ReO_2(\mathbf{L2})_2](Cl)\cdot H_2O$ *cis*-$[\mathbf{16}](Cl)\cdot H_2O$
Dataset	MEB101212	MEB111213
Machine	Stoe IPDS	Xcalibur
Formula	$C_{20}H_{44}NO_5Re$	$C_{18}H_{26}ClN_8O_3Re$
M_w [g/mol]	564.77	624.11
Space group	$P\bar{1}$	$C2_1$
a [Å]	9.6128(10)	12.8965(8)
b [Å]	9.5589(10)	10.6052(10)
c [Å]	14.0719(16)	9.0913(6)
α [°]	87.519(9)	90
β [°]	81.874(9)	106.535(7)
γ [°]	71.367(8)	90
μ [mm^{-1}]	5.036	5.244
Z	2	2
V [$Å^3$]	1213.0(2)	1192.00(16)
ρ_{calc} / [g/cm^3]	1.546	1.739
R1[a, c]	0.0443	0.0335
wR2[b, c]	0.1053	0.0917
CCDC	-	-

[a] R1 = $|F_o - F_c|/|F_o|$; [b] wR2 = $[w(F_o^2 - F_c^2)^2/(wF_o^2)]^{1/2}$; [c] I > 2 sig(I)

	trans-$[ReO_2(\mathbf{L2})_2](PF_6)\cdot 2H_2O\cdot 3THF\cdot LiPF_6$ *trans*-$[\mathbf{16}](PF_6)\cdot 2H_2O\cdot 3THF\cdot LiPF_6$	*trans*-$[ReOCl(\mathbf{L2})_2](PF_6)_2$ *trans*-$[\mathbf{17}](PF_6)_2$
Dataset	MEB100114	MEB170114o
Machine	Xcalibur	SuperNova
Formula	$C_{30}H_{52}F_{12}LiN_8O_7P_2Re$	$C_{18}H_{24}ClF_{12}N_8OP_2Re$
M_w [g/mol]	1119.86	880.02
Space group	I2/a	$P2_1$
a [Å]	19.820(6)	13.48030(6)
b [Å]	12.8130(18)	21.68710(10)
c [Å]	19.006(19)	20.03310(8)
α [°]	90	90
β [°]	115.98(7)	92.0546(4)
γ [°]	90	90
μ [mm^{-1}]	2.978	11.003
Z	4	8
V [$Å^3$]	4339(5)	5852.88(4)
ρ_{calc} / [g/cm^3]	1.714	1.997
R1[a, c]	0.0409	0.0420
wR2[b, c]	0.1010	0.0975
CCDC	-	-

[a] R1 = $|F_o - F_c|/|F_o|$; [b] wR2 = $[w(F_o^2 - F_c^2)^2/(wF_o^2)]^{1/2}$; [c] I > 2 sig(I)

	$[^{99}TcO_2(\mathbf{L2})(\mathbf{L4})]_2(PF_6)_{1.5}(Cl)_{0.5}\cdot 3DMF\cdot 4H_2O$ $[\mathbf{18}](PF_6)_{1.5}(Cl)_{0.5}\cdot 3DMF\cdot 4H_2O$	$[^{99}TcO_2(\mathbf{L2})(\mathbf{L4})]_2(PF_6)_2\cdot 2H_2O$ $[\mathbf{18}](PF_6)_2\cdot 2H_2O$
Dataset	MEB071013	MEB221014
Machine	Xcalibur	Xcalibur
Formula	$C_{41}H_{69}Cl_{0.50}F_9N_{19}O_{11}P_{1.50}Tc_2$	$C_{32}H_{44}F_{12}N_{16}O_6P_2Tc_2$
M_w [g/mol]	1437.29	1236.73
Space group	C2/c	$P2_1/n$
a [Å]	24.5120(8)	12.594(6)
b [Å]	8.4534(2)	7.9045(10)
c [Å]	30.4565(9)	23.382(12)
α [°]	90	90
β [°]	107.835(3)	99.69(6)
γ [°]	90	90
μ [mm^{-1}]	0.619	0.783
Z	4	2
V [$Å^3$]	6007.6(3)	2294.5(16)
ρ_{calc} / [g/cm^3]	1.587	1.787
R1[a, c]	0.0507	0.0459
wR2[b, c]	0.1280	0.1090
CCDC	-	-

[a] R1 = $|F_o - F_c|/|F_o|$; [b] wR2 = $[w(F_o^2 - F_c^2)^2/(wF_o^2)]^{1/2}$; [c] I > 2 sig(I)

	$[ReO_2(\mathbf{L2})(\mathbf{L4})]_2(PF_6)_2 \cdot 2H_2O$ [**19**]$(PF_6)_2 \cdot 2H_2O$	$[^{99}TcOCl_3(\mathbf{L2})]$ [**20**]	$[ReOCl_3(\mathbf{L2})]$ [**21**]
Dataset	MEB011214o	MEB180515o	MEB080615
Machine	SuperNova	SuperNova	Xcalibur
Formula	$C_{32}H_{44}F_{12}N_{16}O_6P_2Re_2$	$C_9H_{12}Cl_3N_4OTc$	$C_9H_{12}Cl_3N_4ORe$
M_w [g/mol]	1411.13	397.58	484.78
Space group	$P2_1/n$	$Pna2_1$	$Pna2_1$
a [Å]	12.62892(16)	15.6427(3)	15.5476(8)
b [Å]	7.90142(8)	11.9894(2)	11.9306(9)
c [Å]	23.4081(3)	7.07153(13)	7.0493(6)
α [°]	90	90	90
β [°]	100.3138(13)	90	90
γ [°]	90	90	90
μ [mm^{-1}]	11.804	14.336	9.898
Z	2	4	4
V [$Å^3$]	2298.07(5)	1326.24(4)	1307.60(17)
ρ_{calc} / [g/cm^3]	2.039	1.986	2.462
R1[a, c]	0.0195	0.0282	0.0363
wR2[b, c]	0.0467	0.0680	0.0665
CCDC	-	-	-

[a] R1 = $|F_o - F_c|/|F_o|$; [b] wR2 = $[w(F_o^2 - F_c^2)^2/(wF_o^2)]^{1/2}$; [c] I > 2 sig(I)

	$[^{99}TcO_2(\mathbf{L2})(bipy)](PF_6) \cdot H_2O$ [**22**]$(PF_6) \cdot H_2O$	$[ReO_2(\mathbf{L2})(bipy)](PF_6) \cdot H_2O$ [**23**]$(PF_6) \cdot H_2O$
Dataset	MEB130815	MEB210815
Machine	Xcalibur	Xcalibur
Formula	$C_{19}H_{22}F_6N_6O_3PTc$	$C_{19}H_{22}F_6N_6O_3PRe$
M_w [g/mol]	626.39	713.59
Space group	Pbcm	Pbcm
a [Å]	13.9938(4)	13.9352(5)
b [Å]	7.7977(2)	7.8149(3)
c [Å]	21.3247(8)	21.3142(7)
α [°]	90	90
β [°]	90	90
γ [°]	90	90
μ [mm^{-1}]	0.771	5.388
Z	4	4
V [$Å^3$]	2326.95(13)	2321.16(13)
ρ_{calc} / [g/cm^3]	1.785	2.042
R1[a, c]	0.0305	0.0281
wR2[b, c]	0.0723	0.0526
CCDC	-	-

[a] R1 = $|F_o - F_c|/|F_o|$; [b] wR2 = $[w(F_o^2 - F_c^2)^2/(wF_o^2)]^{1/2}$; [c] I > 2 sig(I)

	$[ReO_2(\mathbf{L2})(bipy)](Cl)\cdot 4H_2O$ [**23**](Cl)·4H$_2$O	*cis*-[$^{99}TcCl_2(\mathbf{L2})_2](PF_6)_2\cdot THF$ [**24**]$(PF_6)_2\cdot$THF	$[Re(\mathbf{L5})(CO)_3]$ [**25**]
Dataset	DUB030815tw_hklf4	MEB090215o	MEB081013
Machine	Xcalibur	SuperNova	Xcalibur
Formula	$C_{19}H_{28}ClN_6O_6Re$	$C_{22}H_{32}Cl_2F_{12}N_8OP_2Tc$	$C_{21}H_{20}BN_6O_3Re$
M_w [g/mol]	658.12	884.38	601.44
Space group	$P\bar{1}$	$P2_1/n$	$Cmc2_1$
a [Å]	7.7808(3)	11.3360(2)	13.2297(5)
b [Å]	10.2158(5)	24.4127(4)	20.1592(12)
c [Å]	15.3393(6)	12.30960(17)	8.0787(5)
α [°]	99.091(4)	90	90
β [°]	96.940(3)	98.8170(15)	90
γ [°]	99.919(4)	90	90
μ [mm^{-1}]	5.345	6.761	5.676
Z	2	4	4
V [$Å^3$]	1172.14(9)	3366.33(9)	2154.6(2)
ρ_{calc} / [g/cm^3]	1.865	1.743	1.854
R1[a, c]	0.0335	0.0763	0.0374
wR2[b, c]	0.0664	0.1950	0.0581
CCDC	-	-	-

[a] R1 = $|F_o - F_c|/|F_o|$; [b] wR2 = $[w(F_o^2 - F_c^2)^2/(wF_o^2)]^{1/2}$; [c] I > 2 sig(I)

	$(PhB(^{Me}Im\text{-}H)_3)(OTf)_2$ (**L5**-H$_3$)$(OTf)_2$	$[ReBr(\mathbf{L6}\text{-}H)(CO)_3](Br)\cdot H_2O\cdot CH_3CN$ [**27**](Br)·H$_2$O·CH$_3$CN
Dataset	MEB240714	MEB111113
Machine	Xcalibur	Xcalibur
Formula	$C_{20}H_{23}BF_6N_6O_6S_2$	$C_{22}H_{30}Br_2N_7O_4Re$
M_w [g/mol]	632.36	802.53
Space group	$P2_12_12_1$	$P\bar{1}$
a [Å]	6.8544(8)	10.0051(3)
b [Å]	19.227(3)	14.1006(5)
c [Å]	20.181(12)	20.9249(6)
α [°]	90	71.996(3)
β [°]	90	83.153(3)
γ [°]	90	89.460(3)
μ [mm^{-1}]	0.291	7.270
Z	4	4
V [$Å^3$]	2659.7(17)	2786.30(15)
ρ_{calc} / [g/cm^3]	1.579	1.913
R1[a, c]	0.0441	0.0465
wR2[b, c]	0.0863	0.1047
CCDC	-	-

[a] R1 = $|F_o - F_c|/|F_o|$; [b] wR2 = $[w(F_o^2 - F_c^2)^2/(wF_o^2)]^{1/2}$; [c] I > 2 sig(I)

	[^{99}Tc(**L5**)(CO)$_3$] [**28**]	[$^{99}Tc_3O_3(\mu\text{-}O)_3(\mu\text{-}CHO_2)$(**L2**)$_3$(^{Me}Im)](PF$_6$)$_2\cdot 3CH_2Cl_2$
Dataset	MEB010914	MEB221013
Machine	Xcalibur	Xcalibur
Formula	$C_{21}H_{20}BN_6O_3Tc$	$C_{35}H_{49}Cl_6F_{12}N_{14}O_8P_2Tc_3$
M_w [g/mol]	514.24	1593.51
Space group	$Cmc2_1$	$P\bar{1}$
a [Å]	13.261(14)	13.5052(6)
b [Å]	20.284(6)	14.1618(5)
c [Å]	8.0961(14)	16.2659(6)
α [°]	90	96.638(3)
β [°]	90	99.117(3)
γ [°]	90	107.925(4)
μ [mm^{-1}]	0.697	1.142
Z	4	2
V [Å^3]	2178(2)	2877.50(19)
ρ_{calc} / [g/cm^3]	1.565	1.836
R1[a, c]	0.0281	0.0681
wR2[b, c]	0.0681	0.1748
CCDC	-	-

[a] $R1 = |F_o - F_c|/|F_o|$; [b] $wR2 = [w(F_o^2 - F_c^2)^2/(wF_o^2)]^{1/2}$; [c] I > 2 sig(I)

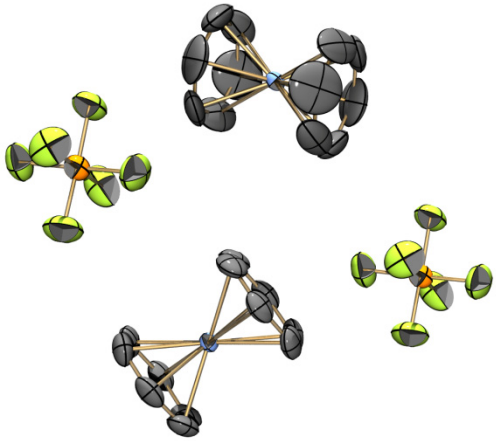

Figure 54: ORTEP representation[51] of the [^{99}Tc(benzene)$_2$](PF$_6$) structure.

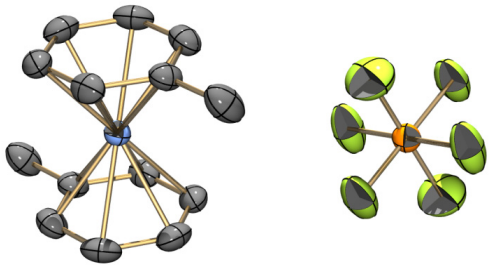

Figure 55: ORTEP representation[51] of the [^{99}Tc(toluene)$_2$](PF$_6$) structure.

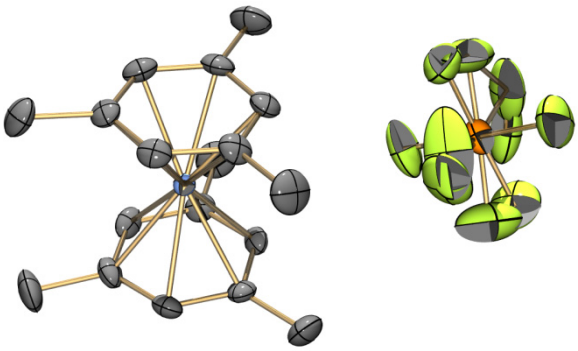

Figure 56: ORTEP representation[51] of the [^{99}Tc(mesitylene)$_2$](PF$_6$) structure.

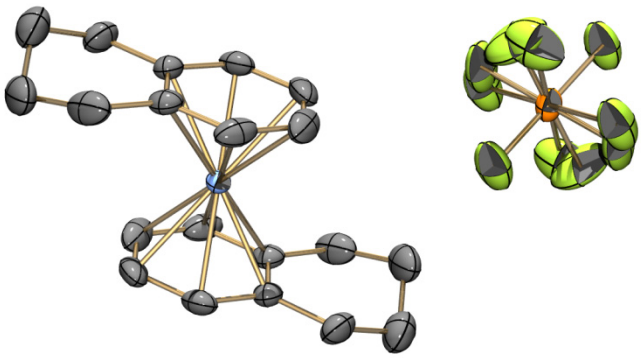

Figure 57: ORTEP representation[51] of the [^{99}Tc(tetralin)$_2$](PF$_6$) structure.

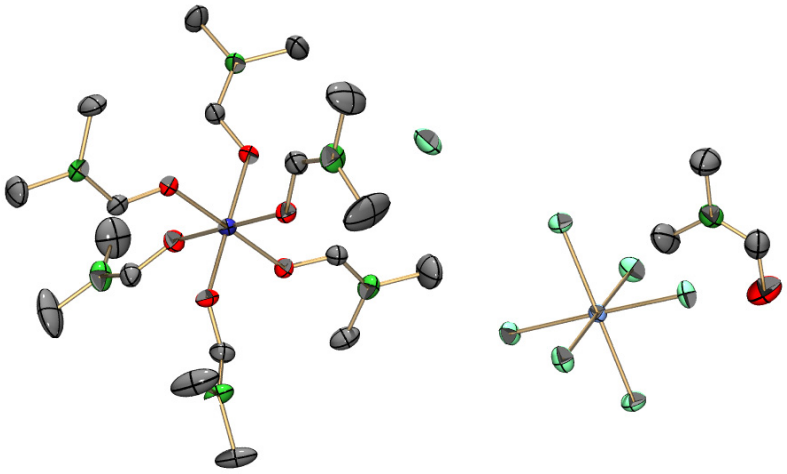

Figure 58: ORTEP representation[51] of the $[Al(DMF)_6][^{99}TcCl_6](Cl)\cdot DMF$ structure.

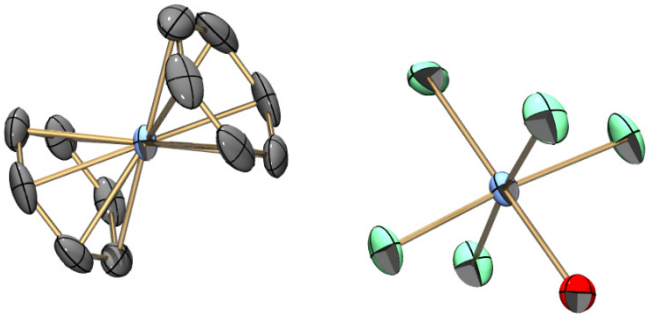

Figure 59: ORTEP representation[51] of the $[^{99}Tc(benzene)_2][^{99}TcCl_5(OH_2)]$ structure.

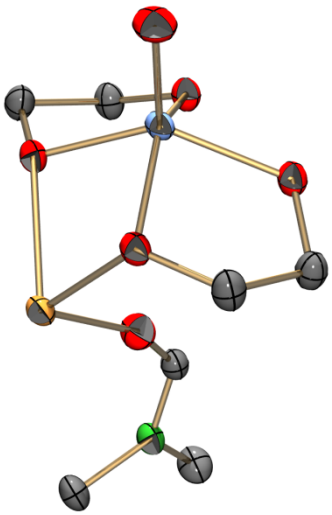

Figure 60: ORTEP representation[51] of the $(Li)[^{99}TcO(glyc)_2]\cdot DMF$ structure.

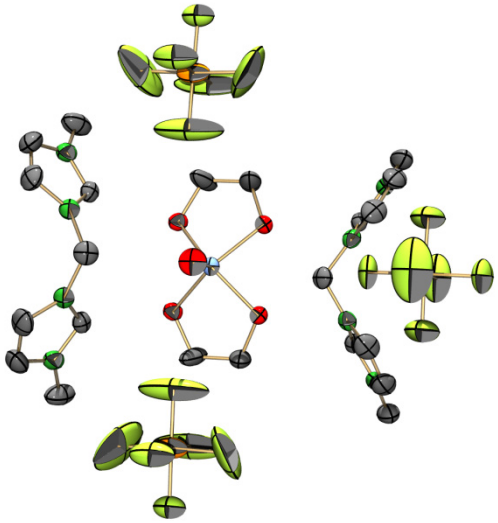

Figure 61: ORTEP representation[51] of the (**L2**-H_2)$_2$[^{99}TcO(glyc)$_2$](PF_6)$_3$ structure.

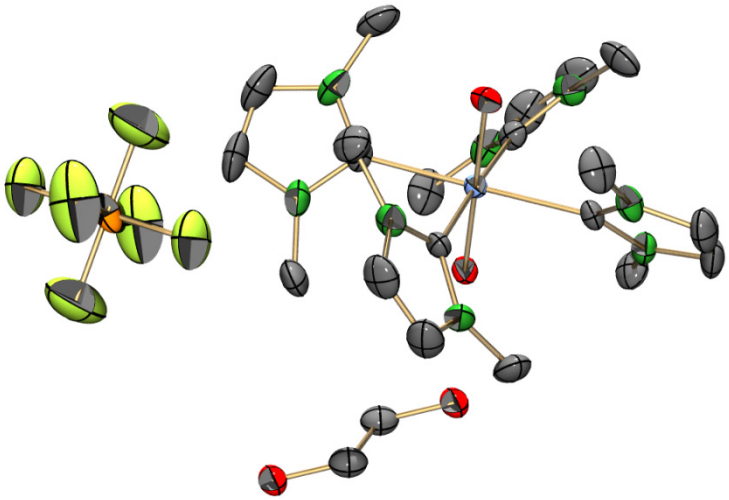

Figure 62: ORTEP representation[51] of the [$^{99}TcO_2$(**L1**)$_4$](PF_6)·glyc-H_2 structure.

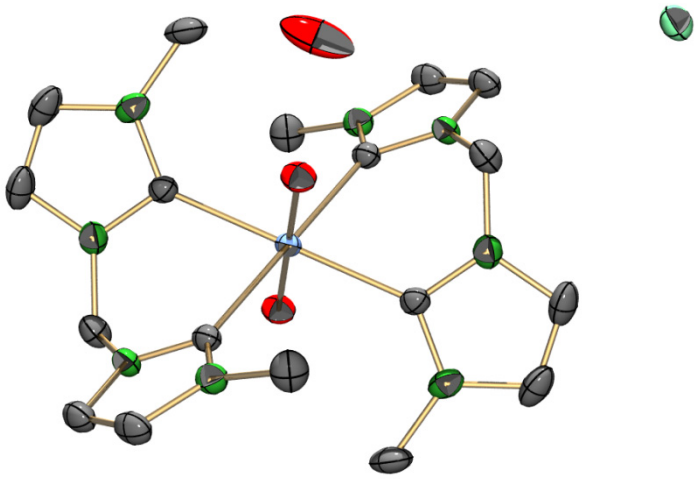

Figure 63: ORTEP representation[51] of the [$^{99}TcO_2$(**L2**)$_2$](Cl)·2H_2O structure.

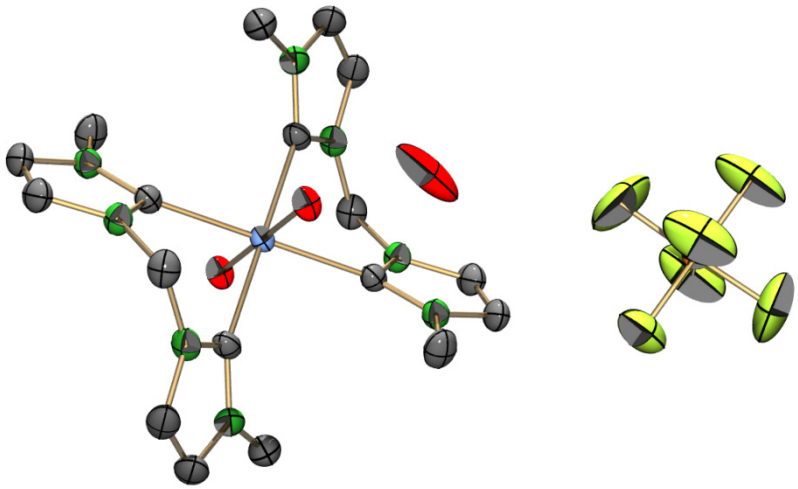

Figure 64: ORTEP representation[51] of the [$^{99}TcO_2$(**L2**)$_2$](PF_6)·H_2O structure.

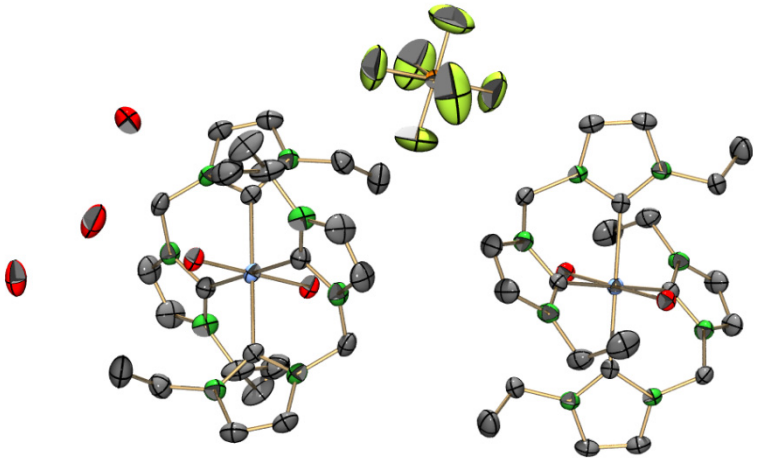

Figure 65: ORTEP representation[51] of the [$^{99}TcO_2$(**L3**)$_2$](PF_6)·2.6H_2O structure.

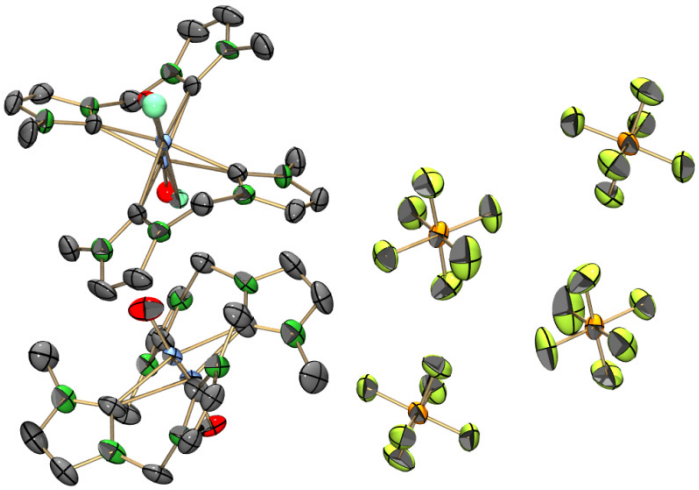

Figure 66: ORTEP representation[51] of the [$^{99}TcOCl$(**L2**)$_2$](PF_6)$_2$ structure.

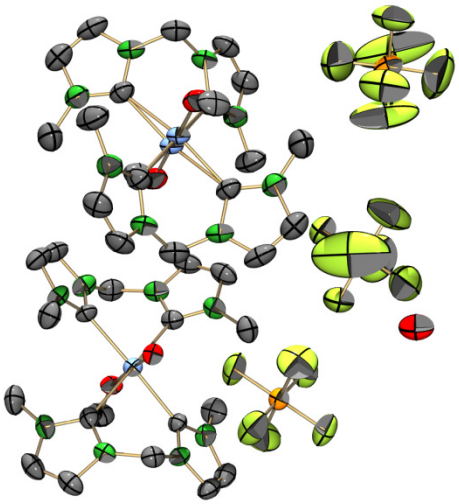

Figure 67: ORTEP representation[51] of the [^{99}TcO(OMe)(**L2**)$_2$](PF$_6$)$_2$·0.67H$_2$O structure.

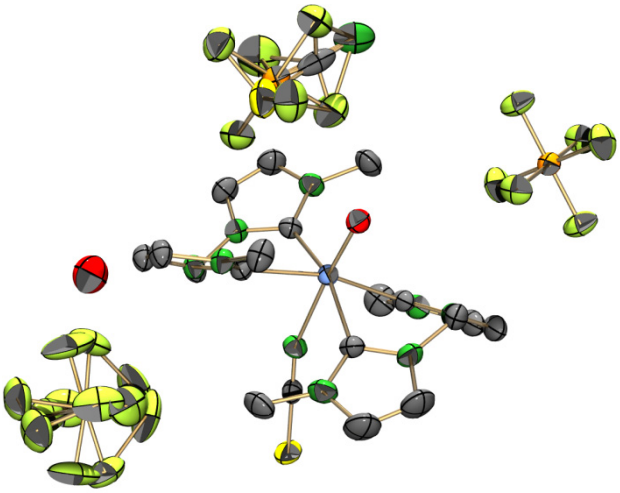

Figure 68: ORTEP representation[51] of the [^{99}TcO(NCS)(**L2**)$_2$](PF$_6$)$_{1.4}$(SCN)$_{0.6}$·H$_2$O structure.

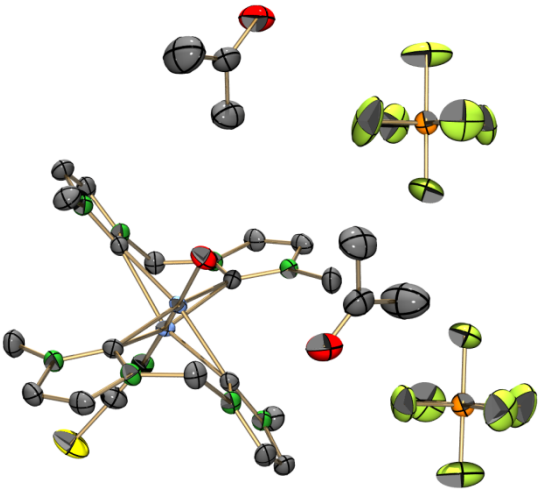

Figure 69: ORTEP representation[51] of the [^{99}TcO(NCS)(**L2**)$_2$](PF$_6$)$_2$·2acetone structure.

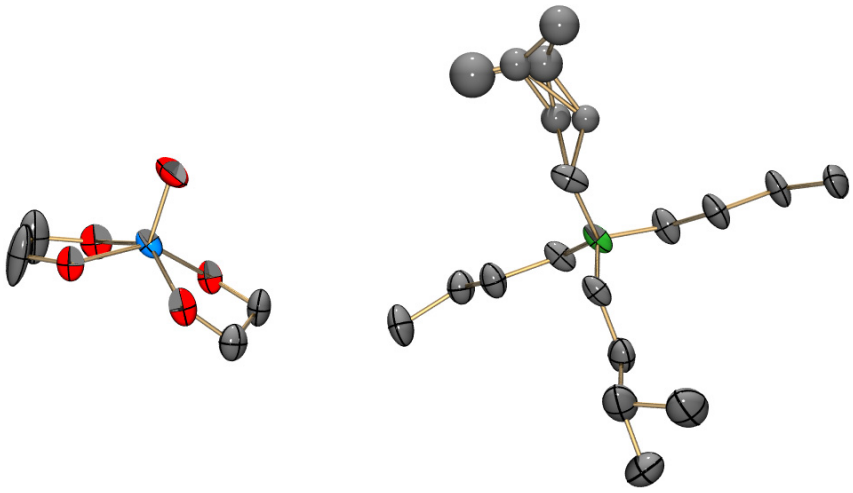

Figure 70: ORTEP representation[51] of the $(N^nBu_4)[ReO(glyc)_2]$ structure.

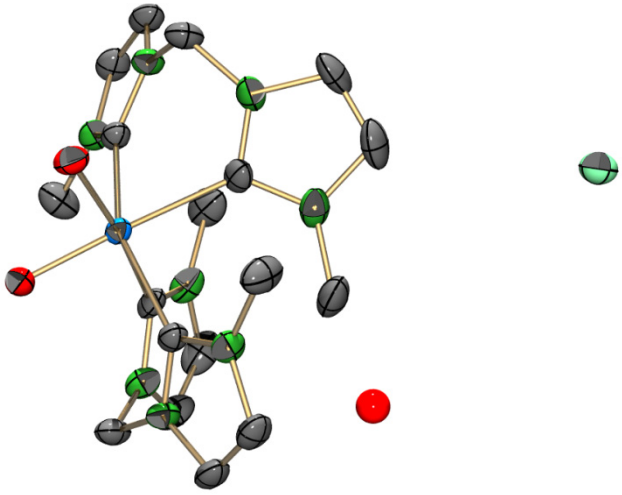

Figure 71: ORTEP representation[51] of the *cis*-$[ReO_2(\mathbf{L2})_2](Cl)\cdot H_2O$ structure.

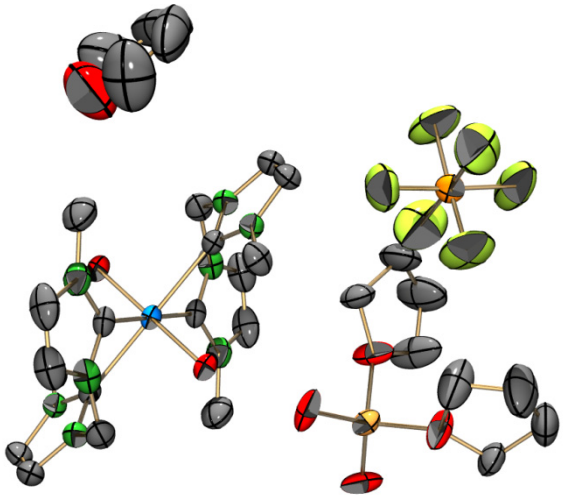

Figure 72: ORTEP representation[51] of the *trans*-$[ReO_2(\mathbf{L2})_2](PF_6)\cdot 2H_2O\cdot 3THF\cdot LiPF_6$ structure.

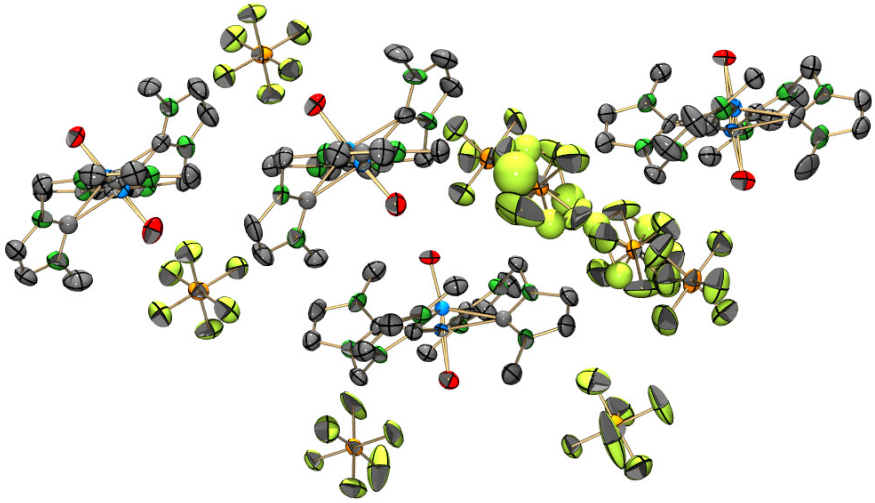

Figure 73: ORTEP representation[51] of the *trans*-[ReOCl(**L2**)$_2$](PF$_6$)$_2$ structure.

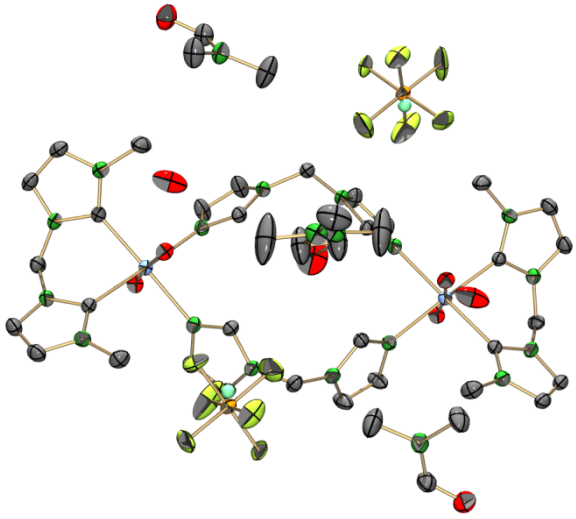

Figure 74: ORTEP representation[51] of the [^{99}TcO$_2$(**L2**)(**L4**)]$_2$(PF$_6$)$_{1.5}$(Cl)$_{0.5}$·3DMF·4H$_2$O structure.

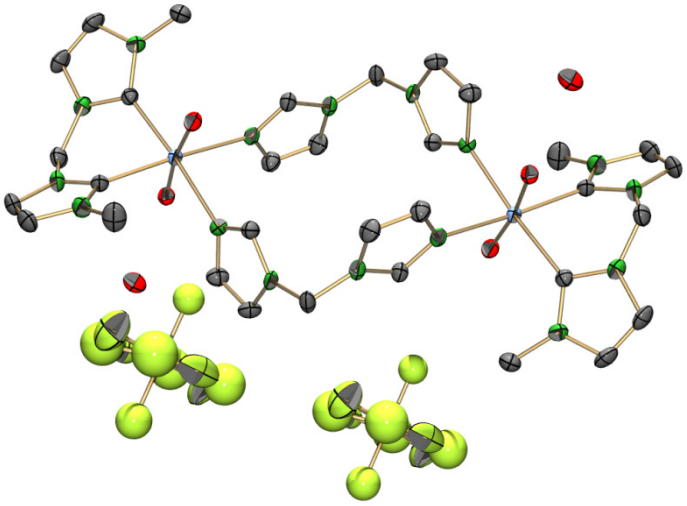

Figure 75: ORTEP representation[51] of the [^{99}TcO$_2$(**L2**)(**L4**)]$_2$(PF$_6$)$_2$·2H$_2$O structure.

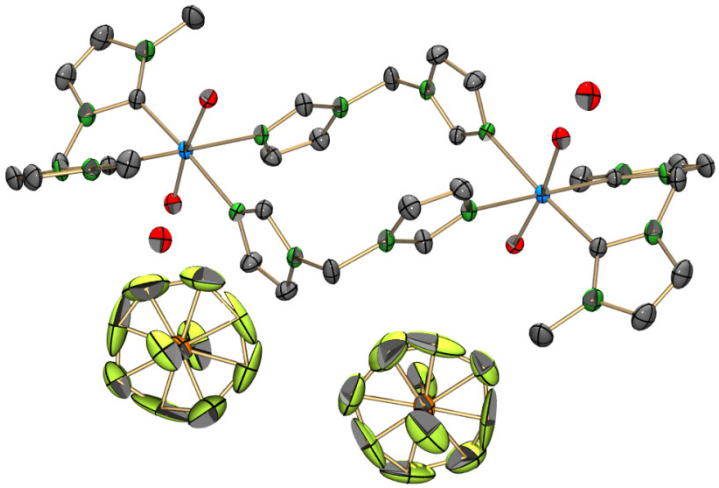

Figure 76: ORTEP representation[51] of the $[ReO_2(\mathbf{L2})(\mathbf{L4})]_2(PF_6)_2 \cdot 2H_2O$ structure.

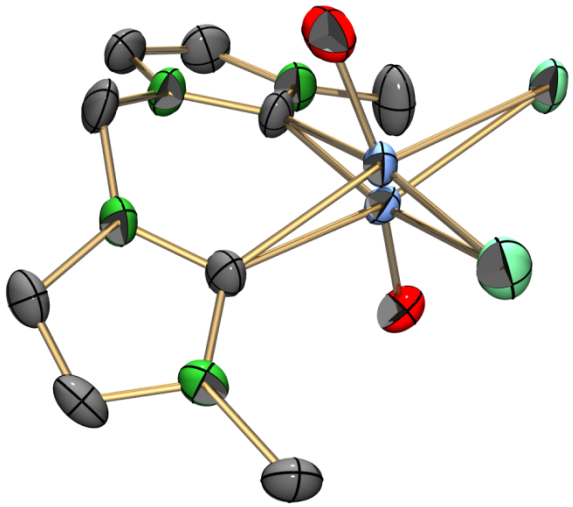

Figure 77: ORTEP representation[51] of the $[^{99}TcOCl_3(\mathbf{L2})]$ structure.

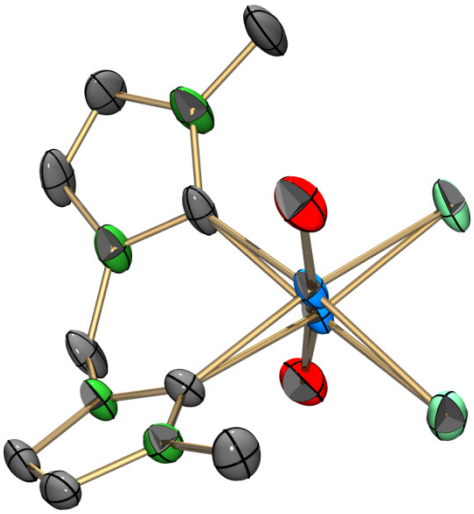

Figure 78: ORTEP representation[51] of the $[ReOCl_3(\mathbf{L2})]$ structure.

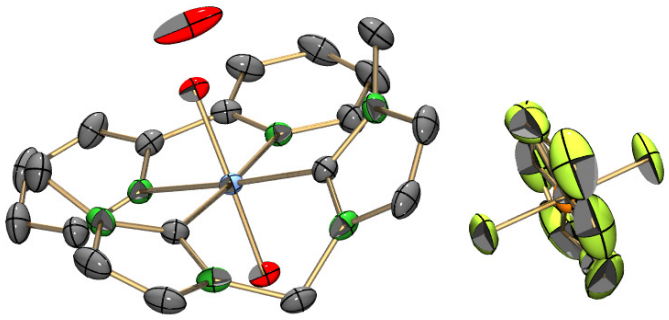

Figure 79: ORTEP representation[51] of the [$^{99}TcO_2$(**L2**)(bipy)](PF_6)·H_2O structure.

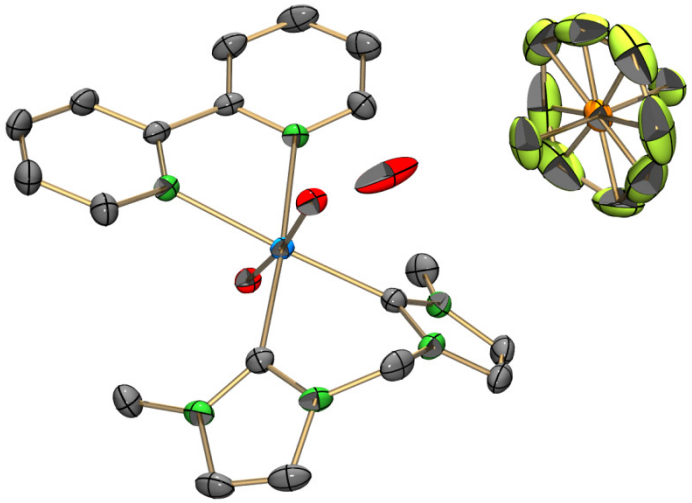

Figure 80: ORTEP representation[51] of the [ReO_2(**L2**)(bipy)](PF_6)·H_2O structure.

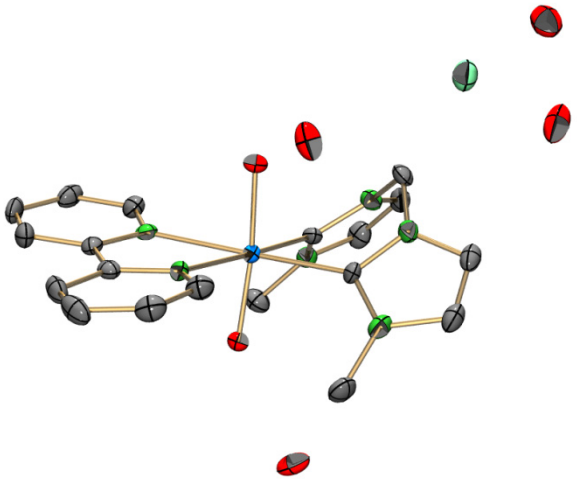

Figure 81: ORTEP representation[51] of the [ReO_2(**L2**)(bipy)](Cl)·$4H_2O$ structure.

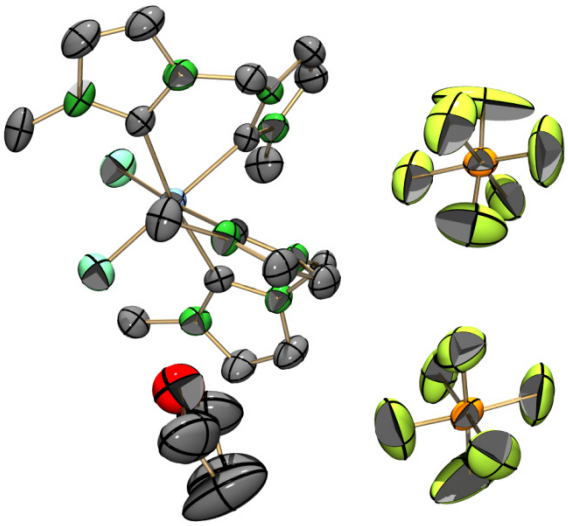

Figure 82: ORTEP representation[51] of the *cis*-[$^{99}TcCl_2$(**L2**)$_2$]$(PF_6)_2$·THF structure.

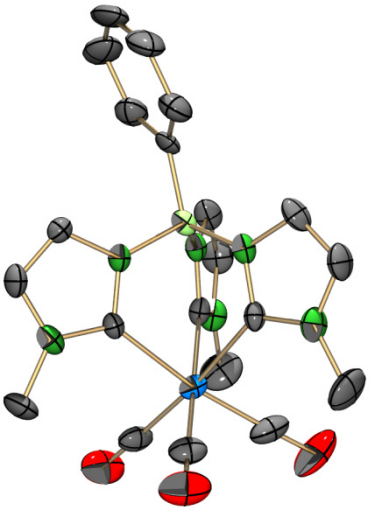

Figure 83: ORTEP representation[51] of the [Re(**L5**)$(CO)_3$] structure.

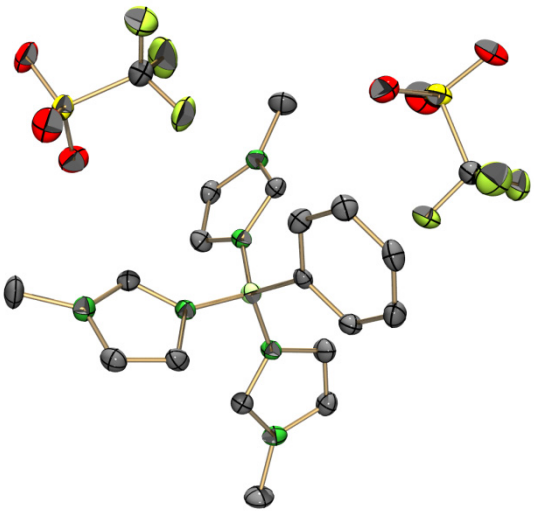

Figure 84: ORTEP representation[51] of the (PhB(^{Me}Im-H)$_3$)$(OTf)_2$ structure.

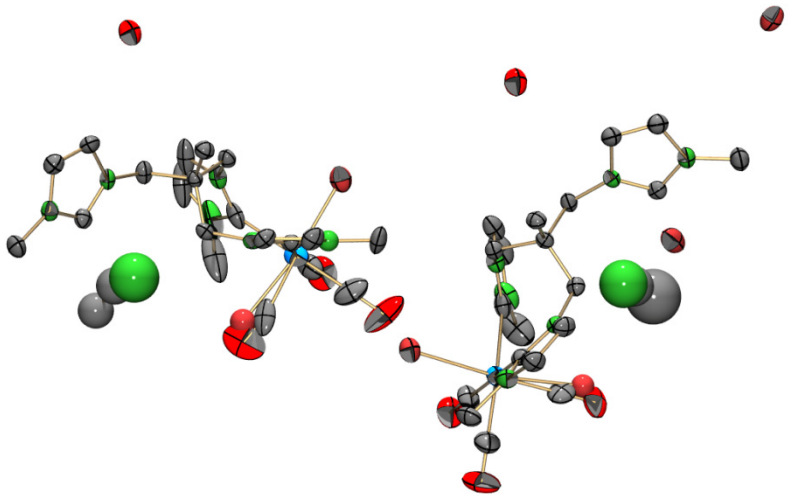

Figure 85: ORTEP representation[51] of the [ReBr(**L6**-H)$(CO)_3$](Br)·H_2O·CH_3CN structure.

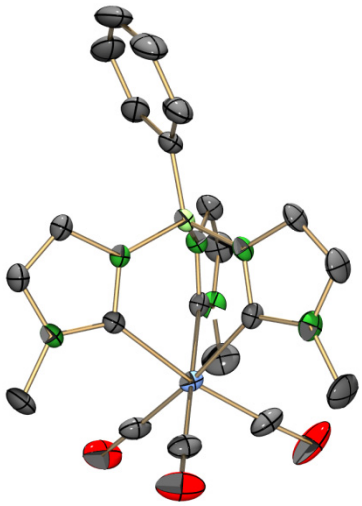

Figure 86: ORTEP representation[51] of the [^{99}Tc(**L5**)$(CO)_3$] structure.

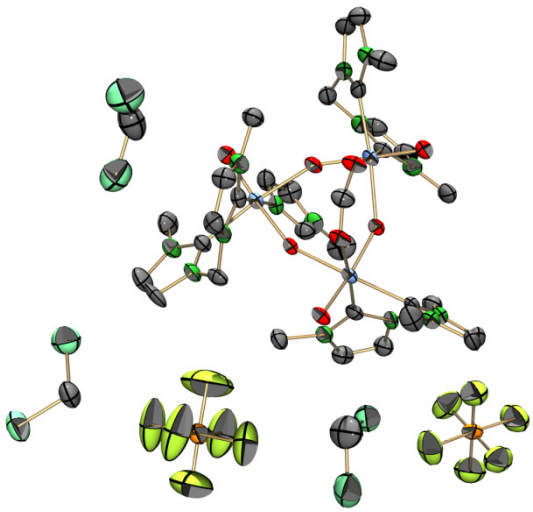

Figure 87: ORTEP representation[51] of the [$^{99}Tc_3O_3(\mu\text{-}O)_3(\mu\text{-}CHO_2)$(**L2**)$_3$(^{Me}Im)]$(PF_6)_2$·$3CH_2Cl_2$ structure.

9 References

1. Hartinger, C. G.; Metzler-Nolte, N.; Dyson, P. J. *Organometallics* **2012**, *31*, 5677-5685.
2. Yan, Y. K.; Melchart, M.; Habtemariam, A.; Sadler, P. J. *Chem. Commun.* **2005**, 4764-4776.
3. Liu, W.; Gust, R. *Chem. Soc. Rev.* **2013**, *42*, 755-773.
4. Hindi, K. M.; Panzner, M. J.; Tessier, C. A.; Cannon, C. L.; Youngs, W. J. *Chem. Rev.* **2009**, *109*, 3859-3884.
5. Perrier, C.; Segrè, E. *J. Chem. Phys.* **1937**, *5*, 712-716.
6. Perrier, C.; Segrè, E. *J. Chem. Phys.* **1939**, *7*, 155-156.
7. Deutsch, E.; Libson, K.; Jurisson, S.; Lindoy, L. F. In *Prog. Inorg. Chem.*; John Wiley & Sons, Inc., **2007**; 75-139.
8. Boyd, R. E. *Radiochim. Acta* **1987**, *41*, 59-63.
9. Pillai, M. R. A.; Dash, A.; Knapp, F. F., Jr. *J. Nucl. Med.* **2013**, *54*, 313-323.
10. Icenhower, J. P.; Qafoku, N. P.; Zachara, J. M.; Martin, W. J. *Am. J. Sci.* **2010**, *310*, 721-752.
11. Dileep, C. S.; Jagasia, P.; Dhami, P. S.; Achuthan, P. V.; Dakshinamoorthy, A.; Tomar, B. S.; Munshi, S. K.; Dey, P. K. *Desalination* **2008**, *232*, 157-165.
12. Sood, D. D.; Patil, S. K. *J. Radioanal. Nucl. Chem.* **1996**, *203*, 547-573.
13. Alberto, R.; Meyer, J. A. M. J. In *Comprehensive Coordination Chemistry II*; Pergamon: Oxford, **2003**; 127-270.
14. Hileman, J. C.; Huggins, D. K.; Kaesz, H. D. *J. Am. Chem. Soc.* **1961**, *83*, 2953-2954.
15. Hieber, W.; Herget, C. *Angew. Chem.* **1961**, *73*, 579-580.
16. Alberto, R.; Schibli, R.; Egli, A.; August Schubiger, P.; Herrmann, W. A.; Artus, G.; Abram, U.; Kaden, T. A. *J. Organomet. Chem.* **1995**, *492*, 217-224.
17. Alberto, R.; Schibli, R.; Egli, A.; Schubiger, A. P.; Abram, U.; Kaden, T. A. *J. Am. Chem. Soc.* **1998**, *120*, 7987-7988.
18. Alberto, R.; Ortner, K.; Wheatley, N.; Schibli, R.; Schubiger, A. P. *J. Am. Chem. Soc.* **2001**, *123*, 3135-3136.
19. Alberto, R.; Schibli, R.; Waibel, R.; Abram, U.; Schubiger, A. P. *Coord. Chem. Rev.* **1999**, *190-192*, 901-919.
20. Joachim, J. E.; Apostolidis, C.; Kanellakopulos, B.; Maier, R.; Marques, N.; Meyer, D.; Müller, J.; Pires de Matos, A.; Nuber, B.; Rebizant, J.; Ziegler, M. L. *J. Organomet. Chem.* **1993**, *448*, 119-129.
21. Baumgärtner, F.; Fischer, E. O.; Zahn, U. *Chem. Ber. Recl.* **1961**, *94*, 2198-2203.
22. Fischer, E. O.; Schmidt, M. W. *Chem. Ber.* **1969**, *102*, 1954-1960.
23. Palm, C.; Fischer, E. O.; Baumgärtner, F. *Tetrahedron Lett.* **1962**, 253-254.
24. Wester, D. W.; Coveney, J. R.; Nosco, D. L.; Robbins, M. S.; Dean, R. T. *J. Med. Chem.* **1991**, *34*, 3284-3290.
25. Öfele, K. *J. Organomet. Chem.* **1968**, *12*, P42-P43.
26. Wanzlick, H. W.; Schönherr, H. J. *Angew. Chem. Int. Ed. Engl.* **1968**, *7*, 141-142.
27. Bourissou, D.; Guerret, O.; Gabbaï, F. P.; Bertrand, G. *Chem. Rev.* **2000**, *100*, 39-92.
28. Herrmann, W. A. *Angew. Chem. Int. Ed.* **2002**, *41*, 1290-1309.
29. Grubbs, R. H. *Angew. Chem. Int. Ed.* **2006**, *45*, 3760-3765.
30. Mercs, L.; Albrecht, M. *Chem. Soc. Rev.* **2010**, *39*, 1903-1912.
31. Hu, X. L.; Castro-Rodriguez, I.; Olsen, K.; Meyer, K. *Organometallics* **2004**, *23*, 755-764.
32. Nemcsok, D.; Wichmann, K.; Frenking, G. *Organometallics* **2004**, *23*, 3640-3646.
33. Hock, S. J.; Schaper, L.-A.; Herrmann, W. A.; Kuhn, F. E. *Chem. Soc. Rev.* **2013**, *42*, 5073-5089.
34. Braband, H.; Zahn, T. I.; Abram, U. *Inorg. Chem.* **2003**, *42*, 6160-6162.
35. Kuhn, N.; Kratz, T. *Synthesis* **1993**, *1993*, 561-562.
36. Braband, H.; Abram, U. *Organometallics* **2005**, *24*, 3362-3364.
37. Oehlke, E.; Kong, S.; Arciszewski, P.; Wiebalck, S.; Abram, U. *J. Am. Chem. Soc.* **2012**, *134*, 9118-9121.
38. Bellemin-Laponnaz, S.; Dagorne, S. *Chem. Rev.* **2014**, *114*, 8747-8774.
39. Forshaw, A. P.; Bontchev, R. P.; Smith, J. M. *Inorg. Chem.* **2007**, *46*, 3792-3794.
40. Flores-Figueroa, A.; Kaufhold, O.; Feldmann, K.-O.; Hahn, F. E. *Dalton Trans.* **2009**, 9334-9342.

41. Liu, C.-Y.; Chen, D.-Y.; Lee, G.-H.; Peng, S.-M.; Liu, S.-T. *Organometallics* **1996**, *15*, 1055-1061.
42. Lum, R.; Zhang, H.; Zhang, W.; Bai, S.-Q.; Zhao, J.; Hor, T. S. A. *Dalton Trans.* **2013**, *42*, 871-873.
43. Chan, C. Y.; Pellegrini, P. A.; Greguric, I.; Barnard, P. J. *Inorg. Chem.* **2014**, *53*, 10862-10873.
44. Trifonova, E. A.; Perekalin, D. S.; Lyssenko, K. A.; Kudinov, A. R. *J. Organomet. Chem.* **2013**, *727*, 60-63.
45. Mausolf, E.; Johnstone, E.; Poineau, F.; Nguyen, S.; Jones, S.; Hartmann, T.; Buck, E.; Czerwinski, K. *J. Radioanal. Nucl. Chem.* **2013**, *298*, 1315-1321.
46. Oehlke, E.; Alberto, R.; Abram, U. *Inorg. Chem.* **2010**, *49*, 3525-3530.
47. Tooyama, Y., PhD Thesis, University of Zürich, **2010**.
48. Tooyama, Y.; Braband, H.; Spingler, B.; Abram, U.; Alberto, R. *Inorg. Chem.* **2007**, *47*, 257-264.
49. Gupta, K.; Mayer, P.; Pandey, A. *Z. Naturforsch., B: Chem. Sci.* **2014**, *69*, 799-803.
50. Hagenbach, A.; Yegen, E.; Abram, U. *Inorg. Chem.* **2006**, *45*, 7331-7338.
51. Farrugia, L. J. *J. Appl. Crystallogr.* **1997**, *30*, 565-565.
52. Yegen, E.; Hagenbach, A.; Abram, U. *Chem. Commun.* **2005**, 5575-5577.
53. Dalziel, J.; Gill, N. S.; Nyholm, R. S.; Peacock, R. D. *J. Chem. Soc.* **1958**, 4012-4016.
54. Raptis, K.; Dornberger, E.; Kanellakopulos, B.; Nuber, B.; Ziegler, M. L. *J. Organomet. Chem.* **1991**, *408*, 61-75.
55. Braga, D.; Cojazzi, G.; Abati, A.; Maini, L.; Polito, M.; Scaccianoce, L.; Grepioni, F. *J. Chem. Soc., Dalton Trans.* **2000**, 3969-3975.
56. Fulmer, G. R.; Miller, A. J. M.; Sherden, N. H.; Gottlieb, H. E.; Nudelman, A.; Stoltz, B. M.; Bercaw, J. E.; Goldberg, K. I. *Organometallics* **2010**, *29*, 2176-2179.
57. SDBSWeb: http://sdbs.db.aist.go.jp; National Institute of Advanced Industrial Science and Technology, **2015**.
58. Stibr, B.; Bakardjiev, M.; Hajkova, Z.; Holub, J.; Padelkova, Z.; Ruzicka, A.; Kennedy, J. D. *Dalton Trans.* **2011**, *40*, 5916-5920.
59. Fischer, E. O.; Elschenbroich, C. *Chem. Ber.* **1970**, *103*, 162-172.
60. Phillips, L.; Dennis, G. R.; Aroney, M. J. *New J. Chem.* **2000**, *24*, 27-32.
61. Silvon, M. P.; Van Dam, E. M.; Skell, P. S. *J. Am. Chem. Soc.* **1974**, *96*, 1945-1946.
62. Halter, J., Master Thesis, University of Zürich, **2014**.
63. Benz, M.; Braband, H.; Schmutz, P.; Halter, J.; Alberto, R. *Chem. Sci.* **2015**, *6*, 165-169.
64. Satou, T.; Takehara, K.; Hirakida, M.; Sakamoto, Y.; Takemura, H.; Miura, H.; Tomonou, M.; Shinmyozu, T. *J. Organomet. Chem.* **1999**, *577*, 58-68.
65. Yur'eva, L. P.; Lev, N. N.; Svetlana, M. P. *Russ. Chem. Rev.* **1993**, *62*, 121.
66. Pampaloni, G. *Coord. Chem. Rev.* **2010**, *254*, 402-419.
67. Oertel, A. M.; Ritleng, V.; Burr, L.; Chetcuti, M. J. *Organometallics* **2011**, *30*, 6685-6691.
68. Buitrago, E.; Tinnis, F.; Adolfsson, H. *Adv. Synth. Catal.* **2012**, *354*, 217-222.
69. Cao, C.; Zhuang, Y.; Zhao, J.; Liu, H.; Geng, P.; Pang, G.; Shi, Y. *Synth. Commun.* **2011**, *42*, 380-387.
70. In, S.; Kang, J. M. *J. Inclusion Phenom. Macrocyclic Chem.* **2006**, *54*, 129-132.
71. Díez-Barra, E.; Delahoz, A.; Sánchezmigallón, A.; Tejeda, J. *Heterocycles* **1992**, *34*, 1365-1373.
72. Shishkov, I. V.; Rominger, F.; Hofmann, P. *Dalton Trans.* **2009**, 1428-1435.
73. Hiltner, O.; Boch, F. J.; Brewitz, L.; Härter, P.; Drees, M.; Herdtweck, E.; Herrmann, W. A.; Kühn, F. E. *Eur. J. Inorg. Chem.* **2010**, *2010*, 5284-5293.
74. Quezada, C. A.; Garrison, J. C.; Panzner, M. J.; Tessier, C. A.; Youngs, W. J. *Organometallics* **2004**, *23*, 4846-4848.
75. Davison, A.; DePamphilis, B. V.; Jones, A. G.; Franklin, K. J.; Lock, C. J. L. *Inorg. Chim. Acta* **1987**, *128*, 161-167.
76. Braband, H.; Abram, U. *Inorg. Chem.* **2006**, *45*, 6589-6591.
77. Braband, H.; Tooyama, Y.; Fox, T.; Alberto, R. *Chem. Eur. J.* **2009**, *15*, 633-638.
78. Benz, M.; Spingler, B.; Alberto, R.; Braband, H. *J. Am. Chem. Soc.* **2013**, *135*, 17566-17572.
79. Kückmann, T. I.; Abram, U. *Inorg. Chem.* **2004**, *43*, 7068-7074.

80. Garrison, J. C.; Youngs, W. J. *Chem. Rev.* **2005**, *105*, 3978-4008.
81. Díez-González, S.; Marion, N.; Nolan, S. P. *Chem. Rev.* **2009**, *109*, 3612-3676.
82. Mata, J. A.; Poyatos, M.; Peris, E. *Coord. Chem. Rev.* **2007**, *251*, 841-859.
83. Braband, H.; Kückmann, T. I.; Abram, U. *J. Organomet. Chem.* **2005**, *690*, 5421-5429.
84. Refosco, F.; Tisato, F.; Bandoli, G.; Bolzati, C.; Dolmella, A.; Moresco, A.; Nicolini, M. *J. Chem. Soc., Dalton Trans.* **1993**, 605-618.
85. Tisato, F.; Refosco, F.; Moresco, A.; Bandoli, G.; Dolmella, A.; Bolzati, C. *Inorg. Chem.* **1995**, *34*, 1779-1787.
86. Roodt, A.; Leipoldt, J. G.; Deutsch, E. A.; Sullivan, J. C. *Inorg. Chem.* **1992**, *31*, 1080-1085.
87. Mokuolu, J. A. A.; Speakman, J. C. *Acta Crystallogr. Sect. B: Struct. Sci.* **1975**, *31*, 172-176.
88. Kabesova, M.; Gazo, J. *Chem. Zvesti* **1980**, *34*, 800-841.
89. Maia, P. I. d. S.; Nguyen, H. H.; Hagenbach, A.; Bergemann, S.; Gust, R.; Deflon, V. M.; Abram, U. *Dalton Trans.* **2013**, *42*, 5111-5121.
90. Muzart, J. *Tetrahedron* **2009**, *65*, 8313-8323.
91. Paul, A.; Connolly, D.; Schulz, M.; Pryce, M. T.; Vos, J. G. *Inorg. Chem.* **2012**, *51*, 1977-1979.
92. Schroer, J.; Wagner, S.; Abram, U. *Inorg. Chem.* **2010**, *49*, 10694-10701.
93. Tisato, F.; Refosco, F.; Mazzi, U.; Bandoli, G.; Nicolini, M. *Inorg. Chim. Acta* **1991**, *189*, 97-103.
94. Boehm, G.; Wieghardt, K.; Nuber, B.; Weiss, J. *Inorg. Chem.* **1991**, *30*, 3464-3476.
95. Pomp, C.; Wieghardt, K. *Polyhedron* **1988**, *7*, 2537-2542.
96. Che, C.-M.; Y. K. Cheng, J.; Cheung, K.-K.; Wong, K.-Y. *J. Chem. Soc., Dalton Trans.* **1997**, 2347-2350.
97. Bandoli, G.; Dolmella, A.; Gerber, T. I. A.; Luzipo, D.; du Preez, J. G. H. *Inorg. Chim. Acta* **2001**, *325*, 215-219.
98. Blackbourn, R. L.; Jones, L. M.; Ram, M. S.; Sabat, M.; Hupp, J. T. *Inorg. Chem.* **1990**, *29*, 1791-1792.
99. Dilworth, J. R.; Ibrahim, S. K.; Roz Khan, S.; Hursthouse, M. B.; Karaulov, A. A. *Polyhedron* **1990**, *9*, 1323-1329.
100. Knapp, F. F.; Beets, A. L.; Guhlke, S.; Zamora, P. O.; Bender, H.; Palmedo, H.; Biersack, H. J. *Anticancer Res.* **1997**, *17*, 1783-1795.
101. Kelkar, S. S.; Reineke, T. M. *Bioconjugate Chem.* **2011**, *22*, 1879-1903.
102. Müller, C.; Schubiger, P. A.; Schibli, R. *Nucl. Med. Biol.* **2007**, *34*, 595-601.
103. Chatterjee, S.; Del Negro, A. S.; Wang, Z.; Edwards, M. K.; Skomurski, F. N.; Hightower, S. E.; Krause, J. A.; Twamley, B.; Sullivan, B. P.; Reber, C.; Heineman, W. R.; Seliskar, C. J.; Bryan, S. A. *Inorg. Chem.* **2011**, *50*, 5815-5823.
104. Kastner, M. E.; Fackler, P. H.; Clarke, M. J.; Deutsch, E. *Inorg. Chem.* **1984**, *23*, 4683-4688.
105. Jin, S.; Wang, D.; Xu, Y. *J. Coord. Chem.* **2012**, *65*, 1953-1969.
106. Cui, G.-H.; Li, J.-R.; Tian, J.-L.; Bu, X.-H.; Batten, S. R. *Cryst. Growth Des.* **2005**, *5*, 1775-1780.
107. Jin, S.-W.; Chen, W.-Z. *Polyhedron* **2007**, *26*, 3074-3084.
108. Shi, R.-B.; Pi, M.; Jiang, S.-S.; Wang, Y.-Y.; Jin, C.-M. *J. Mol. Struct.* **2014**, *1071*, 23-33.
109. Masciocchi, N.; Figini Albisetti, A.; Sironi, A.; Pettinari, C.; Di Nicola, C.; Pettinari, R. *Inorg. Chem.* **2009**, *48*, 5328-5337.
110. Cotton, F. A.; Davison, A.; Day, V. W.; Gage, L. D.; Trop, H. S. *Inorg. Chem.* **1979**, *18*, 3024-3029.
111. Archer, C. M.; Dilworth, J. R.; Griffiths, D. V.; McPartlin, M.; Kelly, J. D. *J. Chem. Soc., Dalton Trans.* **1992**, 183-189.
112. Papachristou, M.; Pirmettis, I. C.; Tsoukalas, C.; Papagiannopoulou, D.; Raptopoulou, C.; Terzis, A.; Stassinopoulou, C. I.; Chiotellis, E.; Pelecanou, M.; Papadopoulos, M. *Inorg. Chem.* **2003**, *42*, 5778-5784.
113. Seifert, S.; Pietzsch, H.-J.; Scheunemann, M.; Spies, H.; Syhre, R.; Johannsen, B. *Appl. Radiat. Isot.* **1998**, *49*, 5-11.
114. Zolle, I. *Technetium 99m Pharmaceuticals - Preparation and Quality Control in Nuclear Medicine*, 1 ed.; Springer-Verlag Berlin Heidelberg, **2007**.

115. International Atomic Energy Agency *Technetium-99m Radiopharmaceuticals: Manufacture of Kits*; International Atomic Energy Agency, **2008**.
116. Gorski, B.; Koch, H. *J. Inorg. Nucl. Chem.* **1969**, *31*, 3565-3571.
117. Grossmann, B.; Muenze, R. *Int. J. Appl. Radiat. Isot.* **1982**, *33*, 189-192.
118. Fišer, M.; Brabec, V.; Dragoun, O.; Kovalík, A.; Ryšavý, M.; Dragounová, N. *Int. J. Radiat. Appl. Instrum., Part A* **1988**, *39*, 943-947.
119. Hess, N.; Xia, Y.; Rai, D.; Conradson, S. *J. Solution Chem.* **2004**, *33*, 199-226.
120. Latimer, W. M. *The Oxidation States of the Elements and Their Potentials in Aqueous Solutions*; Prentice-Hall, **1959**.
121. Huey, C. S.; Tartar, H. V. *J. Am. Chem. Soc.* **1934**, *56*, 2585-2588.
122. Randall, M.; Young, L. E. *J. Am. Chem. Soc.* **1928**, *50*, 989-1004.
123. Alberto, R.; Egli, A.; Abram, U.; Hegetschweiler, K.; Gramlich, V.; Schubiger, P. A. *J. Chem. Soc., Dalton Trans.* **1994**, 2815-2820.
124. Alberto, R.; Schibli, R.; August Schubiger, P.; Abram, U.; Kaden, T. A. *Polyhedron* **1996**, *15*, 1079-1089.
125. Gassman, P. L.; McCloy, J. S.; Soderquist, C. Z.; Schweiger, M. J. *J. Raman Spectrosc.* **2014**, *45*, 139-147.
126. Poineau, F.; Sattelberger, A. P.; Czerwinski, K. R. *J. Coord. Chem.* **2008**, *61*, 2356-2370.
127. Kimura, S.; Umeda, I. O.; Moriyama, N.; Fujii, H. *Bioorg. Med. Chem. Lett.* **2011**, *21*, 7359-7362.
128. *STOE-IPDS Software package*, STOE & Cie, G., vers. Darmstadt, Germany, **1999**.
129. *CrysAlis^{Pro} Software system*, Oxford Diffraction Ltd., vers. 171.32 Oxford, UK, **2007**.
130. Altomare, A.; Burla, M. C.; Camalli, M.; Cascarano, G. L.; Giacovazzo, C.; Guagliardi, A.; Moliterni, A. G. G.; Polidori, G.; Spagna, R. *J Appl Crystallogr* **1999**, *32*, 115-119.
131. Sheldrick, G. M. *Acta Crystallogr., Sect. A: Found. Crystallogr.* **2008**, *64*, 112-122.
132. Spek, A. L. *J. Appl. Crystallogr.* **2003**, *36*, 7-13.

10 Curriculum Vitae

Personal Data

Name:	Benz Michael
Date of birth:	31. October 1987
Place of birth:	Uzwil SG, Switzerland
Place of citizenship	Marbach SG
Nationality:	Swiss

Education

2012 – 2015:	PhD at the Department of Chemistry, University of Zurich, under the supervision of Prof. Dr. Roger Alberto, Prof. Dr. Cristina Nevado and Dr. Henrik Braband.
2010 – 2011:	Master of Science in Chemistry at University of Zurich.
2007 – 2010:	Bachelor of Science at University of Zurich. Major in Chemistry, Minor in Biochemistry.
2002 – 2006:	High School at the Kantonsschule am Burggraben St.Gallen, Switzerland.
2000 – 2002:	Secondary School in Goldach, Switzerland.
1994 – 2000:	Elementary School in Unterägeri (1994 – 1996) and Goldach (1996 – 2000), Switzerland.

Awards

Awarded the Alfred Werner Legat three times (2010, 2011 and 2012) for outstanding achievements during his Bachelor- and Master of Science.

Miscellaneous

Jul. 2006 – Mar. 2007:	Work as a construction worker at Monobeton Speck AG in Goldach, Switzerland.
Mar. 2007 – Sep. 2007:	Military service in Switzerland.

11 List of Publications

From Tc^{VII} to Tc^{I}; Facile Syntheses of bis-Arene Complexes $[^{99(m)}Tc(arene)_2]^+$ from Pertechnetate,
Benz, M.; Braband, H.; Schmutz, P.; Halter, J.; Alberto, R. *Chem. Sci.* **2015**, *6*, 165-169.

Activation of $[^{99(m)}TcO_4]^-$ by Phosphonium Cations,
Braband, H.; Benz, M.; Tooyama, Y.; Alberto, R. *Chem. Commun.* **2014**, *50*, 4126-4129.

Toward Organometallic ^{99m}Tc Imaging Agents: Synthesis of Water-Stable ^{99}Tc-NHC Complexes,
Benz, M.; Spingler, B.; Alberto, R.; Braband, H. *J. Am. Chem. Soc.* **2013**, *135*, 17566-17572.

Combining Bifunctional Chelator with (3 + 2)-Cycloaddition Approaches: Synthesis of Dual-Function Technetium Complexes,
Braband, H.; Imstepf, S.; Benz, M.; Spingler, B.; Alberto, R. *Inorg. Chem.* **2012**, 51, 4051-4057.